Coventry University

DOCTOR OF PHILOSOPHY

Cardioprotective Strategies against Crizotinib Induced Cardiotoxicity

Baderinwa, Ellis

Award date:
2022

Awarding institution:
Coventry University

Link to publication

Cardioprotective Strategies against Crizotinib Induced Cardiotoxicity

Ellis Adewole Baderinwa

Supervisory Team: Dr Afthab Hussain and Prof Helen Maddock

April 2021

Centre for Sport, Exercise and Life sciences

Coventry University

A thesis submitted in partial fulfilment of the requirements for the

degree of Doctor of Philosophy

Certificate of Ethical Approval

Applicant:

Ellis Baderinwa

Project Title:

Investigating the cellular, molecular, and intracellular cardiotoxic effects of the anticancer agent Crizotinib and identifying therapeutic strategies to ameliorate injury.
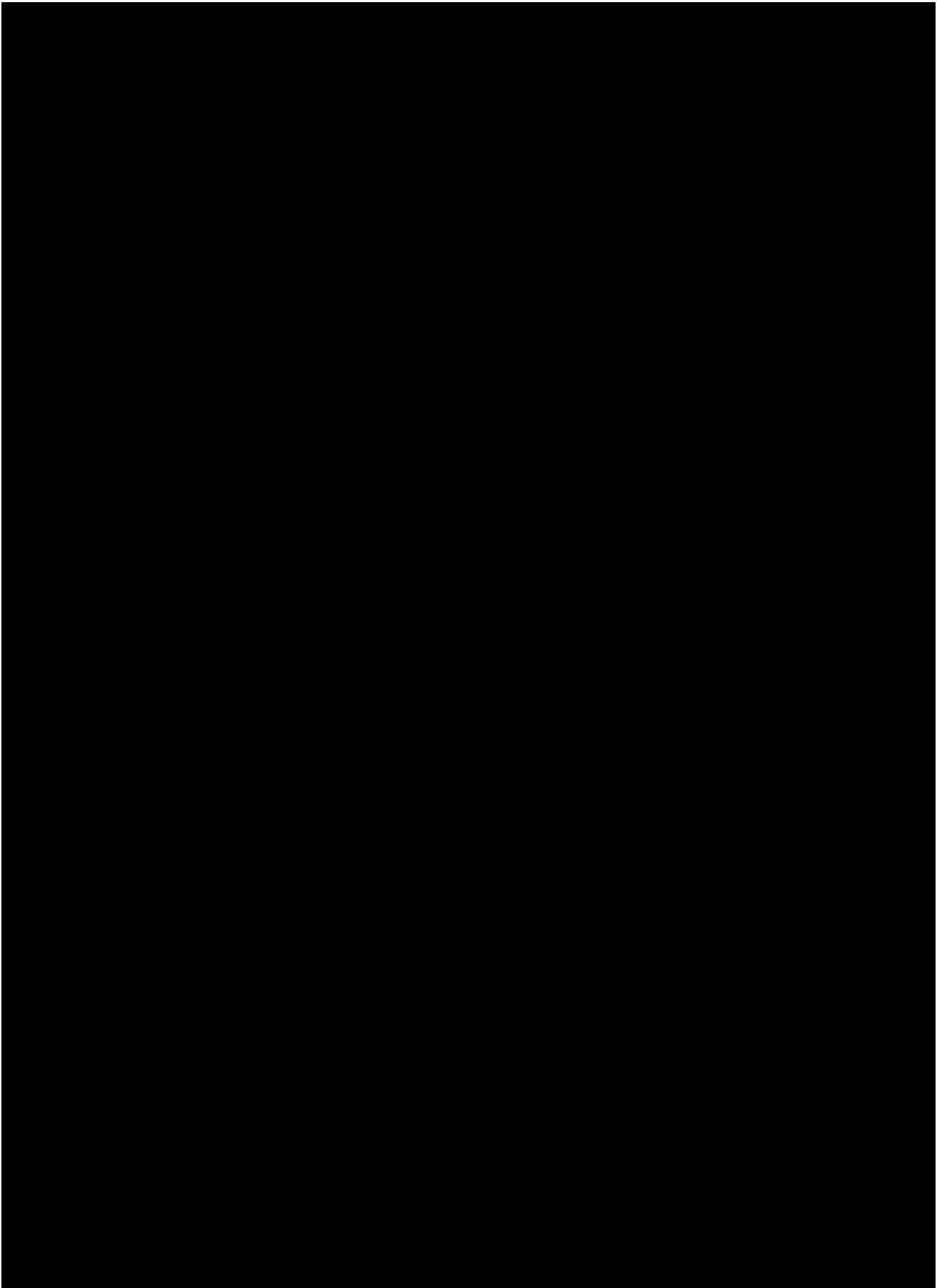
This is to certify that the above-named applicant has completed the Coventry University Ethical Approval process and their project has been confirmed and approved as Medium Risk
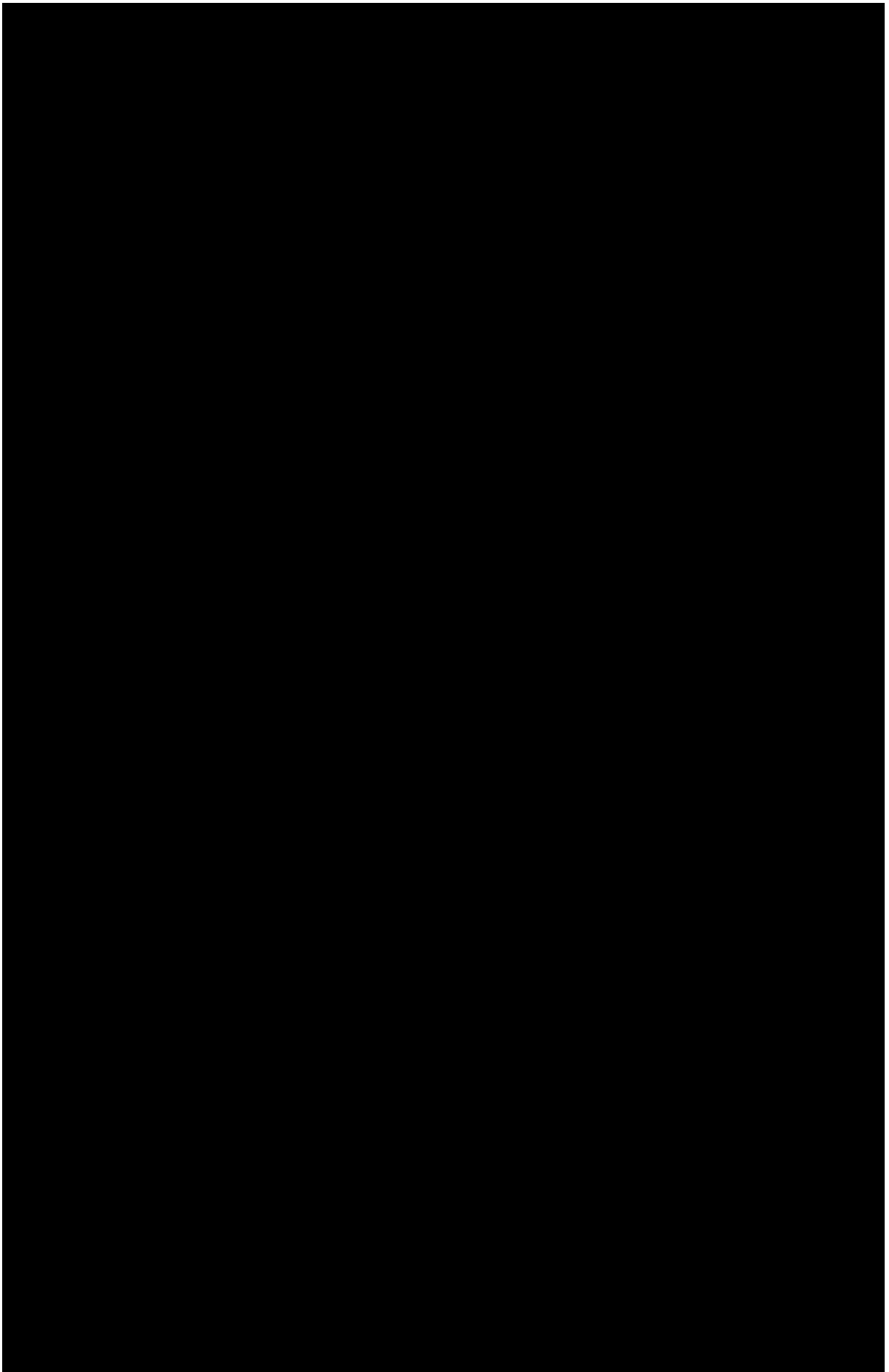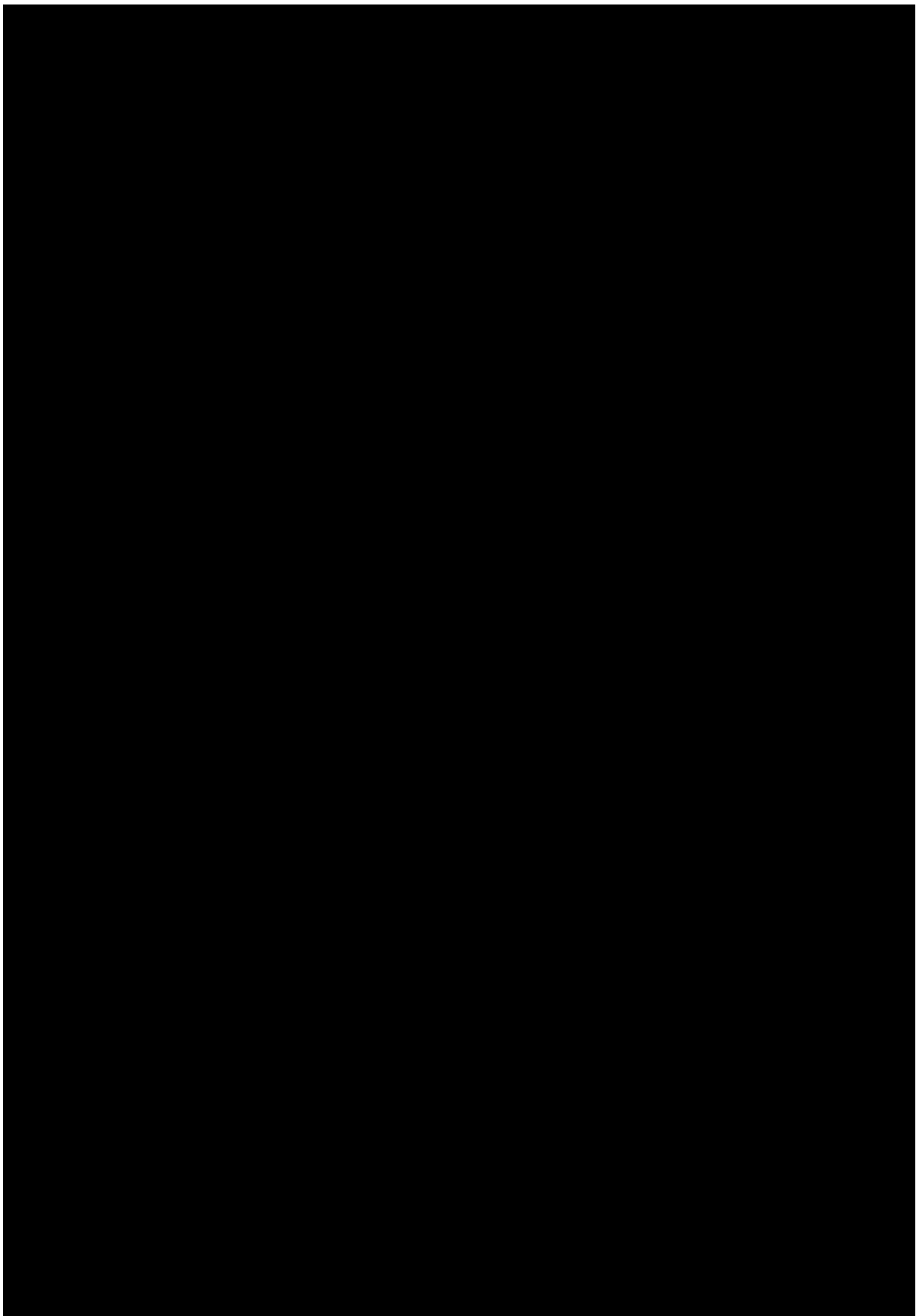
Date of approval:

20 March 2018

Project Reference Number:

P66861
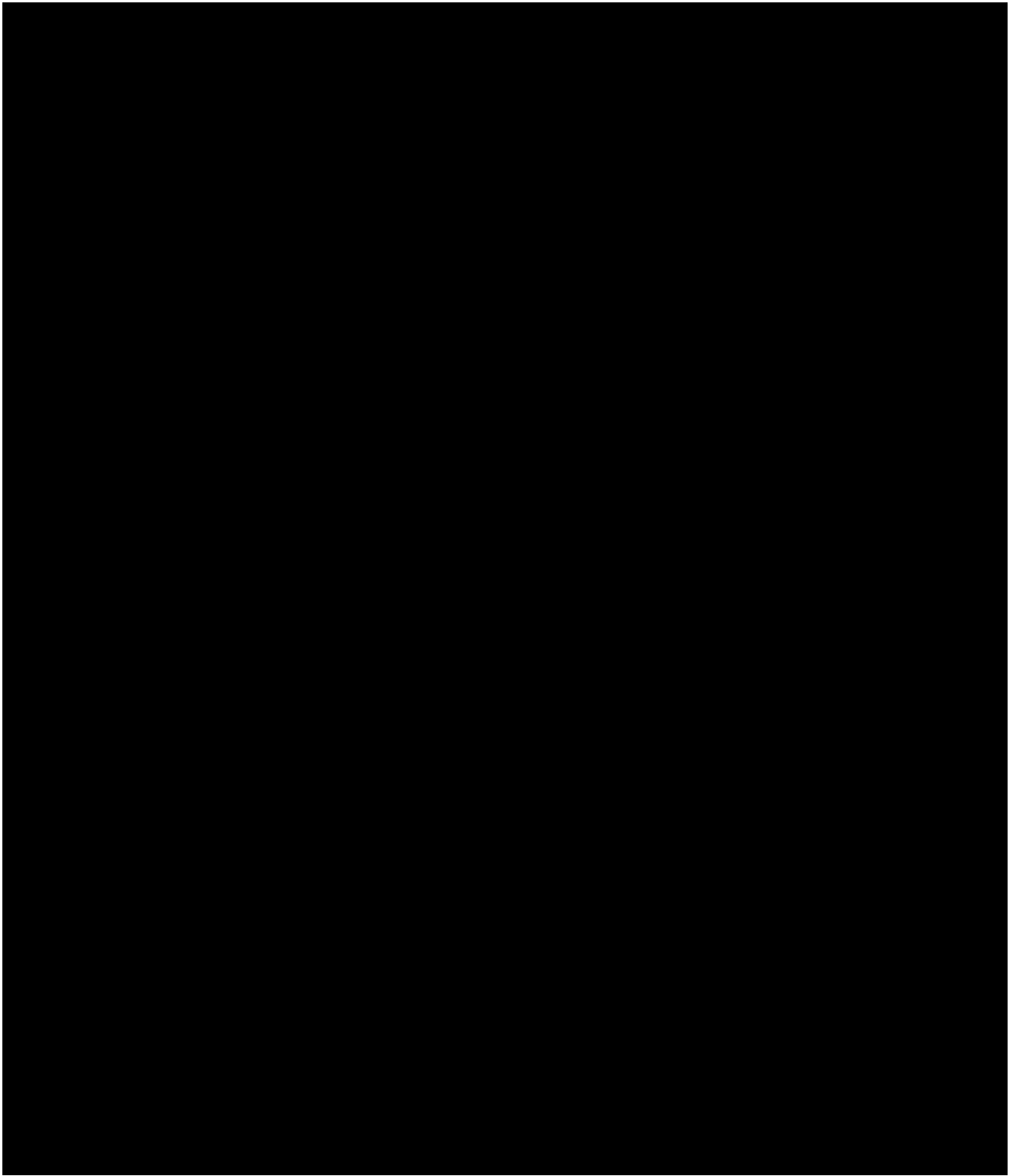
Acknowledgements

I would firstly like to express my deepest gratitude to my supervisor's Dr Afthab Hussain and Professor Helen Maddock, for their support, encouragement, and guidance over these years. I am grateful for the privilege to develop under your guidance.

I would like to thank my family for supporting me emotionally and financially as this would not have been possible without your efforts and many, many sacrifices. I cannot thank you enough or express my full gratitude.

I am grateful to many individuals who have supported me, Mr Mark Bodycote, and Mrs Bethan Grist for providing technical support and training. Hugh Kikuchi for your support at no matter the time of day. A massive thank you to my colleagues for keeping me motivated and supported me throughout this process. I am grateful. My friends who have been on this journey with me and constantly supporting me and encouraging me. I am grateful.

Thank you again,

Ellis Adewole Baderinwa

Abstract

The field of oncology has faced major challenges as cancer therapies are often associated with undesired adverse effects such as cardiotoxicity. Crizotinib treatment has been linked with acute incidences of QT trace prolongation and dysrhythmias in patients during clinical trials. Tyrosine kinase inhibitors primarily display cardiotoxicity due to their activity on multiple receptors.

This present study evaluated concentration dependent cardiotoxicity in adult male Sprague Dawley rat hearts and cultured myoblasts.

Renin angiotensin system antagonists are well known for their cardioprotective effects on the myocardium.

The aim of this study was to assess the potential for renin angiotensin antagonists to limit cardiotoxicity induced by crizotinib treatment.

Crizotinib treatment induced significant concentration dependent impairment of left ventricular developed pressure in isolated langendorff perfused rat hearts. Crizotinib treatment also induced significant concentration dependent infarct to risk ratio development and decreased cultured myoblast viability. It also increased cleaved caspase 3 activity, superoxide generation and disrupted calcium signalling.

Ramipril co-administration with crizotinib significantly improved left ventricular pressure, reduced infarct to risk ratio in isolated rat hearts.

Ramipril co-administration with crizotinib significantly increased myoblast viability, decreased mitochondrial superoxide generation and decreased calcium signalling.

Losartan co-administration with crizotinib similarly improved left ventricular developed pressure, and decreased infarct to risk ratio development. Losartan co-administration with crizotinib significantly increased myoblast viability, decreased cleaved caspase 3 activity, decreased mitochondrial superoxide generation and calcium signalling.

To conclude, the data from this thesis demonstrate concentration dependent toxicity of tyrosine kinase inhibitor crizotinib. The study also presents data that highlights the possible benefit of renin angiotensin system antagonists against crizotinib induced cardiotoxicity.

Contents

List of figures

List Of Abbreviations

- ALK – Anaplastic lymphoma kinase

- HER2 – Receptor tyrosine protein kinase erbB-2

- IP_3R – Inositol triphosphate receptor

- MAPK – Mitogen-activated protein kinase

- MLK1 or MAP3K9 – Mixed lineage kinase 1

- mPTP – Mitochondria permeability transition pore

- NCX – Na^+/Ca^{2+} exchanger

- NSCLC – Non small cell lung cancer

- PI3K – Phosphoinositide 3-Kinase

- RIP1-3 – Receptor interacting serine/threonine-protein kinase 1

- RyR – Ryanodine receptor 1

- SERCA – Sarcoplasmic/endoplasmic reticulum Ca^{2+}-ATPase

- TKI – Tyrosine kinase inhibitor

- VDAC/ANT – Voltage dependent anion channel

Chapter 1 Background

1.1 The Global Burden of Cancer

Fatalities attributed to cancer are considered the second highest cause of death globally and this appears to be independent of the relative developmental differences between countries (Brown and Hahn 2018; Torre et al. 2016) . Despite the increased attention cancer has received over the past few decades, the condition remains a major public health problem globally (Siegel, Miller, and Jemal 2017). According to estimates produced by the World Health Organisation (WHO), as much as 9.6 million deaths in 2018 alone were attributed to cancer globally (Brown and Hahn 2018). Further estimates suggest as much as 1 in 6 deaths worldwide is as a result of cancer and its complications (Brown and Hahn 2018; Ferlay et al. 2015).

The incidence and mortality rates of cancer are reported to be showing an increase globally (Bray et al. 2018a). The underlying cause of this observed increase is difficult to identify (Bray et al. 2018; Ferlay et al. 2015).The widely accepted opinion is that there is a complex interplay between the increased growth of the ageing population and the risk factors of cancer become more prevalent (Ferlay et al. 2015). This is due to increased need for growing innovation to contend with an ever-growing population and slower socioeconomic development in certain regions (Bray et al. 2018; Ferlay et al. 2015). The growth of the aging population due to improvements health

services; resulting in increased likelihood to develop malignancies due to longer term exposure to risk factors (Bray et al. 2018). Increased environmental pollution from increased industrialisation, smoking, obesity and less than adequate dietary changes are often major driving factors in cancer development (Bray et al. 2018).

As previously mentioned, there were an estimated 9.6 million cancer deaths and an estimated 18.1 million newly diagnosed cases in 2018 (Bray et al. 2018). When the figures for both sexes were observed, estimates suggest that Europeans account for 23.4% of new cancer cases and 20.3% of the cancer deaths, while the Americas' accounts for 21% of incidence and 14.4% of cancer deaths globally (Bray et al. 2018). In Africa(7.3%) and Asia(57.3%) however, the cancer deaths are greater than the incidence rates (5.8% and 48.4% respectively) owing to different distribution of the cancer types as well as greater fatality rates in those parts of the world (Bray et al. 2018). Figure 1 below presents the distribution of the incidence and mortality of the 10 more common cancers in 2018, both sex figures combined). These have served as the main driving force behind the vast number of research programs with the aim to characterise the more aggressive and frequently occurring cancer variants (Malvezzi et al. 2015)

A Both sexes

Incidence

Lung 11.6%
Breast 11.6%
Colorectum 10.2%
Prostate 7.1%
Stomach 5.7%
Liver 4.7%
Esophagus 3.2%
Cervix uteri 3.2%
Thyroid 3.1%
Bladder 3.0%
Other 36.6%

18.1 million new cases

Mortality

Lung 18.4%
Colorectum 9.2%
Stomach 8.2%
Liver 8.2%
Breast 6.6%
Esophagus 5.3%
Pancreas 4.5%
Prostate 3.8%
Cervix uteri 3.3%
Leukaemia 3.2%
Other 29.3%

9.6 million deaths

B Males

Incidence

Lung 14.5%
Prostate 13.5%
Colorectum 10.9%
Stomach 7.2%
Liver 6.3%
Bladder 4.5%
Esophagus 4.2%
Non-Hodgkin lymphoma 3.0%
Kidney 2.7%
Leukaemia 2.6%
Other 30.6%

9.5 million new cases

Mortality

Lung 22.0%
Liver 10.2%
Stomach 9.5%
Colorectum 9.0%
Prostate 6.7%
Esophagus 6.6%
Pancreas 4.2%
Leukaemia 3.3%
Bladder 2.8%
Non-Hodgkin lymphoma 2.7%
Other 23.0%

5.4 million deaths

Figure 1 Worldwide distribution of incidence cases and cancer deaths for the 10 most common cancers for both sexes (A), males (B), and females (C) in 2018 [Adapted from (Bray et al. 2018)].

1.2 Non-Small Cell Lung Cancer (NSCLC)

Lung cancer over the past few decades emerged as one of the more common malignancies worldwide (Ferlay et al. 2015). In the year 2008, 1.6 million newly diagnosed cases of lung cancer were reported (Reck et al. 2013). In the same year (2008), lung cancer accounted for 1.4 million deaths worldwide and by 2010, the annual deaths had risen to 1.5 million worldwide (Jemal et al. 2011; Lozano et al. 2012). It was also considered responsible for the most cancer-related morbidities globally for a number of years (Bang 2011).

Lung cancers remain the leading cause of cancer incidence and mortality globally with predicted figures for 2018 estimated to be about 2.1 million new cases and 1.8 million deaths related to lung cancers, which accounts for about 20% of cancer related deaths globally (Bray et al. 2018). In the males, lung cancer is the leading cause of fatalities in majority of Eastern Europe and Western Asia, North Africa, China, and south-east Asia (Bray et al. 2018).

The greatest incidence rates amongst males were reported to be within eastern Asia with rates of above 40 per 100, 000 cases (Bray et al. 2018). In females, lung cancer is the leading cause of death in 28 countries with the highest incidence rates observed in Northern and Western Europe heavily concentrated in Denmark and Netherlands, Australia, New Zealand and finally Hungary which was reported to have the highest incidence in females (Bray et al. 2018).

Non-small cell lung cancer statistics suggest that the condition accounts for about 85% of cases of lung cancer diagnosed worldwide (Roche 2018; Sasaki et al. 2010a). The main types of non-small cell lung cancer are adenocarcinoma, squamous and large cell non-small cell lung cancer (Zarogoulidis et al. 2013). Historically, the subtype of lung cancer had determined the decision in selection of treatment regimens for patients (Bang 2011). More recently, non-small cell lung cancer is considered to be a collective of disease subtypes which all display consistent oncogenic changes (Bang 2011).

The change in consensus was borne out of a combined effort globally to optimise management of cancers based on the distinctive symptoms presented on a patient-to-patient basis (Zarogoulidis et al. 2013). For instance, consideration to extent/stage of disease as well as predictive and prognostic factors are key in current treatment decision making (Zarogoulidis et al. 2013). These changes have contributed towards favourable outcomes in the therapeutic method selection process on the patient-to-patient cases of non-small cell lung cancer (Zarogoulidis et al. 2013).

A major factor as to why NSCLC is considered of great concern globally is the fact that a large number of patients are often diagnosed during the more advanced stages of the disease, at which point treatment is considered palliative with complete disease eradication at this stage rather challenging (Doebele et al. 2012). Most treatment strategies are often more effective at extending patient survival but for only in the short term (Doebele et al. 2012).

A number of therapeutic strategies are effective at prolonging survival in the short term but ultimately rarely prove to be curative (Doebele et al. 2012). Non-small cell lung cancer has a much slower rate of growth and spread significantly slower than small cell lung cancer (Roche 2018). The early stages of non-small cell lung cancer are often associated with fewer specific symptoms; which results in approximately 70% of patient cases remaining undiagnosed until the later advanced stages of disease when symptoms are more specific (Molina et al. 2008a; Roche 2018).

Smoking was considered to be a major contributing factor towards rising lung cancer incidence (Molina et al. 2008). Reportedly, light cigarette smoking had similar risk of lung cancer to smoking cigars or using a pipe (Molina et al. 2008)). The rate of decline in lung cancer diagnoses was predicted to plateau within the 2 decades in the UK and the US with slower rates of smoking cessation (Molina et al. 2008).

Dietary changes contribute towards increased risk of lung cancer with diets high in cured meats, deep-frying products, and excessive chilies considered to be associated with an increased risk of lung cancer development (Molina et al. 2008).

Alcohol intake is also a contributing factor as studies indicated a slightly increased risk of lung cancer among people with consumptions above 30 grams per day of alcohol when compared with individuals who do not drink (Freudenheim et al. 2005; Molina et al. 2008). Genetic influences are always worth consideration as could contribute towards selection treatment (Sasaki et al. 2010).

The idea of familial clustering of lung cancer has been repeatedly reported over a number of decades suggesting hereditary factors might play a role in lung cancer development (Molina et al. 2008). A family with multiple cases of non-small cell lung cancer were all diagnosed with a sequence variation

T790M within their epidermal growth factor receptor (Li and Hemminki 2004; Molina et al. 2008).

1.3 Molecular Changes in Non-Small Cell Lung Cancer

Research over the last two decades has shed light on the varieties of abnormalities occurring molecularly within non-small cell lung cancer patients (Costa et al. 2015). Despite the ever-growing bank of knowledge on tyrosine kinase proteins with regards their role in tumour development and progression, full knowledge about the exact kinases that promote proliferation of most solid tumours remain relatively elusive (Bang 2011). This often serves as a hindrance to the identification and development of potential drug targets as well as making prediction of likely response to new compounds very difficult (Bang 2011).

The nucleophosmin (NPM) anaplastic lymphoma kinase (ALK) fusion protein was initially identified in patients saddled with anaplastic large cell lymphoma as a target for anti-neoplastic agents (Bang 2011).

With regards to non-small cell lung cancer in particular, a survey of the signalling tyrosine kinases, spanning across 41 cell lines and in over 150 tumours led to the identification of already known oncogenic kinases epidermal growth factor receptor (EGFR) and c-MET (Mesenchymal-epithelial transition protein), as well as novel fusion proteins ALK and Proto-oncogene tyrosine-protein kinase (ROS1) (Bang 2011).

The anaplastic lymphoma kinase was named as such as it was initially discovered translocated in the anaplastic large cell lymphoma (Ou 2011). In the latter years of the 1980's, anaplastic lymphoma kinase gene alterations were recognised widely to play major role in the pathogenesis of anaplastic large cell lymphoma which is considered a subset of B cell non-Hodgkin's lymphoma as well as its roles in inflammatory myofibroblast tumours and also in neuroblastoma (Ou 2011). Anaplastic lymphoma kinase belongs to the leukocyte tyrosine kinase receptor superfamily and is a single chain transmembrane receptor (Ou 2011)(Figure 2).
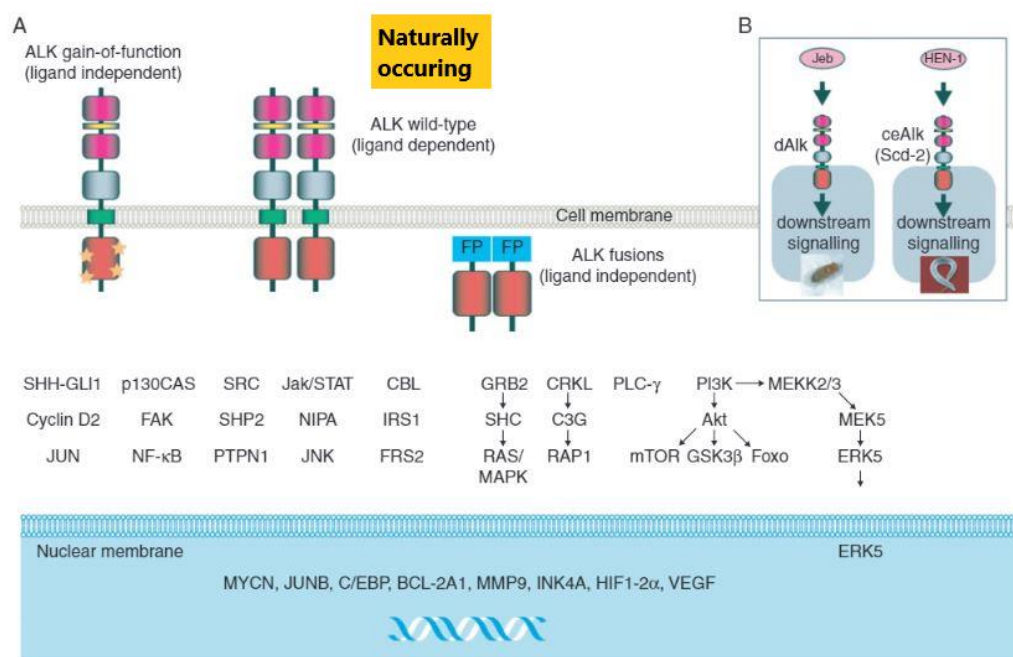
Figure 2 The anaplastic lymphoma kinase (ALK) receptor tyrosine kinase. Ligand dependent activation of wild type ALK results in activation of numerous pathways such as PI3K-Akt which signals

numerous proteins amongst numerous other activities [Adapted from (Hallberg and Palmer 2016)].

The echinoderm microtubule-associated protein like-4(EML4) and anaplastic lymphoma kinase (ALK) fusion gene was identified to be tumorigenic in non-small cell lung cancer cases back in 2007 (Bang 2011). This fusion protein is widely considered to serve as one of the more frequently treated targets in NSCLC (Chen et al. 2017). The EML4-ALK fusion protein is described as an inversion that occurs where the gene coding for EML4 is subjected to a disruption at intron 13 and is conjoined to intron 19 of the gene coding for ALK (Bang 2011). The resultant product was a gene 3926 base pairs long which codes for a protein of 1059 amino acids in length and is associated with constitutive activation of ALK signalling (Bang 2011; Mossé, Wood, and Maris 2009; Soda et al. 2007).

In additional studies involving patients of East Asian origin, found that between 3% - 13% of lung tumours contain EML4-ALK fusions (Sasaki et al. 2010). Based on similar extrapolations, it could be derived that approximately that 5% of all NSCLC diagnosed cases contain an EML4-ALK translocation which equates to just over 70, 000 patients that are diagnosed globally (Sasaki et al. 2010). This translocation induced fusion protein (EML4-ALK) is often observed in younger patients with no history of smoking and also in patients in the more advanced stages of NSCLC (Chen et al. 2017;

Sasaki et al. 2010). ALK fusion genes and such rearrangements are considered to be largely mutually exclusive with other gene mutations such as epidermal growth factor receptor and Kirsten-ras (KRAS) gene mutations (Sahu et al. 2013a; Sasaki et al. 2010). ALK positive tumours are also considered to be highly sensitive towards therapies in the form of ALK-targeting molecules or ALK inhibitors (Ou et al. 2014; Sahu et al. 2013).

The exact intracellular signalling pathways through which EML4-ALK fusion proteins promote/generate the growth and development remain up for debate (Bang 2011).

1.4 Echinoderm Microtubule-Associated Protein Like-4 Anaplastic Lymphoma Kinase Fusion Gene (EML4-ALK) Inhibition as Treatment for Non-Small Cell Lung Cancer

One of the major difficulties encountered during the study of cancers cells is that there often is the plethora of alterations which occur at varying gene sites (Maharsy 2015). These in turn often lead to mutations that could promote oncogenic activation, and repression of tumour suppressor genes in their target organs (Maharsy 2015). Due to the often-unpredictable nature of the mutations observed, the desire to develop efficacious therapies for the malignancies can be quite challenging (Maharsy 2015).

Furthermore, the growing aging population and the perceived increased susceptibility of the wider population to various cancers have corresponded

with the increased numbers of cancer fatalities annually (Maharsy 2015). Robust research drives aimed at characterising the aetiologies and monitoring the routes of progression taken by a number of malignancies has provided invaluable information which proved crucial in the discovery and development of a variety of anticancer therapies and strategies (Maharsy 2015). The strategies often involve one of the following processes: surgical intervention (removal of tumours), the use of chemotherapeutics, the use of radiotherapy and or cell replacement therapy (Maharsy 2015). In most instances however, two or more of these strategies are employed in tandem to treat affected individuals usually in more advanced stages of cancer, with this method referred to as combination therapy (Maharsy 2015). These strategies have proved effective at improving patient outcome and led to increased patient survival even in malignancies which would have been considered beyond treatment previously, as early enough treatment can halt disease progression (Bovelli et al. 2010).

The initial studies carried out leading up to the discovery of EML4-ALK fusion protein proposed the possibility that inhibition of the kinase activity had the potential to be an effective treatment in clinical setting (Sasaki et al. 2010b). Studies conducted by Soda et al. (2007), led to the identification of the transforming EML4-ALK fusion gene in almost 7% non-small cell lung cancer patients with smoking history in a Japanese patient pool and the expression of the EML4-ALK transcript in NSCLC patients was confirmed in a number of

cases from a Japanese patient pool (Inamura et al. 2008; Shinmura et al. 2008; Soda et al. 2007). EML4-ALK protein was predominantly localised within the cytoplasm of transfected cells and initiated the transformation of mouse 3T3 cells which were then introduced into nude mice initiated to the development of tumours (Martelli et al. 2009).

Soda et al. (2007), investigated the use of ALK inhibition as effective treatments of EML4-ALK positive NSCLC (Soda et al. 2007). In BA/F3 cells which were dependent on interleukin-3 for growth, flag-tagged ALK, EML4-ALK or ELM4-ALK (K589M) expression was induced (Soda et al. 2007). In the presence of interleukin 3, the transfected cells showed exponential growth, however in the absence of interleukin 3 only the cells EML4-ALK positive showed proliferation at a similar rate (Soda et al. 2007). This highlighted the kinase-dependent oncogenic properties of EML4-ALK (Soda et al. 2007).

Crizotinib (trade name Xalkori, Pfizer) is described as an orally bioavailable multitarget receptor tyrosine kinase inhibitor which is selective for ALK, MET and proto-oncogene tyrosine-protein kinase (ROS) (Costa et al. 2015; Ou 2011; Sahu et al. 2013b; Sasaki et al. 2010). It is also referred to as an oral ATP-competitive selective inhibitor of ALK and MET receptor tyrosine kinases leading to an inhibition of phosphorylation of tyrosine on activated ALK effectively even at nanomolar doses (Costa et al. 2015; Kwak et al. 2010a). It was initially synthesized to primarily act as an inhibitor of the MET receptor (Ou 2011).

The basis for the drugs development was observed interactions of potent MET inhibitor PHA-665752 at the ATP-binding sites within the MET kinase domain (Ou 2011). The binding of PHA-665752 to the MET kinase signals the displacement of the kinase activation loop leading to interference of the ATP with substrate binding with the MET receptor tyrosine kinase (Ou 2011). PHA-665752 was widely regarded as a very potent dose-dependent inhibitor of MET in a number of cell lines and even xenograft models (Ou 2011). But due to issues such as low solubility at pH level 7.4, high rate of metabolic clearance and poor permeability, PHA-665752 was too limited to be considered for use clinically as a MET tyrosine kinase receptor inhibitor (Ou 2011).

As a result of this, Crizotinib was then designed with the use of a structure-based drug design program aimed originally at the creation of a less lipophilic and more soluble compound, as well as to also possess better interaction with the receptor kinase pocket (Ou 2011). A diagrammatic representation of the comparison of the original compound (PHA-665752) and the resulting compound Crizotinib (Figure 3).

PHA-665752

Crizotinib (PF-02341066)
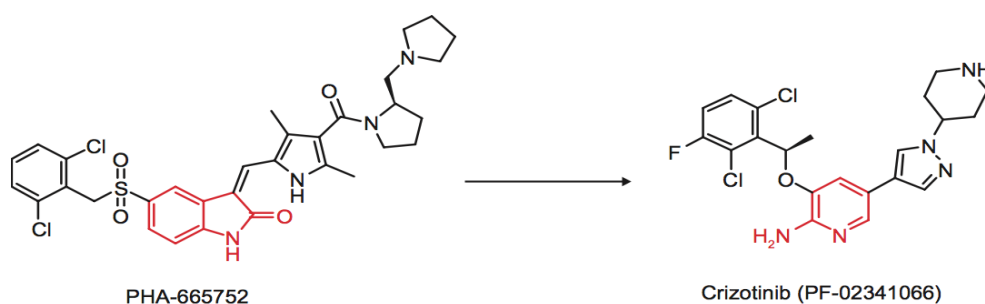
Figure 3 Structural comparison between original MET inhibitor (PHA-665752) and the resulting compound Crizotinib. The structural differences and the sections marked in red on both compounds referred to as the hinge binder with Crizotinib appearing relatively smaller which facilitates it to possess better interaction within the kinase pocket [Adapted from (Ou 2011)].

Crizotinib is described as a potent inhibitor of receptor tyrosine kinases (Sahu et al. 2013). It is also reported to be a potent small-molecule competitive inhibitor of MET, ROS1 and Recepteur d'origine Nantais (RON) (Gridelli, Peters et al. 2014). Crizotinib showed high selectivity for ALK and MET during preclinical tests (Gridelli, de Marinis et al. 2014; Ou 2011). During the Phase II clinical trial of ALK-rearranged NSCLC (PROFILE 1005, NCT00932451), crizotinib had an efficacy response of about 50% at the data cut off point, which formed the basis of the conditional approval of crizotinib in the United States in patients with ALK-rearranged NSCLC and were treated with oral crizotinib continuously in 3-week cycles (Crinò et al. 2011). Similarly, the final results of the large-scale multinational trial (PROFILE 1005), crizotinib

treatment was associated with an objective response rate of 54% in a large patient population previously treated for advanced ALK-positive NSCLC (Blackhall et al. 2017a). 1066 patients received crizotinib and again the observed response rate by the investigators was assessed at 54% (Blackhall et al. 2017b).

Crizotinib, with great potency, initiates inhibition of cell proliferation in a number of tumours such as in mammary tumour cells (Ayoub et al. 2017; Gridelli et al. 2014; Rodig and Shapiro 2010). This action is linked with the G1-S cell cycle phase, leading to cell cycle arrest and promptly induces apoptosis (Gridelli et al. 2014). Crizotinib is reported to be effective at induction of apoptosis in ALK-positive anaplastic large cell lymphoma malignant cells (Ou 2011). Crizotinib is said to inhibit activation of ALK positive tyrosine kinases by ligands even at nanomolar drug concentrations (Kwak et al. 2010).

The inhibitory effect of crizotinib is reliant on its ability to bind to the adenosine triphosphate (ATP) binding site; also referred to as the binding pocket of the ALK-positive kinase, which then prevents autophosphorylation powered by ATP binding hence preventing activation of the kinase (Bang 2011). Crizotinib is widely regarded as the first line treatment for non-small cell lung cancer (Gridelli et al. 2014). Under normal conditions, ALK activation initiates downstream effects such as cell proliferation, survival, and migration, and constitutive activation of ALK can contribute to the survival

and progression of cancer cells (Figure 4). NPM-ALK is considered to partly mediate oncogenesis through activation of pathways PI3K/AKT, JAK/STAT and RAF/MEK/ERK signalling cascades further promoting cancer cell proliferation and apoptosis avoidance (Galkin et al. 2007; Li et al. 2011).
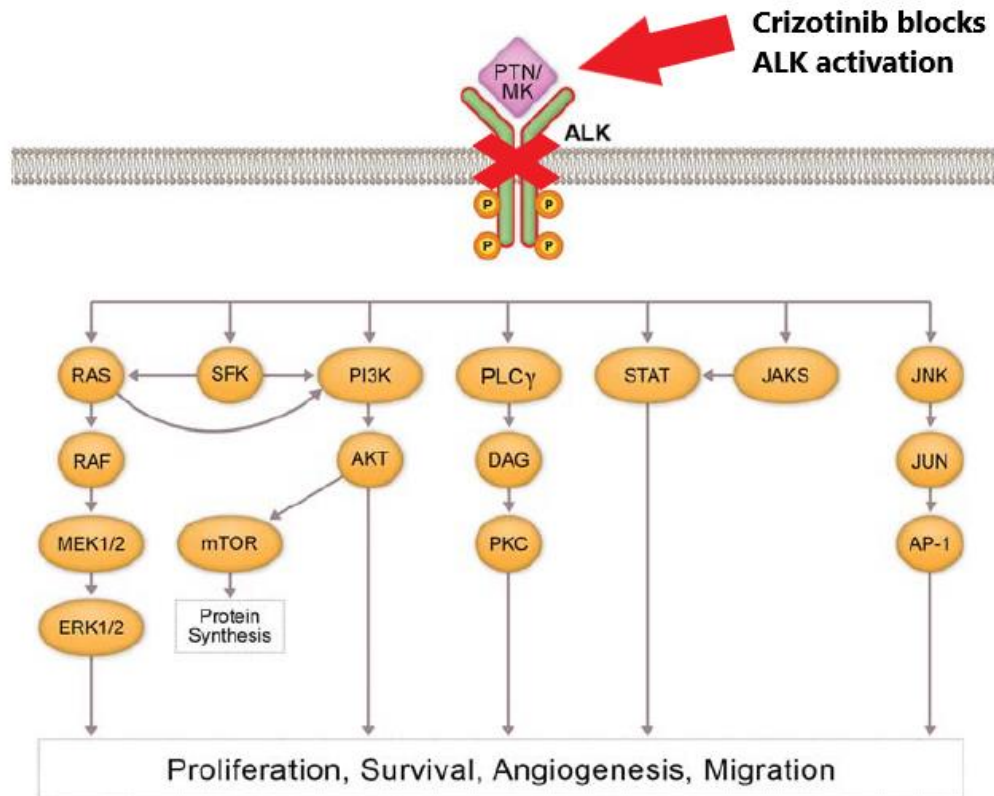
Figure 4 Cascade of Anaplastic lymphoma kinase signalling displaying involvement of a number of pathways. Constitutive activation of Anaplastic lymphoma kinase through mutations or fusions (Echinoderm microtubule-associated protein like-4 anaplastic lymphoma kinase fusion gene (EML4-ALK), chromosomal translocation inv (2) (p21; p23) in NSCLC) can promote cancer development and survival [Adapted from (Holla et al. 2017)].

51

1.5 Anticancer drug induced cardiotoxicity

Drug induced cardiotoxicity has become a prevalent observable side effect during the treatment of a number of malignancies (Maharsy 2015). Antineoplastic agents are no different with patients undergoing chemotherapeutic treatment often reporting cardiotoxicity as a side effect (Le, Cao, and Yang 2014). This has served as a major drawback within the field of developing new antineoplastic agents, being a major obstacle encountered by cardiologists and oncologists alike (Kim et al. 2012; Maharsy 2015).

Despite the massive success observed as a result of more potent and effective anticancer therapeutics have contributed to greater survival rates, dose-dependent cardiotoxicity has limited the use of a number of antineoplastic agents (Le, Cao, and Yang 2014). Conventional chemotherapeutics and targeted therapeutics are associated with a significantly increased risk of cardiovascular damage leading to adverse effects such as; acute left ventricular dysfunction, heart failure, treatment-induced hypertension, ischaemia, dysrhythmias via first-degree heart block (electrical impulses slower through the atrioventricular node) and QTc interval prolongation (Curigliano et al. 2016a).

There has been an enormous focus of clinical research and development of anti-cancer drugs in more recent times, with the ultimate aim of leading to a shift from traditional non-specific anticancer therapies and moving towards

targeted therapies (Han, Zhou, and Liu 2017; Le, Cao, and Yang 2014) . These antineoplastic drugs often are designed to target cellular signalling mediators often further upstream in the affected pathways promoting cell differentiation and proliferation (Le, Cao, and Yang 2014). These in turn then halt the progression of the malignancies which ultimately leads to improvement in survival rates (Le, Cao, and Yang 2014).

The drawback often observed when targeted therapies become apparent during treatment and post- treatment monitoring and manifest as a variety of on- and off-target adverse reactions or toxicities (Le, Cao, and Yang 2014). Cardiotoxicity presents as one of the more frequently diagnosed and more major off-target effect often observed (Le, Cao, and Yang 2014). Cancer therapies have been shown to bear linkage to cardiomyocyte damage which in turn would promote dysfunction to the myocardium (Han, Zhou, and Liu 2017) .

Molecular-targeted antineoplastic agents designed to lead to inhibition of the vascular endothelial growth factor (VEGF) or its associated receptor (VEGFR) with the idea of inhibition of angiogenesis often is associated with the side effect of hypertension (Le, Cao, and Yang 2014). Activation of the vascular endothelial growth factor receptor pathway is reported to carry out roles in the maintenance of vascular homeostasis via the production of nitric oxide (NO)(Le, Cao, and Yang 2014). Nitric oxide is documented to possess vasodilatory effects which actively seek to increase vascular dilation,

permeability, and angiogenesis to bring about reduction of vascular resistance (Förstermann and Sessa 2012; Le, Cao, and Yang 2014).

The fundamental basis advocating the use of VEGF as a genuine target for antineoplastic agents is as a result of the target specific action induced as inhibition of VEGF pathway prevents angiogenesis and therefore limits tumour proliferation significantly (Le, Cao, and Yang 2014). The main inhibitory action generated is due to inhibition of downstream signal pathways such as phosphatidylinositol 3-kinase (PI3K) pathway and also the mitogen-activated protein Kinase (MAPK) pathway (Le, Cao, and Yang 2014). The targeted interruption of the pathways mentioned impairs nitric oxide production and therefore its activity, which leads to alteration in vascular tone which results in increased vascular resistance in the periphery and consequently significantly increases in blood pressure (Le, Cao, and Yang 2014).

1.5.1 Hypertension

Cancer treatment tyrosine kinase inhibitors (TKIs) have been reported to induce hypertension (Le, Cao, and Yang 2014). As earlier introduced TKIs function intracellularly via inhibitory action of phosphorylation of transmembrane receptor tyrosine kinases and do so through formation of high affinity bonds with the receptors effectively blocking the binding of various ligands (Le, Cao, and Yang 2014). A number of TKI's are in clinical use

for the treatment of a variety of malignancies as well as gastrointestinal stromal tumours, metastatic renal cell carcinoma (RCC), soft-tissue sarcoma and advanced hepatocellular carcinoma (Le, Cao, and Yang 2014). Some of the FDA-approved TKIs which target angiogenesis (anti-angiogenic) in their anti-neoplastic function include, Sorafenib, Sunitinib and Pazopanib; and are all described to be small molecule inhibitors (Le, Cao, and Yang 2014).

Zhu, Stergiopoulos, Wu (2009) reports of a meta-analysis which involved close to 5000 individual study patients all documented to have received sunitinib therapy for the treatment of advanced RCC or other malignancies (Le, Cao, and Yang 2014; Zhu, Stergiopoulos, and Wu 2009). The study reported that following evaluation, the incidence of "all-grade" and "high-grade" hypertension was recorded as 21.6% and 6.8% respectively (Le, Cao, and Yang 2014; Zhu, Stergiopoulos, and Wu 2009). Sunitinib was also credited with a significantly increased risk of high-grade hypertension with relative risk of hypertension (RR) reported as 22.72 (Le, Cao, and Yang 2014; Zhu, Stergiopoulos, and Wu 2009).

Similarly, Wu et al (2008) discussed the risks associated with another tyrosine kinase inhibitor sorafenib (Le, Cao, and Yang 2014; Wu et al. 2008). Analysis revealed an overall incidence of high-grade and all-grade hypertension 5.7% and 23.4% respectively following sorafenib treatment (Le, Cao, and Yang 2014; Zhu, Stergiopoulos, and Wu 2009). Sorafenib was also reported to be associated with a significant increase in the relative risk

of hypertension in patients with cancer from database studies (Wu et al. 2008).

The risks associated with another TKI, Pazopanib was reported to be even greater than the observed figures for sunitinib and sorafenib (Le, Cao, and Yang 2014). The relative risk of hypertension for pazopanib versus sunitinib and sorafenib was reported to be 4.97 vs. 2.20 and 1.99 respectively (Le, Cao, and Yang 2014; Qi et al. 2013). The incidence of high-grade and all-grade hypertension observed in patients undergoing pazopanib treatment was 35.9% (Qi et al. 2013).

Hypertension management in the cardiovascular system is essential as it is a major risk factor for adverse cardiac events such as coronary artery disease, stroke, atrial fibrillation, and heart failure (Zahedmehr 2018).

In response to these concerning observations such as with the above treatments, the investigational drug steering committee of the National Cancer Institute made a few recommendations (Le, Cao, and Yang 2014).

The investigational drug screening committee of the national cancer institute recommends pre-treatment evaluation, screening, and monitoring of blood pressure (BP), prior to and during treatment administration of tyrosine kinase inhibitor therapy (Le, Cao, and Yang 2014). The guidelines suggested that investigators should aim for BP targets less than 140/90 mmHg in majority of patients and in patients which fall into the greater risk categories

(Diabetes, Chronic kidney disease, coronary artery disease amongst other conditions), the threshold should be set lower <130/90 mmHg (Le, Cao, and Yang 2014). The committee recommended anti-hypertensive treatment should commence in the instance when BP increases above 140/90 mmHg or in the instance when there is a greater than 20 mmHg magnitude increase in the diastolic BP over the baseline readings (pre-treatment evaluation) (Le, Cao, and Yang 2014).

However, when administering anti-hypertensive medications, agents that inhibit cytochrome P450 enzymes such as diltiazem, verapamil, grapefruit juice; should be avoided as the enzymes play key role in the metabolism of a variety of TKIs (Le, Cao, and Yang 2014). The inhibition of these TKI metabolising enzymes would lead to reduced drug clearance and metabolism further perpetuating the hypertensive state in this situation (Le, Cao, and Yang 2014).

1.5.2 Cardiac Dysfunction

Ventricular dysfunction instigated as a result of cardiotoxicity, in more recent times has become increasingly prevalent with its importance highly paramount as survival rates of cancer patients is on the incline (Le, Cao, and Yang 2014).The drug class Anthracyclines (Doxorubicin), have a vast body of research often characterising their often irreversible, dose-dependent drug induced cardiotoxicity (Le, Cao, and Yang 2014).

Doxorubicin is a member of the anthracycline drug family and is employed in the treatment of a plethora of solid tumours and hematologic malignancies (Desai et al. 2013). Doxorubicin is administered as a single agent or in combination with other agents for the treatment of various malignancies, leukaemia, lymphomas, and soft tissue sarcoma (Gharanei et al. 2013; Takemura and Fujiwara 2007).

Doxorubicin induced damage to myocardium is regarded to be governed by interplay between a number of factors (Gharanei et al. 2013; Volkova and Russell 2011). Increased ROS generation promoting further oxidative stress and intracellular calcium dysregulation indicated by increased calcium detection are said to be key contributors (Chatterjee et al. 2010a; Octavia et al. 2012; Takemura and Fujiwara 2007). Doxorubicin forms irreversible complexes with cardiolipin in the mitochondria disrupting electron transport chain function leading to increased superoxide production (Octavia et al. 2012). ROS in turn directly influences calcium uptake and inherently contractile function in cardiomyocytes (Eiki and Kass David 2007). Through modifications to thiol groups on ryanodine receptor and suppression of L-type calcium channel current leading to inhibition of Ca^{2+} reuptake increasing calcium concentration intercellularly (Eiki and Kass David 2007; Octavia et al. 2012)(Figure 5).
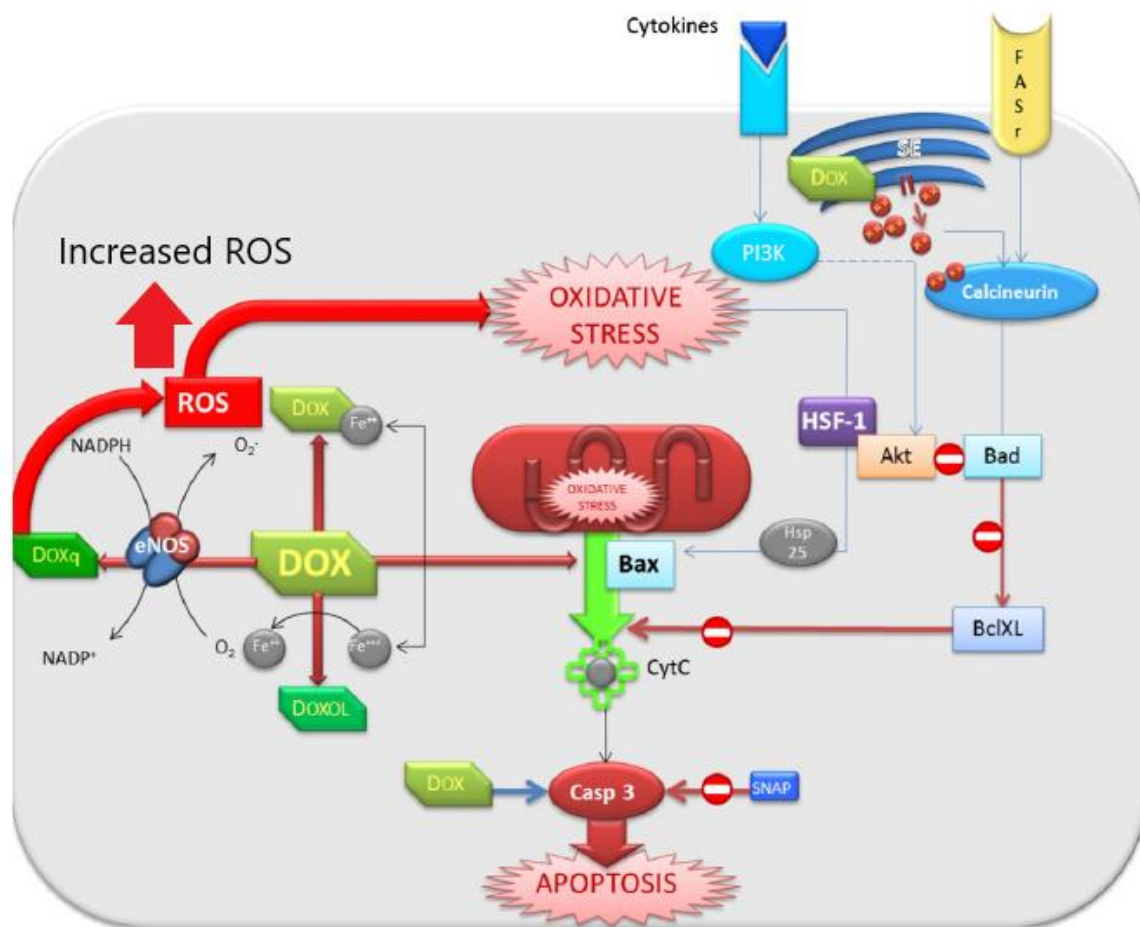
Figure 5 Summary of action doxorubicin intracellularly within cardiomyocyte showing roles with Reactive oxygen species (ROS) generation leading to oxidative stress, oxidative stress leading to mitochondrial release of cytochrome c which leads to increased caspase 3 activation resulting in apoptosis [Adapted from [(Octavia et al. 2012)].

The cardiotoxicity of this class of drug often involves myocardial injury with distinctive features such as mitochondrial dysfunction, myofibrillar disarray, and development of vacuoles which are visible upon microscopic examination (Le, Cao, and Yang 2014). Cardiac dysfunction (CD) with these characteristics

are referred to as type I chemotherapy-related CD (Bloom et al. 2016; Le, Cao, and Yang 2014). This type of cardiac dysfunction associated with free radical generation due to increased oxidative stress is the most frequently proposed mechanism by which myocardial injury occurs (Le, Cao, and Yang 2014). The inherent injury then results in a reduction in the mean ejection fraction (Le, Cao, and Yang 2014). Conversely, type II chemotherapy-related CD is often observed with molecular-targeted drug agents or molecules that target human epidermal growth factor receptor-2(HER2) (Le, Cao, and Yang 2014). Type II CD, however, does not result in a change in cell structure/morphology; the effects are not dose-dependent and are often considered to be reversible resulting to a better prognosis (Le, Cao, and Yang 2014).

The table (Table 1) below presents the characteristics/differences between types I and II chemotherapy induced cardiac dysfunction and was adapted from Le, Cao, Yang 2014.

Characteristic	Type I myocardial injury	Type II myocardial injury
Chemotherapeutic agent	Anthracycline-based *e.g.* doxorubicin	Targeted therapy *e.g.* trastuzumab
Clinical course	Injury often permanent and irreversible, although may stabilize over time	Reversible with good prognosis
Dose effects	Cumulative	Often not dose-related
Mechanism	Free radial injury and oxidative stress	ERBB2 inhibition
Ultrastructure	Vacuoles, myofibrillar disarray, and necrosis	None
Cardiac echocardiography	Depressed LVEF with global hypokinesis	Depressed LVEF with global hypokinesis
Effect of re-challenge	High probability of recurrent dysfunction	Often safe after re-challenge, more data needed
Effect of late sequential stress	High probability of cardiac dysfunction	Low probability of cardiac dysfunction

Table 1 : Comparisons between type I and type II chemotherapy induced cardiac dysfunction [Adapted from (Le, Cao, and Yang 2014)].

As earlier discussed, molecular targeted drugs have proved to be cardiotoxicity and small-molecule TKI's have also been shown to be among these drugs (Le, Cao, and Yang 2014). Lapatinib, which also a member of the TKI family, which targets HER2 and epidermal growth factor receptor (Le, Cao, and Yang 2014). In evaluation of a study involving over 3500 patients, assessed the cardiac safety of lapatinib which revealed previous treatment with anthracyclines, trastuzumab or neither was associated with 2.2, 1.7 and 1.5 % likely incidence of a variety of cardiac events occurring respectively (Le, Cao, and Yang 2014). The observed decline in left ventricular ejection fraction was generally not severe, more than likely asymptomatic and often considered reversible (Le, Cao, and Yang 2014). Sunitinib was reported to show links to increased risk of development of congestive heart failure (Le, Cao, and Yang 2014).

Richards et al. (2011) reported the incidence of all and high-grade congestive heart failure in patients treated with sunitinib were 4.1 and 3.30 % respectively (Le, Cao, and Yang 2014; Richards et al. 2011). The relative risk of congestive heart failure was significantly increased in the sunitinib treated patients compared to placebo treated group (Le, Cao, and Yang 2014; Richards et al. 2011).

Extensive research detailing sorafenib's role in cardiac dysfunction remains rather limited. Data from a smaller study reported that treatment with sunitinib or sorafenib, of the 86 patients involved about 33.8 % experienced

adverse cardiac event (Le, Cao, and Yang 2014; Richards et al. 2011). The patients were also reported to have shown recovery following treatment and were clear to recommence TKI treatment (Le, Cao, and Yang 2014; Richards et al. 2011).

During a single-centre observational study, patients were treated with either sunitinib or sorafenib against metastatic renal cell carcinoma (Schmidinger et al. 2008). 38% of the eligible patients experienced an adverse cardiac event and 18 % developed symptomatic arrhythmia (Schmidinger et al. 2008).

Management of cardiac dysfunction currently is reported to entail thorough pre-treatment evaluation and continual screening for risk factors that could potentially give rise to potential cardiovascular related complications (Le, Cao, and Yang 2014). Baseline transthoracic echocardiograms and electrocardiograms are under advisory to enable physicians to achieve a baseline assessment of left ventricular ejection fraction prior to commencing a course of potentially cardiotoxic molecular-targeted agents (Le, Cao, and Yang 2014).

As mentioned previously, tyrosine kinase inhibitors induce cardiotoxicity through induction of cardiovascular dysfunction (Zamorano et al. 2017). sunitinib which is a multitarget Vascular endothelial growth factor receptor inhibitor was associated with an 8% increase in incidence of heart failure and a 28% increased incidence of greater than 10% decrease in left ventricular

ejection fraction (Lal, Kolaja, and Force 2013). Individuals with imatinib resistant gastrointestinal stromal tumours were treated with sunitinib in a phase I/II protocol to evaluate the efficacy of sunitinib treatment (Chu et al. 2007). Sunitinib treatment was associated with the cardiotoxic effects reported by lal, kolaja and Force (2013) earlier mentioned (Lal, Kolaja, and Force 2013).

This same study also employed isolated cardiomyocytes and mice models to investigate mechanisms of sunitinib induced adverse cardiac effects. Using mice models, animals were treated with sunitinib (40 mg/kg/d) for 12 days, which resulted in mitochondrial swelling and evidence of degeneration in mitochondrial morphology assessed through transmission electron microscopy (Chu et al. 2007). Similarly, in cultured cardiomyocytes, mitochondrial damage was associated with sunitinib treatment as there was significant release of cytochrome c following sunitinib treatment indicative of cell death (Chu et al. 2007).

1.5.3 QT trace Prolongation

Tyrosine kinase inhibitor treatment have the ability to induce QT prolongation during cancer treatment (Zamorano et al. 2017). Crizotinib, sorafenib and sunitinib are associated with QT prolongation (Zamorano et al. 2017). Failure to correctly recognize/diagnose and remedy the disorder in a timely manner has been associated with *torsade de pointes* (Severe form of

ventricular tachycardia often preceding sudden cardiac arrest) a condition that can be fatal (Tisdale 2016).

In the clinical setting, the observed intervals have been used as markers to signify a heightened risk of fatal arrhythmias occurrence (Al-Khatib et al. 2003). The QT interval correlates to ventricular depolarization and repolarization on a surface ECG (Sanguinetti and Mitcheson 2005). Mechanisms that interfere with the repolarization phase therefore interfere with the QT interval (Sanguinetti and Mitcheson 2005). This corresponds to the interruption of the human ether-a-go-go portion in the delayed rectifier potassium (K^+) channel (Sanguinetti and Mitcheson 2005).

The evaluation of Crizotinib reported by Ou et al 2014, proposed that there was an overall mean reduction in the heart rate of patients treated with Crizotinib from when baseline readings were taken pre-treatment and post treatment and the difference was said to be at a magnitude 26.1 bpm less (Ou et al 2014).

This was often indicative of the individual being subjected to bradycardia (Ou et al 2014). The patients at greater risk of bradycardia were the patients that were considered older (55.8 years), had baseline HR (pre-treatment) on the lower side (77.9 BPM) and were on Crizotinib therapy for a longer duration (52.9 weeks treatment) (Ou et al. 2014). Patients with prior manifestation of prolonged QT interval should be monitored closely as they are more likely to

present cardiotoxicity clinically and Crizotinib treatment should be ceased in patients already presenting QT prolongation of 500ms or greater (Drew Barbara et al. 2010).

Sunitinib treatment was also associated with QT prolongation in clinical trials although considered a rarity (Shah, Morganroth, and Shah 2013). Similarly, in a single-arm blinded study, patients with advanced solid tumours were treated with sunitinib for a period of time (Bello et al. 2009). The data from the study confirmed Sunitinib treatment induced a concentration dependent increase in QT prolongation (Bello et al. 2009). Vandatanib treatment on individuals from phase II and III prospective clinical trial data was evaluated (Zang et al. 2012). Individuals prescribed vanatanib were diagnosed with significantly increased risk of QT prolongation (Zang et al. 2012).

1.6 Molecular mechanisms involved in chemotherapy induced Cardiotoxicity

There is an extensive amount of research conducted to identify the molecular mechanisms often implicated in chemotherapy induced cardiotoxicity (Angsutararux, Luanpitpong, and Issaragrisil 2015a). In Doxorubicin induced cardiotoxicity for instance, oxidative stress was discovered to be a major contributor to damage which ultimately could result in cardiomyopathy and heart failure (Angsutararux, Luanpitpong, and Issaragrisil 2015). The key overriding mechanism for anthracycline cardiotoxicity such as seen with

doxorubicin is ROS generation (Chatterjee et al. 2010b). Previous studies regarding anticancer induced cardiotoxicity have focussed on anthracyclines and in some occasion's radiotherapy but more recently, other drug families have gained attention (Force, Krause, and Van Etten 2007).

Tyrosine kinase inhibitor treatment has been linked with increased ROS generation with agents such as sunitinib, pazopanib and sorafenib crediting ROS generation as mechanisms of their toxicity (Teppo, Soini, and Karihtala 2017). Sunitinib in particular is considered to interfere with cardiomyocyte homeostatic energetics which contributes to dysfunction (Gorini et al. 2018). Figure 6 illustrates the processes involved in ROS generation and neutralisation under normal circumstances.
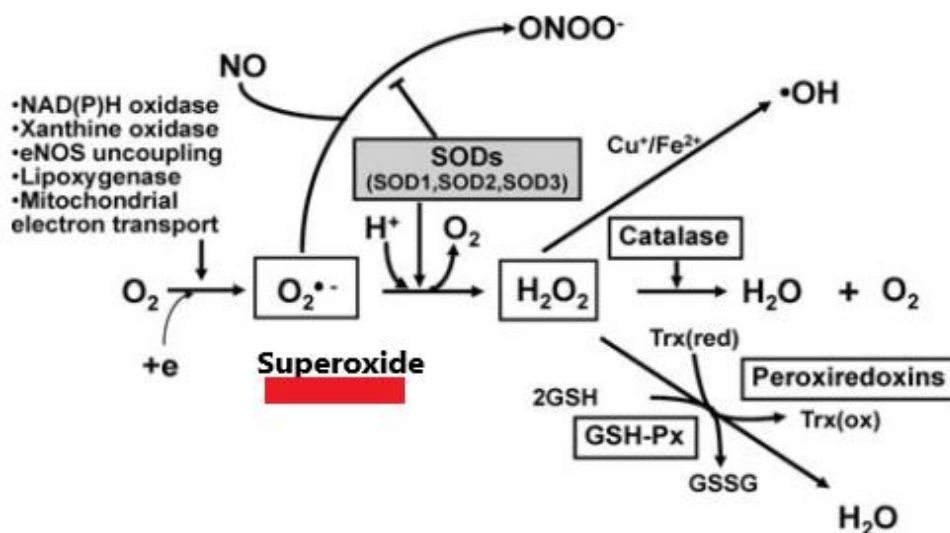
Figure 6 Superoxide generation and role of superoxide dismutase in conversion of superoxide into hydrogen peroxide. Catalase and peroxiredoxins convert hydrogen peroxide to water or oxygen

molecules. Nitric oxide is also inactivated through spontaneous reaction with superoxide ions which then results in the production of the oxidant peroxynitrite. Reduced transition metals such as iron and copper could spontaneously converted to hydroxyl radicals [Adapted from (Fukai 2011)].

1.6.1 Chemotherapy induced oxidative stress, increased reactive oxygen species generation, and disrupted calcium homeostasis

Reactive oxygen species (ROS) play key role in cellular signalling and are generated from multiple sites within the cell (Bou-Teen et al. 2021). NADPH oxidases located within cell membranes and cyclooxygenases located within the cytosol contribute towards overall ROS, however, the mitochondria accounts for up to 90% of physiologically generated ROS within cells (Dan Dunn et al. 2015).

ROS generation within mitochondria occurs as a result of oxidation of the metabolic intermediates of electron transport chain and is usually under strict regulation to prevent oxidative stress (Dan Dunn et al. 2015). Mitochondrial superoxide (O_2^-) is the main ROS which exists in the mitochondria (Dan Dunn et al. 2015). Mitochondrial damage from ROS is attenuated by defence systems such as glutathione peroxidases, dismutase's amongst others as they either catalyse or facilitate breakdown of ROS and some of its more harmful products (Bou-Teen et al. 2021).

Oxidative stress occurs when an imbalance occurs between the ability of the cardiovascular system to generate or accumulate ROS and the ability of the system eliminate or detoxify the products (Burton and Jauniaux 2011; Zhang et al. 2019b). As mentioned previously, increased ROS generation has been implicated in anthracycline cardiotoxicity, especially with doxorubicin associated with ROS damage and oxidative stress (Zhang et al. 2019). The case is similar with tyrosine kinase inhibitors (Gorini et al. 2018).

Under normal circumstances, in response to excessive ROS production and accumulation, systemic activation of the primary antioxidant defence system occurs (enzymes such as superoxide dismutase, catalase, and glutathione peroxidase) to eliminate ROS and its toxic by-products (hydrogen peroxide) in an attempt to prevent oxidative stress (Figure 6) (Fukai 2011; Zhang et al. 2019).

Tyrosine kinase inhibitor treatment has been reported to be able to induce mitochondrial dysfunction, uncoupling components of electron transport chain and promoting ROS generation (Rodríguez-Hernández et al. 2020a). Increased ROS generation is closely related with increased Ca^{2+} due to interesting cross talk between both in which the production of one fuel the increased production of the other (Figure 8)(Bertero and Maack 2018; Görlach et al. 2015).
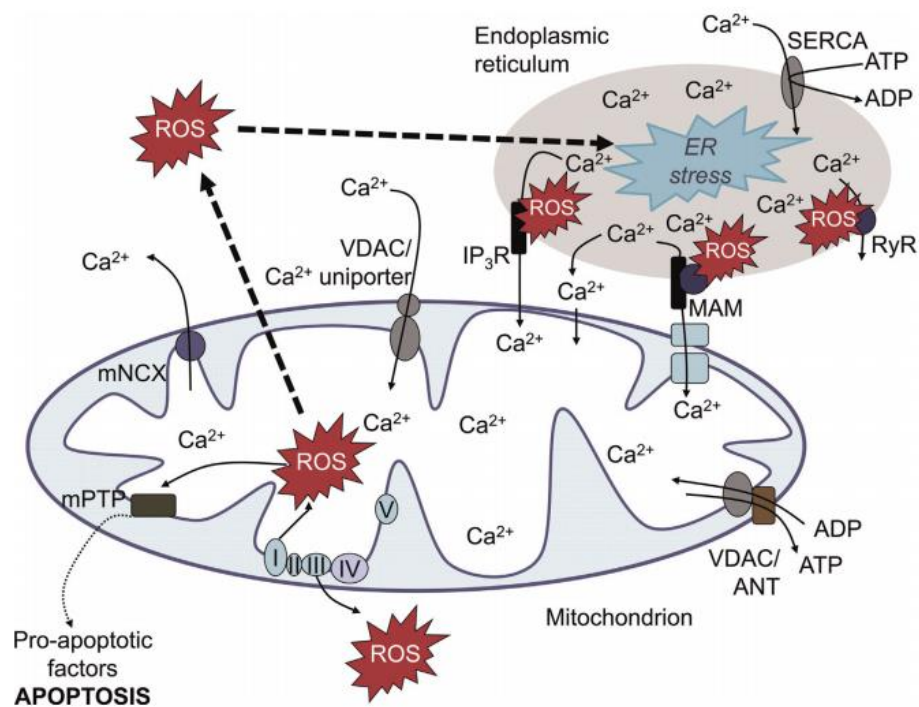
Figure 7 ROS and calcium regulated crosstalk between mitochondria and endoplasmic reticulum. Increased levels of Ca²⁺ stimulate increased ROS generation by directly fuelling of respiratory activity. ROS in turn stimulates calcium release from endoplasmic reticulum (Ca²⁺ stores) via calcium channels and with increased calcium, subsequent increases in ROS production [Adapted from (Görlach et al. 2015)].

Tyrosine kinase inhibitor treatment has been associated with ROS generation and Ca²⁺ signalling disturbances as one of the main mechanisms of cardiotoxicity (Coriat et al. 2012; Kawabata et al. 2015). Paech et al. (2018) assessed the mechanisms of mitochondrial toxicity in tyrosine kinase inhibitor treatment. In HepG2 cells exposed to sorafenib for 24 hours, there

was increase in ROS generation and a decrease in mitochondrial membrane potential (Paech et al. 2018).

Similarly, sorafenib was associated with increased rapid mitochondrial ROS generation and mitochondrial calcium overload in a study to assess apoptotic cell death, in radiotherapy resistant Hep G2 cells detected by confocal microscopy (Chiou et al. 2009). In a study to assess oxidative stress induced by sunitinib treatment, cultured H9C2 cells were treated for 24 hours with sunitinib and results showed an increased accumulation of ROS as well as increased detection of cleaved caspase 3 (Bouitbir et al. 2019a). Isolated ventricular myocytes treated with sorafenib showed an increase in diastolic intracellular calcium levels as well as increased levels of ROS which the study concluded was enough evidence to suggest disruption of calcium homeostasis (Ma et al. 2020). During a multi-parameter in vitro toxicity testing of tyrosine kinase inhibitors, crizotinib and nilotinib treatment was associated with increased ROS production (Doherty et al. 2013). Human cardiac myocytes treated for 24 hours with crizotinib and nilotinib showed significant increases in ROS generation (Doherty et al. 2013).

The above provides evidence for consideration of ROS accumulation and calcium dysregulation with tyrosine kinase inhibitor toxicity (Figure 8).

During apoptosis, Ca^{2+} can induce the opening of the mitochondrial permeability transition pore (mPTP) as a result of calcium overload and

increased oxidative stress (Crow Michael et al. 2004; Xiongwen et al. 2005). Excessive cytoplasmic Ca^{2+} has been linked to cell death (apoptosis) through activation of Ca^{2+} dependent calcineurin which phosphorylates bcl-2 antagonist of cell death protein (BAD), promoting translocation of bcl-2 associated X protein (BAX) into the mitochondria where oligomerisation of Bax/Bad at the mitochondrial outer membrane inducing the release of cytochrome c (Görlach et al. 2015; Xiongwen et al. 2005).
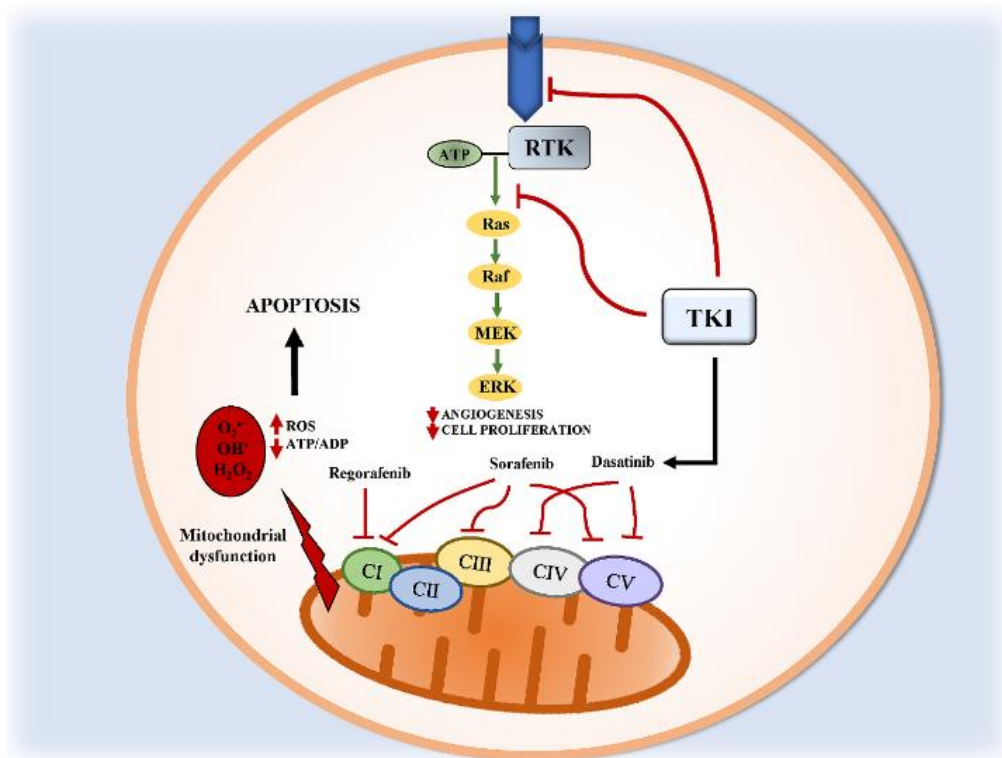
Figure 9 Tyrosine Kinase inhibitor induced mitochondrial dysfunction and ROS generation. Impairment of key complexes within respiratory chain and mitochondrial uncoupling results in ROS production and by products such as hydrogen peroxide could contribute to mitochondrial dysfunction [Adapted from (Rodríguez-Hernández et al. 2020)].

Intracellular levels of Ca^{2+} within cardiomyocytes are subjected to fine regulation to avoid cell death by apoptosis (Giorgi et al. 2012). Under normal conditions, there is reduced Ca^{2+} within cytosol for mitochondria to absorb, but under stressed situation such as oxidative stress from excess ROS generation there is an excess amount of cytosolic Ca^{2+} (Giorgi et al. 2012). Excessive cytosolic Ca^{2+} can trigger apoptosis and mitochondrial Ca^{2+} signalling overload is pro-apoptotic due to induction of mPTP opening, mitochondrial swelling, outer membrane rupture and release of pro-apoptotic factors into cytosol (cytochrome c release) (Giorgi et al. 2008).

Cardiotoxicity induced oxidative stress fuels excess ROS generation, which then contributes to impaired mitochondrial function and Excessive cytosolic Ca^{2+} (Hempel and Trebak 2017). This then leads to Ca^{2+} signalling overload, opening of mitochondrial permeability transition pore and then cell death (Wallace, Sardão, and Oliveira 2020).

1.6.2 Tyrosine Kinase induced Apoptosis

Apoptosis is the crucial genetically regulated process of cell elimination, which is essential for embryogenesis, tissue homeostasis and development of multicellular organisms (Galluzzi et al. 2018; Pinton et al. 2008). Apoptosis also referred to as programmed cell death serves as an internal safety response to cellular damage either in the form of DNA damage or copy errors or abnormal cells in general (Meredith and Dass 2016).

Apoptosis could occur in most instances through caspase enzyme-dependent pathways which could be intrinsic or extrinsic apoptotic pathways (Meredith and Dass 2016). The extrinsic pathway is initiated by the activity of ligands such as Fas ligand, tumour necrosis factor α and tumour necrosis related apoptosis-inducing ligand (Meredith and Dass 2016); these ligands bind to pro-apoptotic membrane bound cell death receptors (Meredith and Dass 2016). Through coupling of these death receptors with procaspase-8 by Fas-associated death domain, resulting in caspase 8 activation further leading to activation of caspases 3, 6 and 7 leading to programmed cell death (Meredith and Dass 2016). The mitochondria are crucial to ROS accumulation and damage and play similar role in the apoptotic process (Rodríguez-Hernández et al. 2020; van Loo et al. 2002).

Apoptosis could either be initiated through extrinsic (death receptor mediated) or the intrinsic (mitochondrial) pathways (Fulda and Debatin 2006). The extrinsic pathway involves activation of death signalling ligands such as tumour necrosis factor-related apoptosis inducing ligand through death receptors (Loreto et al. 2014). The intrinsic mitochondrial pathway is regulated through internal and external stimulus such as DNA damage, ischemia, and oxidative stress (Loreto et al. 2014) (Figure 9).
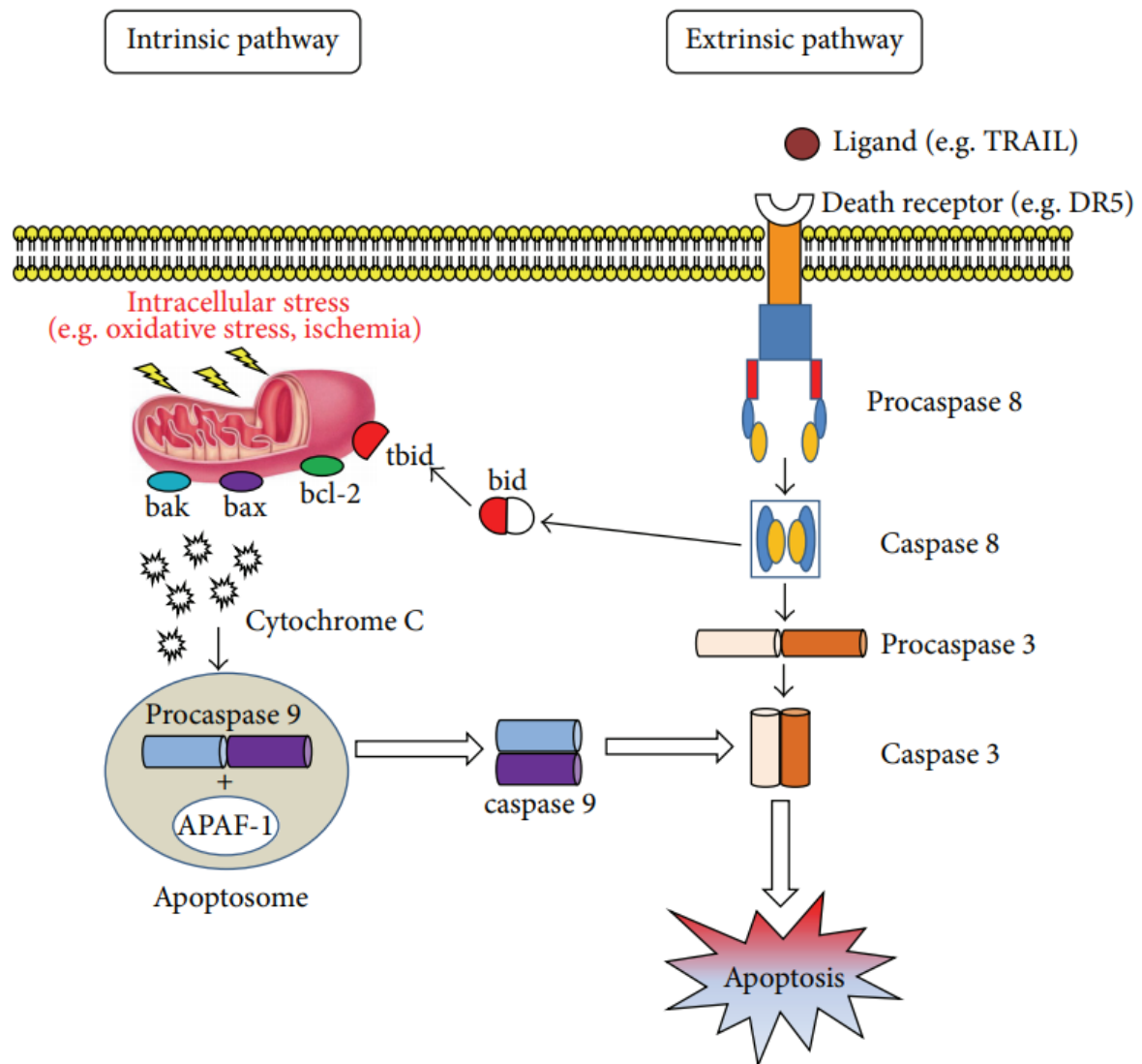
Figure 10 Intrinsic and extrinsic apoptotic pathways: Extrinsic pathway is activated by death receptor ligation which then leads to caspase 8 activation, further cleaving caspase 3. Caspase 3 then promotes DNA fragmentation and cell death. Mitochondrial pathway on the other hand partly influenced by mitochondrial membrane bound pro-apoptotic bcl member proteins promote release of cytochrome c from mitochondria. Cytochrome C and deoxyadenosine triphosphate complex forming

apoptotic protease factor 1 which initiates recruitment and activation of procaspase 9 and again in turn activates caspase 3 resulting in apoptosis [Adapted from (Loreto et al. 2014)].

Tyrosine kinase inhibitor sorafenib treatment was associated with apoptosis determined by cell cycle analysis and DNA damage assessment in Hep G2 cells (Chiou et al. 2009). When Paech et al. (2018) assessed tyrosine kinase induced mitochondrial damage, HEP G2 cells were treated with ponatinib, regorafenib and sorafenib. Treatment with all 3 TKI's was associated with induction of early apoptosis and increased cytochrome c detection within cytoplasm following 24 hours of treatment (Paech et al. 2018). In the multiparameter in vitro testing of tyrosine kinase inhibitors, crizotinib and nilotinib treatment on human cardiomyocytes for 72 hours, was associated with apoptosis as the cultures showed an increase in activation of caspase 3/7 suggestive of apoptotic involvement (Doherty et al. 2013).

1.6.3 Tyrosine kinase inhibitor induced necrosis

Necrosis is a mechanism of cell death characterised by distinctive morphologic changes such as cell swelling, damage to plasma membrane and is ATP independent (Chiong et al. 2011). Necrosis previously was considered to be unregulated and attributed to accidental or dependent on external damages induced as pathogenic infection and ischemic-reperfusion injury (Chiong et al. 2011; Vanlangenakker et al. 2008). However, this is no longer

the case with current consensus that necrotic cell death occurs in a number of forms some of which can be driven by defined molecular pathways (Figure 11)(Chen, yu, and Zhang 2016; Linkermann and Green 2014). Cardiac diseased states and pathological conditions feature necrosis in cardiomyocyte death and can be executed by regulated mechanisms (Lim et al. 2007; Zhang et al. 2019a).
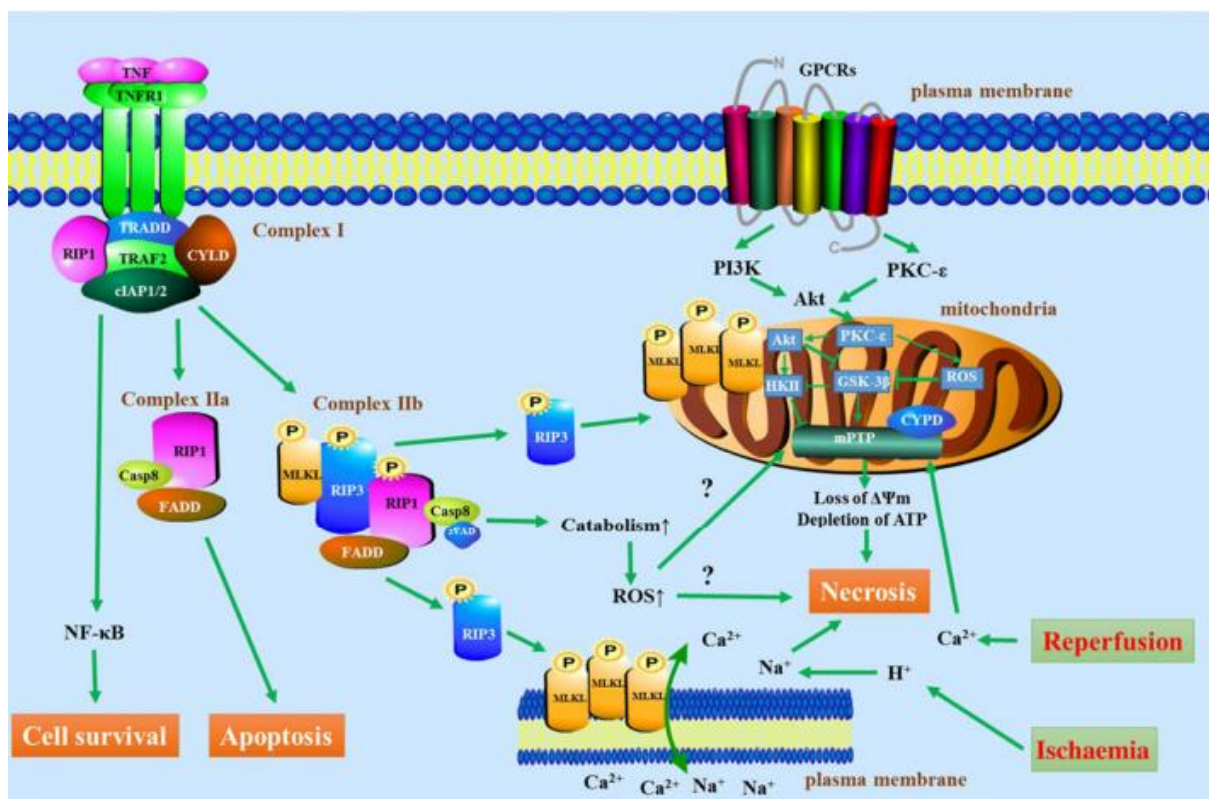
Figure 11 Some of the key signalling pathways implicated in programmed cardiomyocyte necrosis. RIP1 interacts with RIP3 and MLKL to form complex IIB which is involved in mediation of necroptosis. Complex IIB involves phosphorylation of RIP3 and MLKL which then translocate to mitochondrial-associated plasma membranes increasing

Na+ and Ca2+ exchange across the membrane. RIP1 and RIP3 undergo phosphorylation which facilitates necrosis potentially through catabolic pathways and ROS generation. The opening of the mPTP due to increased Ca2+ overload, ROS mediated oxidative stress or ATP depletion result in detrimental changes to mitochondrial morphology and function which could induce necrosis [Adapted from (Zhang et al. 2019)].

Programmed cardiomyocyte necrosis could either be programmed (mitochondria driven) or caspase independent (death receptor mediated) (Vanlangenakker et al. 2008; Zhang et al. 2019).

The mitochondrial driven mechanism of necrosis is of interest with regards TKI induced cardiotoxicity due to the role of ROS and calcium overload mentioned previously. Homeostatic maintenance of inner mitochondrial membrane (IMM) integrity is key to sustained electrical gradient required for ATP production during respiration and key to mitochondrial function (Duprez et al. 2009). However, disturbance of the intracellular microenvironment such as excessive ROS production or calcium overload could affect IMM integrity, leading to mitochondrial membrane potential dissipation, membrane breakdown and ultimately cardiomyocyte death (Duprez et al. 2009; Galluzzi et al. 2018). This sort of cell death is also referred

to as mitochondrial permeability transition (MPT)-driven necrosis (Izzo et al. 2016).

Disrupted calcium signalling is a key mediator in MPT-driven necrosis due to its role in mitochondrial membrane transition pore opening (Duprez et al. 2009). As previously stated, disrupted calcium signalling is usually accompanied by increased ROS production and therefore, both play key role in MPT-driven necrosis (Bertero and Maack 2018; Duprez et al. 2009; Görlach et al. 2015). Tyrosine kinase inhibitors have also been linked with necrosis.

Treatment with sunitinib on isolated cardiomyocytes and mice showed necrosis as one of the mechanisms by which sunitinib is cardiotoxic (Chu et al. 2007). In a study to assess cardiotoxicity of TKI imatinib, the results were suggestive of necrotic damage. Cardiomyocytes were obtained from C7BL6 mice treated with imatinib for between 3 to 6 weeks and analysed. Cytosolic vacuoles observed along accompanied with increased propidium iodide absorption due to loss of integrity which were considered indicators of apoptosis (Kerkelä et al. 2006a). There was also decrease in membrane potential and increased release of cytochrome c, which although the research interpreted as apoptotic indicator, could have be MTP-driven necrosis in part (Kerkelä et al. 2006).

A separate study also indicated that imatinib treatment was associated with caspase independent, necrosis-like cell death mediated by serine protease

activity (Okada et al. 2004). BV173 (an established leukemic cell line from patient with chronic myelogenous leukaemia lymphoid blastic crisis) and K562 (a cell line established from a patient with chronic myelogenous leukaemia erythroid blastic crisis) were treated with imatinib. Inhibition of caspases could not attenuate cell death by imatinib treatment which led investigators to suggest necrotic death (Okada et al. 2004). The results also indicated necrotic morphology was associated with imatinib treated cells (DNA fragmentation and decreased DNA content) (Okada et al. 2004).

1.7 Management and prevention of chemotherapy induced cardiotoxicity

Treatments for oncogenic conditions have come on leaps and bounds showing great progress in more recent times, no longer considered a death sentence with survival rates of cancer patients reported to be show a gradual incline (Bovelli et al. 2010; Csapo and Lazar 2014b). Cardiotoxicity presents as one of the more recurring and more concerning side effects associated with anticancer treatments (Bovelli et al. 2010).

The development of a multitude of cardiac events due to toxicity; despite the asymptomatic nature of some of them, ultimately impacts the prognosis of the cancer patient negatively but also imposes restrictions towards other therapeutic pathways (Raschi et al. 2010). The clinical manifestation of anti-cancer induced cardiotoxicity encompasses a wide range of conditions, from

incidences of mild transient dysrhythmias; to more lethal disorders like myocardial ischemia (Csapo and Lazar 2014).

Damage to the cardiovascular system would severely hinder the achievement of optimal results following antineoplastic treatment and a number of the cardiotoxic events present as irreversible, therefore the level of importance attributed towards characterising the underlying mechanisms of cardiac toxicity and providing effective management regimes could not be understated (Bovelli et al. 2010; Csapo and Lazar 2014).

However, a standard and effective method to mitigate cardiotoxicity remains elusive with investigations still ongoing (Bovelli et al. 2010). Current guidelines recommend better and earlier detection of patients with increased risk, seeking effective preventative regimens & strategies and also rapid treatment of clinical manifestations of cardiotoxicity when made apparent (Bovelli et al. 2010; Csapo and Lazar 2014).

A crucial milestone towards the development of adequate preventative strategies is the identification of the varying risk factors that contribute towards the manifestation of these cardiovascular events (Raschi et al. 2010). The development of chemotherapy-induced cardiac toxicity is often believed to vary, with the apparent variation dependent on a number of risk factors some of which include patient related factors like individuals age, gender, history of cardiovascular disorders/events, imbalances in electrolytes as a

result of diseased conditions, present or previous administration treatment against neoplasms such as anthracycline treatment or radiation therapy (Le, Cao, and Yang 2014).

As mentioned earlier, patients subjected to chemotherapy are expected to undergo rigorous clinical evaluation as well as thorough assessment of their cardiovascular risk factors and screen for the presence of any other comorbidities (Csapo and Lazar 2014; Le, Cao, and Yang 2014). Conditions which could present risk factors include hypertension, dyslipidaemia (increased amounts of lipids in circulation), diabetes and electrolyte disturbances would need to be attended to prior to antineoplastic therapy commencement and should be monitored diligently during the duration of drug therapy as well as post treatment (Csapo and Lazar 2014).

In addition, effective strategies are required in order to implement protective regimens to protect or at least seek to limit the clinical cardiotoxicity (Raschi et al. 2010). Agents such as dexrazoxane, statins and B-blockers have proved relatively promising results against a number of anticancer therapies, but their success has proved limited against targeted therapies (TKIs) (Albini et al. 2010).

1.8 Cardioprotective strategies

Anticancer induced cardiotoxicity fuels the relationship between cancer and cardiovascular disease (Bertero, Ameri, and Maack 2019). As a result of

cancer treatment, patients have increased likelihood to have cardiovascular disease development (Bansal et al. 2017). Similarly, cancer patients with underlying risk factors or pre-existing cardiovascular disease have greater risk of cardiac complications (Armenian et al. 2018; Bansal et al. 2019). The most effective strategy to prevent cardiac deterioration induced by chemotherapy induced cardiotoxicity is the cessation of treatment with the particular agent (Smiseth, Edvardsen, and Skulstad 2013). Interdisciplinary dialogue between cardiology, oncology and haematological specialists along with the primary care givers is crucial to avoiding or minimizing anticancer induced cardiotoxicity (Curigliano et al. 2020). The use of protective therapeutics could be of benefit to maintaining health of myocardium in instances of cardiotoxicity (Bansal et al. 2017; Smith, Phyu, and Akabuogu 2016).

1.8.1 Angiotensin converting enzyme inhibitors

Angiotensin converting enzyme inhibitors were developed as targets for the treatment of hypertension (Heran et al. 2008; Hicks et al. 2018). ACE inhibitors prevent the conversion of Angiotensin I in angiotensin II which has a myriad of physiological actions (Heran et al. 2008; Hicks et al. 2018). The notion that angiotensin converting-enzyme inhibitors (ACEI) possess cardioprotective properties is widely accepted (Blaes et al. 2015; Ma et al. 2020). ACEIs are reported to be routinely administered in clinical setting and have proved to be beneficial in their protective therapeutic properties against

a variety of cardiovascular events (Ghazi-Khansari and Mohammadi-Bardbori 2007; Hiona et al. 2011). ACEIs also facilitate changes affecting mitochondrial metabolism and cardiomyocyte function through alterations in gene expression (Csapo and Lazar 2014).

Treatment of adult male albino rats with captopril was successful at attenuating doxorubicin induced cardiotoxicity with reduction of oxidative stress and reduction of doxorubicin induced myocardial fibrosis, which suggested angiotensin converting enzyme inhibitor co-treatment displayed beneficial effects against doxorubicin induced cardiotoxicity (Ibrahim et al. 2009). Captopril co-administration with doxorubicin significantly improved the oxidative status of the studied animals with significant attenuation in the increase in activity of superoxide dismutase and glutathione peroxidase in animals treated with doxorubicin alone reversing dox-induced cardiotoxicity (Ibrahim et al. 2009a).

Previous research studies have highlighted the role of the renin-angiotensin system (RAS) as being crucial in the development of doxorubicin (Anthracycline)-induced cardiomyopathy and revealed the benefit of ACEIs as being protective against anticancer-induced cardiotoxicity (Blaes et al. 2015). ACEIs effectively lead to the inhibition of the synthesis of angiotensin enzyme 2 which then inhibits angiotensin type-1 receptor activation (Figure 12) (Ma et al. 2020b). ACEIs are also widely accepted to possess anti-oxidative

effects and minimize aldosterone-induced cardiac fibrosis and also minimize observed apoptosis in cardiomyocytes (Sabbatino et al. 2021).
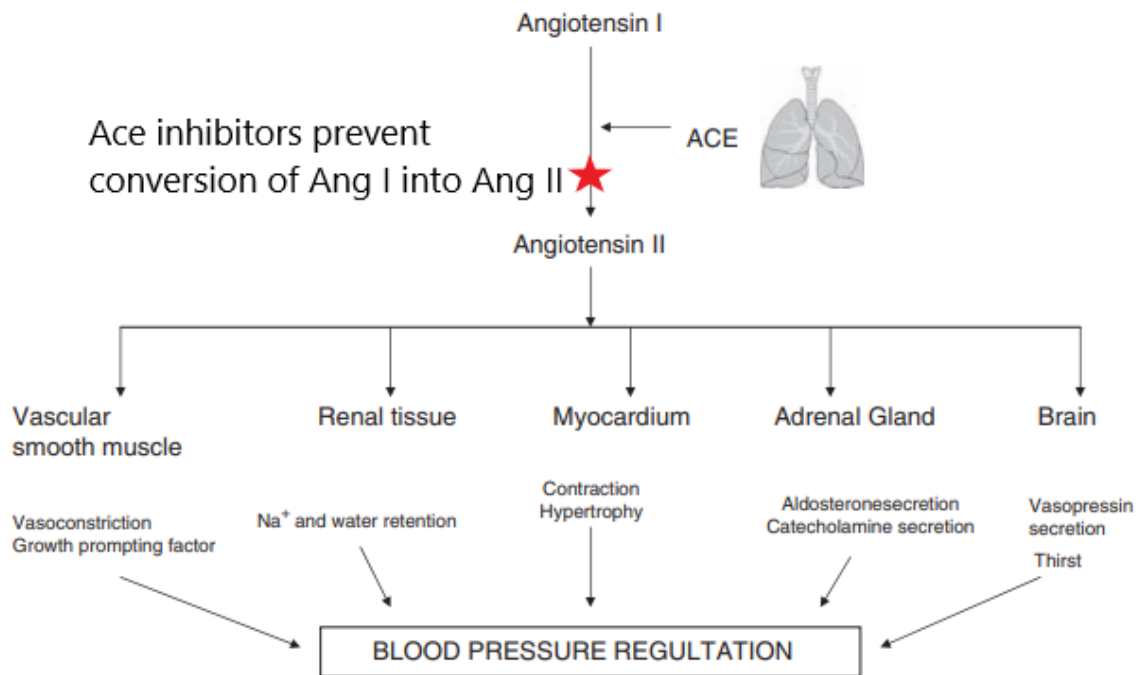
Figure 12 Action of ACE inhibition on production of angiotensin II which leads to blood pressure regulation [Adapted from (Hanif, Bid, and Konwar 2010)].

A meta-analytic study of clinical data sought to evaluate the effects of angiotensin converting enzyme inhibitor treatment in individuals with heart failure (Tai et al. 2017). The study reported that ACE inhibition with drugs such as captopril and trandolapril reduced cardiovascular mortality in heart failure patients following myocardial infarction (Tai et al. 2017). Similarly, during the meta-analysis of randomised clinical trial data of RAAS inhibitor

treatment patients, ACE inhibitor treatment (Lisinopril, enalapril and perindopril) overall significantly reduced mortality in the 4-year follow up period (Fuchs and DiNicolantonio 2015; van Vark et al. 2012).

During the randomised trail assessing the cardioprotective effectiveness of two drugs against trastuzumab cardiotoxicity, the angiotensin converting enzyme inhibitor lisinopril was deemed more effective (Guglin et al. 2019). Lisinopril treatment was associated with less incidence of cardiotoxicity compared to individuals treated with carvedilol (beta blocker) (Guglin et al. 2019).

In vivo studies in canine subjects treated with doxorubicin and enalapril for 4 weeks recommended enalapril treatment was beneficial in the prevention of doxorubicin induced cardiomyopathy (Vaynblat et al. 2002). Enalapril treatment significantly improved survival, significantly increased end diastolic pressure and significantly reduced end diastolic diameter compared to non-enalapril treated animals after 12 weeks. In another *in vivo* study, male Sprague Dawley rats treated with doxorubicin for 3 weeks were also either treated with or without temocapril and after 12 weeks, the animals simultaneously treated with the ACE inhibitor presented reduction in doxorubicin induced myocardial damage compared to their untreated counterparts with significant reduction in heart/body weight ratio and prevented contraction abnormalities and prevented interstitial fibrosis (Tokudome et al. 2000).

Male Wistar rat isolated liver mitochondria treated with paraquat (toxic compound commonly used within herbicides) with or without captopril showed significantly increased total GSH (reduced glutathione which is protective of the mitochondria against ROS-mediated injury) in mitochondria treated with paraquat and captopril compared with paraquat treated mitochondria alone (Ghazi-Khansari and Mohammadi-Bardbori 2007). In the same study, paraquat + captopril treatment was shown to display significant improvement in catalase activity (catalase regulates the conversion of toxic hydrogen peroxide to hydroxyl radical (Ghazi-Khansari and Mohammadi-Bardbori 2007). The study concluded that captopril treatment improved the mitochondrial oxidative status as seen with improved activity of enzymes like GSH and catalase which have roles in reduction of ROS and in turn oxidative stress (Ghazi-Khansari and Mohammadi-Bardbori 2007).

1.8.2 Angiotensin receptor blockers

The renin-angiotensin system (RAS) comprises of a number of mechanisms that plays a central role in a number of physiological processes including cardiovascular regulatory activities (Shetty and DelGrande 2000; Sobczuk et al. 2020). Over-activity of the renin-angiotensin-aldosterone system (RAS) can often lead to a number of detrimental vascular events occurring (figure 13) (Dzau Victor 2001; Munger 2011). Direct vasoconstrictor effects are brought about by the interaction between angiotensin II within the adrenergic, endothelin and vasopressin pathways which ultimately culminate

in scenarios which contribute to further fuelling oxidative stress and a reduction in the activity of nitric oxide (Munger 2011).
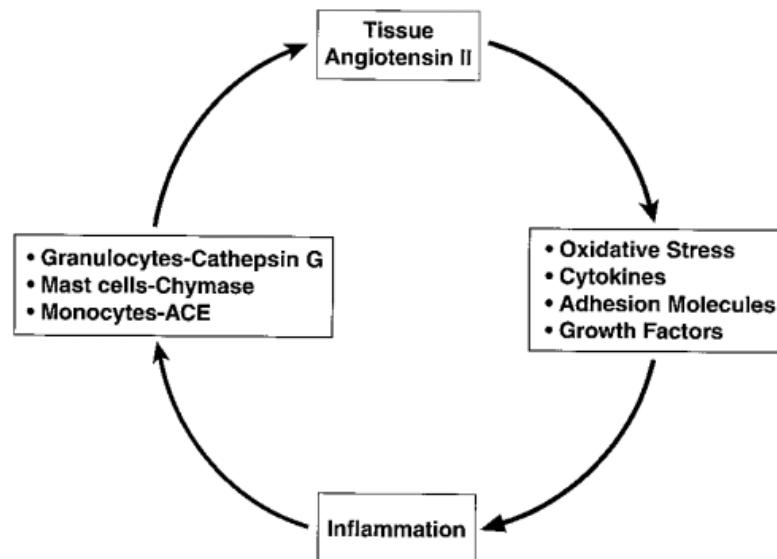
Figure 13 Angiotensin II activation initiates a positive feedback cascade inducing oxidative stress (ROS generation) and inflammation(cytokine and growth factor release) leading to increased cell wall inflammation which in turn further generate more angiotensin II restarting the cycle [Adapted from (Dzau Victor 2001)].

Angiotensin II leads to induction of endothelial dysfunction through the activation of key transcription factors specifically nuclear factor–κβ, which ultimately signals the activation of inflammatory phenotypes within smooth muscle located in the vasculature (Munger 2011). Some of these phenotypic changes include the activation of NADH and NADPH oxidase (which aid production of superoxide anion), activation of monocytes & macrophages, facilitate the secretion of cytokines, proteases, and growth factors and also

initiates the stimulation of leukocyte adherence molecules responsible for inflammatory action within the walls of the different vasculature (Dzau Victor 2001; Munger 2011).

Angiotensin II directly affects smooth-muscle migration, causes vascular hypertrophy, synthesis & then the release of components of the extracellular matrix, which are key components during vascular remodelling (Dzau Victor 2001). Angiotensin II also regulates activities which promote a pro-thrombotic (increased risk of atherosclerosis) state by the initiation of increased synthesis of plasminogen activator inhibitor type 1 and a down regulation of tissue-type plasminogen activator, as well as the activation of platelet aggregation and adhesion (Munger 2011).

As earlier introduced, the renin-angiotensin system (RAS) is crucial in the regulatory processes involved with normal cardiovascular function (Lv et al. 2018). The RAS system is essential in the management of blood pressure changes and as well as playing a crucial role in the maintenance of regular cardiovascular and renal function (Ruschitzka and Taddei 2012).

Blockage of RAS overactivity is of significant health benefit with regards cardiovascular disease (Lv et al. 2018). RAS contributes towards the progression of cardiovascular disease states such as atrial hypertension, vascular injury, and heart failure amongst others (Dessì et al. 2011; Shetty and DelGrande 2000; Sobczuk et al. 2020). Angiotensin II inhibition by

angiotensin I receptor blockade (AT1) is an effective target to manage RAS activity (Min et al. 2009). Blockage of AT1 receptor would also prevent induction of potentially harmful effects such as oxidative stress, apoptosis, and inflammation (Min et al. 2009; van Thiel et al. 2015).

In a study to evaluate the benefit of ARB treatment following coronary artery bypass grafting in individuals (Kim et al. 2020). ARB treatment was associated with reduction of major adverse cardiovascular event occurrence along with stroke prevention in the 12 month follow up period (Kim et al. 2020).

Eight-week-old male stroke prone, spontaneously hypertensive rats were treated with low dose losartan and reported haemodynamic improvement with significant attenuation of systolic blood pressure observed measure via radiotelemetry (McLachlan et al. 2014). Treatment of adult male albino rats with telmisartan was effective at attenuating doxorubicin induced cardiotoxicity with reduction of oxidative stress and reduction of doxorubicin induced myocardial fibrosis, which suggested AT1 receptor blocker treatment was beneficial against doxorubicin cardiotoxicity (Ibrahim et al. 2009). Telmisartan co-administration with doxorubicin significantly improved the oxidative status of the studied animals with significant reduction in the observed activity of superoxide dismutase and glutathione peroxidase in animals treated compared with doxorubicin treatment alone, reversing doxorubicin induced cardiotoxicity (Ibrahim et al. 2009).

1.9 Molecular signalling pathways involved in anaplastic lymphoma kinase signalling

ALK is considered significant in its role in key processes such as development and function of the nervous system, controlling cell proliferation, survival, and differentiation (Holla et al. 2017). ALK proteins activate a number of different pathways which overlap and share connecting mediators (Chiarle et al. 2008). Some of the pathways include the Ras/Raf/MEK/ERK1/2, Janus activated kinase/signal transducer and activator of transcription (JAK/STAT), phosphatidylinositol3-kinase (P13k)/AKT (protein kinase B) and phospholipase C (PLC)-Y pathways (Roskoski 2013). Regarding the regulation of cell survival, PI3K/AKT and JAK/STAT pathways are responsible (Figure 14) (Roskoski 2013).

AKT is a protein-serine/threonine kinase which binds phosphatidylinositol biphosphate and triphosphate with high affinity (Liu et al. 2009; Roskoski 2013). PDK1 and mammalian target of rapamycin complex 2 (mTORC2) catalyse the phosphorylation of AKT Thr308 and Ser473 respectively. The bi-phosphorylated and activated AKT then in turn catalyses the phosphorylation of mTOR which lists cell survival as a downstream effect (Roskoski 2013; Singh et al. 2009).
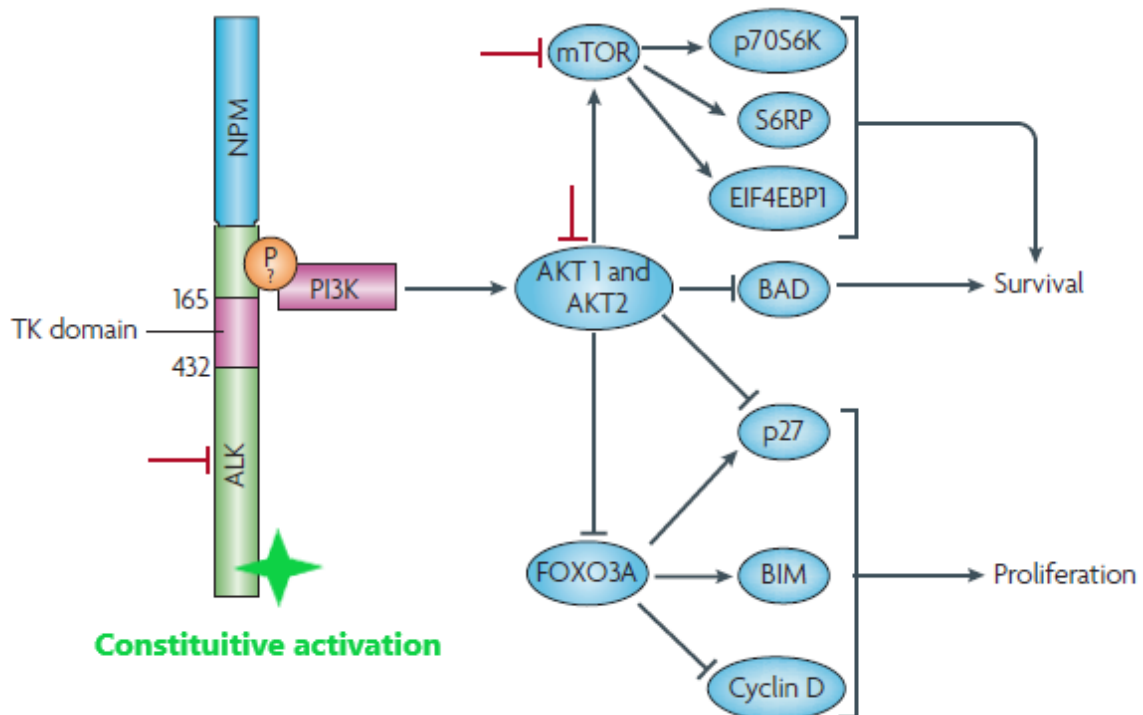
Figure 14 The ALK PI3K signalling cascade which governs cell proliferation and survival. ALK activation leads to AKT phosphorylation which in turn enhance cell survival by blocking pro-apoptotic factors. AKT 1 and 2 phosphorylate forkhead box 03A on Tyr24, Ser256 and Ser319 preventing transcription of target genes promoting apoptosis, cell cycle arrest and cell death. However constitutive activation of ALK facilitates oncogenic cells survival [Adapted from (Chiarle et al. 2008)].

Cardiotoxicity induced by doxorubicin was associated with decreased AKT signalling in a study involving embryonic stem cell transplantation (Singla 2015). Treatment of C57BL/6 mice were treated with doxorubicin intraperitoneally significantly decreased p-Akt expression and increased percentage of apoptotic nuclei detected (Singla 2015). Doxorubicin treatment

on C57BL/6 mice similarly decreased Akt expression in a study conducted to assess the cardioprotection induced by induction of calcium sensitivity (Li et al. 2020). Treatment of mice with doxorubicin significantly decreased p-Akt expression and increased myocardial apoptosis assessed in living mice and myocytes compared to untreated animals (Li et al. 2020).

1.10 Phosphatidylinositol3-kinase / protein kinase B (PI3K/AKT) signalling in cell death.

The PI3K/AKT pathway regulates a variety of cellular processes, such are cell growth, proliferation, survival, and metabolic regulation (Lee, Liao, and Lin 2005). PI3K/AKT activation induces protein phosphorylation promoting tumour cell growth and proliferation, cell survival (apoptosis inhibition) invasion and metastasis amongst other activities (Liu et al. 2020). The signalling pathway also participates in cell survival and apoptotic process (Chiarle et al. 2008; Meng et al. 2017). AKT is the primary effector of downstream PI3k activation cascade (Meng et al. 2017).

AKT is a key inhibitor of cell death by apoptosis due to its ability to inactivate apoptosis promoting molecules such as caspase 9, Bad and by triggering activity of transcription factor NF-κB (triggers innate and adaptive immunity)(Nogueira et al. 2008). AKT also plays role in energy metabolism which accompanies its roles in apoptosis and promote cell cycle progression (Nogueira et al. 2008). AKT activation was shown to induce cell sensitivity to

ROS-induced apoptosis through increased inhibition ROS-scavengers and increased oxygen consumption downstream of FOXO (Nogueira et al. 2008). In primary mouse embryonic fibroblasts, wild type cells with normal AKT expression were significantly more susceptible to hydrogen peroxide (ROS) induced cell death compared to AKT KO fibroblasts (Nogueira et al. 2008). This was attributed to AKT activation and downstream phosphorylation and inactivation of FOXO transcription factors downregulating antioxidant enzymes (Nogueira et al. 2008). Sustained activation of AKT would lead to sustained inhibition of FOXO transmission factors which would in turn reduce secretion of antioxidant enzymes (Los et al. 2009).

During myocardial injury induced by doxorubicin, worsened by ischemic stress was associated with increased phosphorylation of AKT (p-AKT) (Gharanei et al. 2013). Isolated rat hearts from male Sprague-Dawley rats were treated with doxorubicin via langendorff perfusion. Doxorubicin treatment was associated with significant increased detection of p-AKT compared to ischemia reperfusion control (Gharanei et al. 2013). AKT was also shown to inhibit non-apoptotic cell death induced by ceramide (molecule generated in response to cell death stimulus such as oxidative stress and ionizing radiation) (Mochizuki et al. 2002). U251 glioma cells with constitutive activation of AKT kinase showed significant inhibition of cell death with significant increases in cell viability after 48 hours of treatment (Mochizuki et al. 2002). Pro-apoptotic plant derived curcumin was able to

induce apoptotic cell death by PI3K /AKT pathway inhibition (Kuttikrishnan et al. 2019). Curcumin treatment was associated with reduced detection of p-AKT protein and increased detection of unphosphorylated AKT and also induced cell death by apoptosis by inhibition of antiapoptotic protein Bcl-2 (Kuttikrishnan et al. 2019). These highlight the interesting relationship between AKT and cell death.

1.10 Cardiac cell models

Isolated cardiomyocytes have achieved terminal differentiation and do not divide in culture, there has been a need for a suitable alternative (Peter, Bjerke, and Leinwand 2016).

Immortalised cardiac myocytes cell lines although not entirely identical to adult isolated cardiac myocytes present opportunity to assess individual parameters or provide data which could indicate likely processes in isolated cardiomyocytes (Peter, Bjerke, and Leinwand 2016). For instance, H9C2 cells which were derived from embryonic rat ventricular tissue are one of such cell lines (Peter, Bjerke, and Leinwand 2016). These cells display favourable response to hypertrophic stimulus and divide in culture readily reducing the need for isolating cardiomyocytes (Peter, Bjerke, and Leinwand 2016).

1.11 Aims, objectives and hypotheses

1.11.1 Aims

- Does anaplastic lymphoma kinase inhibiton with crizotinib induce cardiotoxicity in cardiac models?

- Is crizotinib induced cardiotoxicity concentration dependent?

- Is the Phosphatidylinositol3-kinase / protein kinase B (PI3K/AKT) signalling pathway involved in crizotinib induced cardiotoxicity?

- Does interference with the renin angiotensin system pathway reverse crizotinib induced cardiotoxicity?

1.11.2 Objectives

- To characterise the concentration dependent cardiotoxic effects of crizotinib in isolated langendorff rat hearts.

- To evaluate the effects of crizotinib treatment on signalling proteins in the PI3K/AKT signalling pathway

- To evaluate the effects of RAS antagonists on crizotinib induced dysfunction

1.11.3 Hypotheses

- Crizotinib treatment induces concentration dependent haemodynamic dysfunction in isolated hearts, increases infarct to risk ratio development and cardiomyocyte death.

- Angiotensin converting enzyme inhibitor co-treatment will protect against crizotinib induced cardiotoxicity.

- Angiotensin receptor blocker co-treatment will protect against crizotinib induced cardiotoxicity.

Chapter 2 General Materials and Methods

2.1 Drugs and materials

Crizotinib (Carbosynth, Europe), Ramipril & Losartan (Tocris, Bristol, UK) powders were all dissolved in DMSO (0.04%) (Dimethyl sulfoxide) for the purpose of experimental procedure. The drugs were then aliquot into 1.5ml eppendorf tubes and stored at -20°C until required. The antibodies anti-rabbit antibody for phospho-Akt at Ser473 (Cell Signalling technologies™), as well as anti-biotin and anti-rabbit IgG were purchased from Cell Signalling technologies™. Cleaved caspase7 and Caspase 7 were also purchased from cell signalling. The Triphenlytetrazolium chloride (TTC) was purchased from Sigma Aldrich, UK. DMEM (Dulbecco's modified eagle medium) which was purchased from ThermoFisher scientific ™. Penicillin streptomycin (10,000 U/mL) purchased from Gibco ™. Foetal bovine serum (FBS) purchased from Gibco ™. Phosphate buffer saline was purchased from Gibco ™.

2.2 Animals

Adult male Sprague-Dawley rats with body weight range between 350±50 grams purchased from Charles River UK limited (Margate, UK) were used for the purpose of this study. They were kept in humane conditions and fed standard pellet diet. Handling and treatment procedures were in full accordance with the Guidelines regarding the operation and handlings of Animals (scientific procedures act 1986).

2.3 Isolated perfused heart: Langendorff perfusion model

For the Langendorff procedure, the animals were sacrificed by cervical dislocation. The hearts were then excised quickly from the rats and were then placed in ice cold krebs-Henseleit buffer (KH) between transit between the prep room and being mounted on the Langendorff apparatus. After being mounted on the system, the hearts were then perfused continually with KH buffer at 37°C and pH 7.4 and saturated with constant 95% O_2 and 5% CO_2 gas supply.

The temperature was monitored and maintained at 37 ºC throughout the procedure with a sensitive thermoprobe inserted into the water circulation system to notify of any deviations from temperature. The KH buffer comprised of buffer (118.5 mM NaCl, 25 mM $NaHCO_3$, 4.8 mM KCl, 1.2 mM $MgSO_4$, 1.2 mM KH_2PO_4, 1.7 mM $CaCl_2$, and 12 mM glucose, pH 7.4).
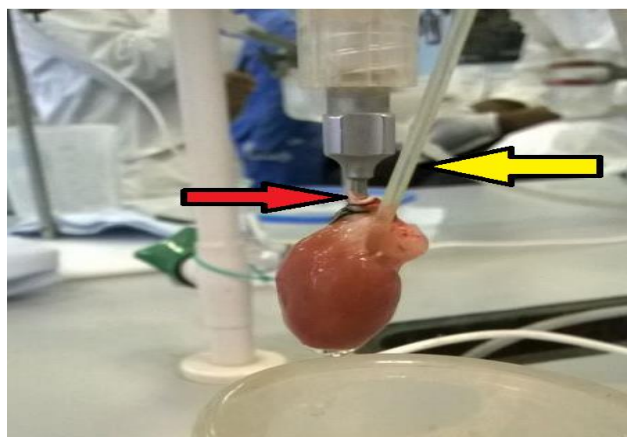
Figure 2.3.1: Image showing heart mounted on Langendorff apparatus. The red arrow indicating the cannulated aorta and the yellow arrow indicating the tube connected to the inflated balloon, through the opening created following excision of the left atrium.

2.3.1 Haemodynamic data monitoring and collection

The left atrium was carefully excised after the aorta had been cannulated. A latex balloon was then inserted into the left ventricle via the opening of the excised aorta and the balloon was then inflated at a constant pressure of 5-10mmHg.

The left ventricular developed pressure in mmHg (LVDP) and heart rate (BPM) were monitored and recorded through a physiological pressure transducer which was connected to a Powerlab (AD instruments Ltd.Chalgrove, UK), which was connected to a computer running the LabChart® software v7.

The coronary flow was measured via collection of the perfusate expelled from the heart over the required time intervals which was for 1 minute. Haemodynamic parameters were measured at 5-minute intervals during the first 50 minutes of perfusion, after which readings were taken at 15-minute intervals (Figure 2.3.2).

Figure 2.3.2: Image from the Lab Chart® software v7 used to measure values for LVDP and Heart rate. The values were measured per minute at the varying intervals.

2.3.2 Experimental Design

The hearts were allowed a 20-minute stabilization period where haemodynamic readings were recorded at 5-minute intervals. Following the stabilization period and 30 minutes into drug treatment, readings were taken at 15-minute intervals. The hearts were then perfused with KH buffer, drug treatment & Drug co-treatment. The total perfusion time was 175 minutes (2 hours 55 minutes). Following the total perfusion time, the hearts were then weighed and then stored in the -20°C to be Triphenyl tetrazolium chloride (TTC) stained for infarct analysis at a later time.

The hearts were perfused with the following treatment groups for the langendorff haemodynamic and tissue collection phases. Vehicle control (KH

buffer), DMSO control, Crizotinib (10nM, 0.1μM, 1μM), Ramipril 1μM ± Crizotinib 1μM, Losartan 4.5μM ± Crizotinib 1μM.
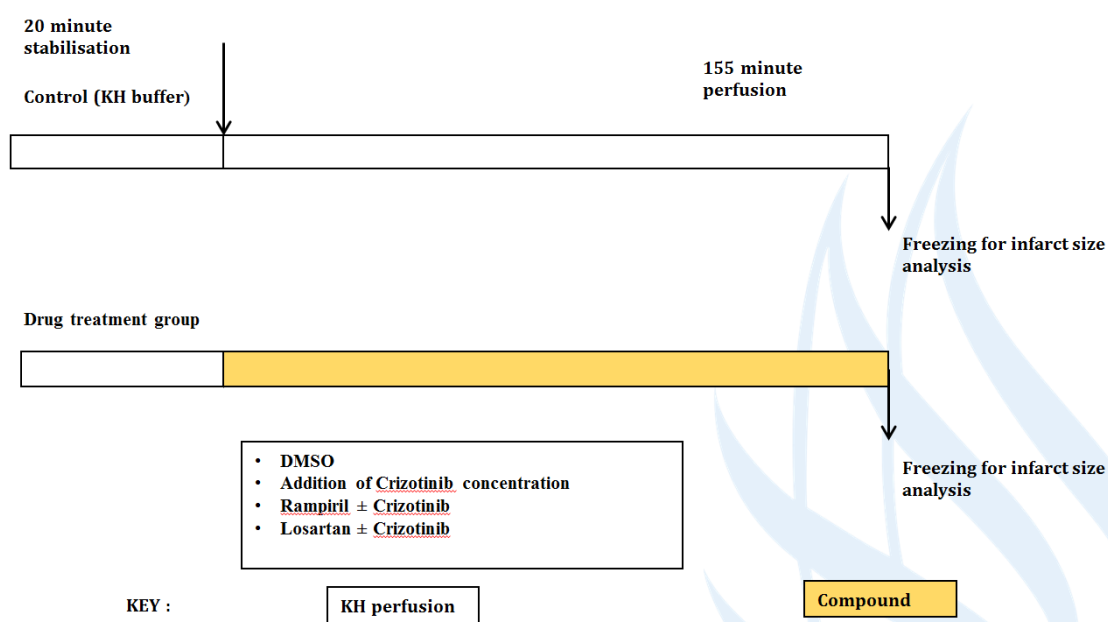
Figure 2.3.3: Illustration of experimental design for Langendorff perfusion procedure

2.3.3 TTC Analysis/ infarcts analysis

The treated hearts were removed from the -20°C storage and then with a scalpel sliced thinly, about 3mm thickness per slice. The thinly cut slices were then transferred to a 50ml falcon tube containing a solution of 0.1g of 2, 3, 5-Triphenyltetrazolium chloride (TTC) powder, 8ml of Na_2HPO_4 and 2ml of NaH_2PO_4.

The samples were then incubated at 37°C for about 15 minutes after which the TTC solution was then decanted off carefully. Following this the samples/slices filled with 10% formaldehyde solution and then incubated at room temperature for a minimum of 4 hours. This was done in order to bring about enhancement of the contrast viable and infarcted areas in the heart slices.

Following the formaldehyde incubation, the Formaldehyde was decanted off (fume cupboard) and discarded appropriately. The slices were then placed in between 2 glass slabs and clamped around the edges to get the slices as thinly flat as possible and also to eradicate bubbles (Figure 2.3.4).

 A transparent acetate sheet was then placed over the glass and under a lamp the risk/infarct areas visible by eye were marked off unto the sheets.

Following this, the acetate sheets were then scanned digitally and analysed with image J computer software. The traced areas recorded to achieve data to be used for statistical analysis subsequently.

Previous studies have employed similar TTC staining protocol to assess infarct development in cardiac and cerebral tissue (Formatting...
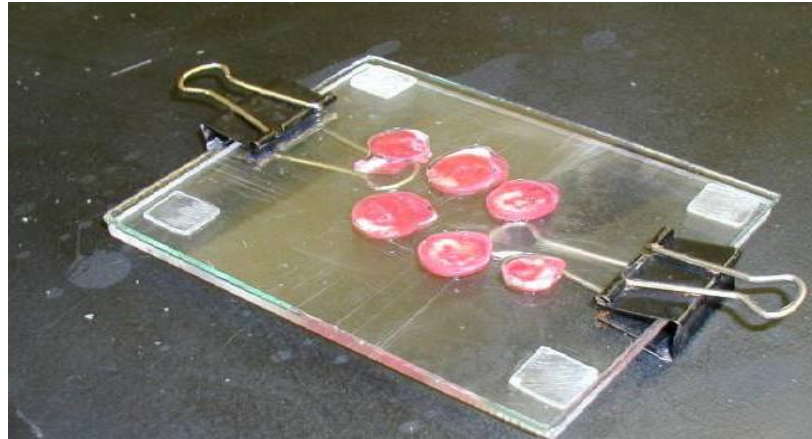
Figure 2.3.4: Image showing heart slices compressed between 2 glass sheets in preparation of acetate tracing.

2.3.4 Tissue collection

For this procedure the hearts were subjected to the same process outlined the langendorff protocol. The hearts were perfused with the appropriate drug treatments and perfused for the stated time period and haemodynamic parameters were measured and recorded as to ensure the hearts were performing optimally. Upon completion of the perfusion, the hearts were removed from the langendorff apparatus and then weighed. The left ventricles were then excised and wrapped in aluminium foil and then flash frozen in liquid nitrogen. The samples were then placed in -80°C storage for later use.

2.5.5 Exclusion criteria during langendorff perfusion

During the initial stabilisation, isolated hearts were excluded from the study if they did not meet any of the following criterion.

1. If contractility of the heart was unstable during the 20-minute period

2. The measured Coronary flow exceeded 30 ml/min in the absence of any visible leakages

3. Heart rate below 150 BPM during the course of stabilisation

4. Appearance of constant and longer lasting severe arrhythmia

2.4 Protein Quantification assay (BCA assay)

The assay that was employed for the determination of protein concentration from tissue samples was the Pierce™ BCA protein assay Kit (ThermoFisher Scientific 2017). This kit displays strong absorbance at wavelength 562nm which appears almost linear with increasing protein concentration and does so over a wide working range (PierceTM BCA protein assay Kit, Thermo Scientific 2017). The assay was selected for its wide working range and also colour change/development is slow enough to facilitate analysis of a number of samples simultaneously.

The protein standards and working reagents were provided along with the kit purchased. The composition of the standards and reagents used were provided in the protocol for the assay.

The formula for the working BCA working reagent employed was as follows;

= (number of standards + number of unknown samples) x (number of replicates) x (volume of working reagent required per sample)

The assay was carried out on 96 well plates as this provided opportunity to analyse large sample numbers and replicates in the least amount of space efficiently. Following optimization, the following protocols and volumes were established.

- 10µl of standards were added to the plates to the appropriate wells

- 2µl of unknown samples were added to the appropriate wells (Excess protein in samples from tissue stocks would provide absorbance values well above the range of any analyser available); same volume of sample outside working range

- 200µl of working reagent was added to each well (standards, unknown samples and replicates)

Following successful inoculations, the plates were covered with aluminium foil incubated for 30 minutes at 37ºc. Following incubation, plates were then left to briefly cool to room temperature.

The absorbance's for the different wells were then measured on the Biotek Epoch 2 Microplate Spectrophotometer™ at 562nm.

2.5 Western Blot protocol

The frozen samples (section 2.3.4 Tissue collection treated with the required compounds) were retrieved from the -80^0C storage. The tissue samples were allowed to defrost on ice briefly. This is to prevent excess protein degradation.

2.5.1 Sample preparation for western Blotting

The work bench was first sprayed down with RNAse solution and wiped down with 70% IMS solution. Then into a 2ml Eppendorf/ flow tube, 400μl of lysis buffer + PhosSTOP™ (Phosphatase stop) + Protease cocktail and then add between 70-100 mg of frozen tissue. All of this was done over ice to prevent unnecessary protein denaturation.

The Eppendorf / flow tube containing the samples then had the homogeniser blade inserted and done so in such a manner that the blades were in contact with the tissue before switching on the motor. The speed of the blade was altered accordingly to ensure maximal homogenisation. Samples kept on ice before and after. The samples were homogenised until a paste-like consistency is achieved and solid tissues have been homogenised. The samples were then returned to being placed on ice.

The sample blade was cleaned with 70% alcohol at the start and at the end of session of homogenisation and was rinsed with fresh RO water in-between samples.

The successfully homogenised samples were then centrifuged (Thermo Scientific™ Pico 17 MicroCentrifuge, 24-Pl Rotor; 230 VAC) for 10 minutes at 11000 RPM at -4°C. The supernatant was then delicately pipetted into newly labelled 1.5ml Eppendorf's on ice. BCA assay was then conducted on the samples with about 10μl used for the purpose of the assay. A 1:1 dilution was done with sample buffer (250 mM Tris-HCl, 10% Glycerol, 0.006% Bromophenol blue, 4% SDS, 2% β-mercaptoethanol) as an equal volume of sample buffer was added to the Eppendorf containing the remainder of the sample. The samples were then boiled at 100 °C in a heating block for 5 minutes. Following which the samples were then stored at -20 °C for later use. Protein concentration should be halved as the samples were diluted 1:1 in sample buffer.

2.5.2 Sample loading for western blotting

The samples were taken out of the -20°C storage and then allowed to defrost while being kept on ice. Samples were then made up into required concentrations and dilutions with sample buffer and were then quickly centrifuged (Thermo Scientific™ Pico 17 MicroCentrifuge, 24-Pl Rotor; 230 VAC) for 2 minutes at 12000 RPM at 4 °C and returned back to being on ice.

The gel packs were then placed into the cartridge with the bottom green strips removed and then cartridge closed when gels placed in correctly and then returned into the gel tanks.

The tank was then filled with running buffer (14.42 g/L glycine, 1.0 g/L SDS, 3.0g/L TrisBase) with the gel cartridge filled first and then the chamber was filled afterwards. The combs were then removed after the wells were sufficiently submerged in running buffer. It was imperative to ensure the gel holding cassette was closed properly to prevent leakage of running buffer.

2.5μl of Kaleidoscope was then pipetted into well 1 of the gel and 2.5 μl of marker pipetted into well 12. The samples are placed in the wells in-between with 15 - 20μl of sample. The gels were then run at 100V for about 60 minutes; however, they were closely monitored in case the samples ran a lot quicker than expected. The figure below provides an image of the filled chamber following successful sample loading.

Figure 2.5.1: Image of a filled gel tank showing gels with loaded samples just prior to separation by electrophoresis.

Following the completion of the run time, the gels were then ready to be transferred. The transfer membranes were then opened with half placed on the transfer cassette. The Gels were then placed unto the membrane and then covered with the second part of the membrane and then smoothed out with the roller to prevent gaps/folds under the membrane. The cassette was then closed and inserted into the blot transfer device and was allowed to run for 7 minutes.

Following successful transfer, the gel area was cut with a scalpel on the membrane. The membranes were then placed in a container with blocking buffer(solution of 15ml 10X TBST ; 10x TBST – 50mM Tris Base, 150mM NaCl, 0.05% Tween-20; pH 7.6) , 5% milk - 0.75 g) and then was incubated at room temperature on the orbital shaker for at least 1 hour.

2.5.5 Antibody staining

Following the blocking phase, the membrane was then washed 3-times, 5-minute duration in 15 ml TBST. Following the washes, the blots were then ready for incubation. The rolled blots were then placed into falcon tubes containing solution of 5ml TBST + 5% BSA with 5 μl primary antibody and incubated overnight on a roller at 4 °C.

Following overnight incubation, the blots were taken out of the falcon tubes and washed twice in 10 x TBST. The secondary antibody was then prepared (15ml TBST, 0.5g BSA and 3μl anti-rabbit IgG). The blots were then incubated

in the secondary solution for 2 hours at room temperature on the orbital shaker. After incubation the blots were then washed 3 times in TBST.

2.5.6 Visualisation

A 1:1 solution of the west femto™ reagents was made (usually about 2-3ml for 2 blots). The blot was then placed on a clear acetate film taking care to remove bubbles underneath the membranes. 1ml of the solution was then pipetted over the membrane generously and then placed into the ChemiDoc. The appropriate settings were then selected, and visualisation could commence.

2.5.7 Blot stripping procedure

The blots were placed in stripping buffer for 5 minutes, and then washed afterwards 3 times in TBST before re-blocking.

2.6 Ventricular Cardiomyocytes isolation procedure

Randomly selected rats were sacrificed humanely by cervical dislocation. The chest cavity was then carefully dissected to expose the heart which was then excised in a timely manner minimizing clot formation and placed in cold KH buffer. The hearts were then taken to the langendorff set up for cannulation.

Following cannulation on the new set up, the heart was then perfused through a rate-controlled pump for 3-5 minutes with calcium free (EGTA) buffer to allow blood to flow completely from the heart and also to halt beating of the heart to avoid further damage to cardiomyocytes. Following perfusion with

EGTA buffer, the hearts were then perfused with collagenase buffer. Collagenase perfusion was again done for about 5 minutes. The end point for this phase was usually indicated by the inflammation of the heart and development of a more translucent appearance. Some of the perfusate containing collagenase was collected in a falcon tube to be used for further digestion of the heart.

Following the exhaustion of the collagenase buffer within the pump, the heart was taken off the apparatus. The heart at this point, was less elastic and showed signs of degradation. The atria were then excised and discarded. The ventricles of the heart were then minced and placed into the falcon tube containing the saved collagenase buffer. With the aid of a large pipette the ventricular tissue was subjected to mechanical breakdown through gentle upwards and downwards pipetting within the collagenase buffer to encourage further tissue digestion and dissociate the cardiomyocytes.

To assess the quality of the isolation at this stage a small sample suspension was viewed under an inverted microscope to visualise the cardiac myocytes and estimate cell viability based on the confluence of visible viable cells.

The contents of the falcon tube were then decanted through a nylon mesh into another falcon tube to remove undigested tissue debris. The debris were then transferred into more collagenase buffer to further digest the remainder of the cells that may not have separated yet and then these were then decanted

into another falcon tube. Both falcon tubes were then centrifuged (Eppendorf™ Centrifuge 5702/ 5702 R/5702 RH - Low-Speed Centrifuge) at 800 RCF for 2 minutes at 20°C. The supernatant retrieved from both tubes were then carefully aspirated and discarded. The pellet was then resuspended in the desired amount of restoration buffer (dependent on the required cell density) and combined into the same tube. This tube contained the resultant isolated cardiomyocytes. The calcium content of the sample was then raised by gradual addition of 34μl of 100mM calcium chloride solution (CaCl$_2$), every 3 minutes for a 15-minute period. The cell suspension was then ready for cell-based assays.

2.7 Cell culturing and incubation protocols

The isolated ventricular myocytes were resuspended in restoration buffer in a falcon tube and were incubated in a water bath 37°C. They were kept at that temperature to avoid excessive cooling prior to culturing.

In order to ensure minimal cross-contamination, cell work was conducted within a flow cabinet. The surfaces were also sprayed and wiped down with Industrial methylated spirit (70% IMS). In addition, any piece of equipment used within the fume hood was sprayed with 70% IMS solution as well.

The different drugs were then added unto the well plates still in the fume cupboard. The cells were then added from the falcon tube into the individual wells with the adequate amount for the required density. Following

successful sample addition gentle up and down pipetting was done to ensure adequate mixing of drug within the drug suspension. The well plates were then carefully taken to the incubator. The plates were placed into the 5% CO_2 incubator and set a temperature of 37°C.

The cells were allowed to incubate for 24 hours in their appropriate treatments. Upon completion of incubation the contents on each well were the transferred labelled Eppendorf tubes (1.5ml) ensuring cells that adhered to the bottom of the wells were dislodged by up and down pipetting. From this stage, the cells were then able to undergo fixation protocols which enables them undergo storage for longer or to have a variety of cell-based assays conducted with the cells.

2.8 H9C2 cell line culture and care protocol

2.8.1 Culturing

The cells were predominantly grown in T75 flasks & T175 flasks. The flasks were supplemented with modified DMEM (Dulbecco's Modified Eagle Medium) which contained 10% FBS (Foetal bovine serum) and 1% PEN-STREP (Penicillin streptomycin). The media within the flasks was changed every couple of days. During the week 12mls of fresh supplemented DMEM was added to the flasks and 15ml of media was added the Friday for over the weekend. The media was always changed on Monday.

2.8.2 Cell passaging

The cells were passaged when the cultures had achieved desired confluence. The media was aspirated off and then a solution of 0.05% trypsin/EDTA which had been warmed to 37°C was added to the flask with 3ml added to T75 flasks for 5 minutes 37°C. The trypsin was then aspirated off and then fresh trypsin was then added, and the flask was then incubated at 37°C for up to 5 minutes.

The flask was then observed under an inverted microscope to assess for cell dissociation from plate and soybean trypsin inhibitor was added to the flasks to inactivate the enzyme. The volume of the inhibitor was a 1:1 with trypsin in the flasks containing the cells or directly into the modified media. The cells were then aspirated from the flask and transferred to a 50ml falcon tube. The tube was then centrifuged for 5 minutes at 1300rpm.

The tube containing the cells were then retrieved from the centrifuge and then the supernatant was carefully aspirated off and discarded. The resultant pellet was then resuspended in supplemented DMEM media. Up and down pipetting was done to ensure complete resuspension however care was taken to avoid excess bubbling.

5ml per T75 flask was then transferred into the new flasks (T25 or T75 or T175). When flasks were passaged at the end of the week the volumes of supplemented DMEM media were doubled.
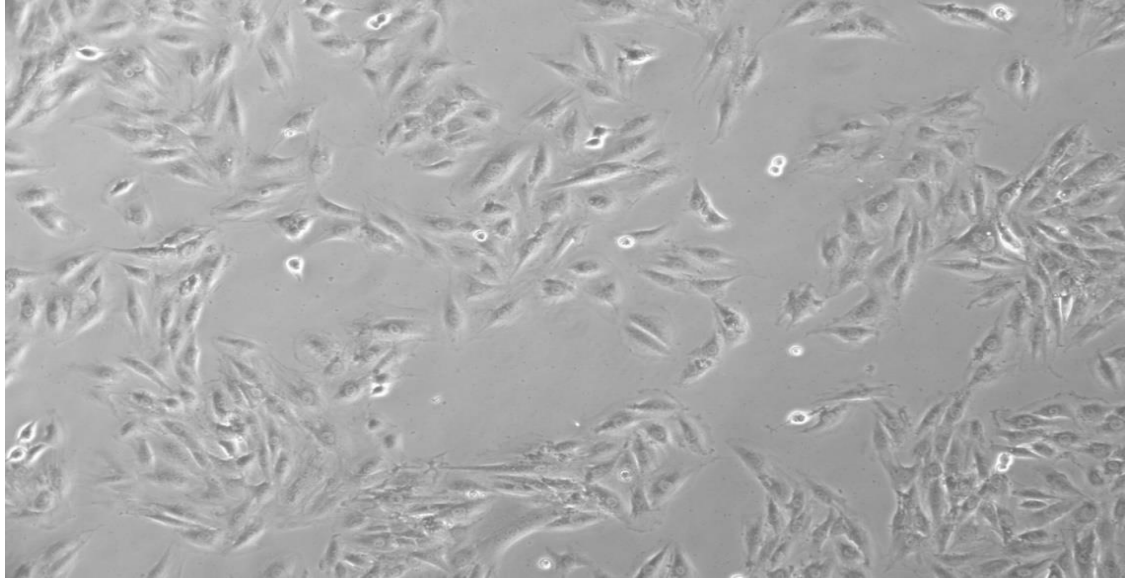
Figure 2.8.2.1 Image showing about 60% confluency when flasks were split into separate flasks
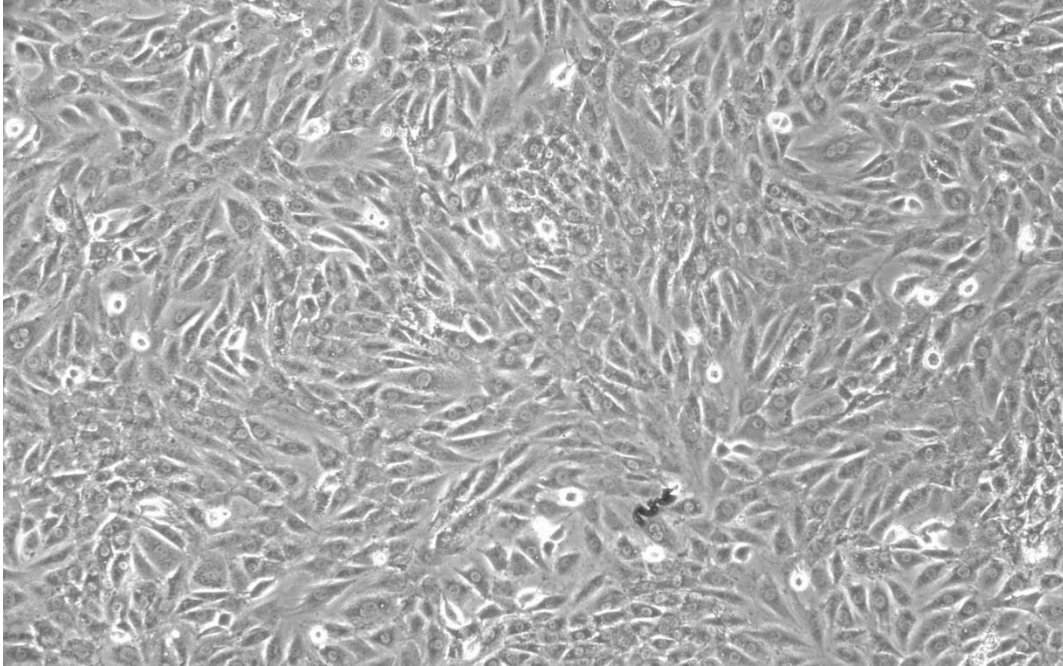
Figure 2.8.2.2 Image showing fully confluent flask

2.8.4 Cell Freezing

Generally, the contents of three fully confluent T75 flask into one cryovial and when the cryovial was thawed, this was usually done in a T75 flask.

Firstly, the media was aspirated from the flask and discarded. The flask was then washed with 5 ml of PBS and then discarded. Then 5ml of 0.05% trypsin/EDTA per T75 was allowed to be incubate at 37°C for up 5 minutes and longer if necessary.

3ml of soybean trypsin inhibitor was added to the flasks containing the dislodged cells to inactivate trypsin. The cells were then transferred into a 50ml falcon tube and was then centrifuged at 1300 rpm for 5 minutes.

The pelleted cells were then retrieved from the centrifuge and then the supernatant was aspirated carefully. The pellet was then resuspended in 1.5ml of freezing medium (70% media/20% FBS/ 10% DMSO which was kept for a week at most when neccesary but usually made fresh). The resuspended cells were then transferred into a cryovial. The cryovial was then transferred into a Nalgene freezing jar which contained room temperature isopropanol.

The freezing jar was then immediately placed into the -80°C storage and the cells were frozen at a rate of -1°C and precenting flash freezing. The samples were left overnight and were then the vial was transferred to a liquid nitrogen Dewar.

2.8.5 Thawing protocol

Firstly, a tissue culture flask (T75) with modified DMEM was placed into the incubator. Cells were warmed for about 2 minutes at room temperature and then transfer the cells into T75 tissue culture flask. The flask was then left for about 4 hours in the flask to allow enough time for the cells to reattach and assessed afterwards.

2.9 Cytotoxicity/Viability studies

The MTT (3-(4, 5-dimethylthiazol-2-yl)-2-5-diphenlytetrazolium bromide) cell proliferation assay kit (ab211091) purchased from Abcam, UK; was employed for the purpose of this study.

The kit provided a fairly straightforward measure of cell proliferation and viability. The fundamental basis for the assay was due to the conversion of water soluble MTT compound into the insoluble formazan product generated. Viable cells possess the ability to perform this conversion due to active metabolism while deceased cells by matter of fact do not perform active metabolism so are incapable of performing the conversion. The viable cells therefore produce this colour change resulting in a signal which acts as an indicator. The signal generated at absorbance OD 590 nm is proportional to the number of viable cells present (Abcam ab211091). Mitochondrial reductase takes part in the conversion process.

Assay protocol

The first step was the culture the cells unto well plates as required. The cell density per well for this study was about 1×10^5 per well. The cells were allowed sufficient time to adhere and reach confluency. This was dependent on the cell line in use but on average 2 days (48 hours) was allowed for all the wells to reach optimal confluency. The following day, the wells had old media discarded and replaced with fresh media and left at 37°C incubation for an hour. This was to ensure cell debris or any cells which were not healthy were removed to limit the chance of interfering with results.

The plates were then inoculated with the appropriate drug treatment and incubated for 24 hours. An automatic pipette was used to remove and replace media and was set to the "low" to ensure minimal disturbance to the cells.

Following the incubation period (24 hours), the media containing the drug treatment was carefully aspirated and discarded. The wells were washed twice carefully with sterile PBS and then directly inoculated with the MTT reagent with serum free media (1:1 ratio). The volume of reagent used was dependent on the plate size used. The cells were then incubated in dark condition at 37°C for 3 hours to allow the viable cells absorb the MTT reagent. After the incubation period, the MTT reagent + Media was then discarded and replaced with 100% DMSO to lyse the cells and then transfer the plate to the orbital shaker for 10 minutes to ensure complete cell lysis.

Upon completion of lysis, the plate was then transferred to the plate reader and absorbance measured at OD590 nm. The data generated was then used to determine the percentage viability. The formula below provides a description of how the data was interpreted.

Normalised absorbance reading = Mean absorbance value **minus (-) ** Mean absorbance of cell free medium

Percentage cytotoxicity (%) = (Control (Untreated)/ Sample absorbance) x 100

2.10 Cell viability assessment by Abcam™ Annexin V-FITC apoptosis detection kit

This kit was selected as it's a more reliable and accurate method of assessment of viable cells. The assays function is reliant on the observation that cells upon initiation of apoptosis, translocate their membrane phosphatidylserine (PS) from its usual location on the inner side of the plasma membrane to being presented externally on the cell surface. When the PS becomes exposed, staining and detection becomes a lot less challenging with a target present on the cell surface. Detection with a fluorescent conjugate of annexin V which possess a high affinity for binding to PS becomes feasible.

Protocol

Similar to all the other studies, the cells were firstly added to the plates at a density of $1\text{-}5 \times 10^5$ per ml. 12 well plates were used for the purpose of this study. The plates were allowed 48 hours for all the wells to reach optimal confluence. On the day the experiment was to be carried out, fresh media was added to the plates about an hour prior to drug administration for the same reasons that were stated during the MTT protocol. The well plates were then inoculated with the different drug treatments and allowed to incubate for 24 hours.

Following the incubation, the cells plate was then taken out of the incubator and transferred into a laminar flow cabinet where the rest of the protocol was carried out.

It was important to note that due to the cells being adherent in nature, the cells required trypsinisation for detachment from the plate. Other studies have suggested using cell scrapers for mechanical detachment; however, these could damage viable cells so was not recommended for more delicate cell lines.

After the plate had been transferred to the hood, the first step was to remove the treatment containing media. The next step was to wash the cells twice with sterile PBS. The trypsin was then added to each well (about 100µl should provide sufficient well base coverage) and the plate was then transferred back into the incubator for 5 minutes.

After 5 minutes, the plates were inspected under a microscope for maximal cell detachment. Equal volume of supplemented media (100µl) to inactivate the trypsin and the contents of each well was then transferred into a labelled Eppendorf tube. The cells were then pelleted in a cold centrifuge (200-300 X g for 5 minutes). The supernatant was then discarded. The pelleted cells were then resuspended in 500µl of 1 X binding buffer.

To each of the Eppendorf tubes, 5 µl of annexin V-FITC and 5 µl of propidium iodide (for necrotic studies) was added. The samples were then kept in the

dark at room temperature for 5 minutes. Upon completion of this 5-minute incubation, the samples were then ready for analysis using the BD Accuri™ C6 Plus personal flow cytometer.

For analysis on the flow cytometer, the samples were analysed using the FL1 channel for the Annexin V-FITC and for the Propidium iodide staining the FL2 channel.

2.11 Cleaved Caspase-3 activity

As discussed previously, caspase activation is a distinctive indicator of the initial stages of the apoptotic process (Walsh et al. 2008). Caspase 3 along with caspase 6 & 7 are downstream effector caspases (Walsh et al. 2008; McIlwain et al. 2013).

Cleaved caspase-3 (Asp175 from cell signalling) secretion indicates apoptosis. Assessment of Caspase activation was employed as a measure for number of cells undergoing apoptosis. Staining procedure was carried out as recommended as per kit manufacturer's protocol (Cleaved Caspase-3 (Asp175) Antibody #9661).

The cells in this assay could be fixed as there was not a requirement for the cells to be viable during flow cytometric analysis. The cells were fixed and made permeable and made into single cell suspension prior to analysis with the BD Accuri™ C6 Plus personal flow cytometer.

Protocol

Firstly, cells were seeded to plates with a density of about 1×10^5 per ml. Again 24 well plates were used generally. The plates were allowed about 48 hours for each well to reach optimal confluence. On the day of treatment, the media in each well was replaced with fresh media at least an hour prior to drug administration. The plates were then inoculated with the appropriate treatments and left to incubate at 37^0C for 24 hours.

Following the incubation periods the media was aspirated and discarded. The cells were then washed twice with sterile PBS. 100μL of trypsin was then added to each well and the plate was then transferred to the incubator for 5 minutes until full cell layer detachment. Equal volume of media was added to inactivate the trypsin and the contents of each well were added into labelled eppendorf tubes. The tubes were then spun at 300g for 5 minutes to pellet the cells.

The supernatant was removed and discarded. The cells were then resuspended in 100μL 4% formaldehyde solution per 1 million cells. Ensure thorough mixing to completely dissociate pellet and prevent cross-linking of individual cells. The samples were then allowed to fix for 15 minutes at room temperature. After the incubation period, the samples were then washed in excess PBS (approximately 200 μl) and pellet. It is imperative to discard

formaldehyde in appropriate waste discard. Resuspend cells in 0.5-1 ml of 1 X PBS. The cells could also be stored overnight in excess PBS at 4^0 C.

For permeabilization, ice cool 100% methanol was added slowly to precooled cells, with intermittent vortexing to produce a final methanol concentration of 90%. The samples were then left to permeabilize for at least 10 minutes while kept on ice. The cells could then be stored at – 20 ^{0}C or could be carried further for immunostaining.

Cells were counted and aliquoted desired number of cells into tubes (approximately $5x10^5$). The cells were then washed in excess PBS to remove methanol and the resultant methanol supernatant solution was discarded appropriately. The pellet was then resuspended in 100μL of diluted primary antibody solution (Cleaved caspase-3 antibody dilution buffer based). This was then allowed to incubate for 1 hour at room temperature. The samples were then washed in 1 x PBS pelleted and washed again for a second time. The samples were then resuspended in the secondary antibody solution (Alexa Flour® conjugate) which was also prepared in antibody dilution buffer. This was then allowed to incubate for 30 minutes at room temperature in dark condition. The samples were then washed 2 times in 1 x PBS. The pellet was finally resuspended in 500 μl of 1 x PBS ready for analysis on the BD Accuri™ C6 Plus personal flow cytometer.

2.12 MitoSOX™ Red Mitochondrial superoxide indicator assay.

Superoxide is the reactive oxygen species by-product which is generated through the mitochondrial respiratory chain (Robb et al 2015). Produced from respiratory complexes, it enacts a crucial role in mechanisms of oxidative stress and redox signalling (Robb et al 2015). These contribute to Superoxide generation being considered an indicator oxidative damage in numerous pathologic conditions and damage to the cardiovascular system.

Protocol

As was the case with the other assays, the cells were seeded on plates with a density of 1×10^5 cells per ml. The plates were allowed 48 hours to reach full confluency. Media was changed at the end of day both days. On the day of running the assay, fresh media was added prior to drug administration. The plates were then inoculated with the appropriate treatments and left to incubate at 37^0C for 24 hours.

The following day, the treatment media was then discarded. The adherent cells were then washed twice with phenol free media twice and not PBS to ensure signal stability. The cells were then covered with 300-500µl of 5µM solution of mitochondrial superoxide red (MitoSox™ reagent). Original stock solution (5mM stock in DMSO) of mitosox red was reconstituted in DMSO, however working (5 µM) solution was diluted in media. The plates were

incubated for 20-25 minutes at 37^0C covered from light. Following the incubation period, the mitosox reagent was carefully aspirated off and transferred to the Epoch 2 microplate spectrophotometer (Biotek UK). The absorbance was then measured between 510/580nm wavelengths.

2.13 Fluo-3AM calcium signalling indicator

Disruptions in calcium signalling and homeostasis could contribute towards apoptosis, with increases in Ca^{2+} a hallmark of early and late stage apoptotic pathway (Pinton et al 2008).

Protocol

As was the case with the other assays, the cells were seeded on plates with a density of 1×10^5 cells per ml. The plates were allowed 48 hours to reach full confluency. Media was changed at the end of day both days. On the day of running the assay, fresh media was added prior to drug administration. The plates were then inoculated with the appropriate treatments and left to incubate at 37^0C for 24 hours.

The treatment media was discarded, and the cells were trypsinised and transferred into eppendorf tubes. The trypsin was then inactivated with equal volume of modified media. The cells were then pelleted in a cold centrifuge (100-300g for 5 minutes at 4°C). Pellets were then resuspended in 1ml of 5µM Fluo-3, AM, Calcium Indicator solution and incubated for 30 minutes

37°C. Following this the cells were then washed twice and resuspended in 1ml 1 X PBS. The samples were than analysed on the BD Accuri™ C6 Plus personal flow cytometer set to count 5000 cells.

2.14 Data analysis

Data were expressed as mean ± SEM and graphs and charts were produced on GraphPad prism (version 9, GraphPad software, inc. USA). Data analysis was conducted using one-way ANOVA with LSD post hoc test or student t-test between 2 groups were compared on SPSS (IBM, USA) software.

Chapter 3: ALK Inhibitor Crizotinib Induces Myocardial Injury

3.1 Abstract

The treatment of cancers with tyrosine kinase inhibitors has been linked to increased risk of adverse cardiovascular events. Crizotinib treatment has been linked with acute QT prolongation and dysrhythmias. Concentration dependent crizotinib induced cardiotoxicity was evaluated in naïve male Sprague Dawley rats and cardiac myoblasts.

Isolated langendorff perfused hearts were treated with different concentrations of crizotinib (10nM, 0.1, 1 and 10µM) and haemodynamic performance and infarct development were assessed. Left ventricular tissue samples were analysed for p-AKT expression by western blotting. H9C2 cardiac myoblasts were assessed for viability, and cleaved caspase-3 expression. H9C2 myoblasts were assessed for superoxide generation and increases calcium ion detection.

Crizotinib 1µM treatment impaired LVDP significantly compared with non-treated controls. Crizotinib 1µM treatment induced significant infarct development and significantly decreased cardiac myoblast viability also compared to non-treated controls. Crizotinib 1µM significantly increased cleaved caspase-3 expression, superoxide generation and calcium ion detection when compared with non-treated control samples.

This study shows that tyrosine kinase inhibition with crizotinib causes significant dysfunction to the myocardium and cardiac myoblasts.

3.2 Introduction

Despite their intended targeted nature, tyrosine kinases inhibitors are often selective for multiple targets (Crizotinib is selective for ALK, MET and ROS1 receptors), which often brings effects on non-malignant cells culminating in on- and off- target toxicities (Costa et al. 2015; Srikanthan et al. 2015). There are a number of cardiac specific toxicities associated with tyrosine kinase inhibitor (TKI) treatment, some of which include; hypertension, congestive heart failure, left ventricular systolic dysfunction, acute coronary syndromes and QT prolongation (Chaar, Kamta, and Ait-Oudhia 2018a; Lamore et al. 2020). Owing to the broad patient eligibility for TKI treatment, as well as the ease and effectiveness of treatment contributing towards improved patient survival; the emergence of increased risk of cardiovascular events is of clinical importance (Khakoo and Yeh 2008).

There are a number of Tyrosine kinase receptors, with involvement in pathways regulating a number of cellular processes such as cell proliferation and survival (Will et al. 2008). Mutations within these receptors in malignant cells leads to overexpression and constitutive activation of said receptors which could result in over signalling further leading to increased cellular proliferation, angiogenesis and apoptotic inhibition promoting malignant phenotype (Orphanos, Ioannidis, and Ardavanis 2009). Tyrosine kinase inhibitors were designed to inhibit the activity of these overactive kinases and are employed heavily in the treatment of malignancies (Chu et al. 2007).

Inhibition of these kinases combats the dysregulation in cellular homeostasis observed in malignant conditions (Lamore et al. 2020). Crizotinib is a tyrosine kinase inhibitor that is selective for anaplastic lymphoma kinase (ALK) and effective against tumour growth and possess good pharmaceutical properties (Cui et al. 2011; Toyokawa and Seto 2014). There are limited studies published detailing crizotinib induced cardiotoxicity, however, following post treatment monitoring programs and during clinical trials, the most common symptoms observed are QT interval prolongation and bradycardia (Lamore et al. 2020; Tartarone et al. 2015b).

Interestingly, not all TKIs that target one specific kinase exert the same cardiotoxic effects, with this occurrence usually the result of off-target effects due to their often multi kinase selectivity (Lamore et al. 2020). TKIs bind to receptors on non-malignant cells resulting in undesired side effects such as above discussed cardiotoxicity (Chu et al. 2007). Certain kinases crucial for tumorigenesis could be critical in the maintenance of normal function in cardiomyocytes as well as the maintenance of associated vasculature ultimately resulting in cardiotoxicity through the inhibition of such kinases (Lamore et al. 2020).

Tyrosine kinase inhibitors main mechanism of action against malignant cells is to block target receptor sites (such as anaplastic lymphoma kinase in the case of crizotinib) on malignant cells inhibiting activation of associated

survival and proliferative signalling pathways (Dl, H, and Lx 2014). Figure

3.2.1 below provides an outline of the ALK signalling pathway.
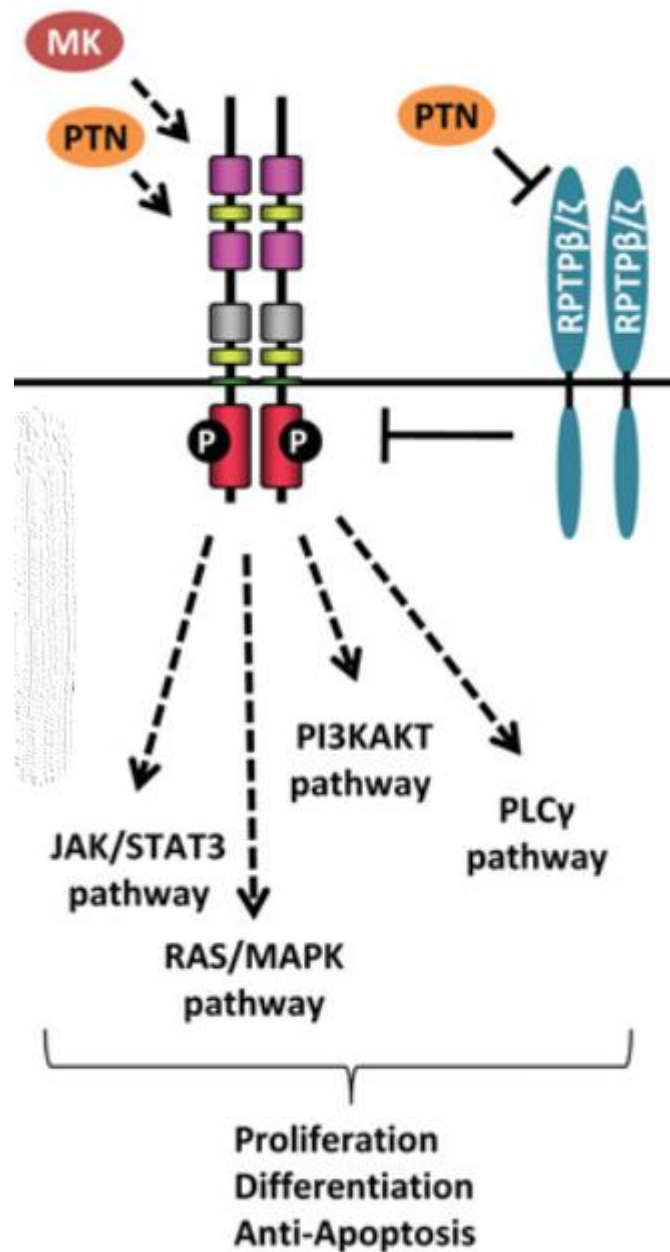
Figure 3.2.1 The anaplastic lymphoma kinase signalling cascade; ligand binding activation during normal conditions. ALK signalling is normally activated by ligand midkine (MK) which is a member of the pleiotrophin

(PTN) family. Constitutive activation during malignant conditions stimulates over-phosphorylation of the kinase leading to activation of PI3K/AKT, MAPK/ERK, & STAT3 pathways. All of which promote cancer proliferation, survival and ultimately metastasis [Adapted from (Palmer et al. 2009)].

Members of the tyrosine kinase inhibitor family of drug molecules have been implicated with cardiotoxicity. For instance, HER2 and epidermal growth factor receptor inhibitor lapatinib was associated with a decline in mean left ventricular ejection fraction in the studied patient pool during the analysis of the cardiac safety of lapatinib (which comprised of individuals that received lapatinib treatment between January 5, 2001 & September 30, 2006), however the decrease observed in these individuals was concluded to be either partial or fully reversed within 7.3 weeks (Perez et al. 2008). Similarly, sunitinib induces inhibition of angiogenesis via blockade of the vascular endothelial cell growth factor receptors (VEGFR) was associated with an increased likelihood of occurrence of congestive heart failure (CHF) (Chu et al. 2007). The study conducted by Chu et al. (2007), reported that 11% of the individuals treated with sunitinib developed either CHF or left ventricular ejection fraction decline of greater than 20% (≥20%) (Chu et al. 2007).

Similarly, trastuzumab is a monoclonal antibody attributed with displaying on target cardiotoxicity due to tyrosine kinase inhibition (Chen, Kerkelä Risto,

and Thomas 2008). Its action is facilitated through binding to the HER2 (human epidermal growth factor receptor 2) protein (Gutierrez and Schiff 2011). Its mechanism of actions include inhibitory activity on intracellular signalling, angiogenesis, ECD cleavage (extracellular domain of the HER2 receptor), as well as increased degradation of intracellular HER2 and the upregulation of antibody dependent cytotoxicity (Codony-Servat et al. 1999; O'Sullivan and Smith 2014). Cardiotoxicity of trastuzumab presents most frequently as declines in ejection fraction (Pinto et al. 2013). Activation of HER2 in cardiomyocytes activates ERK & PI3K/AKT pathways which play key roles in cardiomyocyte proliferation during development and survival in adulthood (Kuramochi, Guo, and Sawyer 2006; Zhao et al. 1998). Additionally, activation of the HER2 by neuregulin's (Nrg-1) activates the Src/focal adhesion kinase pathway which enhances cardiac contractility & blockage of this pathway (with trastuzumab) aggravates left ventricular dysfunction (Kuramochi, Guo, and Sawyer 2006; Zhao et al. 1998). This appears to suggest HER2 inhibition contributes to dysfunction and ultimately death in normal cardiomyocytes (Chen, Kerkelä Risto, and Thomas 2008). Trastuzumab blocks downstream signalling in the HER2 pathway (Figure 3.2.2) & crucially reverses the inhibition of Bad which facilitates activation of bax, cytochrome c release and ultimately apoptosis (Chen, Kerkelä Risto, and Thomas 2008).
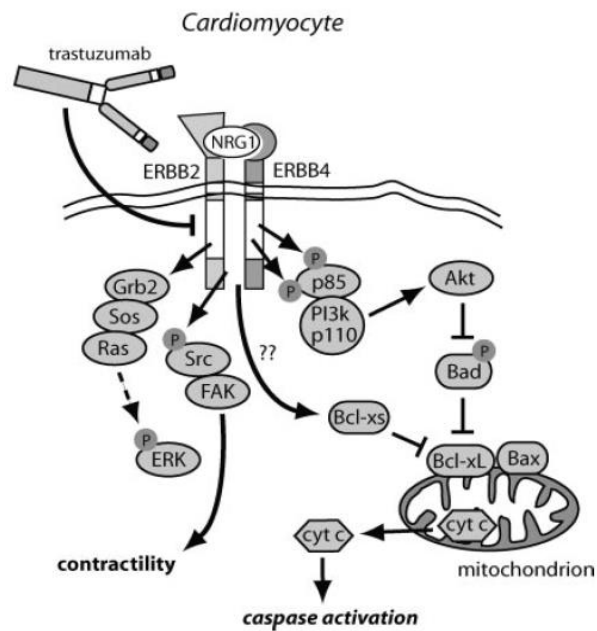
Figure 3.2.2 Mechanism of Trastuzumab induced cardiotoxicity; Inhibition of ERBB2(HER2) by Trastuzumab reverses Bad inhibition in turn activates Bax ultimately resulting in cytochrome c release and caspase activation initiating the apoptotic process in cardiomyocytes [Adapted from (Chen, Kerkelä Risto, and Thomas 2008)].

Imatinib mesylate is a small-molecule inhibitor of the fusion protein Bcr-Abl for the treatment of chronic myelogenous leukaemia (Kerkelä et al. 2006b). In some rare instances, imatinib treatment was associated with heart failures (Kerkelä et al. 2006; Park et al. 2006). Imatinib was also previously linked with declines in ventricular function accompanied with myocardial tissue wasting which was concluded to be indicative of cardiomyocyte loss (Chen, Kerkelä Risto, and Thomas 2008). Imatinib has also been shown to induce cell

death in cultured mouse cardiomyocytes and features hallmarks of both apoptosis and necrosis (Kerkelä et al. 2006). Combining data from myocardial biopsies retrieved from individuals that developed left ventricular dysfunction and mouse tissue from wild-type C57BL6 mice treated with imatinib mesylate (Kerkelä et al. 2006). Combining. Imatinib toxicity was attributed to the induction of endoplasmic reticulum (ER) stress response which is also referred to as the unfolded protein response (Ron and Walter 2007). Sustained stress caused by imatinib within cardiomyocytes ultimately initiates cell death processes (figure3) (Pattacini et al. 2004).
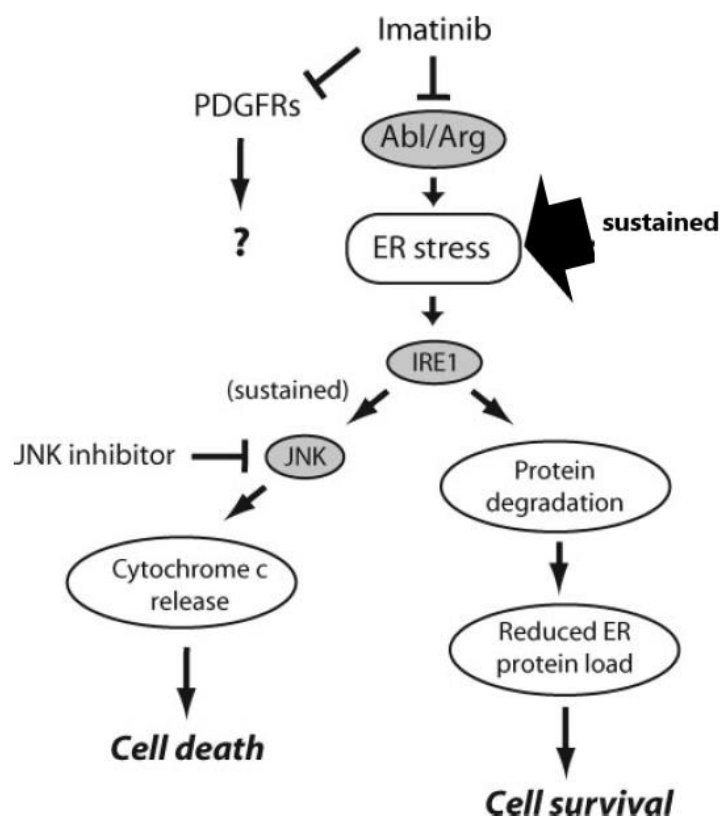
Figure 3.2.3 Mechanism of imatinib induced cardiotoxicity. Imatinib inhibition of Abl/Arg initiates ER stress. This leads to activation of

protein kinase IRE1 and under sustained ER stress IRE1 activates JNK which initiates intrinsic apoptotic pathways and ultimately cell death [Adapted from (Chen, Kerkelä Risto, and Thomas 2008)]

Imatinib induced cardiotoxicity as mentioned previously involves apoptotic and necrotic features in cardiomyocytes (Kerkelä et al. 2006). This provides justification assessment of cell death pathways linked with crizotinib treatment. Additionally, ER stress response occurs within mitochondria which in turn leads to release of cytochrome c release initiating apoptosis. Cleaved caspase 3 which has served as an indicator of apoptosis is implicated in Nilotinib cardiotoxicity (Doherty et al. 2013; Ma et al. 2020). Similarly, sunitinib treatment has been associated with increased caspase3/7 activation (Ron and Walter 2007). Nilotinib as well has been associated with ER stress and ROS accumulation suggestive of mitochondrial dysfunction or impairment in cardiomyocytes (Lekes et al. 2016; Ma et al. 2020).

A few tyrosine kinases have been studied extensively and the general consensus is cardiotoxicity is not often attributed to one direct action or singular mechanism, rather on- and off- target kinase inhibition is the likely cause (Chaar, Kamta, and Ait-Oudhia 2018b). For instance, sorafenib which inhibits the VEGFR pathway to halt angiogenesis and vasodilatory action, directly leads to increased vascular resistance & hypertension as observed in research involving bevacizumab (Syrigos et al. 2011). This may not directly

damage the heart it may serve as a precursor to more severe cardiac conditions occurring (Syrigos et al. 2011). Sorafenib treatment was credited with cardiotoxicity linked with mitochondrial impairment when the effects multitargeted tyrosine kinase inhibitors treatment on isolated rat heart mitochondria and H9C2 cells were assessed. Out of the four TKI's (imatinib, dasatinib, sunitinib and sorafenib), only sorafenib induced direct impairment of mitochondrial function which contribute towards its cardiotoxicity (Schneider et al. 2018; Will et al. 2008).

The intention behind this study was to assess the cardiotoxic effects associated with crizotinib treatment on the cardiovascular system. Preclinical findings on crizotinib included an observed decrease in heart rate and increase in left ventricular end-diastolic pressure in canine studies and myonecrosis (cardiac muscle necrosis) in rats (Cross et al. 2015). Previous clinical studies reported the Cmax for Crizotinib to be observed around 0.73 – 1.06μM during in vitro studies involving human cardiomyocytes (Doherty et al. 2013). Prior articles have also linked crizotinib treatment with asymptomatic sinus bradycardia (Ou et al. 2013). The exact mechanism for crizotinib cardiotoxicity is not fully known however, ROS accumulation, apoptosis and increased synthesis of cholesterol have been proposed as possible mechanisms which contribute to perceived cardiotoxicity (Doherty et al. 2013).

ROS mediated oxidative stress occurs as a result of imbalance between ROS generation and failure of systemic mechanism to effectively eliminate the radicals leading to accumulation (Zhang et al. 2019). Reactive (ROS generation) free radicals interfere with a number of physiologic processes such as protein oxidation, restrict glycolysis and impairment of myocardial energy metabolism and cardiac function (Deres et al. 2005). Tyrosine kinase inhibitor treatment has been associated with induction of mitochondrial dysfunction, uncoupling components of electron transport chain and increased ROS generation (Rodríguez-Hernández et al. 2020).

Increased ROS generation is closely related with increased Ca^{2+} due to interesting cross talk between both in which both fuel the increase of each other (Bertero and Maack 2018; Görlach et al. 2015). Tyrosine kinase inhibitor treatment has been associated with ROS generation and Ca^{2+} disturbances as one of their mechanisms of their cardiotoxicity (Coriat et al. 2012; Kawabata et al. 2015). In a study conducted in HepG2 cells, exposure to sorafenib for 24 hours, there was an increase in ROS generation and a decrease in mitochondrial membrane potential (Paech et al. 2018). Similarly, sorafenib treatment was associated with increased rapid mitochondrial ROS generation and mitochondrial calcium overload in a study to assess apoptotic cell death in radiotherapy resistant Hep G2 cells detected by confocal microscopy (Chiou et al. 2009). Assessment of mitochondrial superoxide

would be a useful target to determine if oxidative stress was associated with cardiotoxicity induced by crizotinib.

In this current study, crizotinib induced cardiotoxicity was assessed using the isolated perfused rat heart model. Naïve-non stressed hearts were treated for 175 minutes during which functional parameters (Left ventricular developed pressure, heart rate and coronary flow) were measured and recorded. Additionally, infarct to risk analysis was employed to assess infarct size (%) following treatment.

Again, the exact mechanisms for crizotinib induced cardiotoxicity are unclear, it was important to consider some hallmark signalling proteins as a means to identify pathways implicated in perceived crizotinib cardiotoxicity. Activation of apoptotic protease caspase 3 has been documented in previous anticancer agents linked with cardiotoxicity such as doxorubicin and sunitinib (Ichihara et al. 2007; Ueno et al. 2006). Serum starved primary cultured cardiomyocytes from neonate Sprague Dawley rats and *in vivo* Sprague Dawley rats were treated with doxorubicin for 5 weeks. Dox treatment was associated with significant increase in caspase-3 activity in both *in vivo* and *in vitro* study arms compared to the controls (Ueno et al. 2006). Therefore, the expression of activated caspase 3 (cleaved caspase) could be a key marker to assess for crizotinib induced cardiotoxicity.

Cell death is often a key contributor to drug induced cardiotoxicity with apoptosis and necrosis regularly implicated (Galluzzi et al. 2018; Ma et al. 2020). In sunitinib induced cardiotoxicity, oxidative stress induced impairment to mitochondria initiates apoptosis in cardiomyocytes (Bouitbir et al. 2019b; Ma et al. 2020). Sunitinib treatment on H9C2 myoblasts and male C57BL/6NRj mice was associated with significant increases in caspase 3 activity (Cleaved-caspase 3), increased mitochondrial hydrogen peroxide leakage (product of superoxide breakdown), free radical release and ROS accumulation (Bouitbir et al. 2019). Similarly, suppression of the electron transport chain complexes by sunitinib induces ROS (superoxide) accumulation, which leads to a decrease in mitochondrial membrane potential damaging the mitochondrial structure and initiates caspase cascade leading to apoptosis (Ma et al. 2020).

Similarly, induction of oxidative stress by imatinib treatment inducing mitochondrial dysfunction ultimately activating caspases 3/7/9 through JNK-related mitochondrial signalling (Chambers et al. 2017). In a study to assess the role of the mitochondrial scaffold sab, in mitochondrial dysfunction in imatinib-induced cardiotoxicity (Chambers et al. 2017). H9C2 myoblasts treated with imatinib mesylate was associated with mitochondrial dysfunction, increased mitochondrial superoxide generation, and significant impairment of ATP production (Chambers et al. 2017). These agents induce apoptosis through mechanisms involving mitochondrial impairment through

oxidative stress. Conversely, nilotinib induces apoptosis through activation of JNK which inhibits phosphorylation of Akt which ultimately results in apoptosis further downstream originating from induction of ER stress (D. Lekes et al. 2016; Yang et al. 2018). Akt (figure 3.2.4) is the crucial downstream signal of the PI3K signalling cascade with its phosphorylation regulating cell survival and proliferation through inhibition of pro-apoptotic transcription factors such as Bad and Foxo (Nitulescu et al. 2018).
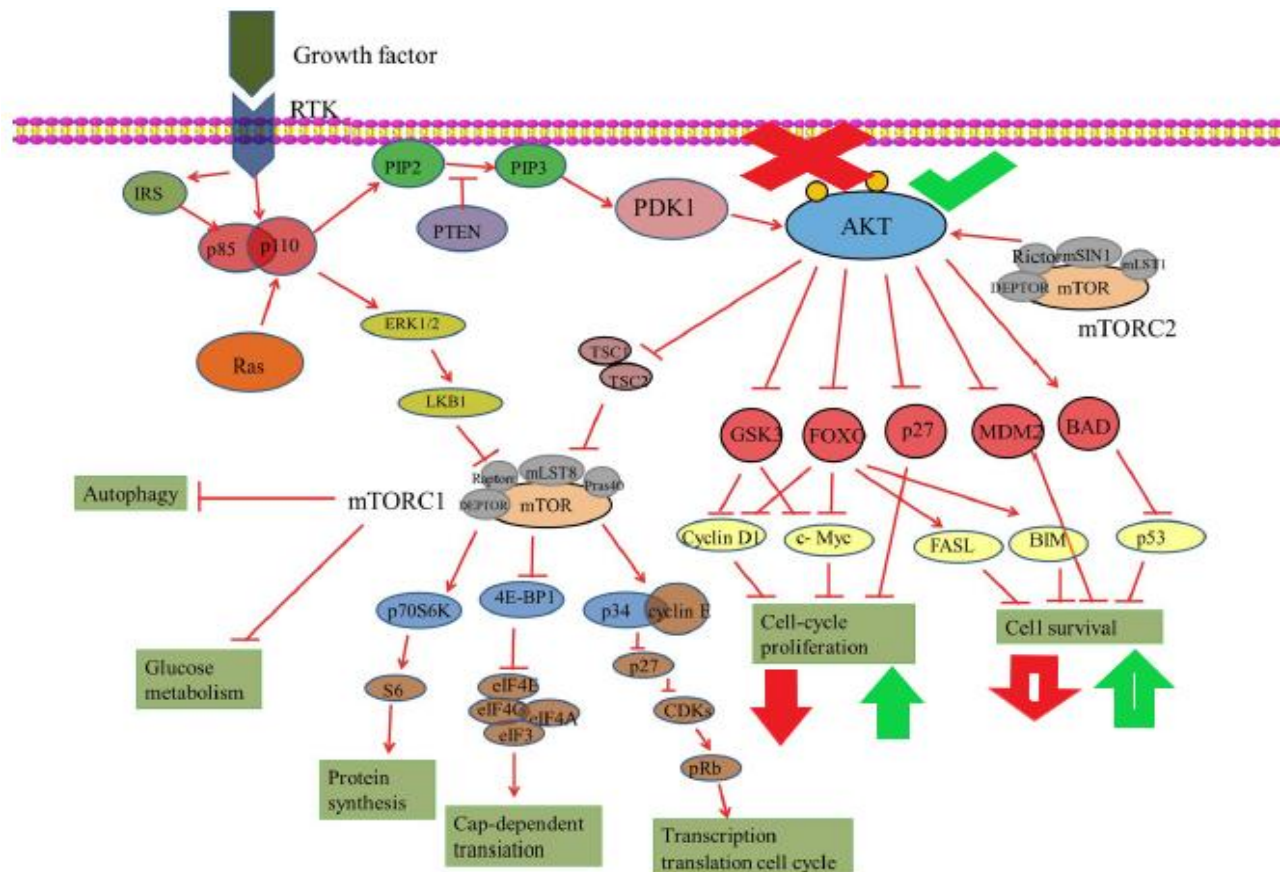
Figure 3.2.4 General overview of PI3K/AKT/mTOR signalling pathways; with green arrows indicative of processes upregulated when AKT

phosphorylation is upregulated while red arrows indicative of processes down regulated by AKT inhibition [Adapted from (Xu et al. 2020)].

The role of Akt in the PI3K signalling cascade is crucial as its phosphorylation contributes to proliferation and survival in cardiomyocytes (Holla et al. 2017) . Akt inhibition activates pro-apoptotic factors leading to cell death (Xu et al. 2020). Its inhibition which occurs through tyrosine kinase inhibition acts as an initiator of cell death via apoptosis (Montaigne, Hurt, and Neviere 2012).

Cell death originating or perpetuated by mitochondrial impairment has been associated with TKIs mentioned previously like with the case with sunitinib & imatinib (Bouitbir et al. 2019; Chambers et al. 2017; Ma et al. 2020). During the multiparameter *in vitro* testing of tyrosine kinase inhibitors, crizotinib and nilotinib treatment on isolated human cardiomyocytes for 72 hours, was associated with apoptosis as the cultures showed an increase in activation of caspase 3/7 suggestive of apoptotic involvement (Doherty et al. 2013).

Similarly, during assessment of tyrosine kinase induced mitochondrial damage, ponatinib, rogafenib and sorafenib treatment were associated with early apoptosis and increased cytosolic cytochrome c detection (Paech et al. 2018). In a study to evaluate cardiotoxicity of TKI imatinib, the results were suggestive of necrotic damage (Kerkelä et al. 2006). Cardiomyocytes were obtained from C7BL6 mice treated with imatinib for between 3 to 6 weeks

and assessed. Cytosolic vacuoles observed along accompanied with increased propidium iodide absorption due to loss of integrity were detected (Kerkelä et al. 2006). A study conducted in BV173 (established leukemic cell line from patient with chronic myelogenous leukaemia lymphoid blastic crisis) and K562 (from a patient with chronic myelogenous leukaemia erythroid blastic crisis) showed caspase inhibition did not attenuate imatinib induced cell death and the presence of DNA fragmentation and DNA decrease suggested necrosis (Okada et al. 2004).

Increased mitochondrial membrane permeabilization brought about by increased calcium overload & oxidative stress was considered a hallmark of apoptotic death (Montaigne, Hurt, and Neviere 2012a). However, severe sustained stress on the mitochondria results in ATP depletion and cardiomyocyte will undergo necrosis (Baines 2009). Sustained oxidative stress and mitochondrial calcium overload aggravates membrane permeability transition in mitochondria resulting in potential (membrane) dissipation, osmotic breakdown of membranes, organelle dissociation and cellular swelling ultimately resulting in necrotic death (Galluzzi et al. 2018; Izzo et al. 2016; Ma et al. 2020). Activation of ER stress and the unfolded protein response by tyrosine kinase inhibition affects expression of key proteins associated with mitochondrial function & pathways which regulate cell metabolism and death (Rodríguez-Hernández et al. 2020b)(Figure 3.2.5).
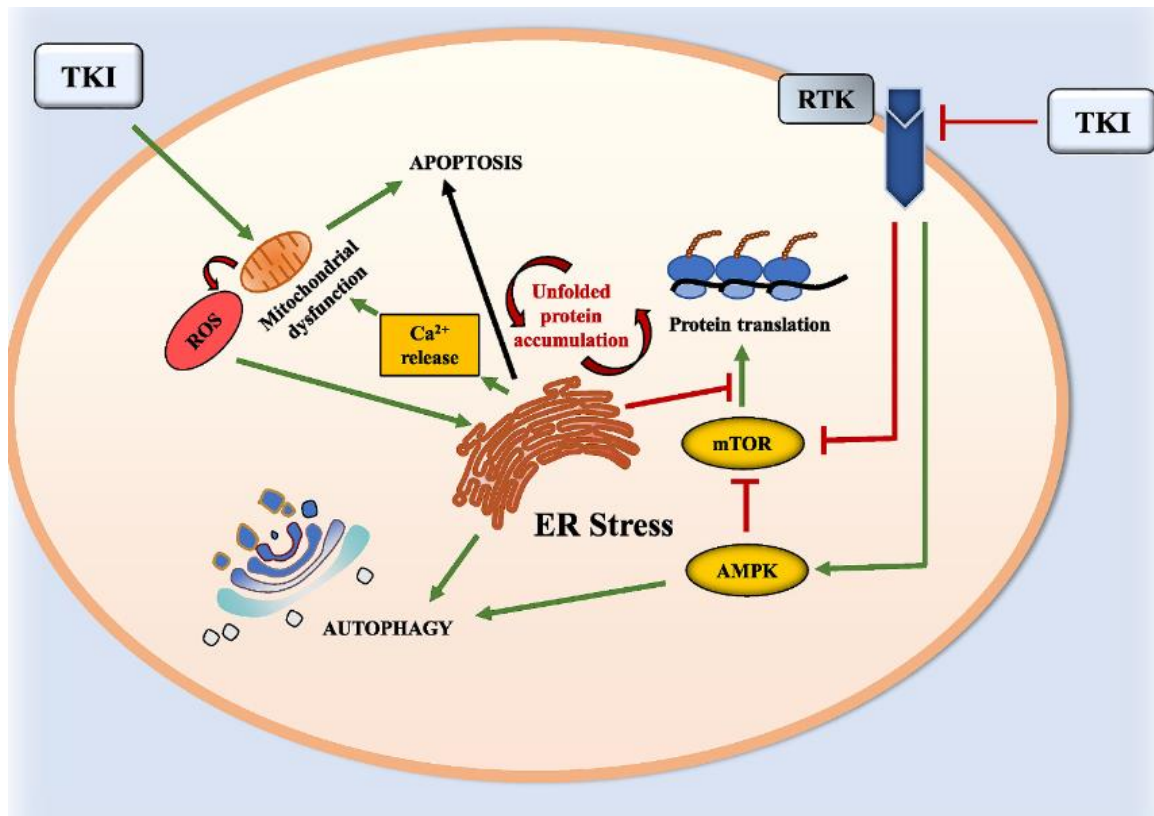
Figure 3.2.5 Tyrosine kinase mediated activation of ER stress. Downstream activation of unfolded protein response, increased Ca2+ release which results in mitochondrial dysfunction and ROS generation further contributing to ER stress & apoptosis [Adapted from (Rodríguez-Hernández et al. 2020)].

The aims of the project outlined in this chapter were to assess the cardiotoxic properties of crizotinib in in-vitro whole heart model and cellular models. The effects of a set of crizotinib concentrations would be assessed on cultured H9C2 cells for cytotoxicity and the haemodynamic performance of a langendorff isolated perfused heart as well as assessing myocardial injury. Additionally, left ventricular tissue will be collected to assess AKT protein

expression levels. Furthermore, the expression of cleaved caspase 3, mitochondrial superoxide and calcium overload was assessed in the cultured H9C2 cells.

3.3 Materials and Methods

3.3.1 Materials

Crizotinib was purchased from Carbosynth limited (UK) and dissolved in dimethyl sulphoxide to a stock solution of 10mM prior to storage at -20 °C. krebs-Henseleit buffer (KH) salts (118.5 mM NaCl, 25 mM NaHCO$_3$, 4.8 mM KCl, 1.2 mM MgSO$_4$, 1.2 mM KH$_2$PO$_4$, 1.7 mM CaCl$_2$, and 12 mM glucose), were purchased from Fischer scientific(UK). The antibodies anti-rabbit antibody for phospho-Akt at Ser473 (Cell Signalling), Akt (pan) (11E7) Rabbit mAb (cell signalling) as well as anti-biotin and anti-rabbit IgG were purchased from cell signalling. Triphenlytetrazolium chloride (TTC) was purchased from Sigma Aldrich, UK. DMEM (Dulbecco's modified eagle medium) which was purchased from ThermoFisher scientific ™. Penicillin streptomycin (10,000 U/mL) purchased from Gibco ™. Foetal bovine serum (FBS) purchased from Gibco ™. Phosphate buffer saline was purchased from Gibco ™.

3.3.2 Animals and ethics

Adult male Sprague-Dawley rats with body weight range between 350±50 grams were purchased from Charles River UK limited (Margate, UK) were used for the purpose of this study (Ethics number P66861). Animals were

kept in humane conditions, suitably housed, and had free access to standard pellet diet. Handling and treatment procedures were in full accordance with the Guidelines regarding the operation and handlings of Animals (Scientific Procedures Act 1986). Animals were selected at random for drug treatment. Tissue collected for infarct analysis were blinded and stored for later analysis.

3.3.3 Langendorff isolated perfused heart preparation

Adult male Sprague-Dawley rats were humanely sacrificed by cervical dislocation and the hearts were quickly excised and placed in ice-cool KH buffer. The rat hearts were then mounted unto the langendorff apparatus and perfused continually with KH buffer. The KH buffer was maintained at PH 7.4 by continual gas supply of 95% O_2 and 5% CO_2 with the temperature maintained at 37 °C using a water-jacketed organ chamber. The left atria were then excised and a latex iso-volumic balloon carefully inserted into the left ventricle and inflated to between 5-10mmHg. Functional parameters measured, which were the left ventricular developed pressure (LVDP), Heart rate (HR) and coronary flow (CF) which were monitored and recorded at regular intervals. The LVDP and HR were measured and recorded with a physiological pressure transducer and Powerlab Software, AD Instruments (UK). CF on the other hand was measured by collecting volume of perfusate for a minute in a measuring cylinder.

The functional parameters measured were expressed as mean of the stabilisation period to facilitate easy comparison between different treatment groups. At the end of the perfusion protocol, the hearts were carefully removed from the apparatus, weighed and frozen at -20°C for infarct analysis.

3.3.4 Infarct size analysis

After 12 hours/overnight, the now frozen pieces heart tissue were sliced into about 2mm thick transverse sections and incubated in 2, 3, 5-Triphenyltetrazolium chloride (TTC) solution (1% phosphate buffer solution) and kept at 37°C for 12 minutes to determine infarct regions. Following this the slices were then fixed in 10% formaldehyde solution for at least 4 hours. Regions of risk stained red while regions of infarct in tissue stained white/pale. The risk areas and infarct areas were traced onto acetate sheets and used to calculate a percentage of infarct to risk ratio (%). The sheets were scanned, and traces were assessed using the image J software. A ratio of infarct to risk size was calculated for each of the heart slices. The mean infarct to risk ratio (%) was then normalised to the weight of each heart.

3.3.5 Langendorff perfused heart experimental protocol

The hearts following excision were allowed a stabilisation period of 20 minutes prior to drug treatment for 155 minutes outlined by figure 3.3.1 below. Hearts were randomly assigned to the following treatment groups; 1) Perfusion with KH buffer alone (vehicle control), 2) Hearts treated with

crizotinib 10nM, 3) hearts treated with crizotinib 0.1µM, 4) Hearts treated with crizotinib 1µM, 5) Hearts treated with 10µM.
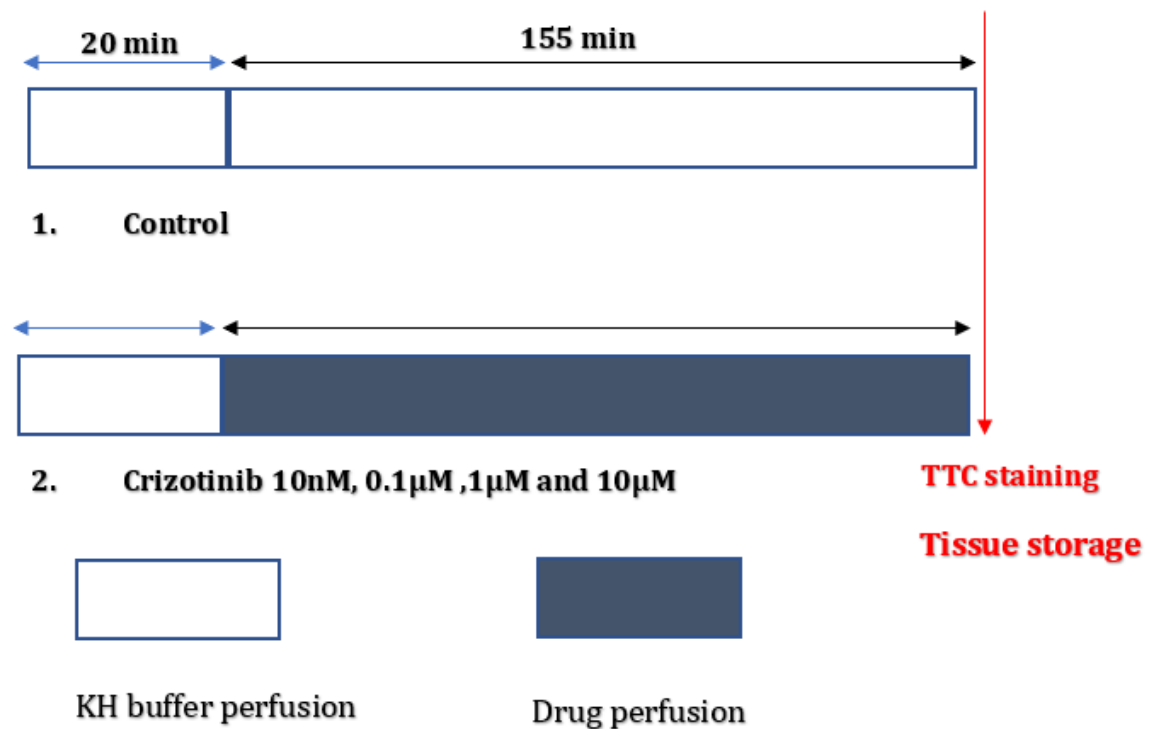
Figure 3.3.1 Langendorff drug treatment protocol

3.3.6 Western Blot analysis

For the western blot protein studies, the hearts were carefully removed from the langendorff apparatus following completion of perfusion period. The left ventricles were then excised and quickly flash-frozen in liquid nitrogen and stored away at -80°C for analysis.

After thawing briefly on ice, into a 2ml Eppendorf 400µl of lysis buffer (NaCl 0.1 M,Tris base 10 µM, EDTA 1 mM, sodium pyrophosphate 2 mM, NaF 2 mM, β-glycaophosphate 2mM, 4-(2-Aminoethyl) benzene sulfonyl fluoride hydrochloride + PhosSTOP™ (Phosphatase stop) + Protease cocktail tablet (Roche, Switzerland) and then add between 70-100 mg of frozen tissue. All of this was done over ice to prevent unnecessary heating of samples to prevent protein denaturation.

The Eppendorf with the samples were homogenised at 11000 RPM for 2 minutes and returned on ice as soon as possible. The samples were homogenised until a paste-like consistency is achieved. Homogenised samples were then subjected to BCA assay for protein quantification. Then 30µg of protein was loaded to 4–15 % Mini-Protean TGX Gel from Bio-Rad (UK) and separated at 10 V for 45 – 50 minutes. After separation, the proteins were transferred to the Bond-P polyvinylidene difluoride membrane from Bio-Rad (UK) by using the Trans-Blot Turbo transfer system from Bio-Rad (UK). Following successful transfer, the gel area was cut with a scalpel on the membrane. The membranes were then placed in a container with blocking buffer (solution of 15ml 10X TBST ; 10x TBST – 50mM Tris Base, 150mM NaCl, 0.05% Tween-20; pH 7.6) , 5% milk - 0.75 g) and then was incubated at room temperature on the orbital shaker for at least 1 hour. After blocking, blots were washed 3 times in 10 X TBST & probed for the phospho-Akt at Ser473 (Cell Signalling). The blots were placed into falcon tubes containing solution

of 10ml TBST + 5% BSA with 5 μl primary antibody and incubated overnight on a roller at 4 °C.

Following overnight incubation, the blots were taken out of the falcon tubes and washed twice in 10 x TBST. The secondary antibody was then prepared (15ml TBST, 0.5g BSA and 3μl anti-rabbit IgG). The blots were then incubated in the secondary solution for 2 hours at room temperature on the orbital shaker. After incubation the blots were then washed 3 times in TBST.

A 1:1 solution of the West Femto™ reagents was made (usually about 2-3ml for 2 blots). The blot was then placed on a clear acetate film taking care to remove bubbles underneath the membranes. 1ml of the solution was then pipetted over the membrane generously and then placed into the Bio-rad ChemiDoc™ for imaging. The appropriate settings were then selected, and visualisation could commence.

Following imaging of the bands phospho-Akt at Ser473 (Cell Signalling), the membranes were stripped (0.1 L Stripping buffer for 5 minutes – 20ml SDS 10%, 12.5ml Tris HCl, pH 6.8, 0.5M, 67.5ml distilled water, add 0.8ml β-mercaptoethanol under the fume hood and warmed to 50°C) and washed 3 times 10 x TBST. The blots were then blocked again for 2 hours and then incubated overnight in Akt (pan) (11E7) Rabbit mAb (cell signalling) 10ml TBST + 5% BSA with 5 μl primary antibody and incubated overnight on a roller at 4 °C.

Following overnight incubation, the blots were taken out of the falcon tubes and washed twice in 10 x TBST. The secondary antibody was then prepared (15ml TBST, 0.5g BSA and 3μl anti-rabbit IgG). The blots were then incubated in the secondary solution for 2 hours at room temperature on the orbital shaker. After incubation the blots were then washed 3 times in TBST.

A 1:1 solution of the west femto™ reagents was made (usually about 2-3ml for 2 blots). The blot was then placed on a clear acetate film taking care to remove bubbles underneath the membranes. 1ml of the solution was then pipetted over the membrane generously and then placed into the Bio-rad ChemiDoc™ for imaging. The appropriate settings were then selected, and visualisation could commence. For additional details refer to chapter 2.5 in the general methods section.

3.3.7 Culturing H9C2 cells

H9C2 cells were cultured in T75 flasks and supplemented with modified DMEM (Dulbecco's Modified Eagle Medium) which contained 10% FBS (Foetal bovine serum) and 1% PEN-STREP (Penicillin streptomycin). Cells were then seeded on 6-well plates and given between 48 hours for the plates to achieve 70% confluency. The first step was the culture the cells unto well

plates as required. The cell density per well for this study was about 1×10^5 per well

The plates were then treated with the appropriate drug treatments and incubated overnight (24 hours). The treatment media was then discarded, and the cells were trypsinised. The dislodged cells were then transferred into eppendorf tubes with equal volume of modified media to inactivate trypsin and pelleted (100-300g for 5 minutes at 4°C). The pellets were then analysed for cleaved-caspase 3, cell death, mitochondrial superoxide, and calcium analysis.

3.3.8 Cell viability analysis via MTT assay

Cultured cells in T75 flasks were first trypsinised and incubated for 5 minutes in 5% CO_2 incubator and set a temperature of 37°C to remove them from the culture flasks. About 2-3ml of supplemented media was added into the flasks to inactivate the trypsin. The cells were then pelleted and resuspended in fresh media, counted, and then seeded unto plates with a density of about 1×10^5 per well about 48 hours prior to allow enough time to adhere and reach full confluency on a 24-well plate. A few wells were filled with media alone to serve as background control.

The cells were then incubated for 24 hours with crizotinib 10nM, crizotinib 0.1µM and crizotinib 1µM. Following the incubation period, the media was

discarded, and the wells directly inoculated with 100µl of 5mg/ml MTT reagent and the wells were then incubated for 3 hours.

Following incubation, the solution was discarded and 100% DMSO solution was added to lyse the cells as previously described in the general results in chapter 2.9. The absorbance values were then read at 590nm. The data was normalised using the formula below.

Normalised absorbance reading = Mean absorbance value minus (-) Mean absorbance of cell free medium

Percentage cytotoxicity (%) = (Control (Untreated) absorbance / treated absorbance) x 100

3.3.9 Analysis of protein expression in isolated perfused tissue following drug treatment through western blotting

Following protein separation via electrophoresis, the protein bands were transferred onto the PVDF membrane and probed for the phosphorylated and total forms of AKT (Ser 473). The resultant banding on the membranes were analysed with the aid of Image J© software. The changes in relative expression were assessed and calculated and corrected for differences in as established by probing for total protein (total AKT).

3.3.10 Assessment of crizotinib cytotoxicity in cultured h9c2 cardiac fibroblasts following drug treatment via annexin v detection (Abcam™ Annexin V-FITC apoptosis detection kit)

The H9C2 cardiac cell line was used for this study. The cells were first stripped from flasks and plated to a density of about 1×10^5 per well about 48 hours prior to allow enough time to adhere and reach full confluency on a 24-well plate. The plates were then inoculated with the required drug treatments and then incubated for 24 hours at 37°C. Following the incubation period, the plates were retrieved from the incubator and transferred to a laminar flow hood for the rest of the protocol.

The treatment media was discarded, and the cells required trypsinisation for detachment from the plate. The trypsinised cell suspension was then transferred into eppendorf tubes. The trypsin was then inactivated with equal volume of modified media. The cells were then pelleted in a cold centrifuge (100-300g for 5 minutes at 4°C) and the pellet was then resuspended in 500µl of 1 X binding buffer. To each of the eppendorff tubes, 5 µl of annexin V-FITC and 5 µl of propidium iodide (for necrosis) was added. The tubes were then transferred into a dark drawer at room temperature for 5 minutes. Upon completion of the incubation period, the samples were then analysed BD Accuri™ C6 Plus personal flow cytometer set to count 5000 cells.

3.3.11 Assessment of cleaved caspase 3 activity (asp175) in cultured H9C2 fibroblasts following drug treatment

The H9C2 cardiac cell line was used for this study. The cells were first stripped from flasks and plated to a density of about 1×10^5 per well about 48 hours prior to allow enough time to adhere and reach full confluency on a 24-well plate. The plates were then inoculated with the required drug treatments and then incubated for 24 hours at 37°C.

The treatment media was discarded, and the cells required trypsinisation for detachment from the plate. The trypsinised cell suspension was then transferred into eppendorf tubes. The trypsin was then inactivated with equal volume of modified media. The cells were then pelleted in a cold centrifuge (100-300g for 5 minutes at 4°C) and the resultant pellet was resuspended in 100μl of 4% formaldehyde solution to fix the cells at room temperature for 15 minutes. The suspension was then washed afterwards in excess 1 X PBS solution and pellet and discard the supernatant. The samples were then resuspended in 0.5 – 1ml of PBS solution.

The fixed cells were then permeabilized with ice chilled 100% methanol added dropwise to the prechilled cells bringing the final concentration to 90% methanol solution. The samples were left for 10 minutes on ice and transferred to then be stored at – 20 °C or could be carried further for immunostaining.

The first step leading up to the immunostaining procedure was to count cells and aliquot desired number of cells into tubes (approximately 5×10^5). The samples were then washed in PBS to remove methanol and the resultant pellet was then diluted in 100μL of diluted primary antibody solution (Cleaved caspase-3 antibody dilution buffer based). This was then allowed to incubate for 1 hour at room temperature. The samples were then washed in 1 x PBS, pelleted and washed again for a second time. The samples were then resuspended in the secondary antibody solution (Alexa Flour 488® conjugate) which was also prepared in antibody dilution buffer. This was then allowed to incubate for 30 minutes at room temperature in dark condition. The samples were then washed 2 times in 1 x PBS. The pellet was finally resuspended in 500 μl of 1 x PBS ready for analysis on the BD Accuri™ C6 Plus personal flow cytometer set to count 10000 cells.

3.3.12 Assessment of mitochondrial superoxide generation following treatment of cultured H9C2 cardiac fibroblasts

The H9C2 cardiac cell line was used for this study. The cells were first stripped from flasks and plated to a density of about 1×10^5 per well about 48 hours prior to allow enough time to adhere and reach full confluency on a 24-well plate. The plates were then inoculated with the required drug treatments and then incubated for 24 hours at 37°C.

The following day, the treatment media was then discarded. The adherent cells were then washed twice with phenol free media twice and not PBS to ensure signal stability. The cells were then covered with 300-500μl of 5μM solution of mitochondrial superoxide red (MitoSox™ reagent). Original stock solution (5mM stock in DMSO) of MitoSox red was reconstituted in DMSO, however working (5 μM) solution was diluted in media. The plates were incubated for 20-25 minutes at 37^0C covered from light. Following the incubation period, the mitosox reagent was carefully aspirated off and transferred to the Epoch 2 microplate spectrophotometer (Biotek UK). The absorbance was then measured between 510/580nm wavelengths.

3.3.13 Assessment of calcium ion detection following treatment of cultured H9C2 cardiac myoblasts

Disruptions in calcium signalling and homeostasis could contribute towards apoptosis, with increases in Ca^{2+} a hallmark of early and late stage apoptotic pathway (Pinton et al 2008).

The H9C2 cardiac cell line was used for this study. The cells were first trypsinised from flasks and plated to a density of about 1×10^5 per well about 48 hours prior to allow enough time to adhere and reach full confluency on a 24-well plate. The plates were then inoculated with the required drug treatments and then incubated for 24 hours at 37°C.

The treatment media was discarded, and the cells required trypsinisation for detachment from the plate. The trypsinised the cell suspension was then transferred into eppendorf tubes. The trypsin was then inactivated with equal volume of modified media. The cells were then pelleted in a cold centrifuge (100-300g for 5 minutes at 4°C). Pellets were then resuspended in 1ml of 5μM Fluo-3, AM, Calcium Indicator solution and incubated for 30 minutes 37°C. Following this the cells were then washed twice and resuspended in 1ml 1 X PBS. The samples were than analysed on the BD Accuri™ C6 Plus personal flow cytometer set to count 5000 cells.

3.3.14 Statistical analysis

As previously stated, the processed data was presented as mean ± Standard error of the mean (SEM). Haemodynamic data was tested for differences using Two-way analysis of variance (ANOVA) with Fischer's LSD post hoc tests for the different time points using GraphPad prism 8 software. Infarct data was assessed so statistical differences between the individual groups using the one-way ANOVA and Tukeys post hoc test. MTT data was assessed so statistical differences between the individual groups using the two-way ANOVA and Fischer's LSD post hoc tests. Fold changes for AKT expression was assessed so statistical differences between the individual groups using one-way ANOVA and Fischer's LSD post hoc tests. One-way ANOVA was employed for the other sets of data with Fischer's LSD post hoc tests. P-values less than 0.05($P < 0.05$) were considered statistically significant.

3.4 Results

3.4.1 The effect crizotinib treatment on myocardial function in isolated perfused rat hearts (haemodynamic assessment)

In order to determine the effects of the crizotinib on cardiac function, isolated rat hearts were perfused with the different concentrations of crizotinib for a total of 175 minutes. Each of the hearts haemodynamic performance In Left Ventricular Developed Pressure (LVDP), Heart Rate (HR) and Coronary Flow (CF) were monitored and recorded. During the first 55 minutes of perfusion, readings were taken at 5-minute intervals and following 55 minutes the reading intervals was extended to 15 minutes. The crizotinib concentrations assessed during this study were, 10nM, 100nM, 1μM and 10 μM. The hearts treated with 10 μM did not complete the treatment period.

3.4.1 Haemodynamic parameters LVDP, HR and CF

3.4.1a Variations in LVDP (%) for isolated adult male rat hearts treated with different concentrations of crizotinib

Crizotinib treatment decreased LVDP (%) in all 4 concentrations of crizotinib with the lower concentrations displaying moderate decreases but the treatment concentration 1μM displaying the greatest significant reduction

compared to the control for the full treatment period (figure 3.4.1). The group

treated with 10μM displayed greatest disparity to the control, but hearts did

not complete treatment period.

A)

162

B)
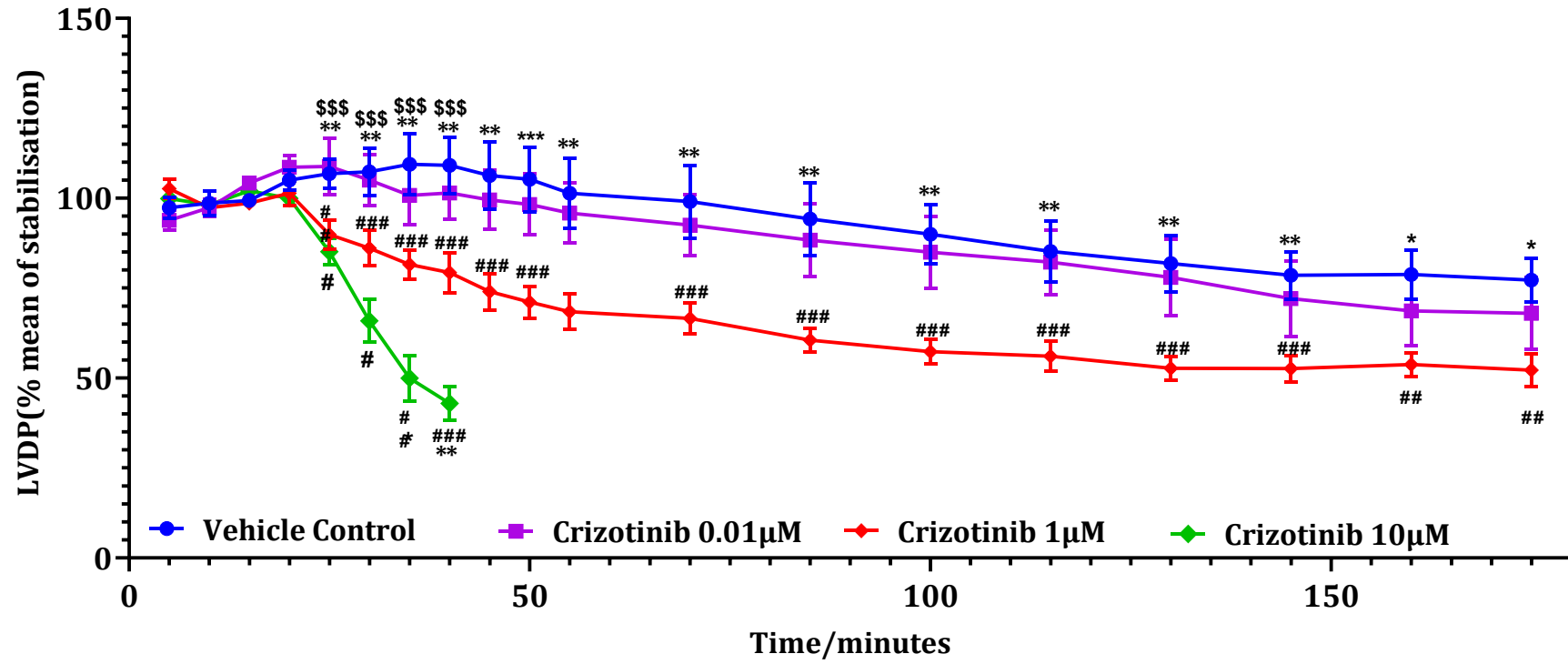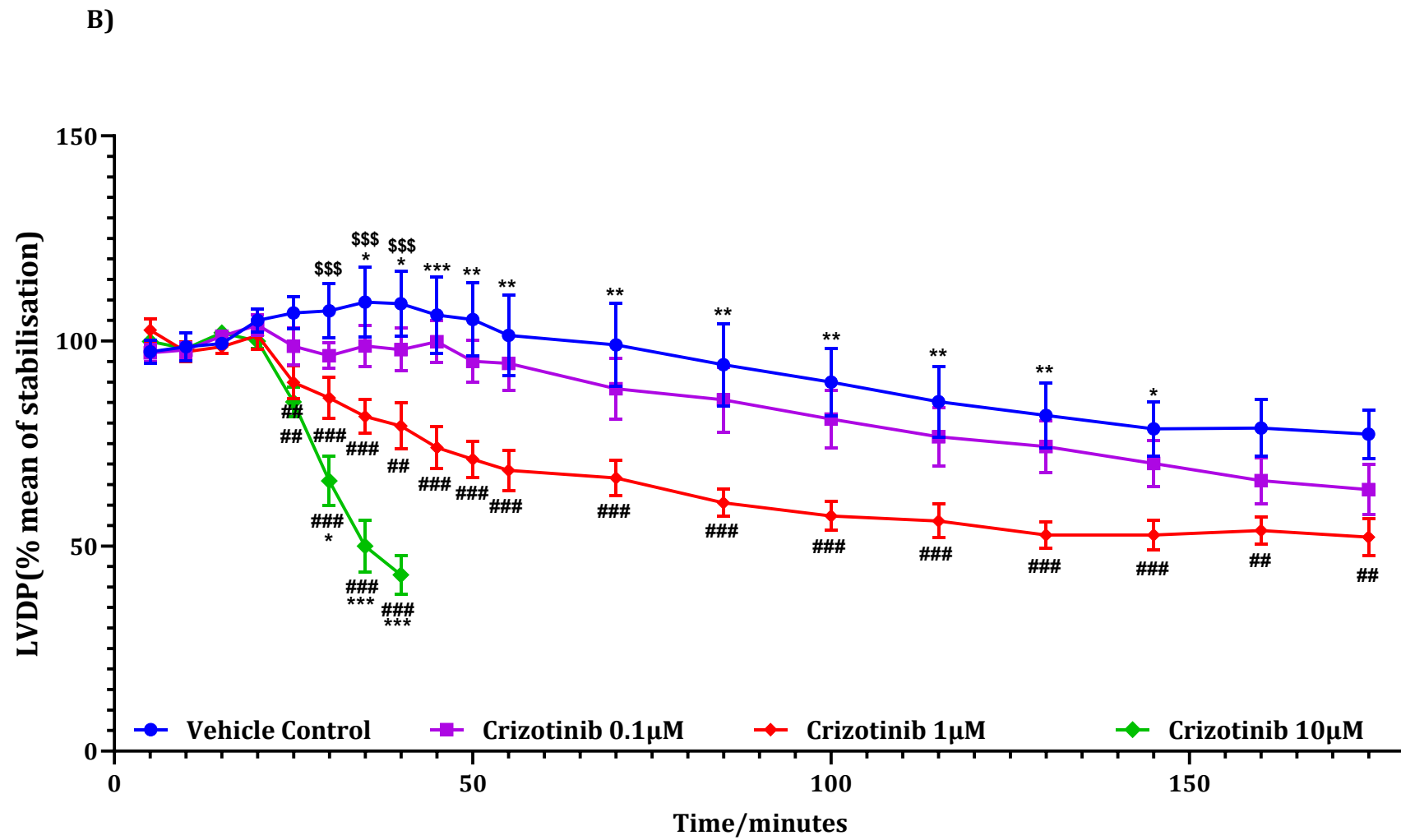
Figure 3.4.1 - The effects of treatment with crizotinib 0.01µM, 0.1µM, 1µM, 10µM and vehicle control on Left Ventricular Developed Pressure (LVDP) in adult Sprague-Dawley rats treated for 175 minutes. A) Shows the trend observed between vehicle control, crizotinib 0.01µM, 1µM and 10µM. B) shows the trend observed between vehicle control, crizotinib 0.1µM, 1µM and 10µM treated rat hearts with 20 minutes stabilisation followed by 155 minutes of drug perfusion. (#$P<0.05$, ##$P<0.01$, ###$P<0.001$ versus the time matched vehicle control; *$P<0.05$, **$P<0.01$ versus the time matched crizotinib 1µM treatment, \$$P<0.05$, \$\$ $P<0.01$ versus treatment with crizotinib 10µM where n=3 for crizotinib 10µM and n=6 for all other treatments). Data was presented as mean ± SEM and statistical tests for each experiment was provided in chapter 2.14 in the general methods, One-way anova with LSD post hoc test.

During the stabilisation period there was no difference observed between the groups which was expected as the hearts were all treated with KH buffer during that period (figure 3.4.2).

Figure 3.4.2 Assessment of LVDP (%) in isolated adult male Sprague-Dawley rat hearts at the 20-minutes into perfusion (5-miutes pre-drug perfusion). There was no significant difference observed between the treatment groups (Data was presented as the mean ± SEM).

30 minutes into perfusion, the groups treated with crizotinib 1μM and 10μM displayed significant differences compared to the non-treated control hearts as indicated in the following figure (Figure3.4.3).

Figure 3.4.3 Assessment of LVDP (%) in isolated adult male Sprague-Dawley rat hearts at 30-minute time interval. There was significant difference observed between groups (### P<0.001 versus vehicle control treatment, ** P<0.01 versus Crizotinib 1μM and $$$ P<0.001 versus treatment with Crizotinib 10μM.)
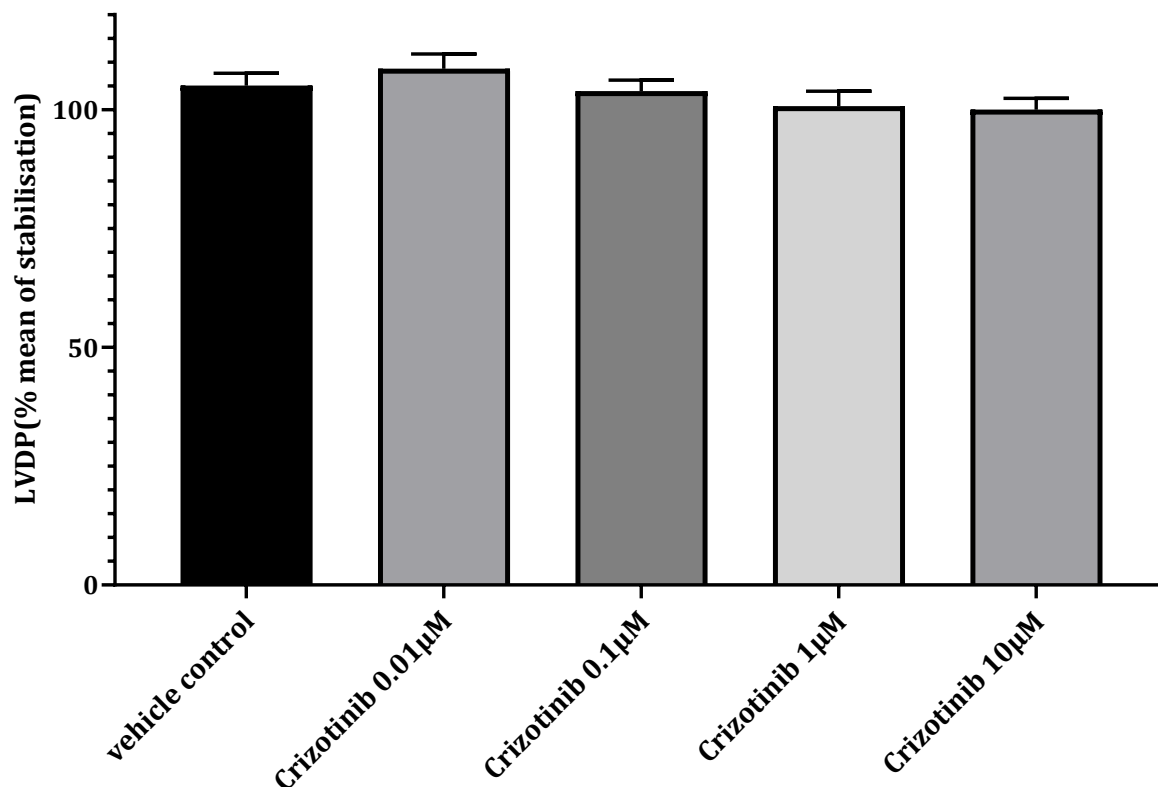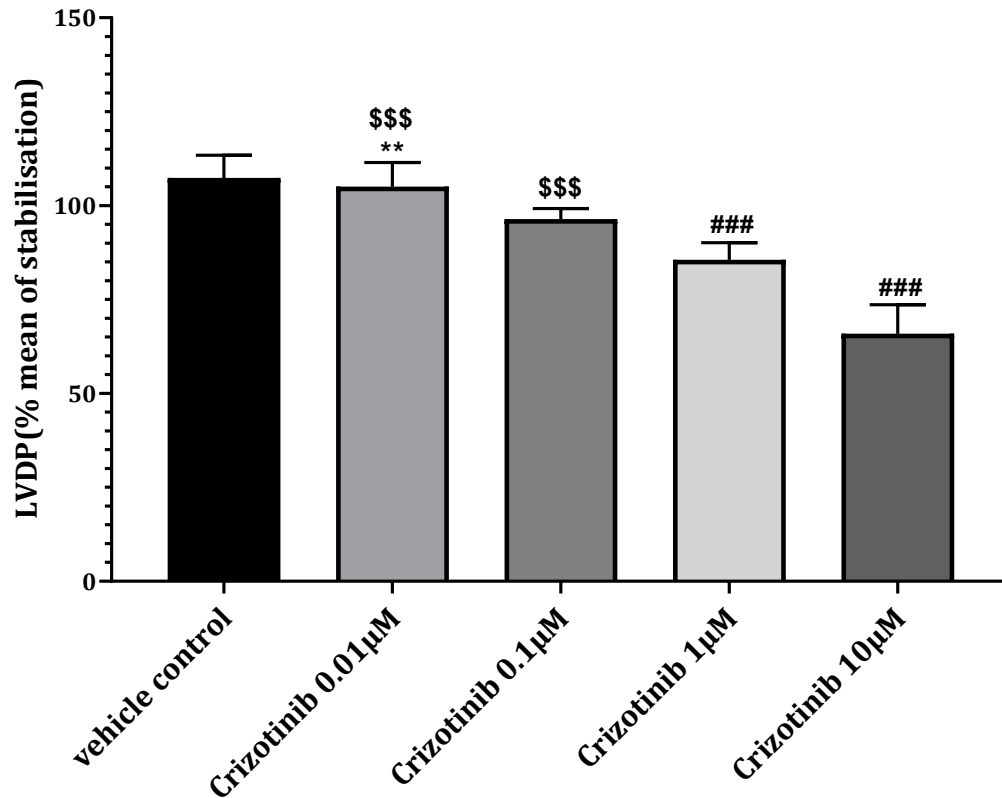
After 30 minutes, crizotinib (1μM) treatment significantly reduced LVDP (%) compared with time matched non-treated control hearts (86.09 ± 4.96% versus 107 ± 6.63% respectively, P<0.001) (Figure 3.4.3). Crizotinib 1μM again significantly reduced LVDP (%) versus time matched treatment with crizotinib 0.01μM treated hearts (86.09 ± 4.96% versus 105.04 ± 7.03% respectively, P<0.01). Crizotinib 1μM also reduced LVDP (%) versus treatment with crizotinib

0.1μM treated hearts however the variance was not deemed statistically significant (86.09 ± 4.96% versus 96.38 ± 3.09% respectively). Crizotinib 10μM also significantly reduced LVDP (%) versus control, crizotinib 0.01μM and 0.1μM (65.90 ± 5.98% versus 107.34 ± 6.23%, P<0.05, 105.03±7.03% P<0.05 and 96.376±3.09% P< 0.05 respectively) (Figure 3.4.3).

After 50 minutes, the hearts treated with crizotinib (10μM) were no longer responsive and attempts to revive the hearts with cold KH buffer proved unsuccessful. Crizotinib (1μM) treatment however, reduced the LVDP (%) versus non-treated control, crizotinib (0.01μM and0.1μM) treated hearts (71.16± 4.46% < 105.23 ± 8.89% P<0.001, 98.28 ± 8.5 P<0.001, 95.084 ± 5.1% P < 0.01 respectively) (Figure 3.4.4).
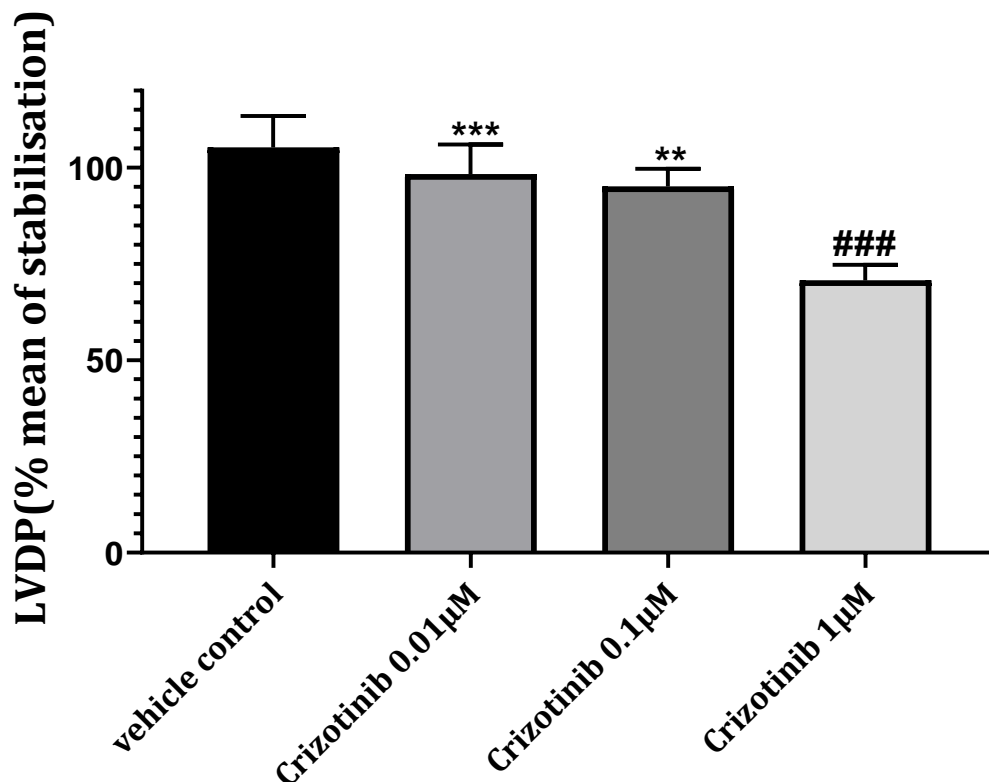
Figure 3.4.4 Assessment of Left Ventricular Developed Pressure performance of isolated adult male Sprague-Dawley rat hearts 30 minutes post stabilisation period. There was significant difference observed between groups. (Data is presented as mean ± SEM P<0.001 ### versus Control treatment, *** P<0.001 versus Crizotinib 1µM, ** P<0.01 versus Crizotinib 1µM, n=6)

Crizotinib (1µM) treatment significantly reduced LVDP (%) versus the non-treated control and both crizotinib (0.01µM and 0.1µM) treated hearts at a number of time points (35 minutes, 50 minutes, 85 minutes and 115 minutes, amongst others) (Figure 3.4.1 A & B).

3.4.1b Heart rate (%) variations following treatment of isolated adult rat hearts with varying concentrations of crizotinib

There did not appear to be any significant differences observed between any of the treatment groups (Figure 3.4.5).

The vehicle control treated animals displayed the most stable trend but not significantly different to any of the other treatments.
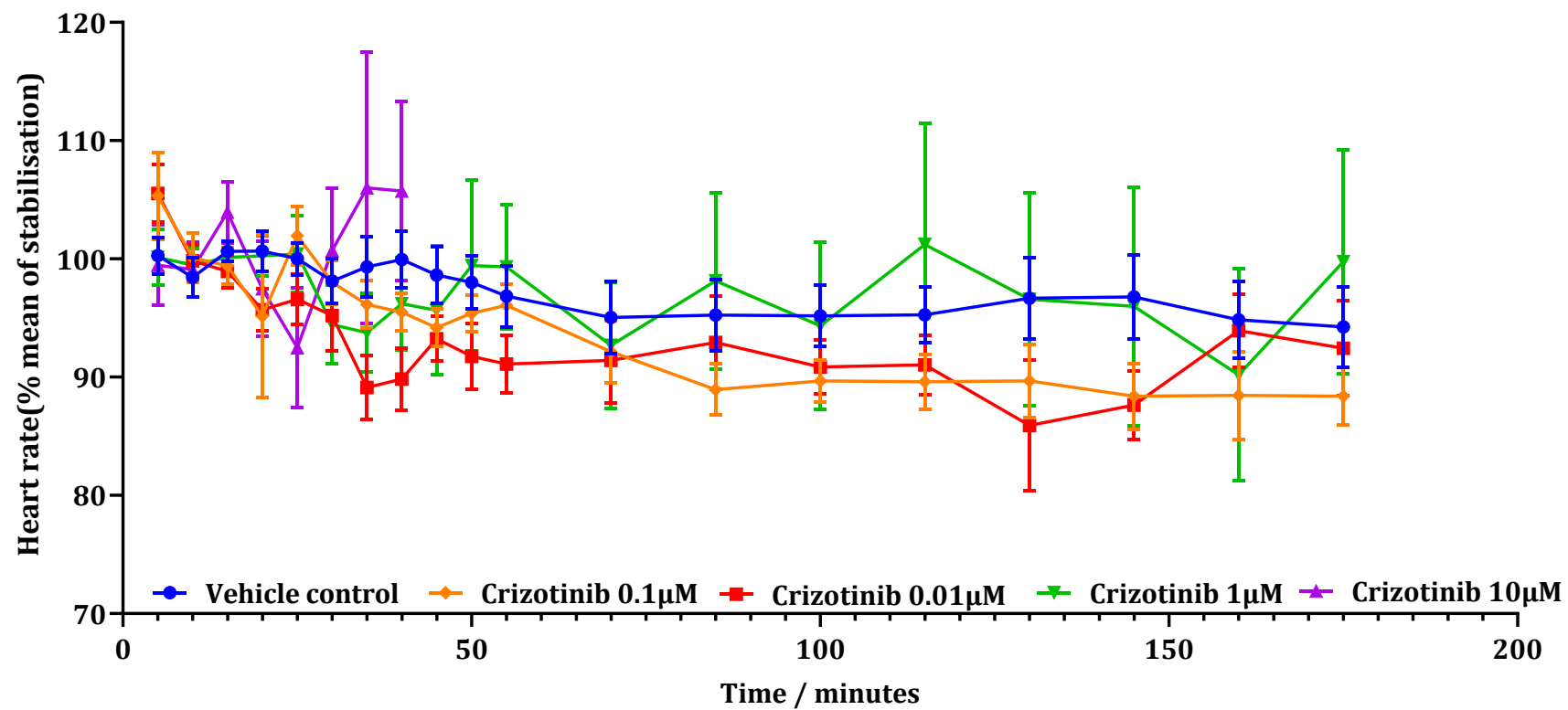
Figure 3.4.5. The effects of treatment with crizotinib (Cz) 0.01μM, 0.1μM, 1μM, 10μM and vehicle control on heart rate (HR) in adult Sprague-Dawley rats treated for 175 minutes. A) The response observed between vehicle control, Crizotinib 0.01μM and 1μM. B) The response observed between vehicle control, Crizotinib 0.1μM and 1μM treated rat hearts with 20 minutes stabilisation followed by 155 minutes of drug perfusion. (N=3 for samples treated with Crizotinib (10 μM) and N=6 for all other treatment conditions).

3.4.1c Coronary flow

The hearts treated with crizotinib (10μM) recorded the greatest percentage increases for coronary flow (%). Crizotinib (10μM) significantly increased coronary flow (%) compared with the control at the 35-minute interval (125±5.97% versus 109.46±8.53%, P<0.05) (Figure 3.4.6).

Interestingly, the hearts treated with treated with Crizotinib (0.01μM) produced least observed coronary flow and was significantly less than the non-treated control and crizotinib (1μM) at various time points (Figure 3.4.6). For instance, at the 100-minute interval, crizotinib (0.01μM) significantly reduced coronary flow significantly than that observed for control and crizotinib (1μM) (67.1 ± 8% versus 84.52 ± 7.73% where P<0.01 and 67.1 ± 8% versus 90.5 ± 4.68% where P<0.01 respectively) (Figure 3.4.6).
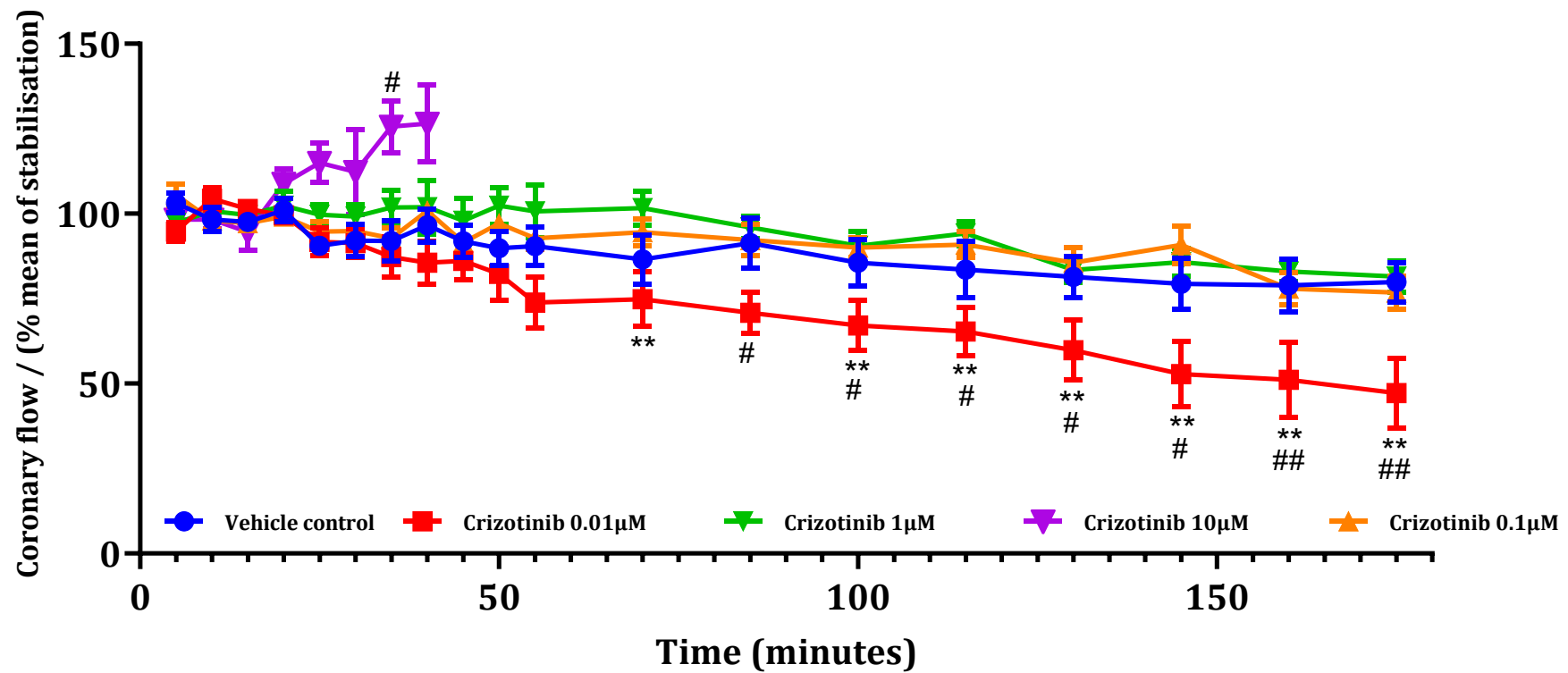
Figure 3.4.6 the effects of treatment with crizotinib (Cz) 0.01 µM, 0.1µM, 1µM, 10µM and vehicle control on coronary flow in adult Sprague-Dawley rats treated for 175 minutes. A) shows the response observed between vehicle control, crizotinib 0.01µM, 1µM and 10µM. B) shows the response observed between vehicle control, crizotinib 0.1µM 1µM and 10µM treated rat hearts with 20 minutes stabilisation followed by 155 minutes of drug perfusion. (Where #P<0.05, ##P<0.01, versus the control; **P<0.01 versus the time matched crizotinib (1µM), N=3 for samples treated with crizotinib (10 µM) and N=6 for all other treatment conditions).

3.4.2 The effect of crizotinib treatment on mean infarct size to risk ratio (%) developed in isolated langendorff perfused adult male Sprague-Dawley rat hearts.

As stated previously, sectioned whole hearts were stained with the aid of 2, 3, 5-Triphenyltetrazolium Chloride (TTC™) and incubated prior to analysis of infarct size to risk ratio (%) with the Image J software (Image J®).

Treatment of the hearts with Crizotinib 1µM produced the greatest infarct risk ratio (%) observed following TTC staining (Figure 3.4.7). It was significantly greater than the ratio developed versus the vehicle control, suggesting Crizotinib 1µM treatment produced significantly greater damage (23.4±5.6% vs. 6.9 ± 0.96% respectively, where P<0.001) (Figure 3.4.7).

Hearts treated with Crizotinib 1µM produced a significantly greater mean infarct risk ratio (%) than the two submaximal concentrations of crizotinib in Crizotinib0.01µM (23.4±5.6% Crizotinib 1µM versus vs 4.59±0.91%, where P<0.001 n=6) and Crizotinib 0.1µM (24.57±5.6 % versus 7.71±1.14%, where P<0.001 n=6) respectively. Indicating that crizotinib 1µM induced the greatest injury to heart tissue in this study.

For the submaximal concentrations, there was no significant difference between the both groups. The Crizotinib 10nM treated group generated the least infarct development (4.59±0.91% for Crizotinib 10nM versus vs 7.71±1.14% for Crizotinib 0.1µM, Where P>0.05 n=6). Another interesting note observed was that the group treated with Crizotinib 0.01µM (10nM), produced the least infarct risk ratio (%), slightly less than versus the vehicle control (4.59±0.91% versus 6.9± 0.96% respectively, where P>0.05) however the difference between the groups was not deemed significant.
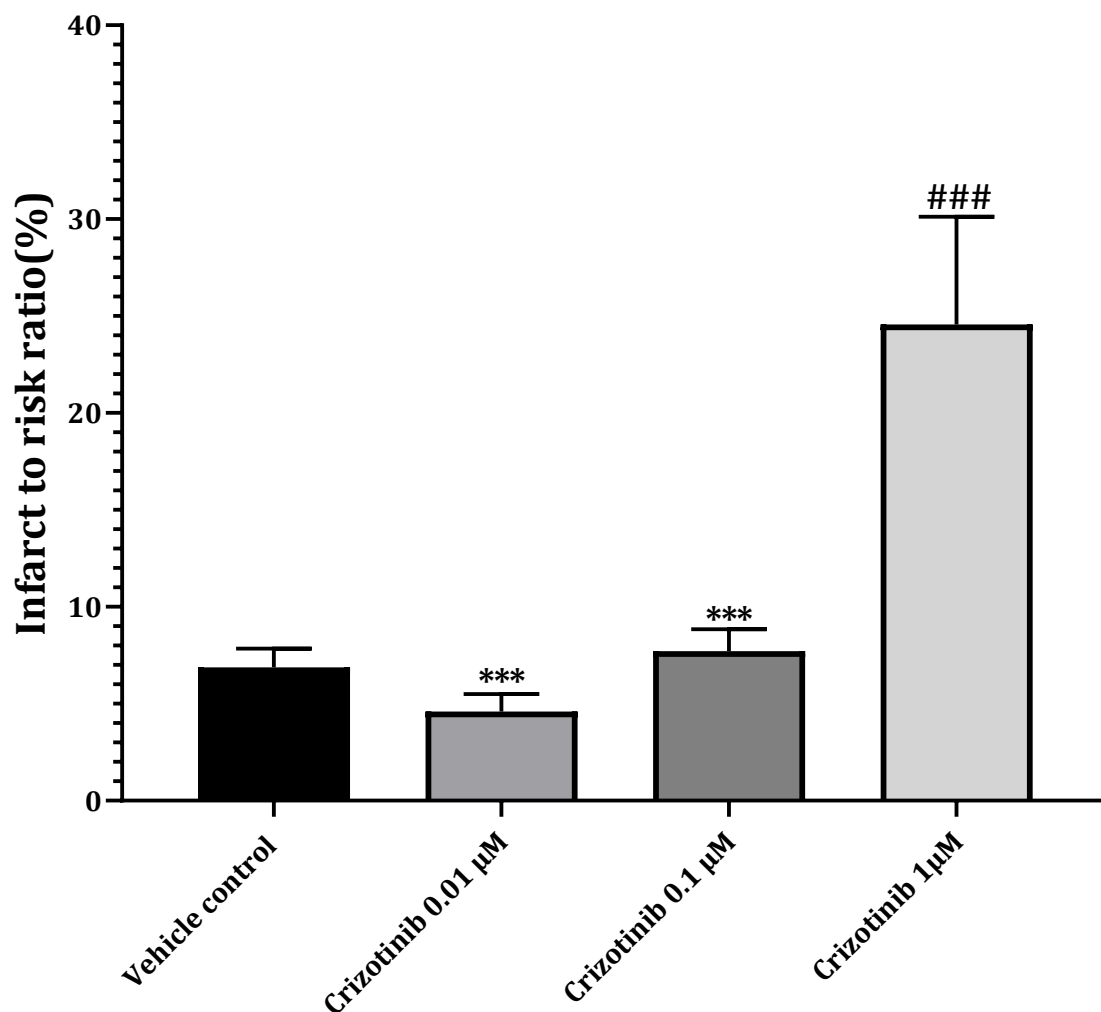
Figure 3.4.7 Assessment Mean infarct size to risk ratio (%) developed in isolated adult male Sprague-Dawley rat hearts following treatment for 175-minutes with vehicle control, crizotinib 0.01μM, crizotinib 0.1μM and crizotinib 1μM added 20 minutes into perfusion (Data was presented as mean ± SEM. ***P<0.001 vs crizotinib 1μM, ###P<0.001 vs control, n=6)

3.4.3 The effect of crizotinib treatment on observed cell viability in cultured H9C2 cardiac myoblasts

The MTT (3-(4,5-dimethylthiazol-2-yl)-2-5-diphenlytetrazolium bromide) assay was employed as a mechanism to assess cell viability. The assay served to identify cells which are participating in active respiration (viable). The intensity of the colour produced through the assay analysed using the microplate reader was an indication to the number of viable cells present within each of the wells.

Treating cultured H9C2 cardiac myoblasts with Crizotinib 1µM significantly reduced cell viability compared to non-treated control (35.51 ± 3.98% versus 104.8 ± 5.6% respectively, where P<0.001) (Figure 3.4.8). Treating cells with Crizotinib 1µM significantly reduced cell viability compared with the cardiac myoblasts treated with Crizotinib 0.01µM and 0.1µM (35.51 ± 3.98% versus 108.5 ± 8.6%, where P<0.001 and 35.51 ± 3.98% versus 94.64± 6.23% respectively, where P<0.001) (Figure 3.4.8).
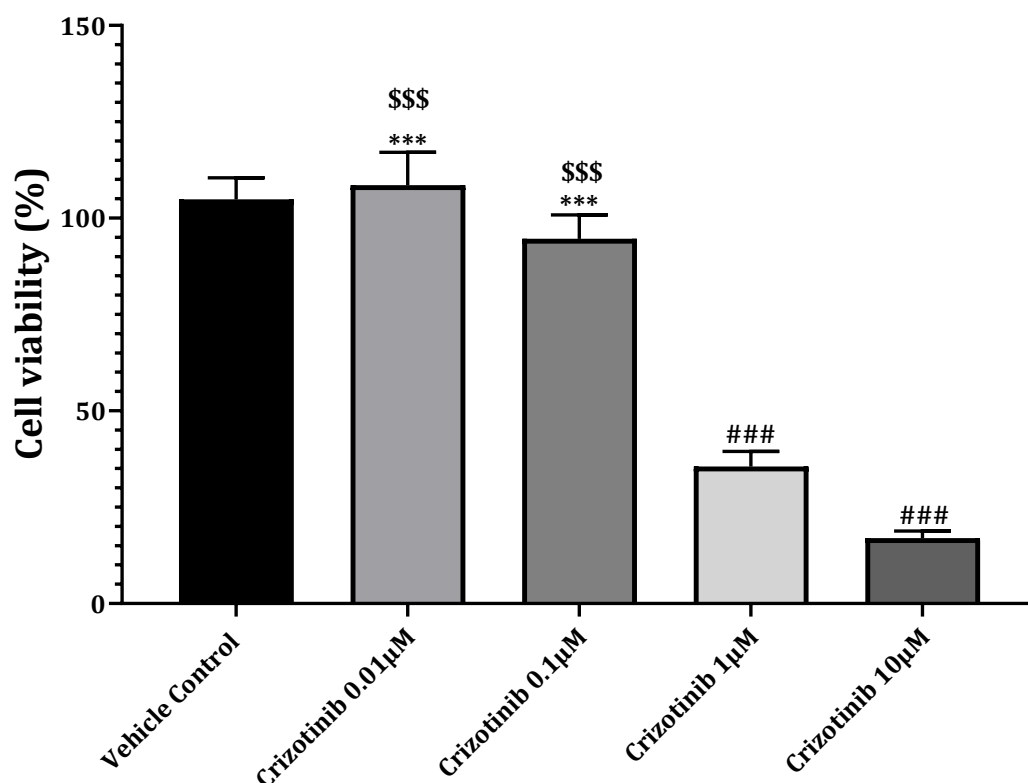
Figure 3.4.8 Assessment of MTT (3-(4,5-dimethylthiazol-2-yl)-2-5-diphenlytetrazolium bromide) assay derived cell viability of H9C2 cardiac cells treated for 24 hours with vehicle control, crizotinib 0.01μM, crizotinib 0.1μM , crizotinib 1μM and crizotinib 10μM incubated for 3 hours in MTT reagent (Data was presented as mean ± SEM. ###P<0.001 vs control ***P< 0.005 vs crizotinib 1μM, *P< 0.05 vs crizotinib 1μM, $$$ P<0.001 versus crizotinib 10μM n=6).

H9C2 cardiac myoblasts treated with Crizotinib 0.01μM appeared to display an increase in viability compared to the non-treated control however difference was not deemed statistically significant (108.5 ± 8.6% versus 104.8 ± 5.62% respectively, where P >0.05).

Similarly, cardiac myoblast treated with Crizotinib 10μM displayed a significantly reduced viability compared to the non-treated controls (16.92 ± 1.9% versus 104.8 ± 5.62% respectively, where P<0.001). In addition, Crizotinib 10μM treatment induced significant reduction in viability (%) assessed in cultured H9C2 myoblasts compared to myoblasts treated with Crizotinib 1μM (16.92 ± 1.9% versus 36.78 ± 5.82% respectively, where P<0.05) (Figure 3.4.8).

3.4.4 The effect of Crizotinib treatment on expression of phosphorylated AKT (ser473) in left ventricular tissue of adult male Sprague-Dawley rat hearts

Following the protocol outlined in the methods section (Section 3.3.9) the band intensities were analysed. The band intensities (signal) were normalised and the data depicted was the ratio of the phosphorylated protein to the total protein.
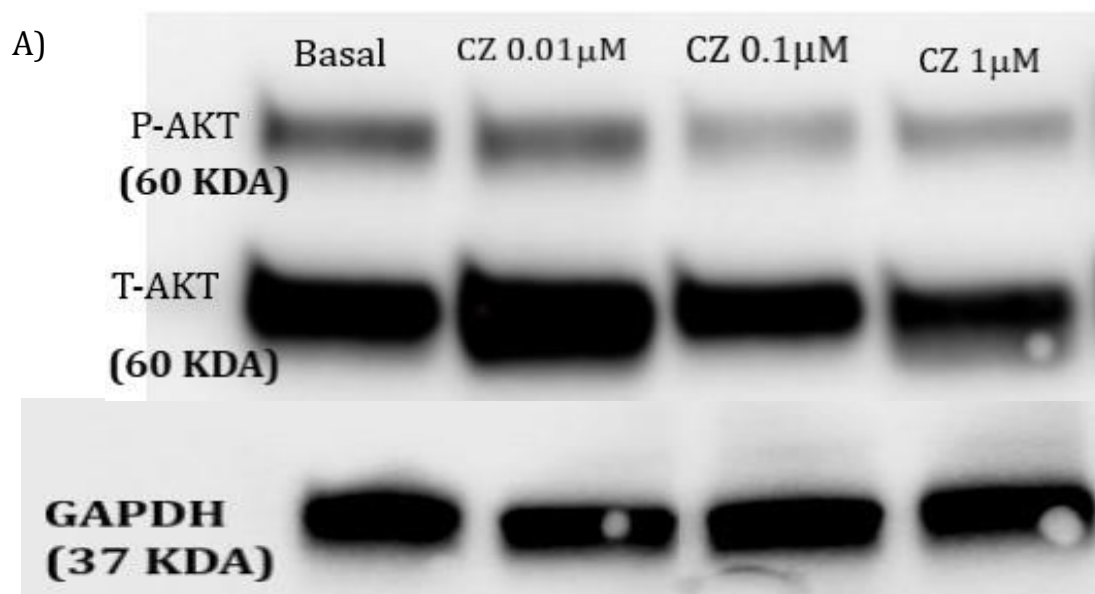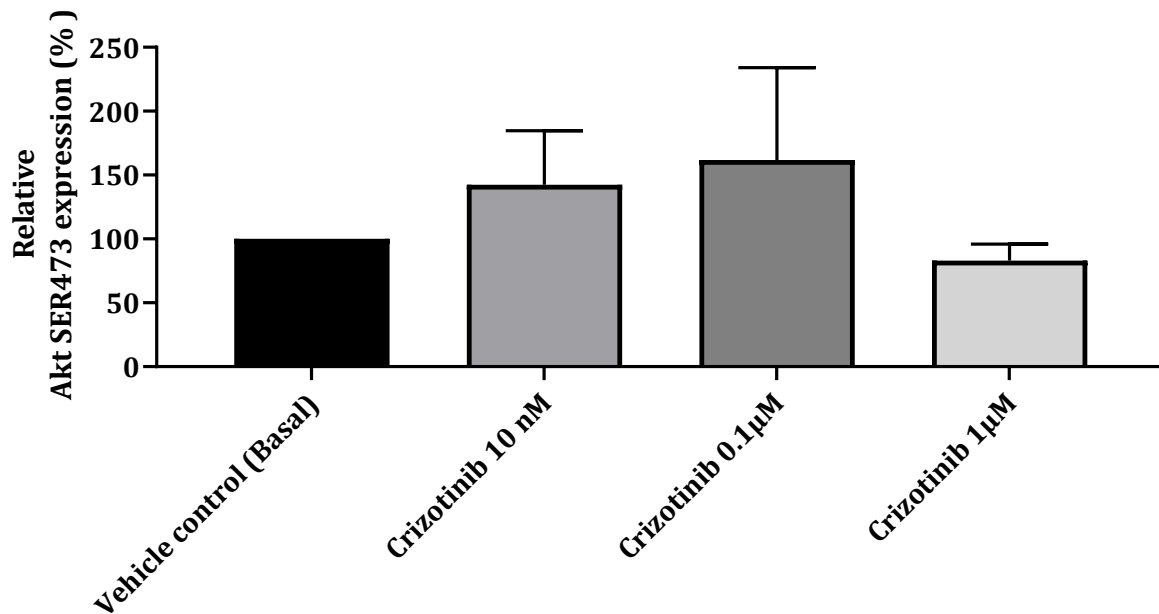
Figure 3.4.9 a & b Assessment of relative ratio of phosphorylated AKT/Total AKT in adult isolated Sprague-Dawley rat hearts treated for 175 minutes with Crizotinib 10nM, Crizotinib 0.1μM and Crizotinib 1μM added 20 minutes into perfusion. (Data presented as mean ± SEM. where n=4)

The figure above provides comparison between the varying Crizotinib concentrations (1μM-0.01μM) and on the expression of phosphorylated AKT (ser473). From figure 3.4.9 a & b, it was apparent the samples treated with Crizotinib 1μM showed the least relative expression of phosphorylated AKT.

Comparing the samples treated with Crizotinib 1μM to the samples treated with Crizotinib 10nM. From the figure it was easy to conclude that there was difference however also looking at the error values the difference could not be considered

significant and this was confirmed by statistical analyses (83 ± 13% versus 142 ± 42% respectively, where P > 0.05).

Considering the next treatments revealed a similar trend. Again, the group treated with Crizotinib 1µM showed a relative expression which was less than that of the group treated with Crizotinib 0.1µM which was the case with the previous comparison. The difference again was not deemed statistically significant (83 ± 13% versus 162 ± 72% respectively, P>0.05).

The two submaximal concentrations of Crizotinib were then compared. By looking at their trend in figure 3.4.9 b, there did not appear to be significant difference between the two treatments. Comparing both groups, Crizotinib 0.1µM induced the greater of relative expression of AKT compared to the samples treated Crizotinib 0.01µM (162 ± 72% versus 142 ± 42%, where P>0.05) respectively.

3.4.5 Effect of crizotinib treatment on cell viability determined through annexin V expression in cultured H9C2 cardiac myoblasts

As described previously in the methods section, the Abcam™ Annexin V-FITC apoptosis detection kit for these results. Annexin V has strong affinity for external membrane phosphatidylserine as an apoptotic response in cells.

Following the treatment and staining protocol, the samples were analysed using flow cytometry.

Treatment with Crizotinib (1μM) significantly decreased annexin V detection compared with the cells treated with crizotinib (0.01μM) (41.43±0.91% versus 48.73±1.27%, where P<0.05) (Figure 3.4.10).
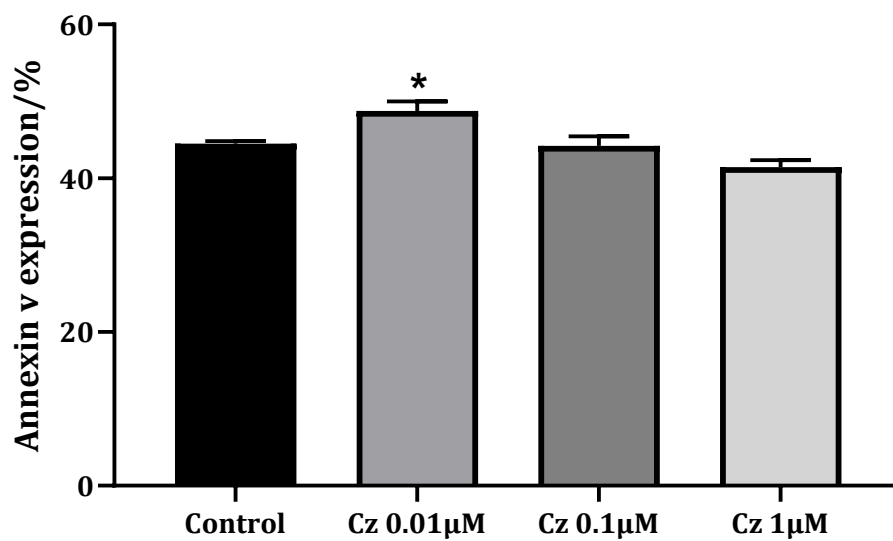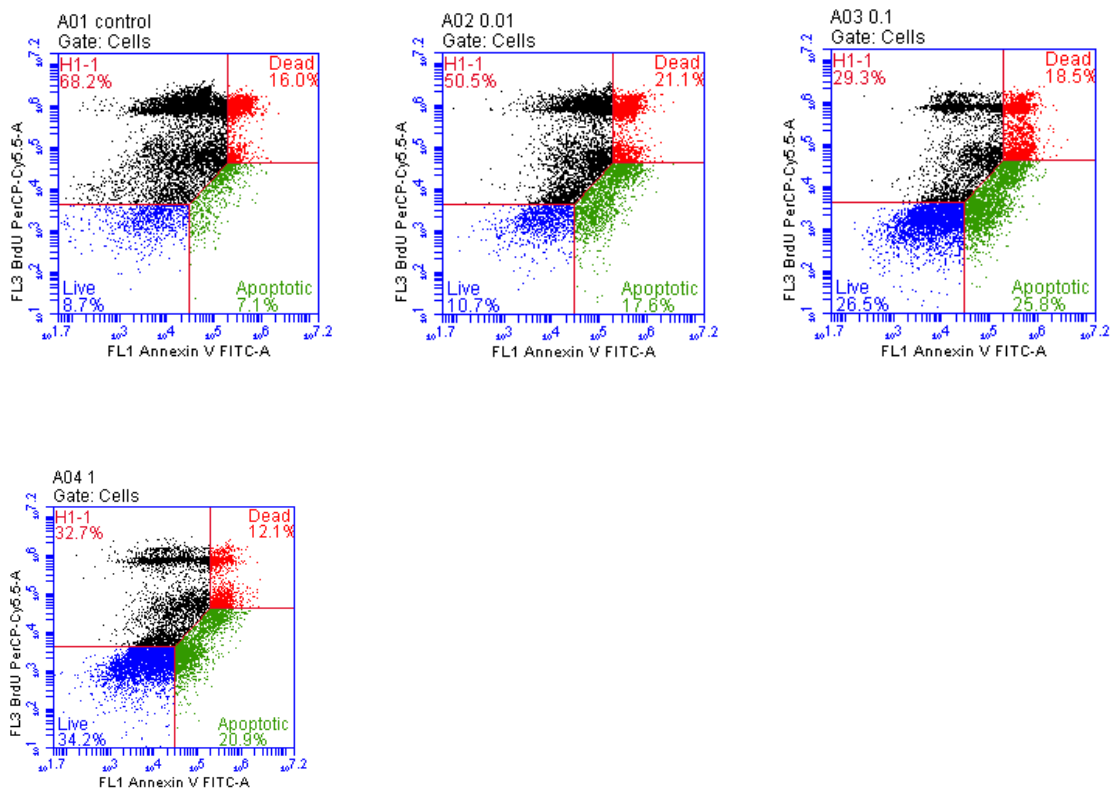
Figure 3.4.10 Assessment of annexin v expression Cultured H9C2 cells treated for 24 hours with Crizotinib 0.01μM, Crizotinib 0.1μM and Crizotinib 1μM (Data was presented as mean ± SEM. Where *P<0.05 versus Crizotinib 1μM). Figures A01 – A04 depict the raw flow cytometric data dumps.

There was no significant difference observed between the other treatment groups.

3.4.6 The effect of crizotinib treatment on cleaved caspase 3 expression in cultured H9C2 cardiac myoblasts

Cleaved caspase 3 expression served as an indicator of cells undergoing apoptosis. Following the treatment and staining protocol the samples were then analysed using the flow cytometer counted 10000 cells.

The 3 concentrations of Crizotinib appeared to produce greater cleaved caspase 3 expression/activity than the non- treated control. However, only cells treated with crizotinib (1μM) and crizotinib (0.1μM) significantly increased cleaved-caspase 3 expression compared to the non-treated cell controls (5292±245.9 AU versus 1701.3±436.8 AU P<0.001) (Figure 3.4.11).
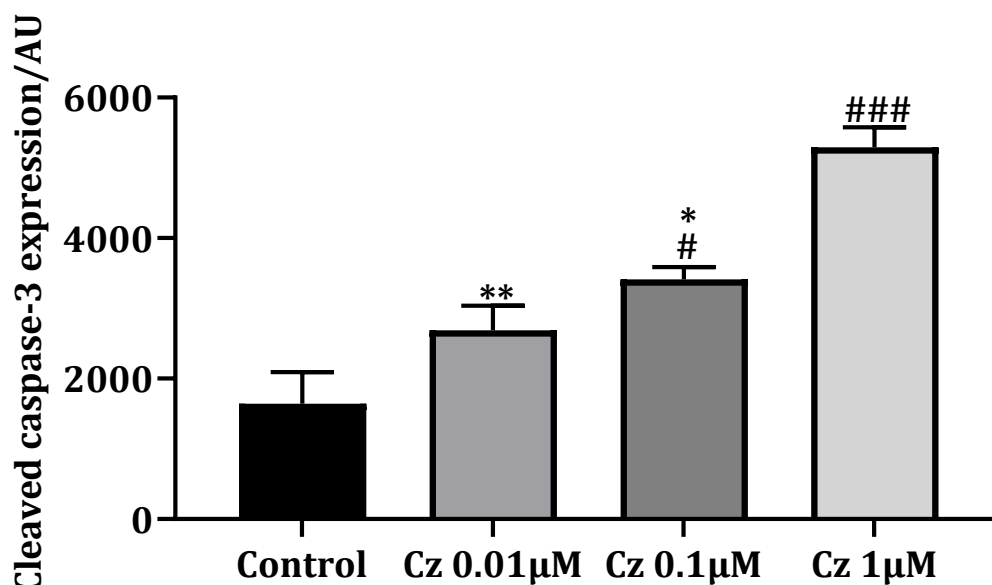
Figure 3.4.11 Assessment of cleaved caspase 3 activity in cultured H9C2 cardiac fibroblasts subjected to 24 hours treatment with either Control, Crizotinib 0.01μM ,0.1μM and 1μM. (Data was presented as mean ± SEM, where # P<0.05 ### P<0.001 versus control; *P<0.05 **P<0.01 versus crizotinib 1μM n=3).

Cells treated with crizotinib (1μM) significantly increased cleaved-caspase 3 expression compared to the cells treated with crizotinib (0.01μM) and (0.1μM) (5292±245.9 AU versus 2755.3±306.8 AU where P<0.01 and 5292±245.9 AU versus 3412.3±152.8 AU where P<0.05 respectively). There was no observed significance in the difference observed in the expression of cleaved caspase 3 between crizotinib 0.1μM and 0.01μM although treatment with crizotinib (0.01μM) increased cleaved caspase 3 expression.

The data suggests treatment with Crizotinib (1μM) induced the greatest increase cleaved caspase 3 activity in cultured H9C2 myoblasts recorded compared to the

control treatment. The two other concentrations also appeared to induce increased cleaved caspase 3 activity however the differences were not deemed statistically significant.

3.4.7 The effect of crizotinib treatment on mitochondrial superoxide generation in cultured H9C2 cardiac myoblasts

Upon completion of the prior described treatment and incubation period MitoSOX™ Red Mitochondrial superoxide indicator assay the samples were analysed using a microplate reader.

The different concentrations of crizotinib treated cultured H9C2 myoblasts all displayed significant increases in mitochondrial superoxide generation (%) compared to the non-treated cell controls. Cultured H9C2 myoblasts treated with crizotinib (1μM) showed the greatest significant increase in mitochondrial superoxide generation compared to then non-treated cell controls (55.25±0.48% versus 77.50±0.29%, P<0.001) (Figure 3.4.12).

In addition, cultured H9C2 myoblasts treated with crizotinib (1μM) showed significant increase in mitochondrial superoxide generation compared to the myoblasts treated with crizotinib (0.1μM and 10μM). Significant increases in mitochondrial superoxide production was observed in myoblasts treated with crizotinib (1μM) compared to cells treated with crizotinib (0.1μM and 10μM) respectively (77.50±0.29% versus 68.67±0.0.88% and 77.50±0.29% versus 72±0.91% P<0.001 in both comparisons).
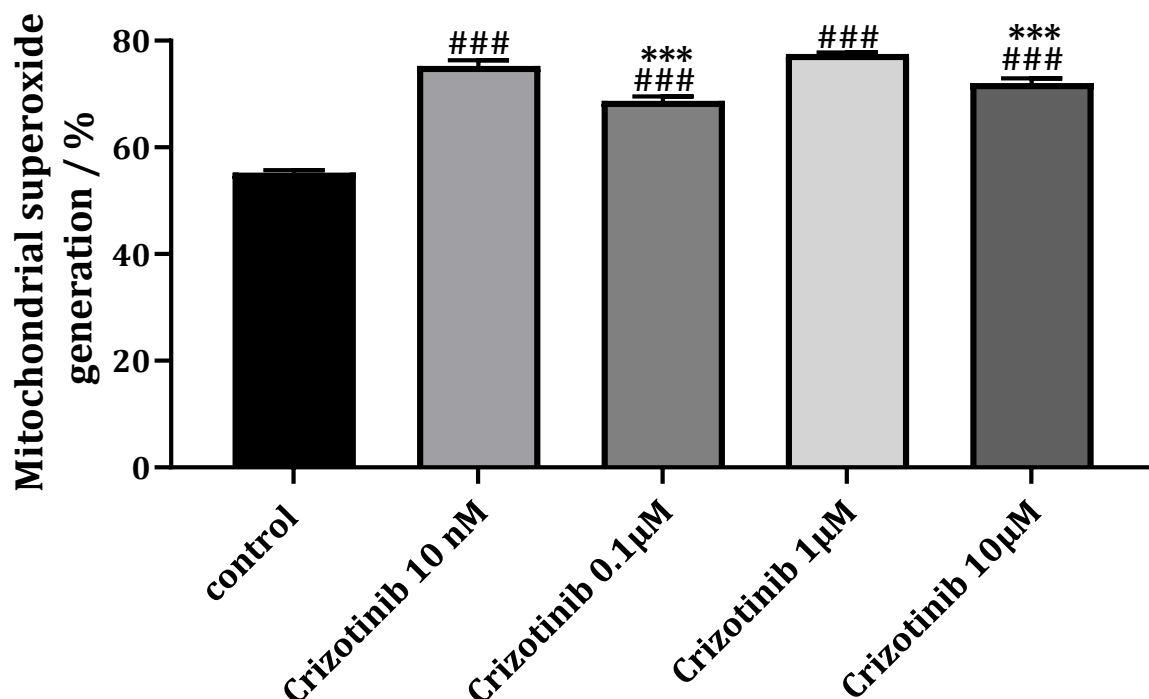
Figure 3.4.12 Assessment of mitochondrial superoxide generation in cultured H9C2 cardiac cells subjected to 24 hours treatment with either non-treated Control (DMSO 0.04%), Crizotinib 10nM, 0.1μM, 1μM and 10μM. (Data presented as mean ± SEM. ### P<0.001 versus control treatment, *** P< 0.001 versus Crizotinib 1μM treatment, where n=3)

The data generated suggests crizotinib treatment was associated with a significant increased generation of mitochondrial superoxide with the greatest increased observed with the samples treated with crizotinib (1μM) (3.4.12).

3.4.8 The effect of crizotinib treatment on the detection calcium ions (Ca^{2+}) in cultured H9c2 Cardiac myoblasts

Following treatment with the appropriate drugs and assay implemented as stated in the methods section (3.3.13). The following deductions could be drawn from the data generated.

Treatment of H9C2 myoblasts with crizotinib (0.01μM, 0.1μM and 1μM) for 24 hours produced greater calcium ion detection compared to the non-treated cell control, however only treatment with crizotinib 1μM produced significantly greater Ca^{2+} detection (95.38±3.62% versus 77.52±3.08%, where P<0.05 respectively).
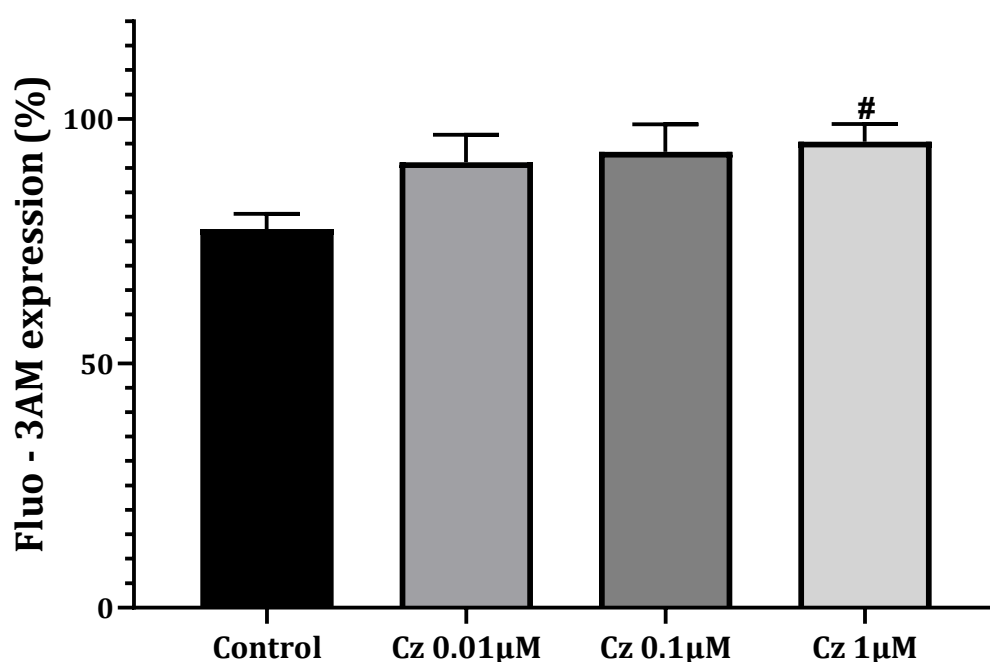
Figure 3.3.14 Assessment of Ca^{2+} activity in cultured H9C2 cardiac cells subjected to 24 hours treatment with either Control (DMSO 0.04%),

Crizotinib 0.01µM ,0.1µM and 1µM. (where # P<0.01 v versus vehicle control treatment).

There was no significant different between any of the other treatment groups.

3.4 Discussion

Despite the great promise shown by tyrosine kinase inhibitors towards improved safety profile regarding anticancer treatment, the increasing concerns regarding their cardiotoxicity are difficult to ignore (Will et al. 2008). Previous research studies have failed to identify a single general mechanism for tyrosine kinase inhibitor induced cardiotoxicity, the widely acceptabed view attributes toxicity to the interruption of multiple signalling pathways (Chaar, Kamta, and Ait-Oudhia 2018). This study highlighted crizotinib induced left ventricular dysfunction on the observed haemodynamic parameters and identified upregulation of cleaved caspase 3 and identified mitochondrial superoxide increase and indication of disrupted intracellular calcium signalling.

Administration of crizotinib (1µM) to isolated langendorff hearts induced decreases in left ventricular developed pressure and increased coronary output compared with the non-treated time matched controls, suggestive of drug induced cardiovascular dysfunction. Bradycardia and QT prolongation are symptoms frequently associated with acute crizotinib treatment in patients (Lamore et al. 2020; Tartarone et al. 2015). Bradycardia is observed in human and animal subjects undergoing treatment with crizotinib, with lower heart rate relative to relevant factors (Lamore et al. 2020). Tyrosine kinases are also often associated

187

with arrythmias as a by-product of on- and off-target toxicities such as inhibition of the hERG ion channel which contributes to QT prolongation leading to increased risk of arrythmias and polymorphic ventricular tachycardia (Lamore et al. 2020; Shopp et al. 2014). The heart rate data from this study showed that the hearts treated with crizotinib (1µM) appeared to be disrupted compared to the non-treated control hearts, while crizotinib (10µM) treatment on hearts showed non-significant increase in heart rate. Hearts treated with Crizotinib (10nM and 0.1µM) did appear to reduce the heartrate compared to non-treated control however differences were not deemed statistically significant.

As mentioned earlier, bradycardia and QT prolongation were associated symptoms of crizotinib treatment (Lamore et al. 2020). The crizotinib (10nM and 0.1µM) treatment in this study appeared to induce bradycardia symptoms with reduction in heart rate compared to non-treated controls however, this was not deemed statistically significant. In published studies with other tyrosine kinase inhibitors, data from a pooled study of electrocardiograms involving another TKI, dasatinib (multiple kinase inhibitor), where dasatinib treatment led to between 3-6 second prolongation of the QT interval and 2 individuals displayed 5 beat runs of asymptomatic, non-sustained ventricular tachycardia (Brave et al. 2008). Similarly, nilotinib (a Bcr-Abl inhibitor) was associated with induction of arrhythmic beating (Schwach, Slaats, and Passier 2020). During the multiparameter *in vitro* testing of tyrosine kinase inhibitors, nilotinib treatment on isolated human cardiomyocytes for 72 hours was associated with induction of arrhythmic heart beats (Doherty et al. 2013). However, despite QT prolongation

observed in patients subjected to crizotinib treatment, associated arrythmias was not reported with sinus bradycardia recorded (Ou et al. 2011).

In addition to the underlying molecular mechanisms implicated in TKI cardiotoxicity, structural alterations of cardiotoxicity have been observed (Jacob et al. 2016). The first manifestation of such was recorded in patients undergoing treatment with imatinib developing heart failure (Kerkelä et al. 2006). Treatment with crizotinib (1μM) in this present study led to a significantly increased infarct to risk ratio development indicative of increased risk of cardiac damage (Figure 3.4.7). Myocyte mortality was also evidenced in section 3.4.3 involving MTT assessment of cell viability which showed Crizotinib 1μM treatment on cultured H9C2 cardiac myocytes resulted in significant reduction in viability compared to the non-treated control. This data was consistent with previous work by Doherty et al. (2013) during the multiparameter *in vitro* testing of tyrosine kinase inhibitors, crizotinib treatment was associated with decreased human cardiomyocyte viability, however the reported significant decreases occurred after Crizotinib 3μM concentration in that study (Doherty et al. 2013).

Similarly, sunitinib treatment which also at similar drug concentrations (sunitinib 3μM) in the same study conducted by Doherty et al. 2013, showed sunitinib treatment significantly reduced human cardiomyocyte viability (Doherty et al. 2013). A study reporting sunitinib-induced cardiotoxicity mediation was regulated by off-target AMP-activated protein kinase inhibition similar results were reported (Kerkela et al. 2009). The study assessed endomyocardial biopsies

from a patient that had undergone sunitinib treatment and in C57Bl/6 mice treated with sunitinib. Cardiomyocyte injury was reported *in vivo* and *in vitro* from biopsy retrieved from patients that underwent treatment with sunitinib and from mouse heart tissue, with structural alterations in mitochondria detected by transmission electron micrography which revealed swollen mitochondria with altered or absent cristae, characteristics which highlight cardiomyocyte mitochondrial damage and ultimately cardiomyocyte damage (Kerkela et al. 2009). The study assessing the involvement of mitogen activated kinase 7 signalling in sunitinib induced cardiotoxicity, sunitinib induced cardiac tissue damage was observed (Cooper, Samantha Louise et al. 2018). Langendorff perfusion of isolated hearts with sunitinib significantly increased infarct to risk ratio (%) compared to control (Cooper, Samantha Louise et al. 2018). The same was the case in a study to evaluate the influence of ageing on sunitinib cardiotoxicity, which again showed langendorff perfusion of isolated hearts sunitinib treatment to significantly increase infarct to risk ratio (%) compared to the corresponding controls across the age groups (Cooper, Samantha et al. 2019).

Crizotinib treatment was also reported to induce to impair viability in human induced-pluripotent stem cell-derived cardiomyocytes with a maximum concentration tested around 10μM concentration similar to what was observed in section 3.4.3 (Doherty et al. 2015). Human-induced pluripotent stem cell derived cardiomyocytes were treated for 48 hours with crizotinib and were shown to induce significant decrease to viability at 10μM concentration (Doherty et al. 2015). Similarly, Sunitinib and imatinib treatment significantly reduced viability

in cardiac fibroblasts similar to what was observed in section 3.4.3 (Burke et al. 2019). Adult cardiac fibroblasts treated with sunitinib and imatinib for 48 hours showed significant impact on viability (Burke et al. 2019). Additionally, cardiac troponin which has been a useful indicator for diagnosing myocardial infarction and early detection of adverse cardiovascular events (Paul et al. 2019). A correlation was shown between crizotinib induced decrease cardiomyocyte viability and corresponding to increased cardiac troponin detection (Doherty et al. 2015).

Section 3.4.5 described the results generated from the annexin V viability staining assessed from cultured H9C2 fibroblasts. Treatment with crizotinib 1μM did not significantly increase annexing V expression compared to the non-treated control. This appeared suggestive that crizotinib induced damage was not solely reliant on cardiomyocyte death by apoptosis. However, in section 3.3.6 accounting the cleaved caspase 3 expression, treatment with crizotinib 1μM appeared to produce increased expression of cleaved caspase 3 and this increase was deemed significant (P<0.05) compared to the non-treated control treatment. This appeared to be supported by studies conducted with nilotinib and crizotinib (Doherty et al. 2013; Schwach, Slaats, and Passier 2020). In the study conducted by Doherty et al. (2013), nilotinib and crizotinib treatment were associated with significant fold change increases in caspase 3/7 activation in human cardiomyocytes (Doherty et al. 2013). In a study to assess ER stress and cell death induction by nilotinib in H9C2 myoblasts; concentration, and time dependent increases in cleaved caspase were associated with nilotinib treatment (D. Lekes et

al. 2016) . Cells were treated for up to 48 hours with nilotinib and were associated with significant increase caspase 3/7 positive cells as well as significant increases in apoptotic and necrotic cells detected (D. Lekes et al. 2016). Imatinib treatment on isolated mice cardiomyocytes was also associated was associated with increased cleaved caspase 3 expression and significant increase in the activity of caspases 3/7 (Kerkelä et al. 2006c). A study evaluating imatinib-induced cardiotoxicity in rats, concluded that imatinib treatment was associated with cardiotoxic effects through a myriad of cellular alterations (Herman et al. 2011). Male Sprague Dawley rats were treated with imatinib showed significant increase in the number of apoptotic cardiomyocyte nuclei detected by tunnel staining compared to the control animals (Herman et al. 2011).

The present study showed that crizotinib treatment was associated with significantly increased calcium ion detection (increased signalling) compared to the non-treated control at the 1µM concentration (Section 3.4.8). Calcium signalling dysregulation has been implicated in mitochondrial dysfunction and inherently cell death with calcium overload inducing opening of the mitochondrial permeability transition pore, triggering apoptotic cascade, and increasing oxidative stress (Görlach et al. 2015; Xiongwen et al. 2005). The increase in calcium signalling observed in this study was similar to results on a study assessing sorafenib induced apoptosis on HEP G2 cells conducted by Chiou et al. (2009). Sorafenib treatment on cultured HEP G2 cells (20µM of sorafenib) was associated with calcium signalling overload detected by confocal microscopy (Chiou et al. 2009). Similarly, pathological hypertrophy induced by imatinib occurs

through alterations to calcium signalling regulation in cardiomyocytes (Barr et al. 2014). Neonatal rat ventricular myocytes were isolated from Sprague Dawley rats, and placed unto glass cover slips coated with laminin and treated with imatinib and perfused with tyrode's solution on an inverted microscope (Barr et al. 2014). The results showed that imatinib treatment was associated with significant increase in the peak amplitude of Ca^{2+} transient, significantly increased the decay rate of Ca^{2+} transient and significantly shorted the time to 50% decay. The investigators also showed imatinib treatment was associated with significant phosphorylation of Ca^{2+} regulatory proteins (Barr et al. 2014). These studies indicate that tyrosine kinase inhibition is associated with increased calcium overload.

Previous studies have attempted to establish an overriding mechanism of chemotherapy induced cardiotoxicity, with extensive work done with anthracyclines (Doxorubicin) highlighting a number of possible mechanisms (Angsutararux, Luanpitpong, and Issaragrisil 2015b). The involvement of the mitochondria and oxidative stress is often implicated due to the importance regarding energy metabolism in the cardiovascular system (Murabito, Hirsch, and Ghigo 2020a). The involvement of mitochondria in tyrosine kinase inhibitor induced cardiotoxicity and dysfunction was explored. This present study (section 3.4.7) reported significant increases in mitochondrial superoxide generation following treatment with crizotinib. Mitochondrial superoxide (ROS) is considered a major contributor towards oxidative damage and contribute towards sustained oxidative stress (Indo et al. 2015). The result of this ultimately furthers

193

mitochondrial dysfunction and ultimately cardiomyocyte damage (D. Lekes et al. 2016).

A study on imatinib cardiotoxicity implicated imatinib treatment with impairment of mitochondrial function linked with decreases in mitochondrial membrane potential, decrease in ATP concentration and cytochrome c release indicative of severe mitochondrial impairment and dysfunction (Kerkelä et al. 2006). Overall, mitochondrial dysfunction has been detected in tyrosine kinase inhibitor induced cardiotoxicity, however, it cannot be conclusively established as the overriding event which contributes to cardiotoxicity. This was evidenced in another study which sought to identify a direct relationship between mitochondrial impairment and cardiomyocyte toxicity. In a model adapted from Marroquin et al. (2007), established ATP depletion in H9C2 cells grown in glucose environment following treatment with imatinib, dasatinib, sunitinib and sorafenib , showed sorafenib treatment induced increased sensitivity to ATP depletion in galactose grown cells (Marroquin et al. 2007; Will et al. 2008). This led to the assumption that only sorafenib impaired mitochondrial function. This was also suggestive that although mitochondrial damage was observed, it is not always the major contributing factor towards cardiotoxicity. During the multiparameter *in vitro* toxicity testing of tyrosine kinase inhibitors, nilotinib and crizotinib treatment on human cardiomyocytes significantly induced ROS generation compared to control treated cells measured by dihydroethidium staining (Doherty et al. 2013).

The PI3K/AKT pathway is crucial towards cell survival and apoptotic activation (Chiarle et al. 2008). AKT phosphorylation (p-AKT) is crucial in apoptotic avoidance as it inhibits pro-apoptotic proteins (Meng et al. 2017). This present study did not reveal any changes in p-AKT expression (Section 3.4.4) although the isolated hearts treated with crizotinib 1μM produced reduced AKT expression although not significantly lower compared to non-treated control. This was consistent with studies conducted with ponatinib treatment on zebrafish and isolated neonate cardiomyocytes (Singh et al. 2019). Ponatinib treatment induced significant reduction in phosphorylation of AKT in a study to evaluate ponatinib induced cardiotoxicity. This decrease was also associated with significant decreases to cardiomyocyte viability and increased cleaved caspase-3 expression (Singh et al. 2019). These results from the study with ponatinib were similar to the results of the current study, as crizotinib 1μM treatment was associated with significant decreased cardiomyocyte viability, significant increased cleaved caspase-3 expression and slight non-significant decreased p-AKT expression.

AKT phosphorylation (p-AKT) has been shown to preserve cardiovascular function and attenuate injury following cardiac ischemia (Takashi et al. 2001). In transgenic Sprague Dawley rats with constitutively activation of Akt, these rats were evaluated for changes in cardiac function when the animals were subjected to ischemia. The animals with constitutively activated Akt were associated with significant decreases infarct regions (%) and prevented cardiomyocyte dysfunction and preserved cardiomyocyte contractility (Takashi et al. 2001).

Overall, this study provides evidence that treatment with crizotinib induced cardiotoxic events. The data produced appears to suggest severity of damage appears to follow a concentration dependent pattern, with increasing concentrations appearing to increase damage. The study does suggest an increased expression of cleaved caspase 3 and this was similar with studies using the same cell line with another tyrosine kinase inhibitor nilotinib (D. Lekes et al. 2016).

Chapter 4: Angiotensin Converting Enzyme Inhibitor Ramipril Attenuates Crizotinib Induced Myocardial Injury

4.1 Abstract

Cancer treatment with tyrosine kinase inhibitors has been implicated with cardiotoxicity. Ramipril and other ACE inhibitors have been shown to offer cardioprotection against the occurrence adverse cardiac events and preserve the myocardium against treatment induced damage. The suitability of ramipril treatment to attenuate crizotinib induced myocardial injury was evaluated

Isolated perfused hearts were treated with ramipril in combination with crizotinib for 175 minutes, haemodynamic performance and infarct development were assessed. Western blot analysis of left ventricular tissue was conducted to evaluate p-AKT expression. Ramipril in combination with crizotinib was administered to H9C2 cardiac myoblasts which were evaluated for cleaved caspase-3 expression, mitochondrial superoxide generation and calcium signalling disruption.

Ramipril co-administration with crizotinib significantly improved left ventricular developed pressure. Ramipril co-administration reduced infarct to risk ratio development, treatment increased cardiac myoblast viability, decreased mitochondrial superoxide generation and calcium ion detection, compared to treatment with crizotinib alone.

This study advocates the possible use of ramipril as an adjunctive therapy alongside crizotinib treatment to limit damage to the myocardium induced by crizotinib treatment.

4.2 Introduction

Cancers are projected to account for the leading cause of death in the 21st century and in turn act as the greatest barrier to increased life expectancy worldwide (Bray et al. 2018b). It has been widely reported that lung cancer over the last few decades has presented as one of the leading causes of cancer related deaths globally independent of gender (Costa et al. 2015). Non-small cell lung cancers account for over 80% of all lung cancer case with a dismal survival rate of about 19% overall (16% in men and 22% in females) for 5 years following late diagnosis (Molina et al. 2008). The low overall 5-year survival figures have showed marginal change the last few decades further reinforcing the burden of the condition (de Groot et al. 2018; Siegel, Miller, and Jemal 2018).

Clinically a large majority of patients are diagnosed at advanced stages of the disease, treatment at that point tends to be a lot more palliative (Sasaki et al. 2010c). Research into more effective therapies led to the approval of crizotinib (receptor tyrosine kinase inhibitors) for the treatment of advanced non-small cell lung cancer, positive for anaplastic lymphoma kinase (ALK) rearrangements (Costa et al. 2015). Crizotinib, a potent inhibitor of receptor tyrosine kinases is prescribed as the first line treatment for ALK positive non-small cell lung cancer (Gridelli et al. 2014).

Clinically, crizotinib treatment was associated with longer disease progression-free survival, significantly greater response rates, significant decrease in symptoms observed and greater improvement in overall quality of life (Shaw et al.

2013). Crizotinib activity is attributed to inhibitory action on ALK receptor (Cui et al. 2011; Toyokawa and Seto 2014). Tyrosine kinases inhibitors are often selective for multiple receptors, which leads to undesired toxicities due to dysfunction in non-malignant cells (Srikanthan et al. 2015). Along with the improved effectiveness of treatments, undesired injury to other organs often accompanies, with disruption in cardiovascular health of particular interest (Curigliano et al. 2016b). Cardiovascular dysfunction often linked to cardiotoxicity presents as a leading cause of mortality and long-term morbidity experienced by patients surviving cancers (Curigliano et al. 2016).

There are concerns regarding cardiac toxicity associated with tyrosine kinase inhibitors (Henderson et al. 2013; Le, Cao, and Yang 2014). Some of the more frequently observed toxicities specific to the cardiovascular system include, hypertension, left ventricular dysfunction and QT prolongation amongst others in patients undergoing crizotinib treatment (Lamore et al. 2020). Any potential health improvement achieved through crizotinib treatment could be offset by increased risk of adverse cardiovascular dysfunction (Khakoo and Yeh 2008). These present a dilemma to healthcare providers as the effectiveness of these therapies is essential to improved patient prognosis and survival non-small cell lung cancer, but increased risk of cardiovascular events ultimately reduces patient outcome.

There are a number of strategies employed to reduce the risk cardiotoxic events occurring. Some of which include administering synthetic analogues with less

cardiotoxicity associated with these agents and the administration of cardioprotective agents in combination with anticancer treatment (Curigliano et al. 2020; Zamorano et al. 2017). Compounds such as Dexrazoxane have been approved by the FDA for the treatment of anthracycline induced cardiac toxicity in adults(Angsutararux, Luanpitpong, and Issaragrisil 2015; Özdoğru 2014), Beta blockers(β Blockers) and statins are considered to display protective effects against different forms of cardiotoxicity such as diminished mortality in patients with systolic heart failure in the case of β Blockers (Anju 2013; Csapo and Lazar 2014a; Gujral, Lloyd, and Bhattacharyya 2018). Angiotensin converting-enzyme inhibitor therapy is another strategy (Curigliano et al. 2016).

The notion of ACE inhibition as a cardioprotective strategy is not novel (Tokudome et al. 2000). ACE inhibitors have been reported to display beneficial effects in a number of diseases associated with a reduced risk of heart failure (Tokudome et al. 2000). Through the inhibition of various physiological mechanisms ACE inhibitors have been credited with displaying protective properties through oxidative stress reduction, limitation of left ventricular remodelling and reduction of cell death through apoptosis (Cruz, Duarte-Rodrigues, and Campelo 2016). In addition, ACE inhibitors have been reported to reduce progression of left ventricular dysfunction in clinical settings (López-Sendón et al. 2004). This reputation is mainly borne out of the notion that the renin-angiotensin system elicits crucial role in the progression of cardiovascular disease state (Daniela et al. 2006; López-Sendón et al. 2004). These agents are usually recommended for the

treatment of heart failure, hypertension and in both acute & chronic manifestations of myocardial infarction (López-Sendón et al. 2004).

ACE inhibitors have been widely accepted to show protective properties with studies attributing credit for their roles in lowering progression of left ventricular dysfunction as well as reducing the occurrence of poor patient cardiovascular outcome (Daniela et al. 2006; López-Sendón et al. 2004). For instance, a randomised clinical study conducted to assess the effects of enalapril treatment following high-dose chemotherapy treatment reported reduction in the development of cardiotoxicity as well as reduction in the occurrence of clinically adverse events manifesting (Daniela et al. 2006). The study reported treatment with enalapril resulted in reduced cardiac troponin release (Cardiac troponin indicative of cardiomyocyte damage) as well as preserved ventricular function versus the patients that remained untreated.

A randomised trial of lisinopril (ACE) versus carvedilol (beta blocker) to prevent trastuzumab cardiotoxicity in breast cancer patients was conducted to determine which treatment was more protective against cardiotoxicity (Guglin et al. 2019). The study concluded that lisinopril treatment displayed effective reduction in cardiotoxicity incidence amongst participants compared with individuals on the beta blocker treatment (Guglin et al. 2019).

Ramipril is another ACE inhibitor which has been shown to display favourable properties regarding cardiovascular events occurrence. For instance, a study which sought to identify a link between rheumatoid arthritis and cardiovascular

complications occurring and identify whether ramipril was effective at preventing disadvantageous occurrences such as oxidative stress, tissue inflammation and fibrosis (Shi et al. 2012). The study concluded that ACE inhibition via ramipril treatment presented a novel pathway to prevention of cardiovascular events in rheumatoid arthritis.

Additionally, a study which sought to assess the effects of ramipril on cardiac hypertrophy and myocardial contractility in a right ventricular pressure model in rabbit subjects (Rouleau Jean et al. 2001). Ramipril was concluded to induce reduction in right ventricular hypertrophy, although the study admitted the difference was not significant. The study also concluded that ramipril treatment corresponded with almost total prevention of decreased contractility. Finally, a study which was conducted to assess the role of ramipril treatment in combination with candesartan against an *in vitro* model of myocardial ischemic reperfusion injury (Sheik Uduman et al. 2016). The study concluded that in combination with candesartan, ramipril was effective at producing significant reduction in oxidative stress, preserved the morphology of tissue in the myocardium and also preserved the ultrastructure of the myocardium and there was less evidence of myocyte damage in the combination treatment (Sheik Uduman et al. 2016). The above studies appear favourable to the notions of ramipril cardioprotection.

Cardiotoxicity can manifest subacute, acute, or chronic as a result of treatment from a number of targeted therapies (Albini et al. 2010). Mitochondrial dysfunction related to excessive ROS generation and Ca^{2+} homeostasis

dysregulation has been attributed to anticancer cancer therapies such as tyrosine kinases & anthracyclines (Lamore et al. 2020; Murabito, Hirsch, and Ghigo 2020b; Orphanos, Ioannidis, and Ardavanis 2009). Elevated levels of ROS contribute to cellular damage associated with oxidative stress (Angsutararux, Luanpitpong, and Issaragrisil 2015).

Ma et al. (2020) showed that sorafenib induces mitochondrial damage through increased ROS and disruption of Ca^{2+} homeostasis (Ma et al. 2020a). Isolated cardiac myocytes from male Sprague-Dawley rats treated with sorafenib showed significant induction of ROS detected by mitochondrial superoxide generation(MitoSOX), the opening of mitochondrial permeability transition pore, and dysregulated calcium homeostasis indicated by Ca^{2+} overload all indicative of mitochondrial dysfunction (Ma et al. 2020). Similarly, Chiou et al showed that sorafenib treatment was effective at inducing mitochondrial dependent oxidative stress apoptotic death in Hep G2 cells (Chiou et al. 2009). Sorafenib treatment was credited with inducing rapid generation of ROS detected by confocal microscopy (Chiou et al. 2009). Sorafenib treatment was also credited with induction of localised Ca^{2+} overload within mitochondria cytosol (Chiou et al. 2009).

Sunitinib (TKI) treatment was associated with increased ROS accumulation and increases in caspase 3/7 activity following in vivo & in vitro treatment with age (Bouitbir et al. 2019). There was also increased free radical detection further indicating mitochondrial oxidative stress (Bouitbir et al. 2019). Caspase 3 is a common effector associated with cardiotoxic agents due to its role in cell death

pathways (Siu and Alway 2009). This provide justification for considering ROS (superoxide) and calcium alteration during cardiotoxicity assessment.
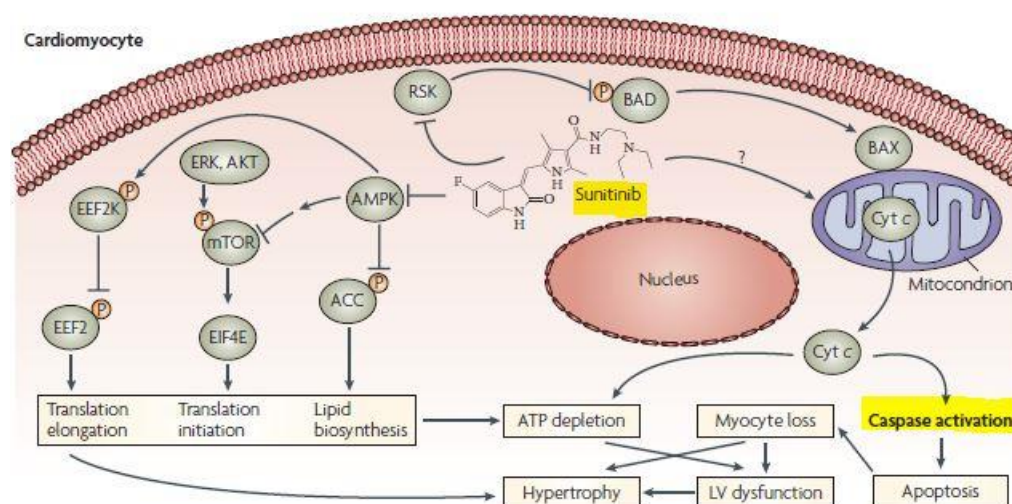
Figure 4.2.1 Role of sunitinib in initiating myocyte damage through mitochondrial involvement to promote oxidative stress through ATP depletion & myocyte loss through initiation of apoptosis [Adapted from (Force, Krause, and Van Etten 2007)].

TKI treatment with sorafenib and sunitinib had been linked with apoptotic cell death mentioned earlier (Bouitbir et al. 2019; Chiou et al. 2009; Ma et al. 2020). Sorafenib treatment was associated with mPTP opening (apoptotic hallmark) & calcium overload while sunitinib was associated with increased caspase 3 activity as earlier introduced (Bouitbir et al. 2019; Chiou et al. 2009; Ma et al. 2020). The phosphatidylinositol3-kinase (P13k)/protein kinase B (AKT) pathway is key in the regulation of cell survival (Roskoski 2013). Malignant cells hijack this pathway in their quest for survival as activation of the pathway and subsequent

phosphorylation of downstream proteins promotes processes like tumour proliferation, inhibition of apoptosis and metastasis (Franke et al. 2003; Liu et al. 2020). AKT phosphorylation(activation) is crucial as it leads to phosphorylation of several substrate specific events within the cytoplasm and nucleus making it a key figure in cell survival and apoptosis avoidance (Franke et al. 2003; Hemmings and Restuccia 2015).

In a study attempting to inhibit apoptosis via Akt-mTOR pathway in a drug induced cardiotoxicity (doxorubicin) model involving embryonic stem cell transplantation (Singla 2015). C57BL/6 mice were treated with doxorubicin intraperitoneally and the doxorubicin treated animals were associated with a significant decreased expression of phosphorylated AKT and increase in apoptosis compared to the non-treated mice (Singla 2015). Li et al. 2020 investigated whether levosimendan (induces calcium sensitivity) induced protective effects against doxorubicin induced cardiotoxicity via regulation of PTEN/Akt pathway (Li et al. 2020). Male C57BL/6 mice were administered drugs by oral gavage for 4 weeks (Li et al. 2020). Doxorubicin treatment significantly decreased p-akt expression as well as significantly increased cleaved caspase 3 expression and increased myocardial apoptosis (*in vivo* and *in vitro*) compared to the control (Li et al. 2020). These provide justification for assessment of p-AKT during cardiotoxicity evaluation.

The aims of this study were to assess the potential of ACE inhibition through ramipril co-treatment to minimise cardiovascular injury as a result of crizotinib induced cardiotoxicity. The effects were assessed in *in-vitro* whole heart models

and cardiac myocyte models. Haemodynamic performance was assessed as well as p-AKT expression heart models. Furthermore, the expression of cleaved caspase 3, mitochondrial superoxide and calcium dysregulation were assessed in cultured cardiac myoblasts.

4.3 Materials and Methods

4.3.1 Materials

Crizotinib was purchased from Carbosynth limited (UK) and dissolved in dimethyl sulphoxide prior to storage at -20 °C. Krebs-Henseleit buffer (KH) salts (118.5 mM NaCl, 25 mM NaHCO3, 4.8 mM KCl, 1.2 mM MgSO4, 1.2 mM KH2PO4, 1.7 mM CaCl2, and 12 mM glucose), were purchased from Fisher scientific (UK). The antibodies anti-rabbit antibody for phospho-Akt at Ser473 (Cell Signalling), Akt (pan) (11E7) Rabbit mAb (cell signalling) as well as anti-biotin and anti-rabbit IgG were purchased from cell signalling. Triphenlytetrazolium chloride (TTC) was purchased from Sigma Aldrich, UK. DMEM (Dulbecco's modified eagle medium) which was purchased from ThermoFisher scientific ™. Penicillin streptomycin (10,000 U/mL) purchased from Gibco ™. Foetal bovine serum (FBS) purchased from Gibco ™. Phosphate buffer saline was purchased from Gibco ™. Ramipril purchased from Tocris, Bio-techne limited (UK).

4.3.2 Animals and ethics

Adult male Sprague-Dawley rats with body weight range between 350±50 grams were purchased from Charles River UK limited (Margate, UK) were used for the

purpose of this study (Ethics number P66861). Animals were kept in humane conditions, suitably housed, and had free access to standard pellet diet and water. Handling and treatment procedures were in full accordance with the Guidelines regarding the operation and handlings of Animals (Scientific Procedures Act 1986). Animals were selected at random for drug treatment. Tissue collected for infarct analysis were blinded and stored for later analysis.

4.3.3 Langendorff isolated perfused heart preparation

Adult male Sprague-Dawley rats were humanely sacrificed by cervical dislocation and the hearts were quickly excised and placed in ice-cold KH buffer. The rat hearts were then mounted unto the langendorff apparatus and perfused continually with KH buffer. The KH buffer was maintained at pH 7.4 by continual gas supply of 95% O_2 and 5% CO_2 with the temperature maintained at 37 °C using a water-jacketed organ chamber. The left atria were then excised and a latex iso-volumic balloon carefully inserted into the left ventricle and inflated to between 5-10mmHg. Functional parameters measured, which were the left ventricular developed pressure (LVDP), heart rate (HR) and coronary flow (CF) which were monitored and recorded at regular intervals. The LVDP and HR were measured and recorded with a physiological pressure transducer and Powerlab Software, AD Instruments (UK). CF on the other hand was measured by collecting volume of perfusate for a minute in a measuring cylinder. The functional parameters measured were expressed as mean of the stabilisation period to facilitate easy

comparison between different treatment groups. At the end of the perfusion protocol, the hearts were carefully removed from the apparatus, weighed and frozen at -20°C for infarct analysis.

4.3.4 Infarct size analysis

The following morning, the now frozen hearts were sliced into about 2mm thick transverse sections and incubated in 2, 3, 5-Triphenyltetrazolium chloride (TTC) solution (1% phosphate buffer solution) and kept at 37°C for 12 minutes to determine infarct regions. Following this the slices were then fixed in 10% formaldehyde solution for at least 4 hours. Regions of risk stained red while regions of infarct in tissue stained white/pale. The risk areas and infarct areas were traced onto acetate sheets and used to calculate a percentage of infarct to risk ratio (%). The sheets were scanned, and traces were assessed using the image J software. A ratio (%) of infarct to risk size was calculated for each of the heart slices. The mean infarct to risk ratio (%) was then normalised to the weight of each heart analysed.

4.3.5 Langendorff protocol

The hearts following excision were allowed a stabilisation period of 20 minutes prior to drug treatment for 155 minutes outlined by figure 4.3.1 below. Hearts were randomly assigned to the following treatment groups; 1) Perfusion with KH buffer alone (vehicle control), 2) hearts treated with crizotinib 1μM, and 3) hearts treated with ramipril 1μM ± crizotinib 1 μM. The drugs stocks made up in DMSO were then diluted appropriately into buffer.
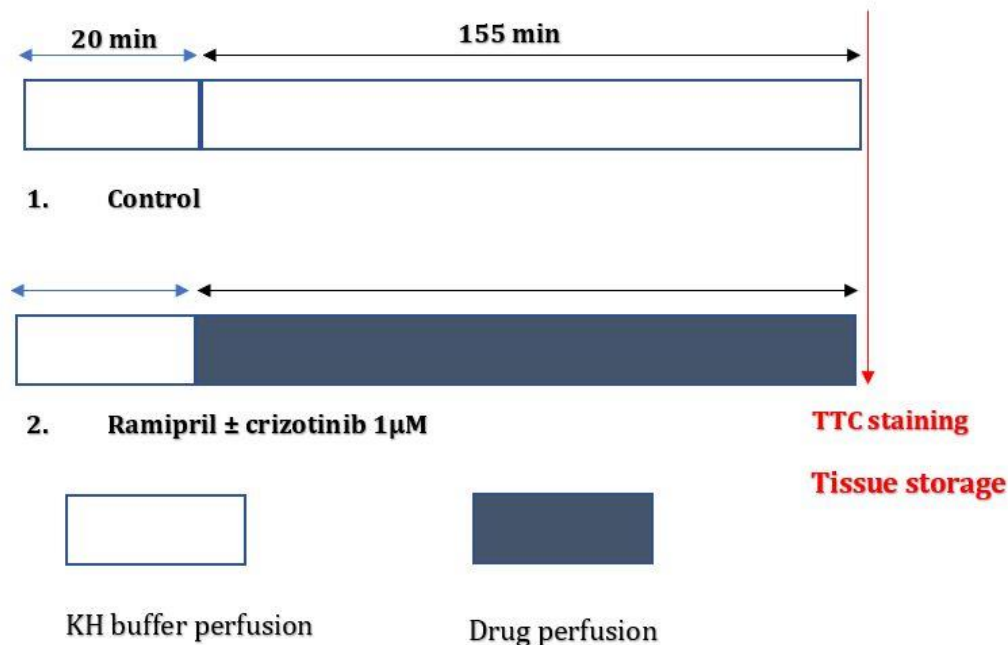
Figure 4.3.1 Langendorff drug treatment protocol

4.3.6 Western blot analysis

For the western blot protein studies, the hearts were carefully removed from the langendorff apparatus following completion of perfusion period. The left ventricles were then excised and quickly flash-frozen in liquid nitrogen and stored away at -80°C for analysis.

After thawing briefly on ice, into a 2ml Eppendorf 400μl of lysis buffer(NaCl 0.1 M,Tris base 10 μM, EDTA 1 mM, sodium pyrophosphate 2 mM, NaF 2 mM, β-glycaophosphate2 mM, 4-(2-Aminoethyl) benzene sulfonyl fluoride hydrochloride + PhosSTOP™ (Phosphatase stop) + Protease cocktail(Roche, Switzerland) and then add between 70-100 mg of frozen tissue. Throughout samples were kept on ice to prevent unnecessary heating of samples to prevent protein denaturation.

The Eppendorf with the samples were homogenised at 11000 RPM for 2 minutes and returned on ice as soon as possible. The samples were homogenised until a paste-like consistency is achieved. Homogenised samples were then subjected to BCA assay for protein quantification. Then 30µg of protein was loaded to 4–15 % Mini-Protean TGX Gel from Bio-Rad (UK) and separated at 10 V for 45 – 50 minutes. After separation, the proteins were transferred to the Bond-P polyvinylidene difluoride membrane from Bio-Rad (UK) by using the Trans-Blot Turbo transfer system from Bio-Rad (UK). Following successful transfer, the gel area was cut with a scalpel on the membrane. The membranes were then placed in a container with blocking buffer(solution of 15ml 10X TBST ; 10x TBST – 50mM Tris Base, 150mM NaCl, 0.05% Tween-20; pH 7.6) , 5% milk - 0.75 g) and then was incubated at room temperature on the orbital shaker for at least 1 hour. After blocking, blots were washed 3 times in 10 X TBST & probed for the phospho-Akt at Ser473 (Cell Signalling). The blots were placed into falcon tubes containing solution of 10ml TBST + 5% BSA with 5 µl primary antibody and incubated overnight on a roller at 4 °C.

Following overnight incubation, the blots were taken out of the falcon tubes and washed twice in 10 x TBST. The secondary antibody was then prepared (15ml TBST, 0.5g BSA and 3µl anti-rabbit IgG). The blots were then incubated in the secondary solution for 2 hours at room temperature on the orbital shaker. After incubation the blots were then washed 3 times in TBST.

A 1:1 solution of the West Femto™ reagents was made (usually about 2-3ml for 2 blots). The blot was then placed on a clear acetate film taking care to remove bubbles underneath the membranes. 1ml of the solution was then pipetted over the membrane generously and then placed into the Bio-rad ChemiDoc™ for imaging. The appropriate settings were then selected, and visualisation commenced.

Following imaging of the bands phospho-Akt at Ser473 (Cell Signalling), the membranes were stripped (0.1 L Stripping buffer for 5 minutes – 20ml SDS 10%, 12.5ml Tris HCl ,pH 6.8, 0.5M, 67.5ml distilled water, add 0.8ml β-mercaptoethanol under the fume hood and warmed to 50°C) and washed 3 times 10 x TBST. The blots were then blocked again for 2 hours and then incubated overnight in Akt (pan) (11E7) Rabbit mAb (cell signalling) 10ml TBST + 5% BSA with 5 μl primary antibody and incubated overnight on a roller at 4 °C.

Following overnight incubation, the blots were taken out of the falcon tubes and washed twice in 10 x TBST. The secondary antibody was then prepared (15ml TBST, 0.5g BSA and 3μl anti-rabbit IgG). The blots were then incubated in the secondary solution for 2 hours at room temperature on the orbital shaker. After incubation the blots were then washed 3 times in TBST.

A 1:1 solution of the West Femto™ reagents was made (usually about 2-3ml for 2 blots). The blot was then placed on a clear acetate film taking care to remove bubbles underneath the membranes. 1ml of the solution was then pipetted over the membrane generously and then placed into the Bio-rad ChemiDoc™ for

imaging. The appropriate settings were then selected, and visualisation could commence.

4.3.7 Culturing H9C2 cells

H9C2 cells were cultured in T75 flasks and supplemented with modified DMEM (Dulbecco's Modified Eagle Medium) which contained 10% FBS (Foetal bovine serum) and 1% PEN-STREP (Penicillin streptomycin). Cells were then seeded on 6-well plates and given between 48 hours for the plates to achieve full confluency. The first step was the culture the cells unto well plates as required. The cell density per well for this study was about 1×10^5 per well.

The plates were then treated with the appropriate drug and incubated overnight (24 hours). The treatment media was then discarded, and the cells were trypsinised. The dislodged cells were then transferred into eppendorf tubes with equal volume of modified media to inactivate trypsin and pelleted (100-300g for 5 minutes at 4°C). The pellets were then analysed for Cleaved caspase 3, cell death, mitochondrial superoxide, and calcium internalisation.

4.3.8 Cell viability via MTT assay

Cultured H9C2 cells in T75 flasks were first trypsinised and incubated for 5 minutes in 5% CO_2 incubator and set a temperature of 37°C to remove them from the culture flasks. About 2-3ml of supplemented media was added into the flasks to inactivate the trypsin. The cells were then pelleted and resuspended in fresh media, counted and then seeded unto plates with a density of about 1×10^5 per well about 48 hours prior to allow enough time to adhere and reach full confluency

on a 24-well plate. A few wells were filled with media alone to serve as background control.

The outer wells were filled with media alone to serve as background control. The cells were then incubated for 24 hours with crizotinib 1μM and crizotinib 1μM ± Ramipril 1 μM. Following the incubation period, the media was discarded, and the wells directly inoculated with 100μl of 5mg/ml MTT reagent and the wells were then incubated for 3 hours.

Following incubation, the solution was discarded and 100% DMSO solution was added to lyse the cells as previously described in methods section. The absorbance values were then read at 590nm. The data was normalised using the formula below.

Normalised absorbance reading = Mean absorbance value minus **(-)** Mean absorbance of cell free medium

Percentage cytotoxicity (%) = (Control (Untreated) absorbance / treated absorbance) x 100

4.3.9 Analysis of protein expression in isolated perfused tissue following drug treatment through western blotting

Following protein separation via electrophoresis, the protein bands were transferred onto the PVDF membrane and probed for the phosphorylated and total forms of AKT (Ser 473). The resultant banding on the membranes were analysed

with the aid of Image J© software. The changes in relative expression were assessed and calculated and corrected for differences in protein loading as established by probing for total protein (total AKT).

4.3.10 Assessment of cytotoxicity in cultured H9C2 cardiac myoblasts following drug treatment via annexin v detection (Abcam™ Annexin V-FITC apoptosis detection kit)

The H9C2 cardiac cell line was used for this study. The cells were first stripped from flasks and plated to a density of about 1×10^5 per well about 48 hours prior to allow enough time to adhere and reach full confluency on a 24-well plate. The plates were then inoculated with the required drug treatments and then incubated for 24 hours at 37°C. Following the incubation period, the plates were retrieved from the incubator and transferred to a laminar flow hood for the rest of the protocol.

The treatment media was discarded, and the cell suspension was then transferred into eppendorff tubes. The cells were then pelleted in a cold centrifuge and the pellet was then resuspended in 500µl of 1 X binding buffer. To each of the eppendorff tubes, 5 µl of annexin V-FITC and 5 µl of propidium iodide (for necrosis) was added. The tubes were then transferred into a dark drawer at room temperature for 5 minutes. Upon completion of the incubation period, the samples were then analysed BD Accuri™ C6 Plus personal flow cytometer set to count 5000 cells.

4.3.11 Assessment of cleaved-caspase-3 (Asp175 from cell signalling) in cultured H9C2 cardiac fibroblasts following drug treatment

The H9C2 cardiac cell line was used for this study. The cells were first stripped from flasks and plated to a density of about 1×10^5 per well about 48 hours prior to allow enough time to adhere and reach full confluency on a 24-well plate. The plates were then inoculated with the required drug treatments and then incubated for 24 hours at 37°C.

The treatment media was discarded, and the cells required trypsinisation for detachment from the plate. The trypsinised cell suspension was then transferred into eppendorff tubes. The trypsin was then inactivated with equal volume of modified media. The cells were then pelleted in a cold centrifuge (100-300g for 5 minutes at 4°C) and the resultant pellet was resuspended in 100μl of 4% formaldehyde solution to fix the cells at room temperature for 15 minutes. The suspension was then washed afterwards in excess 1 X PBS solution and pellet and discard the supernatant. The samples were then resuspended in 0.5 – 1ml of PBS solution.

The fixed cells were then permeabilized with ice chilled 100% methanol added dropwise to the pre-chilled cells bringing the final concentration to 90% methanol solution. The samples were left for 10 minutes on ice and transferred to then be stored at – 20 °C or could be carried further for immunostaining.

The first step leading up to the immunostaining procedure was to count cells and aliquot desired number of cells into tubes (approximately 5×10^5). The samples

were then washed in PBS to remove methanol and the resultant pellet was then diluted in 100μL of diluted primary antibody solution (Cleaved caspase-3 antibody dilution buffer based). This was then allowed to incubate for 1 hour at room temperature. The samples were then washed in 1 x PBS, pelleted and washed again for a second time. The samples were then resuspended in the secondary antibody solution (Alexa Flour® conjugate) which was also prepared in antibody dilution buffer. This was then allowed to incubate for 30 minutes at room temperature in dark condition. The samples were then washed 2 times in 1 x PBS. The pellet was finally resuspended in 500 μl of 1 x PBS ready for analysis on the BD Accuri™ C6 Plus personal flow cytometer set to count 10000 cells.

4.3.12 Assessment of mitochondrial superoxide generation following treatment of cultured H9C2 cardiac Myoblasts

The H9C2 cardiac cell line was used for this study. The cells were first stripped from flasks and plated to a density of about 1×10^5 per well about 48 hours prior to allow enough time to adhere and reach full confluency on a 24-well plate. The plates were then inoculated with the required drug treatments and then incubated for 24 hours at 37°C.

Following the treatment period, the media was discarded. The cells were then washed and stripped from the plates. The cells were then pelleted in eppendorff tubes. Pellets were then resuspended in 5μM MitoSOX™ reagent and left to incubate for 10 minutes at 37^0C in a dark incubator. Following this the cells were

then washed twice and resuspended in 1ml 1 X PBS. The samples were than analysed on the BD Accuri™ C6 Plus personal flow cytometer set to count 5000 cells.

4.3.13 Assessment of calcium ion detection following treatment of cultured H9C2 cardiac Myoblasts

Disruptions in calcium signalling and homeostasis could contribute towards apoptosis, with increases in Ca^{2+} a hallmark of early and late stage apoptotic pathway (Pinton et al 2008). Therefore, calcium internalisation could serve as an indicator of cell death.

The H9C2 cardiac cell line was used for this study. The cells were first trypsinised from flasks and plated to a density of about 1×10^5 per well about 48 hours prior to allow enough time to adhere and reach full confluency on a 24-well plate. The plates were then inoculated with the required drug treatments and then incubated for 24 hours at 37°C.

The treatment media was discarded, and the cells required trypsinisation for detachment from the plate. The trypsinised the cell suspension was then transferred into eppendorf tubes. The trypsin was then inactivated with equal volume of modified media. The cells were then pelleted in a cold centrifuge (100-300g for 5 minutes at 4°C). Pellets were then resuspended in 1ml of 5μM Fluo-3, AM, Calcium Indicator solution and incubated for 30 minutes 37°C. Following this the cells were then washed twice and resuspended in 1ml 1 X PBS. The samples

were than analysed on the BD Accuri™ C6 Plus personal flow cytometer set to count 5000 cells.

4.3.14 Statistical analysis

As previously stated, the processed data was presented as mean ± Standard error of the mean (SEM). Haemodynamic data was tested for differences using Two-way analysis of variance (ANOVA) with Fischer's LSD post hoc tests for the different time points using GraphPad prism 8 software. Infarct data was assessed so statistical differences between the individual groups using the one-way ANOVA and Tukeys post hoc test. MTT data was assessed so statistical differences between the individual groups using the one-way ANOVA and Fischer's LSD post hoc tests. Fold changes for AKT expression was assessed so statistical differences between the individual groups using one-way ANOVA and Fischer's LSD post hoc tests. P-values less than 0.05($P< 0.05$) were considered statistically significant.

4.4 Results

4.4.1 The effect of ramipril on crizotinib induced myocardial dysfunction (haemodynamic assessment)

Isolated rat hearts were perfused for 175 minutes with crizotinib (1µM) in the absence and presence of ramipril (1µM) and cardiac function was measured and recorded at regular intervals. Each of the hearts haemodynamic performance In Left Ventricular Developed Pressure (LVDP), Heart Rate (HR) and Coronary Flow (CF) were monitored and recorded. During the first 55 minutes of perfusion, readings were taken at 5-minute intervals and following 55 minutes the reading

intervals was extended to 15 minutes. The drug concentrations considered in this study were Crizotinib (1µM) and Ramipril (1µM) ± Crizotinib (1µM) and the non-treated vehicle controls.

4.4.1a Variations in LVDP (%) for isolated adult male rat hearts treated with Ramipril (1µM) ± Crizotinib (1µM)

The hearts with the ramipril co-treatment appeared to produce a greater LVDP (%) compared to the crizotinib treated samples over the treatment period.

There was no significant difference observed between the groups within the first 20-minute time period (Figure 4.4.1). However, following the 20-minute period, the samples began to display more dissimilarity.
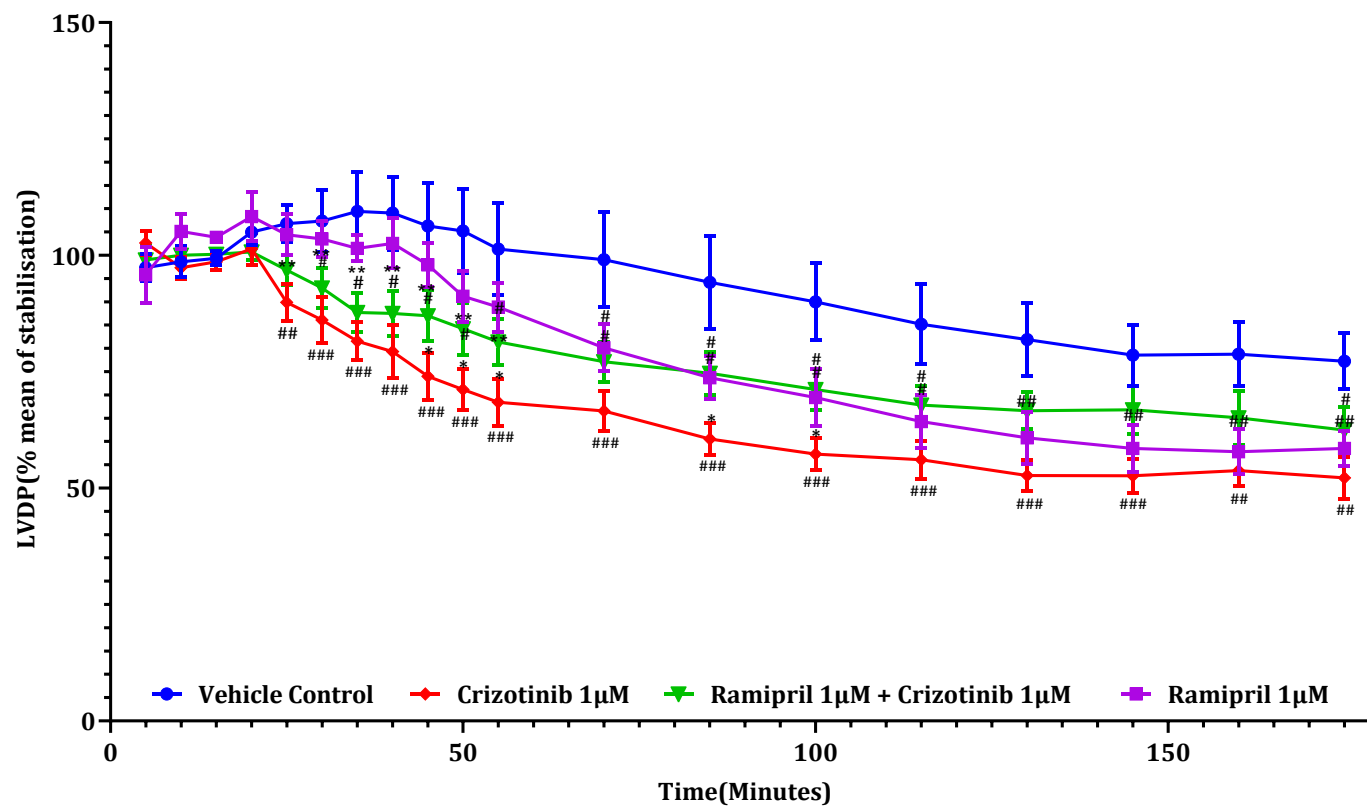
Figure 4.4.1 The effects of treatment with crizotinib 1µM, ramipril 1µM ± crizotinib 1µM and vehicle treatment on left ventricular developed pressure (LVDP) in adult Sprague-Dawley rats treated for 175 minutes (where #P<0.05,

##P<0.01, ###P<0.001 versus time matched vehicle control treatment; *P<0.05 versus the time matched crizotinib (1µM) treatment. N=6).

At the 30-minute measurement period, isolated hearts treated with crizotinib alone and ramipril in combination with crizotinib significantly reduced LVDP (%) compared to the non-treated control hearts (107.35±6.63% versus 86.1±5%, where P<0.05 for crizotinib treatment alone and 107.35±6.63% versus 93±4.21% respectively, where P<0.001 for ramipril in combination with crizotinib respectively) (Figure 4.4.2). Treating isolated rat hearts with crizotinib alone significantly reduced LVDP (%) compared to hearts treated with ramipril alone (86.1±5% versus 103.52±3.9%, where P<0.001).There was no significant difference between the treatment for the crizotinib treatment alone and the ramipril alone treatment at this time interval.
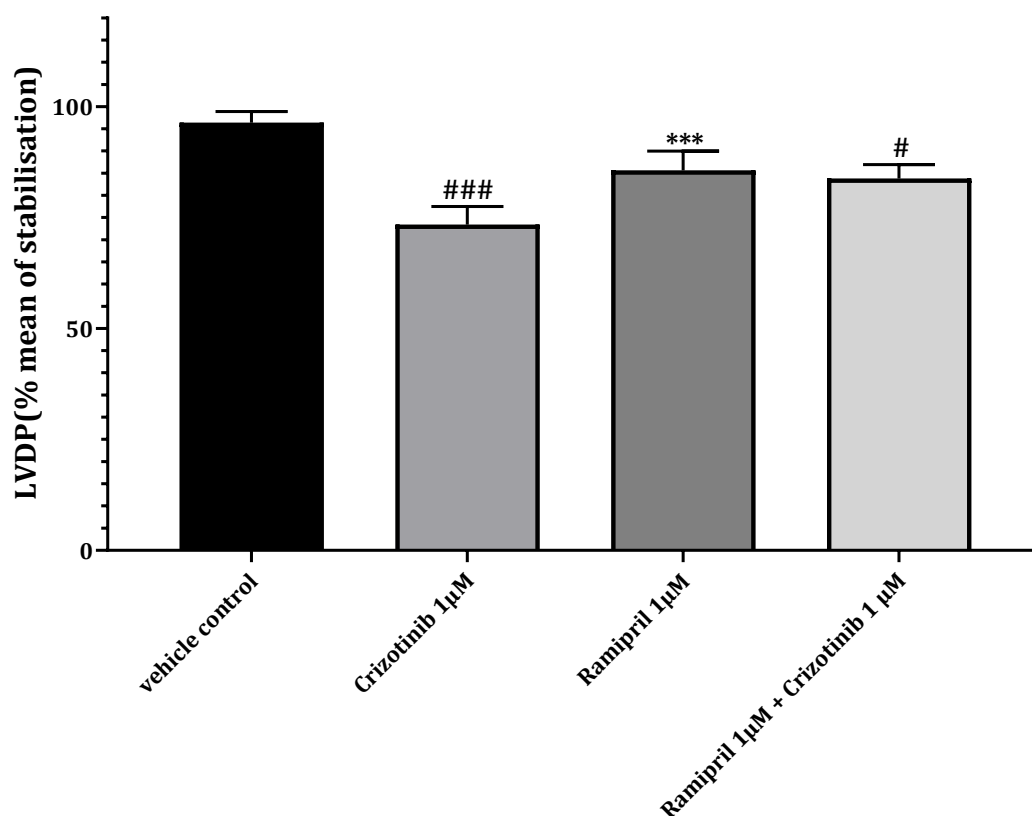
Figure 4.4.2 Assessment of left ventricular pressure performance in isolated adult male Sprague-Dawley rat hearts at the 30-minute measurement period. There was evidently significant difference between the treatment regimens versus the time matched control treatment. (Data was presented as mean ± SEM where #P<0.05 and ### P<0.001 versus time matched vehicle control, ***P<0.001 versus treatment with crizotinib alone).

Similar to the case at the 30-minute interval, crizotinib treatment alone and the ramipril co-treatment both significantly reduced the LVDP (%) in isolated hearts compare to the non-treated control hearts 45 minutes into perfusion (97.4±3.94% versus 74.99±5.11%, P<0.001, 97.4±3.94% versus 86.99±5.56%, P<0.05 respectively). Interestingly, ramipril co-treatment improved the LVDP (%)

compared to the isolated hearts treated with crizotinib alone (87±5.56% versus 74.02±5.11% respectively, P<0.05). Treating isolated rat hearts with crizotinib alone significantly reduced LVDP (%) compared to hearts treated with ramipril alone (74.99±5.11% versus 97.93±4.76% respectively, P<0.01) (figure 4.4.3).
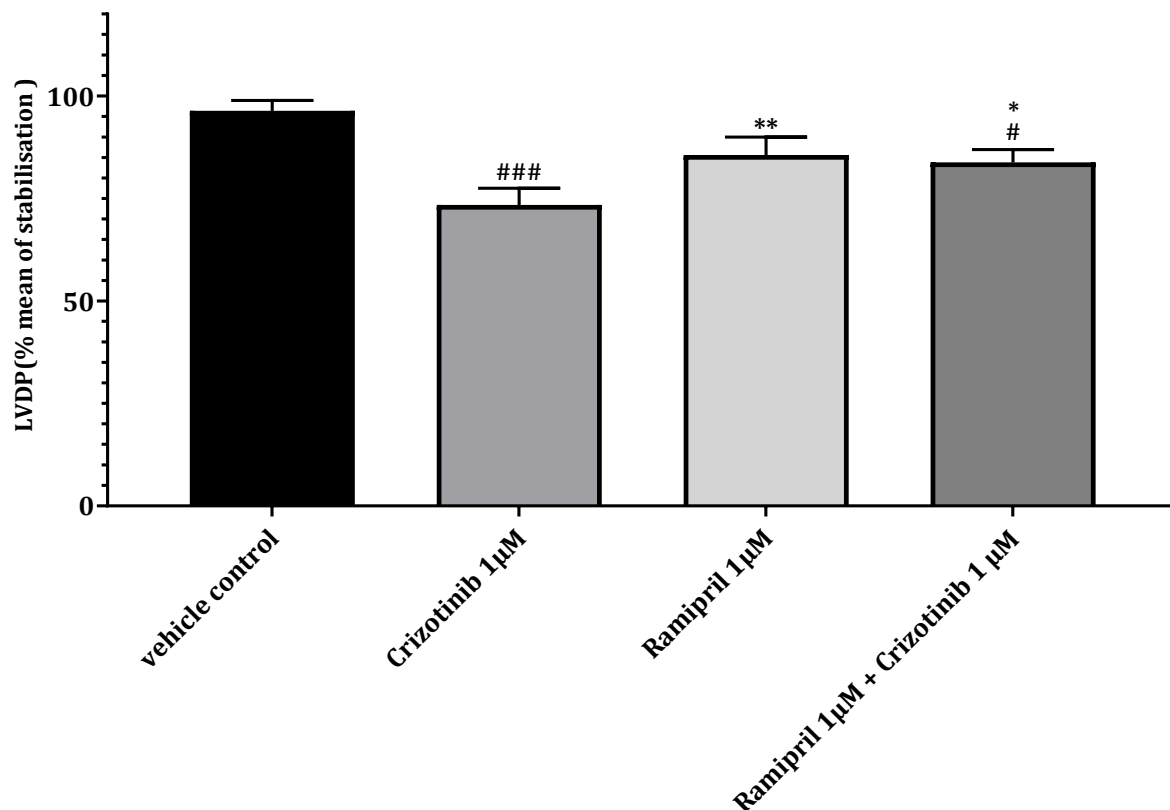
Figure 4.4.3 Assessment of left ventricular pressure performance in isolated adult male Sprague-Dawley rat hearts at the 45-minute measurement period. There was evidently significant difference between the treatment regiments versus the time matched control treatment. (Data was presented as mean ± SEM where #P<0.05 and ### P<0.001 versus time matched control, *P<0.05 versus time matched crizotinib treatment).

Similar significant improvements were observed at the 50-minute, 55, 80 and 100-minute measurement intervals where the ramipril co-treatment improved the LVDP (%) compared to isolated hearts treated with crizotinib alone at the stated intervals.

At the 50-minute measurement period, co-treatment with ramipril significantly increased LVDP (%) in isolated hearts versus hearts treated with crizotinib alone (84.24±5.55% versus 71.16±4.46% where $P<0.05$). Similarly, at the 55-minute interval, the co-treatment significantly increased LVDP (%) in isolated hearts versus hearts treated with crizotinib alone (81.38±4.94% versus 68.45±4.1% where $P<0.05$).

At the 100-minute measurement period hearts treated with ramipril co-administered again significantly improved the LVDP (%) versus the crizotinib treated alone (71.20±4.47% versus 57.32±3.45% where $P<0.05$) (Figure 4.4.4).
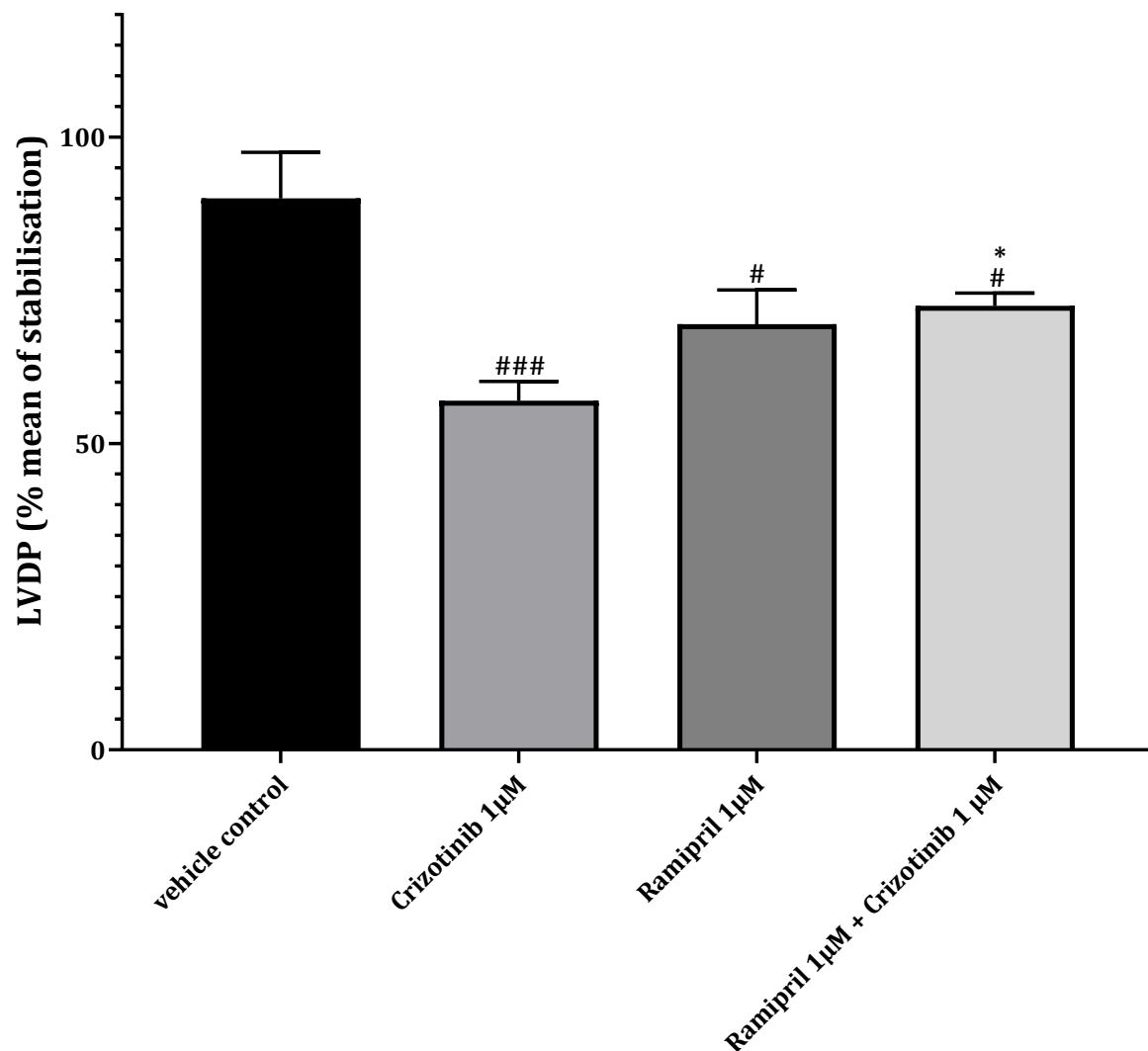
Figure 4.4.4 Assessment of left ventricular pressure performance in isolated adult male Sprague-Dawley rat hearts at the 100-minute measurement period. There was evidently significant difference between the treatment regiments versus the time matched control treatment. (Data was presented as mean ± SEM where #P<0.05, ### P<0.001versus time matched control, *P<0.05 versus time matched crizotinib treatment).

Co-treatment with ramipril (1μM) and crizotinib (1μM) on isolated rat hearts significantly improved LVDP (%) versus Crizotinib (1μM) treatment alone at 45, 50, 55, 80 and 100-minute measurement intervals (Figure 4.4.1).

4.4.1b Heart rate (%) variation in response to treatment with Crizotinib (1μM) ± Ramipril (1μM) recorded in adult isolated rat hearts

Rat hearts treated with Crizotinib (1μM) displayed an unstable response. The ramipril co-treatment sample displayed a more stable initial increase and achieved its peak heart rate (%) at the 25-minute interval (corresponding to 5 minutes into perfusion). Subsequently the trend showed decline and maintained a more response (figure 4.4.5).

The ramipril co-treatment significantly increased the heart rate (%) at 30 minutes in isolated hearts compared with crizotinib (1μM) treated hearts alone (103.9 ± 2 % versus $94.43\pm3.35\%$, where $P<0.01$) (Figure 4.4.6). Interestingly, the ramipril co-treatment also significantly increased the heart rate (%) compared in the isolated rat hearts compared to hearts treated with ramipril alone ($103.9\pm1.99\%$ versus $92.16\pm2.88\%$, where $P<0.01$).

At the 50-minute measurement interval, the heartrate (%) for the ramipril co-treated hearts decreased below the crizotinib treated hearts remaining fairly uniform.
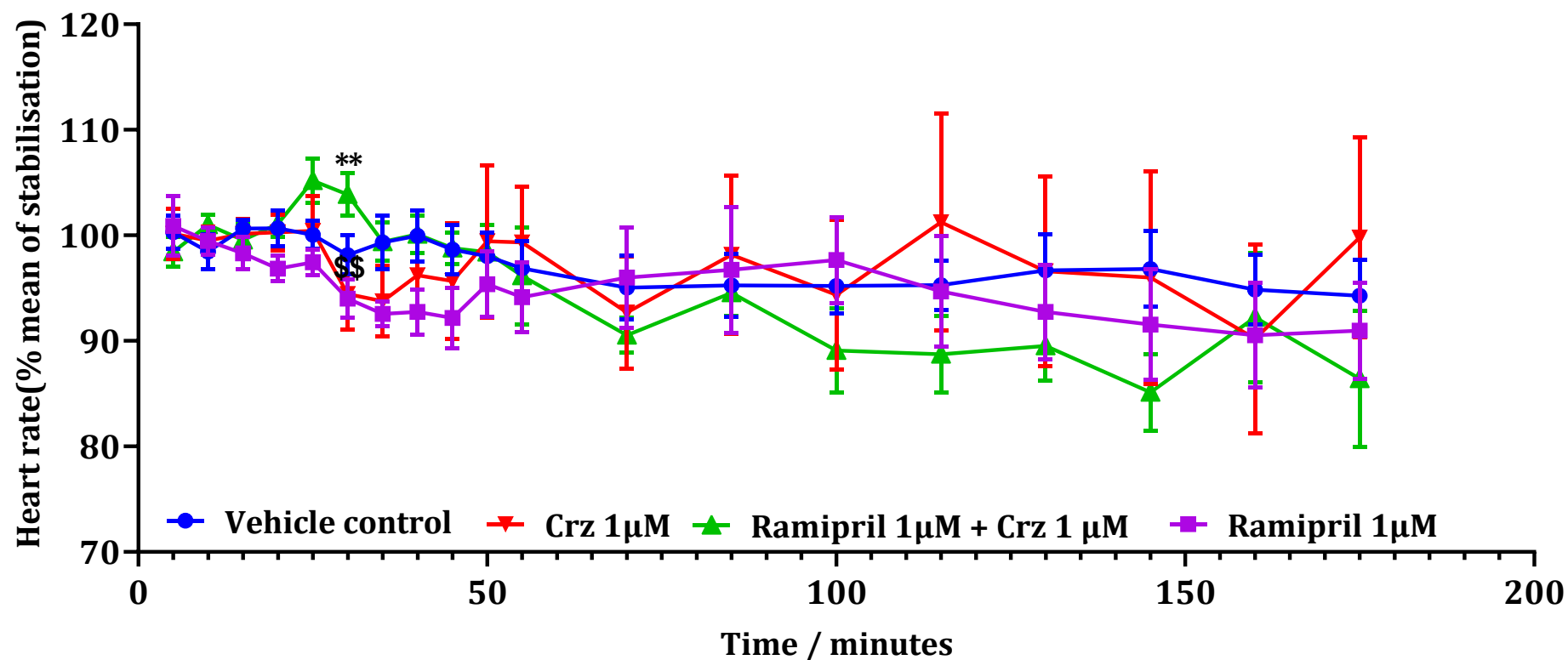
Figure 4.4.5 The effects of treatment with vehicle control, crizotinib 1μM and ramipril 1μM + crizotinib 1μM on heart rate (HR) in adult Sprague-Dawley rats treated for 175 minutes. The figure shows the trend observed between vehicle control, crizotinib 1μM and ramipril 1μM + crizotinib 1μM treated rat hearts with 20 minutes stabilisation followed

by 155 minutes of drug perfusion (Where **P<0.01 versus samples treated crizotinib 1µM, $$P<0.01 versus treatment with Ramipril 1µM + Crz 1 µM, n=6).

Figure 4.4.6 Assessment of heart rate measurement in isolated adult male Sprague-Dawley rats at 30 minutes of measurement. The figure shows the trend observed between vehicle control, crizotinib 1µM and ramipril 1µM + crizotinib 1µM treated rat hearts with 20 minutes stabilisation followed by 155 minutes of drug perfusion (Where **P<0.01 versus samples treated Crizotinib 1µM, n=6).

4.4.1c Variations in coronary flow in adult isolated rat hearts in response to treatment with Crizotinib (1µM) ± Ramipril (1µM)

The hearts co-treated with ramipril displayed an increased coronary output (%) over the perfusion period with significant increases observed at 35 minutes, 85 minutes, 100 minutes, and 130 minutes compared to the non-treated control and crizotinib treated hearts (4.4.7). Treatment with co-treated ramipril and crizotinib significantly increased coronary flow (%) compared to treatment with hearts treated with ramipril alone at every time point from 30 minutes till 175-minute measurement point (Figure 4.4.7).

Figure 4.4.7: The effects of treatment with vehicle control, crizotinib 1μM and ramipril 1μM + crizotinib 1μM on coronary flow in adult Sprague-Dawley rats treated for 175 minutes. The figure shows the trend observed between vehicle control, crizotinib 1μM and ramipril 1μM + crizotinib 1μM treated rat hearts with 20 minutes stabilisation followed by 155 minutes of drug perfusion (Where *P< 0.05 versus samples treated crizotinib 1μM **P<0.01 versus samples treated crizotinib 1μM alone, #P<0.05, ##P< 0.01, ###P<0.001 versus treatment with vehicle control, $$$P<0.001 versus treatment with ramipril and crizotinib n=6)
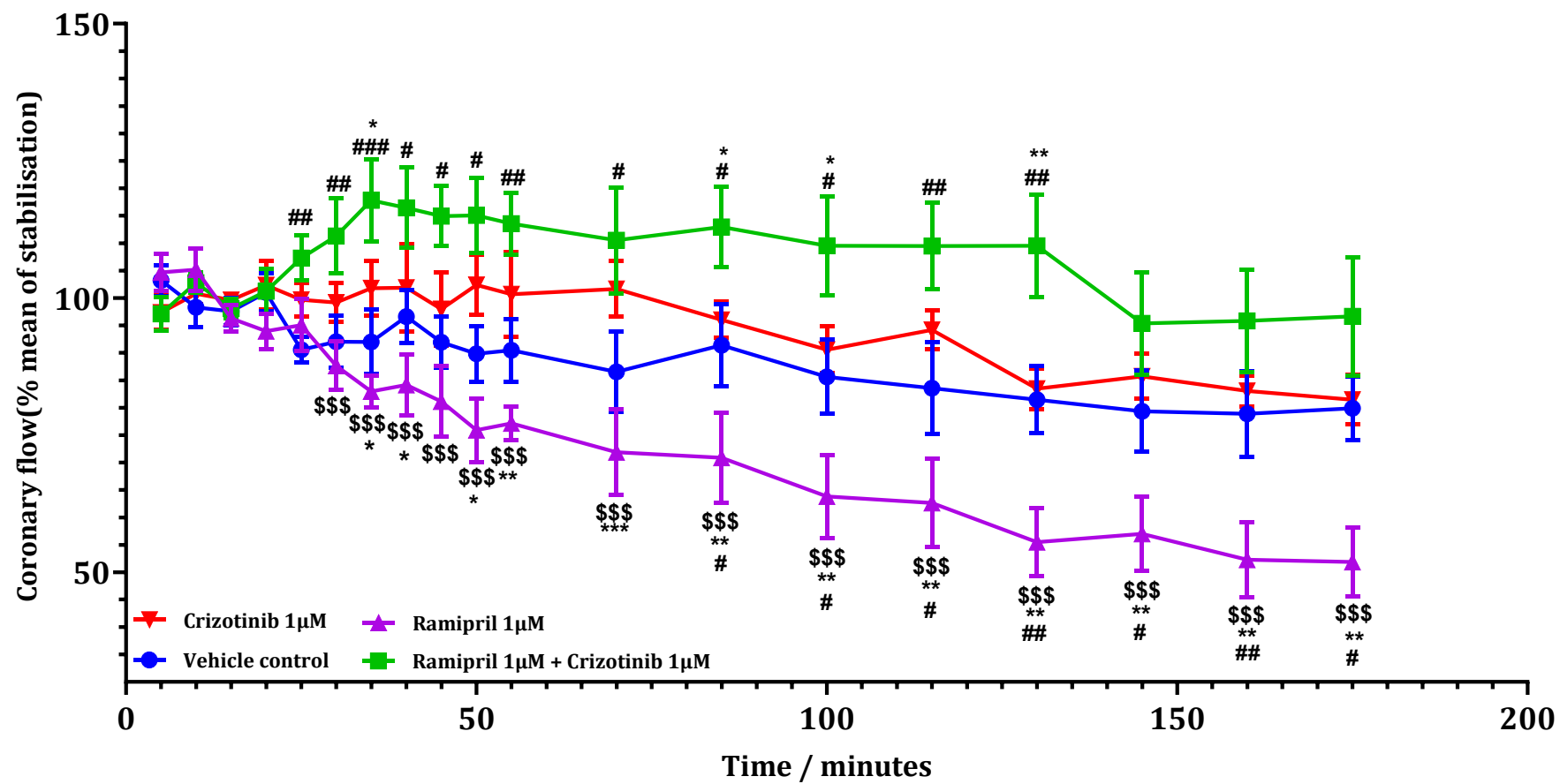
After 35 minutes, the hearts co-treated with ramipril increased coronary flow (%) compared to non-treated control and crizotinib treated hearts (117.8±7.47% versus 91.96±5.87%, where P<0.001 compared to non-treated control and 117.8±7.47% versus 101.8±5.06%, where P<0.05 compared to crizotinib treatment alone). The hearts co-treated with ramipril increased coronary flow (%) significantly compared to hearts treated with ramipril alone (117.8±7.47% versus 82.94±2.86%, P<0.001) (figure 4.4.8).
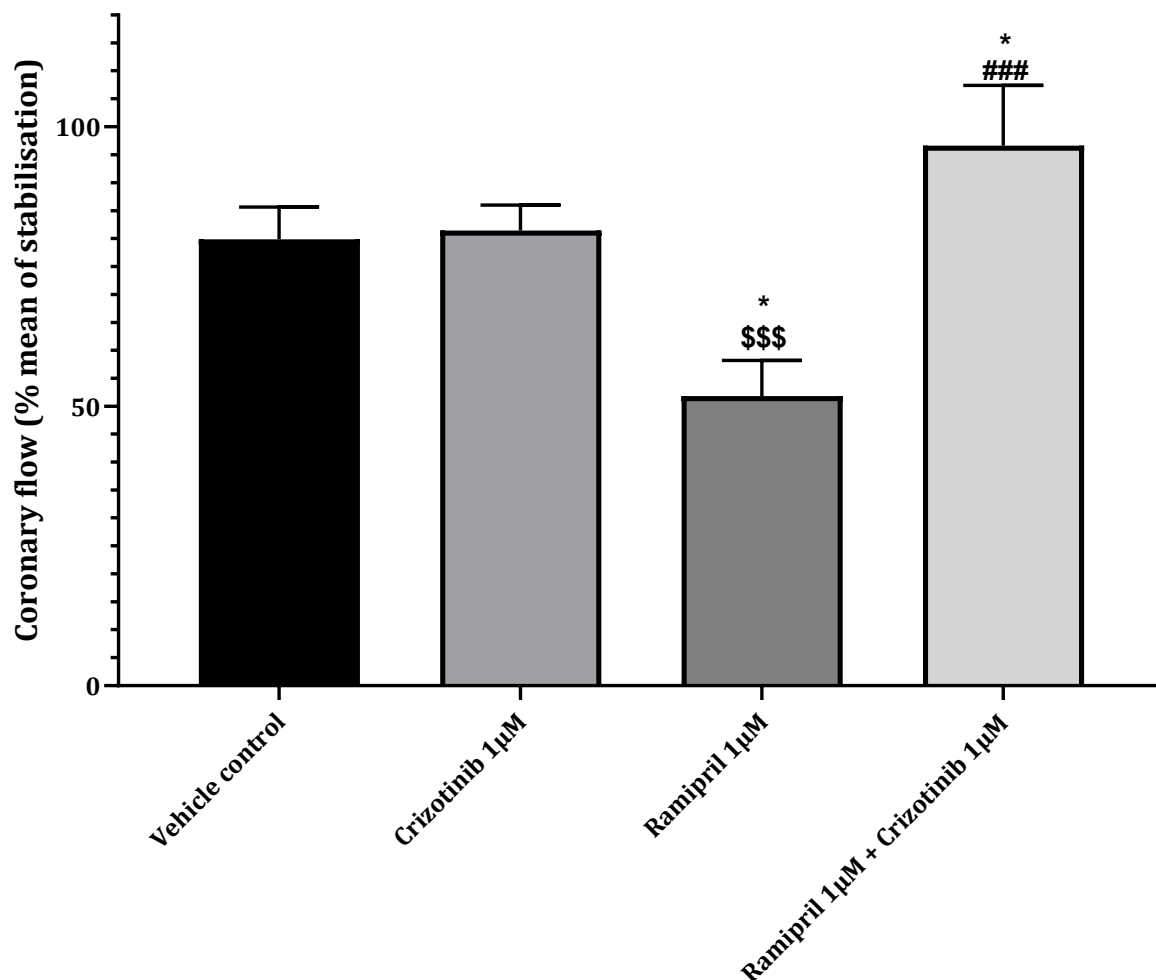
Figure 4.4.8 Assessment of Coronary flow generated from adult male Sprague-Dawley rats at 35 minutes. The figure shows the response observed between vehicle control, Crizotinib 1μM and ramipril 1μM + crizotinib 1μM treated rat hearts with 20 minutes stabilisation followed by 155 minutes of drug perfusion (Where *P<0.05 versus samples treated Crizotinib 1μM, ###P<0.001 versus time matched vehicle control, \$\$\$P<0.001 versus treatment with ramipril and crizotinib N=6).

Similarly, after 130 minutes ramipril co-treatment increased coronary flow (%) compared to non-treated control hearts and crizotinib treated hearts

(109.5±10.24% versus 81.43±6.67% where P<0.01 compared to non-treated control hearts and 109.5±10.24% versus 83.47±4.1% compared to hearts treated with crizotinib alone where P<0.01). ramipril co-treatment increased coronary flow (%) compared to ramipril treatment alone (109.5±10.24% versus 55.48±6.25%, where P<0.001) (Figure 4.4.9).
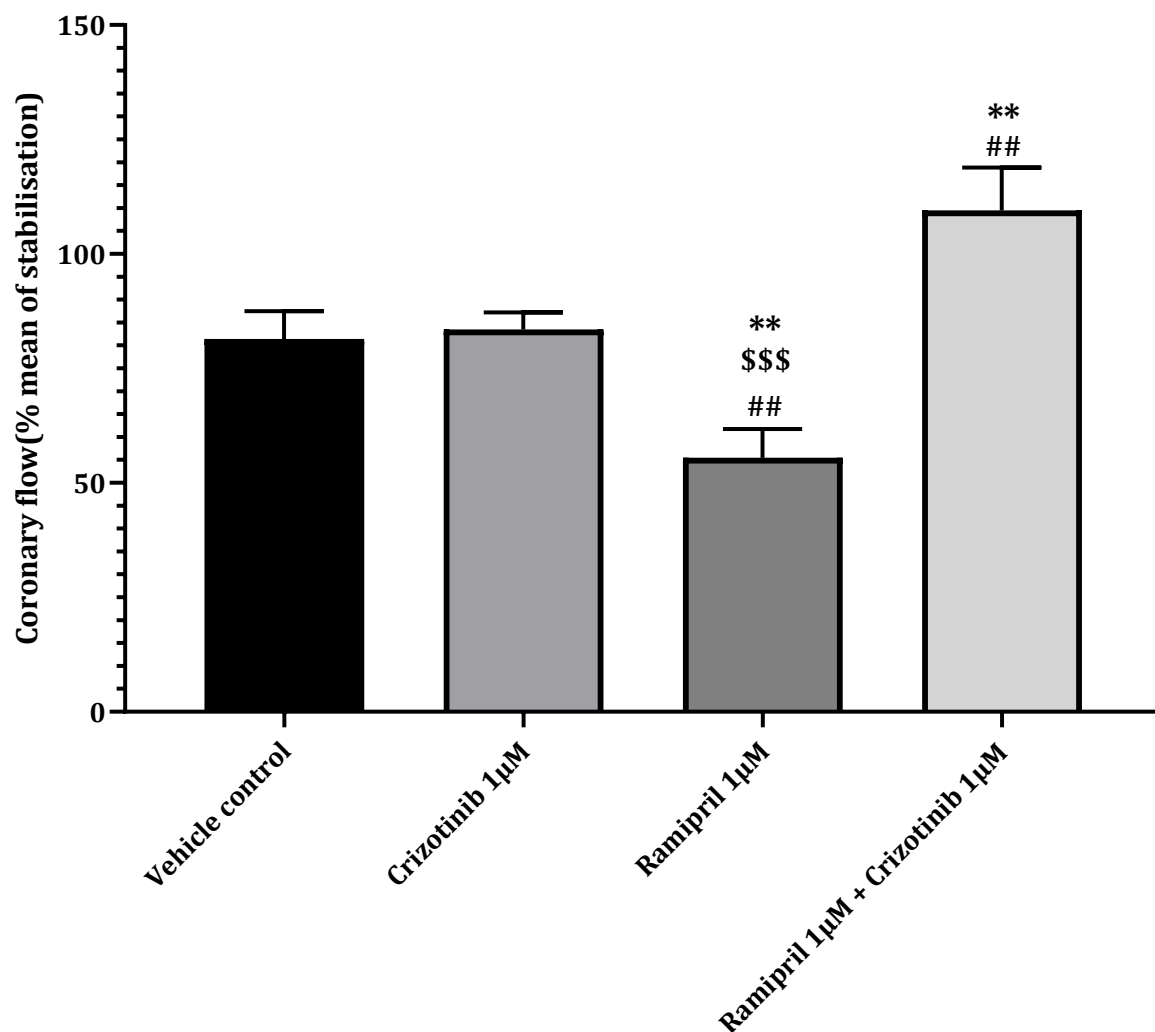
Figure 4.4.9 Assessment of Coronary flow generated from adult male Sprague-Dawley rats at 130 minutes. The figure shows the response observed between vehicle control, crizotinib 1μM and ramipril 1μM +

crizotinib 1μM treated rat hearts with 20 minutes stabilisation followed by 155 minutes of drug perfusion (Where **P<0.01 versus samples treated crizotinib 1μM, ##P<0.01 versus time matched vehicle control $$$P<0.001 versus treatment with ramipril and crizotinib n=6).

The data appears suggestive that the ramipril co-treatment was inducing a sustained increase in coronary flow compared with non-treated hearts and hearts treated with crizotinib alone.

The data also shows hearts treated alone recorded significantly lower flow values compared to the other treatments (figure 4.4.7).

4.4.2 The effect of ramipril co-treatment on crizotinib induced changes in mean infarct size to risk ratio (%) developed in isolated adult male Sprague-Dawley rat hearts following langendorff perfusion

Upon completion of the heart perfusions with the different drug conditions, the heart tissue was frozen for infarct analysis at a later time previously described.

Hearts treated with crizotinib alone produced the greatest infarct/risk ratio (%). Treatment with ramipril in combination with crizotinib decreased the infarct/risk ratio (%) in samples treated with crizotinib alone (11.27±1.624% versus 23.4±5.58%, % where P<0.001). Similarly, treatment with ramipril alone significantly reduced infarct to risk ratio (%) development in hearts compared to hearts treated with the co-treatment of ramipril and crizotinib (7.342839±1.61 versus 13.11±2.87%, where P<0.05) (figure 4.4.9).
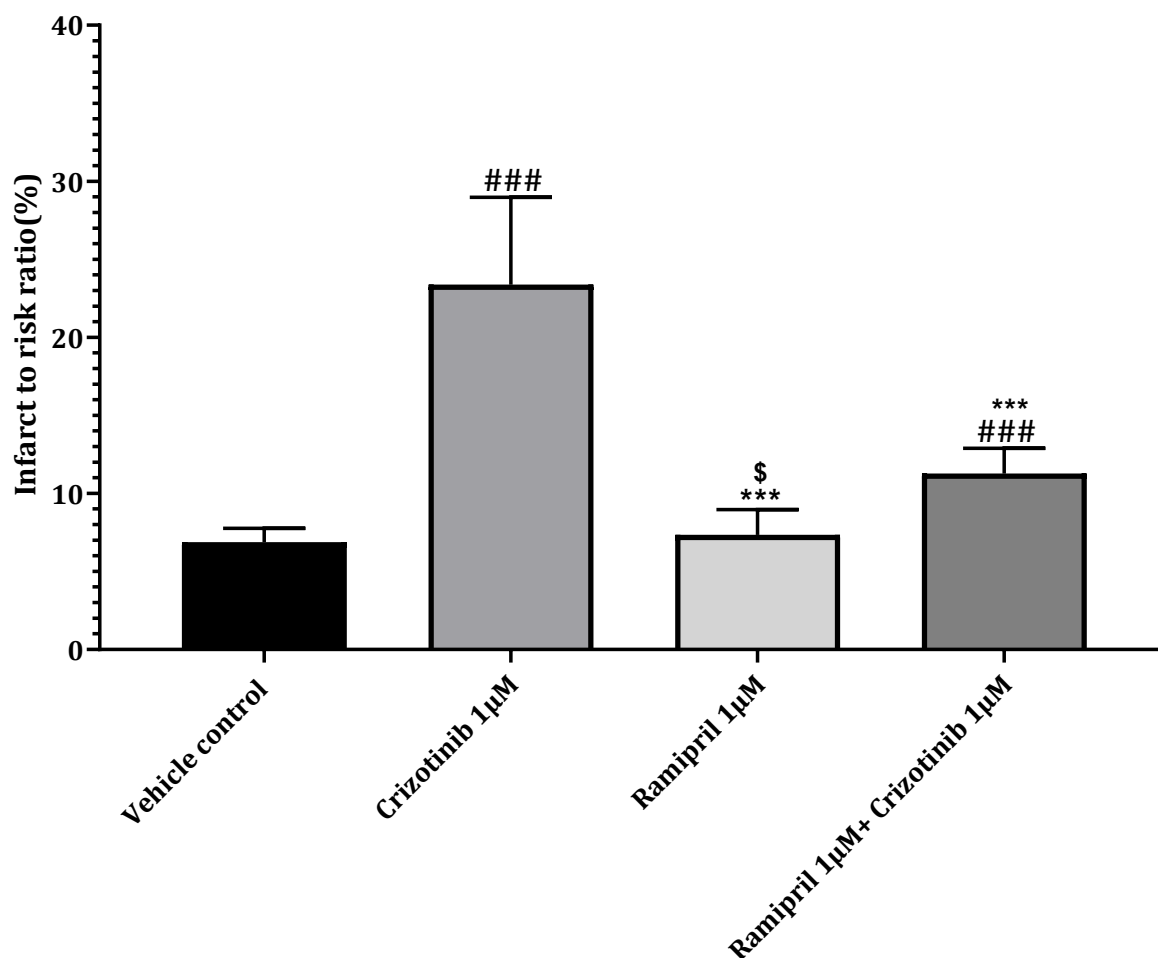
Figure 4.4.10 Assessment Mean infarct size to risk ratio (%) developed in isolated adult male Sprague-Dawley rat hearts following treatment for 175-minutes with Vehicle control, crizotinib 1μM ± ramipril 1μM added 20 minutes into perfusion (Data was presented as mean ± SEM, **P<0.01 vs crizotinib 1μM, ###P<0.001 vs control, $P<0.001 versus treatment with ramipril and crizotinib where n=6)

Hearts treated with ramipril in combination with crizotinib significantly increased infarct/risk ratio (%) compared to non-treated control hearts (11.27±1.624% versus 3.805±0.0.4046%, where P<0.001) (figure 4.4.9).

The deduction from this set of data again was ramipril may have been limiting infarct development as opposed to complete prevention.

4.4.3 The effect of ramipril co-treatment on crizotinib induced reduction in cell viability in cultured H9C2 cardiac Myoblasts

A. Ramipril co-treatment on crizotinib induced reduction in viability determined by MTT assay

The MTT (3-(4, 5-dimethylthiazol-2-yl)-2-5-diphenlytetrazolium bromide) assay was employed as a mechanism to assess cell viability. The assay served to identify cells which are participating in active respiration (viable cells). The intensity of the colour produced through the assay analysed using the microplate reader was an indication to the number of viable cells present within each of the wells.

The cultured H9C2 myoblasts incubated with the ramipril co-treatment significantly reduced viability (%) compared to the non-treated control cells 64.22±5.95% versus 102.69±7.57%, where P<0.001 versus the non-treated controls) (Figure 4.4.11).

The cultured H9C2 myoblasts incubated with the ramipril co-treatment significantly increased cell viability (%) compared to the cells treated with crizotinib alone (64.22±5.95% versus 36.78±5.82% where P<0.001) (Figure 4.4.11).

The cultured H9C2 myoblasts incubated with the ramipril treatment alone significantly reduced observed viability compared to hearts treated with ramipril in combination with crizotinib (94.08±3.85% versus 64.22±5.95%, where P<0.001).
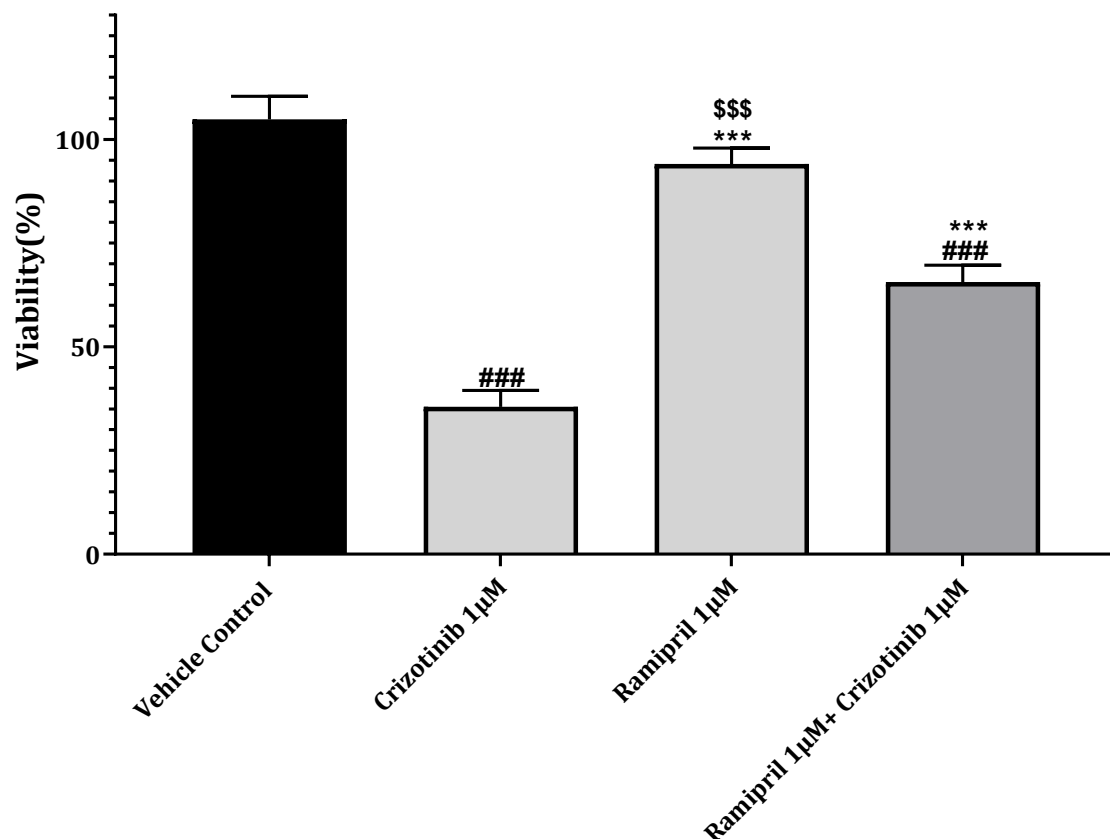
Figure 4.4.11 Assessment of MTT (3-(4,5-dimethylthiazol-2-yl)-2-5-diphenlytetrazolium bromide) assay derived cell viability of H9C2 cardiac cells treated for 24 hours with vehicle control, Crizotinib 1μM ± ramipril 1μM (Data was presented as mean ± SEM; where n=6, ***P<0.005 vs Crizotinib 1μM, ###P<0.005 vs vehicle control, \$\$\$ P<0.005 versus ramipril 1μM ± crizotinib 1μM).

Co-treatment with ramipril and crizotinib on cultured H9C2 myoblasts significantly improved cell viability compared to cells treated with crizotinib (1μM) alone.

4.4.3.b The effects of ramipril co-treatment on cell viability determined through Annexin V expression in cultured H9C2 cardiac fibroblasts

As was described previously in the methods section, the Abcam™ Annexin V-FITC apoptosis detection kit for the purpose of this experiments. Annexin V has strong affinity for external membrane phosphatidylserine as an indicator of apoptosis in studied cells.

Upon completion of treatment and staining protocols, samples were analysed by flow cytometry.

The cultured H9C2 cardiac myoblasts treated with ramipril & crizotinib cotreatment did not appear to significantly increase annexin v expression compared to the non-treated vehicle controls and myoblast treated with crizotinib alone. It did however significantly increase annexin v expression compared to samples treated with ramipril alone (36.41±3.82% versus 44.63±4.03% respectively, where P<0.05) (Figure 4.4.12).
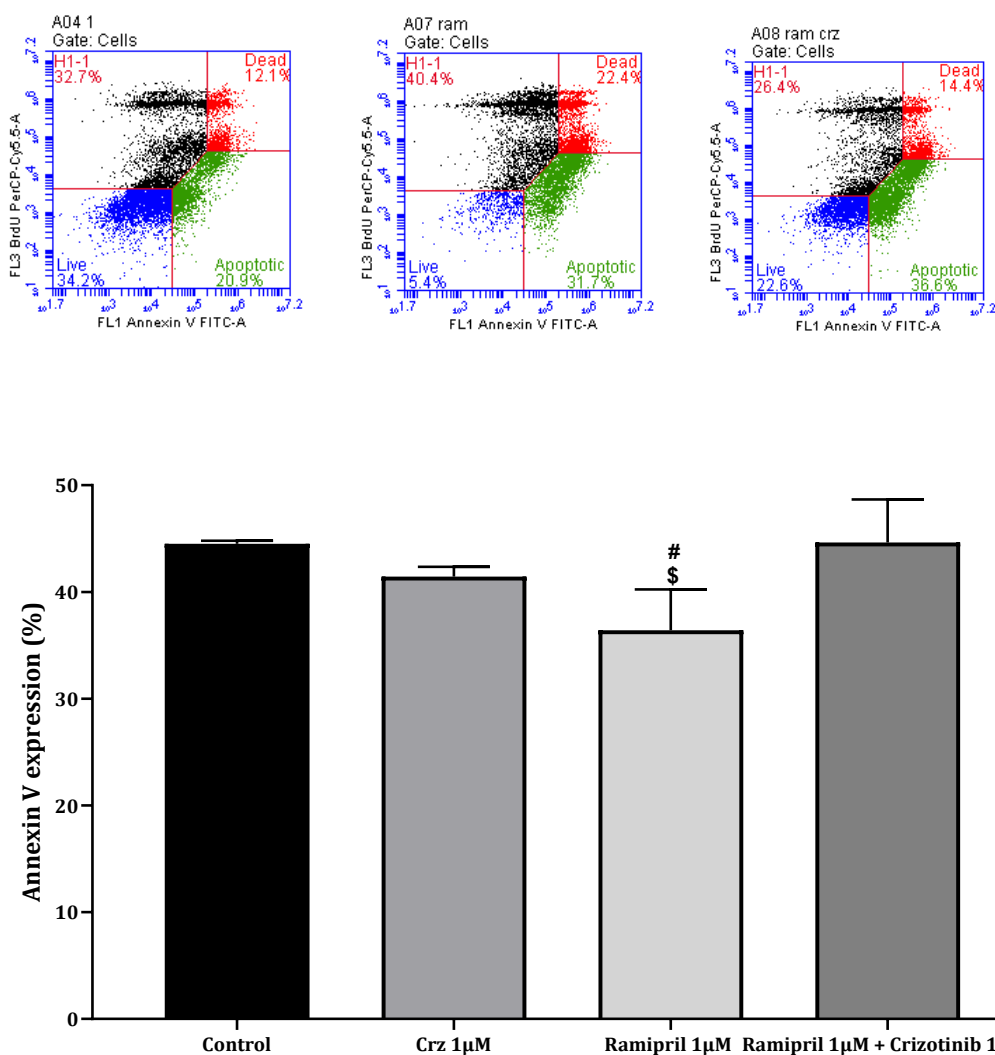
Figure 4.4.12 Assessment of annexin V expression in cultured H9C2 cells treated for 24 hours with ramipril, crizotinib ± ramipril (data presented as mean ± SEM, #P<0.05 versus vehicle control treatment, $P<0.05 versus treatment with ramipril + crizotinib).

Cultured H9C2 myoblasts treatment alone also significantly reduced annexin v activity compared to samples treated with vehicle control (36.41±3.82% versus 44.51±0.29% respectively, where P<0.05).

4.4.4 The effect of ramipril co-treatment on crizotinib induced expression of phosphorylated AKT in left ventricular tissue of adult male Sprague-Dawley rat hearts

Following the protocol outlined in the methods section the band intensities were analysed. The band intensities (signal) were normalised and the data depicted was the ratio of the phosphorylated protein to the total protein. Figure 4.4.13 provided a representation of the expression of phosphorylated AKT protein to total AKT.

A)

B)
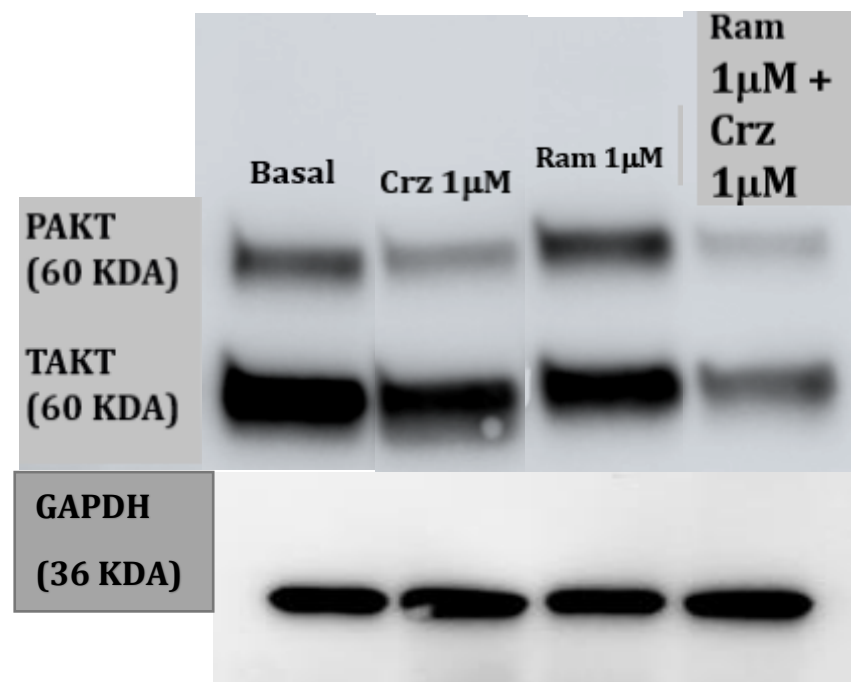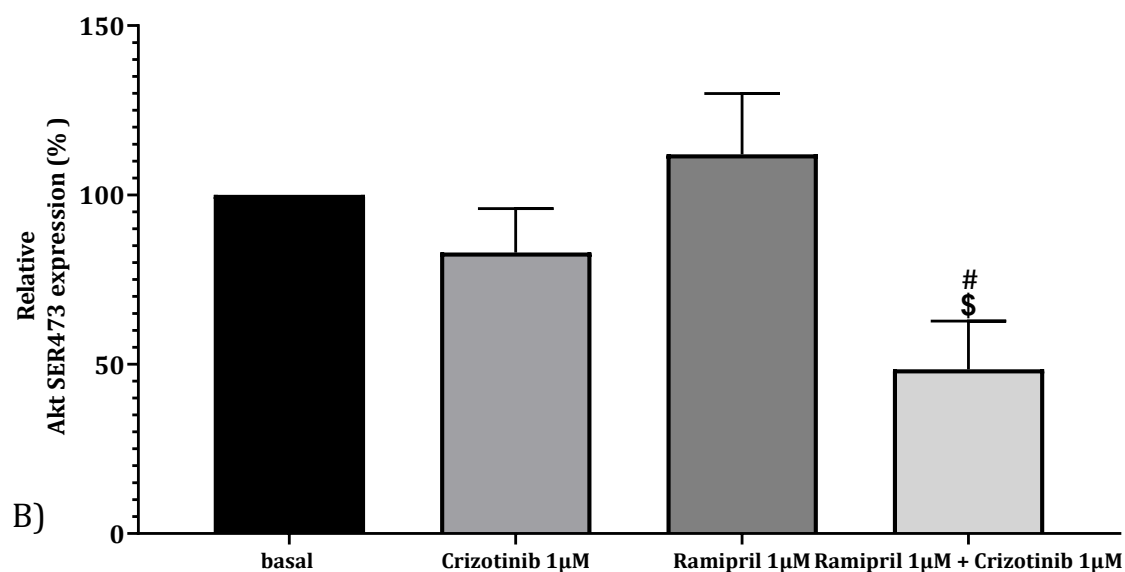
Figure 4.4.13 Assessment of relative expression of phosphorylated AKT SER473 in isolated adult rat hearts for 175 minutes with crizotinib 1μM, Ramipril 1μM ± crizotinib 1μM added 20 minutes into perfusion. (Data presented as mean ± SEM where # P<0.05 versus non-treated control, $ P<0.05 versus Ramipril 1μM treatment, n=4).

The figure above is a representation of the relative expressions of phosphorylated Akt. The ramipril & crizotinib cotreated hearts produced the least mean protein expression but statistical analyses did not show it to be significantly lower than treatment with crizotinib treatment alone.

Treatment of isolated hearts with Ramipril (1μM) + crizotinib (1μM) significantly reduced relative Akt SER473 expression compared to hearts treated with Ramipril 1μM alone (48.5±14.24% versus 112±18% respectively, where P<0.05).

Treatment of isolated hearts with Ramipril (1μM) + crizotinib (1μM) significantly reduced relative Akt SER473 expression compared to hearts with the non-treated control groups (48.5±14.24% versus 100%, where P<0.05).

Interestingly, a comparison between the relative expressions produced by the different treatments shows ramipril treatment alone produced the greatest relative protein expression but was not significantly greater than the three other treatments.

4.4.5 The effect of ramipril co-treatment on crizotinib induced cleaved caspase 3 expression in cultured H9C2 cardiac myoblasts

Cleaved caspase 3 expression served as an indicator of cells that undergo or will undergo apoptosis. Cells are not required to viable during analysis.

Upon treatment protocol completion and the staining protocols, the samples were analysed with the flow cytometer.

Cultured H9C2 myoblasts treated with crizotinib alone and ramipril co-treated with crizotinib significantly increased cleaved-caspase 3 expression compared to the non-treated cell controls (5292±284 RFU versus 1644±447 RFU where P<0.001 and 3945±913 RFU versus 1644±447RFU respectively, where P<0.01) (figure 4.4.14). Cultured H9C2 myoblasts treated with ramipril alone showed significant decrease in cleaved caspase 3 expression compared to samples treated with crizotinib treatment alone (2619±310 RFU versus 5292±284 RFU).
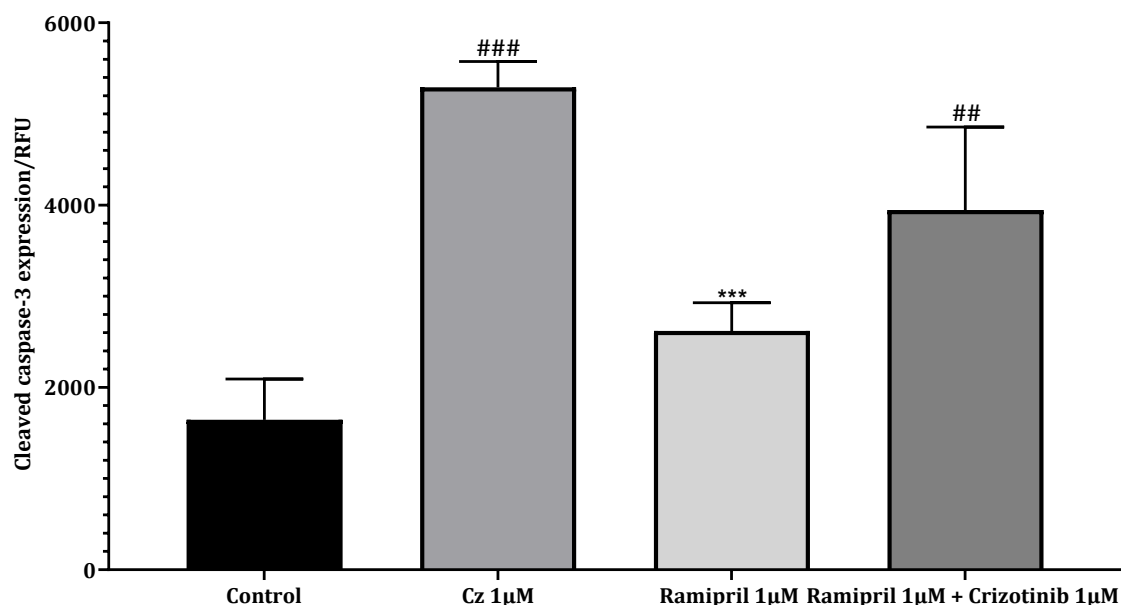
Figure 4.4.14 Assessment of cleaved caspase 3 activity in cultured H9C2 cardiac myoblast subjected to 24 hours treatment with either control, Crizotinib 1μM ± ramipril 1μM (Data presented as mean ± SEM. Where ## P<0.01, ###P<0.001 versus control n=3).

However, cultured H9C2 myoblasts with ramipril co-treated with crizotinib did not significantly reduce cleaved caspase-3 expression compared with the myoblasts treated with crizotinib alone (figure 4.4.14).

4.4.6 The effect of ramipril co-treatment on mitochondrial superoxide generation in cultured H9C2 myoblast

Upon completion of the prior described treatment and incubation period MitoSOX™ Red Mitochondrial superoxide indicator assay (4.2.7), the samples were analysed using the flow cytometer.

Cultured H9C2 myoblasts treated with crizotinib alone significantly increased mitochondrial superoxide expression compared to non-treated cell controls (figure 4.4.15).
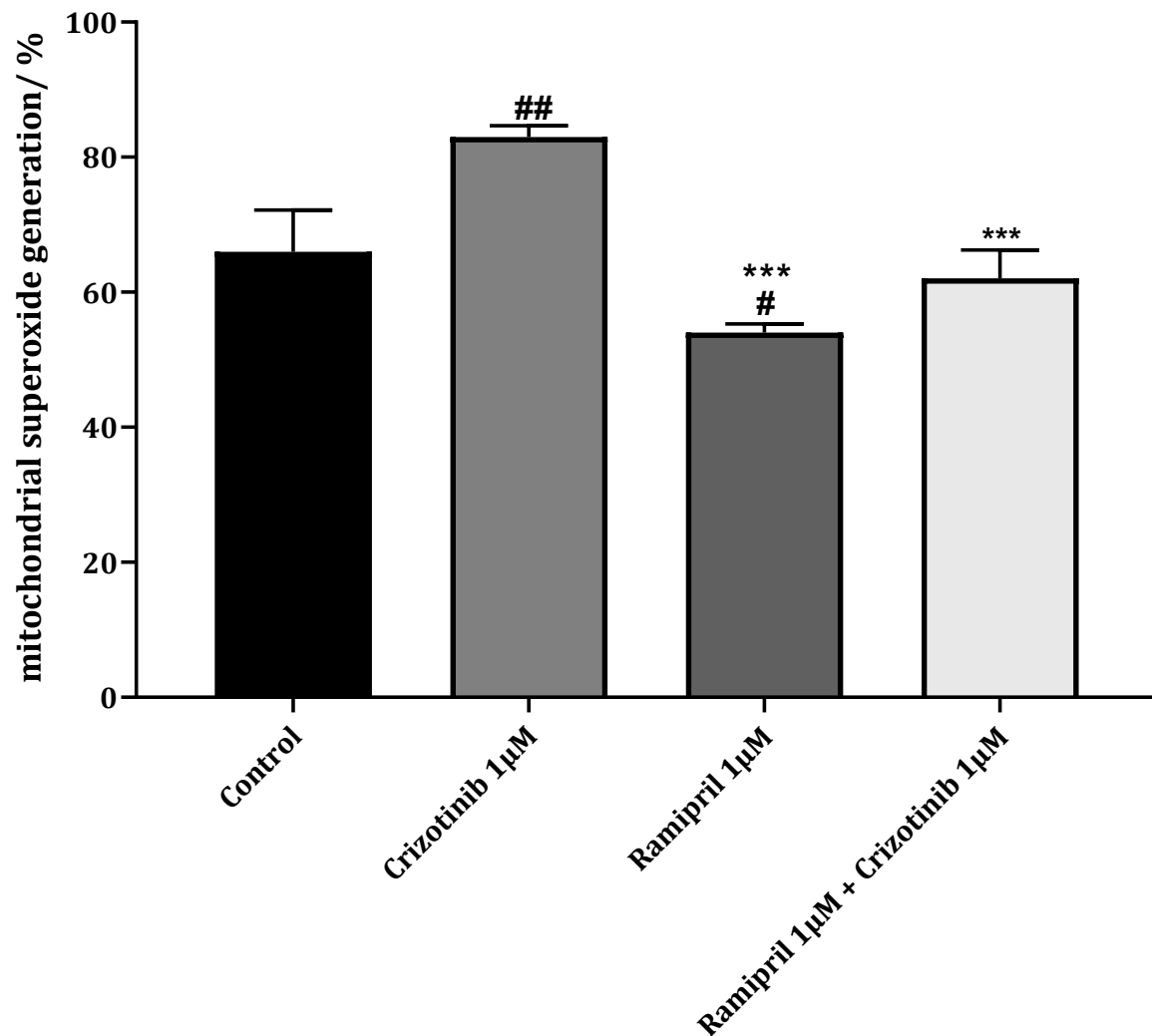
Figure 4.4.15 Assessment of mitochondrial superoxide generation in cultured H9C2 Cardiac myoblasts subjected to 24 hours treatment with either vehicle control, crizotinib 1μM ± ramipril 1μM (Data presented as

mean ± SEM #P<0.05 and ##P<0.01 versus control treatment, *** P< 0.01 versus Crizotinib 1μM treatment).

Cultured H9C2 myoblasts treated with Crizotinib (1μM) significantly increased mitochondrial superoxide expression compared to non-treated cell control (82.98±1.69% versus 65.99±6.152% respectively, where P<0.01). Treatment of cultured H9C2 myoblasts with ramipril cotreated with crizotinib significantly reduced mitochondrial superoxide expression compared to myoblasts treated with crizotinib alone (63.92±3.75% versus 82.98±1.69% respectively, where P<0.01) (Figure 4.4.15).

The data suggests that cotreatment with ramipril & crizotinib resulted in a reduction in mitochondrial superoxide expression compared to the samples that underwent treatment with crizotinib (1μM) alone.

4.4.7 The effects of ramipril co-treatment on crizotinib induced changes in calcium ion detection in H9C2 cardiac myoblast

Treatment of cultured H9C2 myoblasts with Crizotinib (1μM) alone significantly increased fluo-3am detection compared to the cultured H9C2 myoblasts treated with the vehicle non-treated controls (95.38±3.62% versus 77.52±3.08% respectively, where P<0.05).
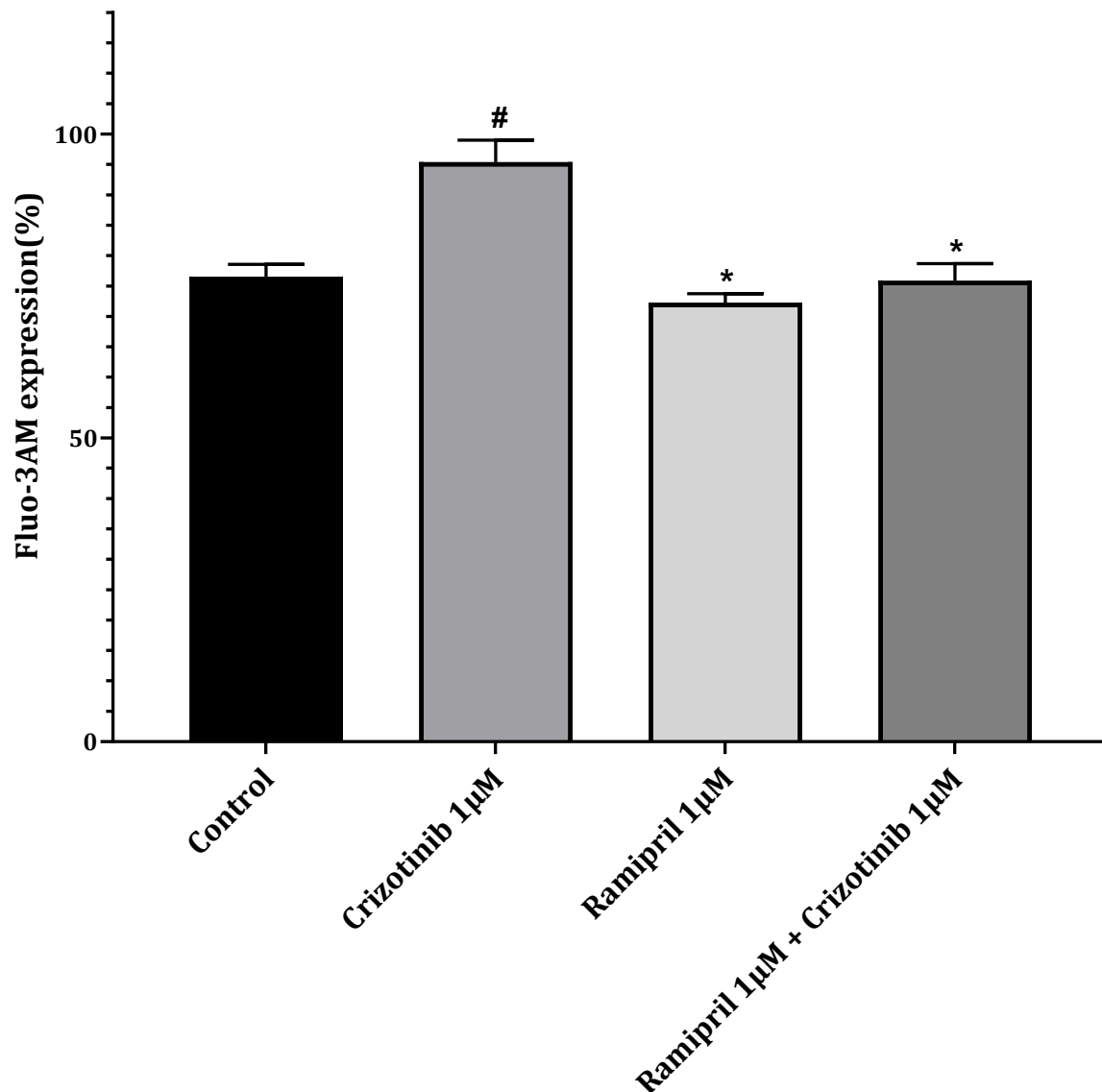
Figure 4.4.16 Assessment of Ca^{2+} activity in cultured H9C2 cardiac myoblast subjected to 24 hours treatment with either vehicle control, crizotinib 1μM ± ramipril 1μM (Data presented as mean ± SEM where *P<0.05 versus crizotinib 1μM, #P<0.001 versus control treatment)

Ramipril co-administered with crizotinib significantly decreased calcium detection in cultured H9C2 myoblasts compared to cells treated with crizotinib alone (75.84±2.84% versus 95.38±3.62% respectively, P<0.05).

Ramipril cotreatment appeared to limit the increase in calcium ion activity associated with treatment of cultured H9C2 myoblasts with crizotinib treatment alone.

4.5 Discussion

In this study, the aim was to observe and characterise the effects of the angiotensin converting enzyme inhibitor ramipril on tyrosine kinase inhibitor crizotinib induced myocardial injury. Angiotensin-converting enzyme (ACE) inhibitors have been reported to decrease the risk of deaths related to cardiovascular defects, myocardial infarction, and stroke in individuals with impaired systolic function, heart failure and diseased vasculature (Jackie Bosch et al. 2005). Ramipril cardioprotection is not a novel concept and studies with ramipril have documented desirable properties to the cardiovascular system such as inhibition of decreased cardiac contractility and reduction in right ventricular hypertrophy to name a few (Rouleau Jean et al. 2001; Shi et al. 2012). This study highlighted ramipril co-treatment with crizotinib attenuating the effects of crizotinib treatment alone.

The langendorff studies could be summarised to significant improvement in left ventricular developed pressure (%), decreased heart rate (%) and significant increases in coronary flow (%) were associated with co-treatment with ramipril and crizotinib compared to hearts treated with crizotinib alone. Inhibition of Angiotensin II action on AT1 receptors inhibits increases in blood volume,

vasoconstriction and ultimately leads to an increase in blood pressure (Figure 4.5.1) (Houston Miller 2010).
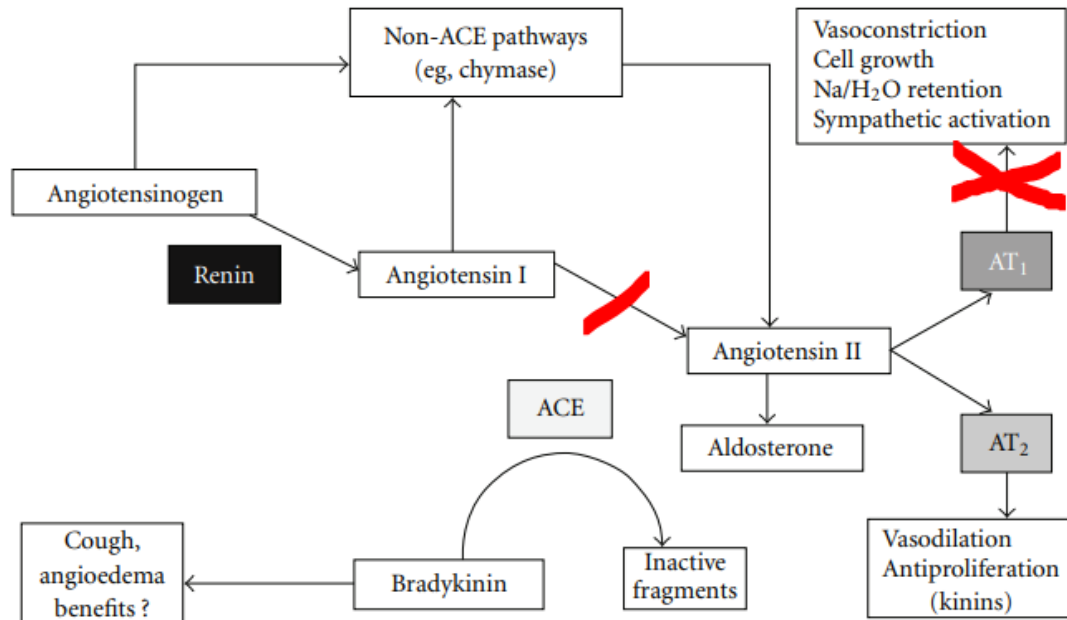
Figure 4.5.1 The role of ACE inhibition preventing angiotensin II formation which amongst other actions leads to decreased of vasoconstriction, attenuation of ROS generation and increased water reabsorption amongst other activities. [Adapted from (Houston Miller 2010)

The data from the langendorff study suggested ramipril co-treatment with crizotinib resulted in overall improvement in the left ventricular developed pressure (LVDP(%) in time matched comparisons versus crizotinib treatment alone, with statistically significant improvement in a number of measurement intervals (45, 50, 55, 80 and 100-minute intervals). This appeared to be consistent with prior studies describing effects of ramipril treatment. The study conducted by Wei et al. (2016) describes an investigation which suggests ramipril

administration following implementation of a myocardial infarction model in rats displayed protective properties (Wei et al. 2016). The study was conducted on female Wistar rats which were either subject to ligation of the anterior descending branch of the left coronary artery (myocardial infarction imitation) or a sham operation (no artery ligation), while animals were subjected to halothane anaesthesia (Wei et al. 2016). Animals were treated with either sodium carboxymethyl cellulose or ramipril 7 weeks post-surgery and treated for 5 weeks. Hemodynamic measurements were taken via a catheter inserted into heart chambers. The results of the study reported improvement in overall systolic and diastolic blood pressures and improved left ventricular systolic pressure in myocardial infarcted animals treated with ramipril compared to the animals subjected to MI without ramipril treatment (Wei et al. 2016). This appeared similar to what was reported in this present study. The hearts treated with ramipril & crizotinib co-treatment appeared to induce improvement in pressure performance versus the treatment with crizotinib treatment alone.

ACE inhibitors are widely recommended for confirmed cancer therapy related cardiac dysfunction (Pituskin et al. 2017). The results presented in the MANTICORE trial study on trastuzumab-mediated cardiotoxicity reported attenuation of declines in left ventricular ejection fraction following treatment with ACE inhibitor perindopril and was also associated with fewer incidences of anticancer induced cardiotoxicity in the patient cohort (Pituskin et al. 2017), which can be compared to the observations on the effects of ramipril co-treatment with crizotinib in this present study.

Additionally, the improvements in left ventricular developed pressure in this current study appeared to be consistent with data from a previous investigation. A prior study sought to investigate the cardioprotective properties of the active component of ramipril (Ramiprilat). Isolated male guinea-pig hearts were subjected to free radical damage and assessed the ability for ramiprilat to protect against superoxide anion damage and 2,2-diphenyl-1-picrylhydrazyl (DPPH) free radical damage (Jin and Chen 2000). The study reported improvements observed in mean left ventricular developed pressure and left ventricular end-diastolic pressure in the isolated male guinea-pig hearts (Jin and Chen 2000).

With regards heart rate component of the haemodynamic parameters presented in section 4.4.1, the overall effect of the co-treatment with ramipril & crizotinib appeared to be a reduction in the heart rate although the reduction was only marginal and rarely statistically significant. A key characteristic of ACE inhibition includes the potential to lower peripheral vascular resistance but their mechanism of this does not involve a compensatory heart rate elevation (Hanif, Bid, and Konwar 2010). This perhaps accounts for the significantly reduced heart rate figures recorded for the ramipril co-treatment with crizotinib compared to time matched measurements taken from crizotinib treatment alone. This also appeared consistent with previous clinical studies advocating positive chronotropic effects of ramipril treatment during stress conditions. For instance, ramipril treatment was effective at leading to reduced heart rate in hypertensive models simulated by mental stress tests and in addition, reduction of cardiac workload was observed as an additional benefit (Kahan and Eliasson 1999; Warner and Perry 2002) .

Significant improvements were also observed in guinea-pig isolated hearts in assessed heart rate and pressure performance (LVDP) and coronary flow (Jin and Chen 2000). With regards the coronary flow, ACE inhibition by function leads to increases in cardiac output which appears consistent with this current study as the co-treatment with ramipril appeared to lead to increased coronary flow with significant increases observed versus time-matched crizotinib treatment (Aronow 2016). Similar improvements in coronary flow was also reported in the study by Jin and Chen (2000). conducted in isolated guinea-pig isolated hearts treated with ramiprilat (Jin and Chen 2000). This is presumably as a result of reduced vasoconstriction achieved via AT1 receptor inhibition which ultimately improves output (Vaduganathan et al. 2020).

Section 4.4.3 took into consideration the effects of ramipril co-treatment with crizotinib induced on isolated H9C2 rat cardiac myoblasts. In this current study it was observed that co-administration with ramipril & crizotinib resulted in a significantly improved cell viability compared to treatment with crizotinib alone (Section 4.4.3.). This was suggestive ramipril treatment was inducing cytoprotective properties or at least limiting the ability of crizotinib to induce greater cellular mortality. This appeared to be corroborated by infarction risk data generated in section 4.4.2, showed that isolated male Sprague Dawley rat hearts subjected to the ramipril and crizotinib co-treatment regimens produced a significantly reduced infarct risk ratio compared to samples treated with crizotinib alone. Further providing evidence that ramipril was limiting cardiac tissue and cellular damage induced by the activity of crizotinib. This appeared consistent

with prior clinical data which reported pre-treatment with ramipril (ramiprilat) in induced free radical injury models resulted in reduction lactate dehydrogenase in coronary effluent which was considered an indicator for decreased myocardial tissue damage (Jin and Chen 2000). Similarly, in a separate study, chronic treatment with ramipril in ischemic models in male Wistar rats reported significantly increased production of bradykinin; leading to increased production of prostaglandins such as PGE2 which in the heart, leads to decreases cardiac hypertrophy during infarct conditions (Dumoulin et al. 2005; Sun and Wang 2012).

Inhibition of angiotensin converting enzyme displays protective properties in the cardiovascular system in a number of mechanisms such as reduction in myocardial remodelling following myocardial infarction (Simonis et al. 2003). Left anterior descending coronary artery ligation was performed in ramiprilat pre-treated male Wistar rats to induce myocardial infarction to assess protection against early remodelling after infarction (Simonis et al. 2003). Ramiprilat treatment was effective at preventing induction of PKC which was considered a key contributor to signal transduction in early remodelling during infarction (Simonis et al. 2003). Similarly, in a separate study involving an analysis of the morphological changes following induction of myocardial infarction, ramipril treatment proved successful in producing significant reduction in heart infarct length and size, six weeks following treatment of male Wistar rats (Sandmann et al. 2006a).

A separate study involving combination therapy with apstatin (an amino peptidase P inhibitor) and a number of ACE inhibitors reported the co-treatment regimens on Sprague Dawley rats involving ramipril resulted in the least percentage infarct generated and was also significantly less than control (Veeravalli et al. 2003). This appeared consistent with data generated in the present study with overall improvements observed in the myocardium following ramipril co-administration. This bore similarity with data collected in the present study, with co-treatment with ramipril yielding significant improved cardiomyocyte viability and significant reduction in infarct development.

In addition, during in vivo studies involving baseline observation and follow up assessment in patients, ramipril was demonstrated to produce favourable effects on left ventricular structure as well as function by effects such left ventricular mass reduction and left ventricular volume reduction (Lonn et al. 2004). A separate study designed to assess the efficacy of ramipril co-administration with angiotensin receptor blockers (Telmisartan and losartan) in individuals with stage 2 hypertension revealed both to be effective at reducing blood pressure but suggested the telmisartan proved to be more effective due to greater values generated (Jain et al. 2005).

In this current study, treatment with ramipril co-administered with crizotinib reduced cleaved caspase-3 expression however decrease was not deemed statistically significant (Section 4.4.5). Caspases since their identification have been studied extensively and are known for their role in the apoptotic signal

transduction cascade (Hirokazu et al. 2004; Siu and Alway 2009). Caspase-3 is a common downstream effector caspase & promotes a number of cytotoxic events when activated and plays prominent role in apoptosis (Siu and Alway 2009). Caspase-3 is frequently activated in the death protease facilitating catalysation of cleavage of key cellular proteins (Brentnall et al. 2013; Porter and Jänicke 1999). In this current study, ramipril co-treatment with crizotinib did not induce significant change in annexin v expression compared to samples treated with crizotinib alone. This could suggest ramipril cytoprotective properties could be operating against cell death independent of caspase activation or apoptotic process such as mitochondrial & oxidative stress mediated or more necrotic processes (Bröker, Kruyt, and Giaccone 2005; Tait and Green 2008).

In the current study, ramipril co-administration with crizotinib was effective at significantly reducing indicators of oxidative stress with reduced mitochondrial superoxide (%) and a decrease in calcium ion detection (%) compared to the increases in the levels induced by treatment with crizotinib alone (Section 4.4.6 and 4.4.7). Elevated ROS levels contribute to cardiomyocyte damage causing oxidative stress (Angsutararux, Luanpitpong, and Issaragrisil 2015). Excessive ROS generation within myocytes leads to peroxidation of myocyte membranes which then facilitates Ca^{2+} influx (Ca^{2+} overload) intracellularly which further causes myocyte damage through mitochondrial dysfunction (Curigliano et al. 2016).

In male albino rat hearts subjected to ischemia reperfusion, ramipril alone & ramipril plus candesartan treatment both significantly reduced Thiobarbituric acid reactive substances (TBARS) detection (Sheik Uduman et al. 2016). Ramipril & ramipril plus candesartan treatment was associated with significant increases in glutathione (GSH) detection compared to ischemic controls. Ramipril plus candesartan treatment was associated with significant increases in superoxide dismutase (SOD) and myocardial catalase levels in comparison to ischemic control (Sheik Uduman et al. 2016). TBARS serve as indicator for lipid peroxidation in response to cardiomyocyte damage by free radicals therefore reduced TBARS indicate reduction in oxidative stress similar to what was observed in this present study (Curigliano et al. 2016; Sheik Uduman et al. 2016). Oxidants such as SOD, GSH and myocardial catalase are protective of the myocardium by inhibition of ROS accumulation (Dhalla et al. 2000; Fukai 2011). Increased activity of these oxidants by ramipril is cardioprotective as they result in inhibition of ROS accumulation and in turn oxidative stress again which correlates to data from the present study (Sheik Uduman et al. 2016).

Calcium (Ca^{2+}) is considered a key regulator of mitochondrial function and energy synthesis (ATP) (Brookes et al. 2004). Sustained generation of mitochondrial ROS is in part controlled by Ca^{2+} (Edoardo and Christoph 2018). Therapeutics that increase mitochondrial oxidative stress disrupt calcium homeostatic concentration (Montaigne, Hurt, and Neviere 2012b). Increased intracellular mitochondrial calcium overload triggers permeability transition of mitochondria, dissipating transmembrane potential, swelling, energy depletion, increased ROS

generation and promotes cell death (Montaigne, Hurt, and Neviere 2012). ACE inhibition was effective at preventing Ca^{2+} overload in a myocardial infarction model (Zalvidea et al. 2012). Male swiss mice were subjected to induced myocardial infarction (left coronary artery ligation) and treated with delapril for 6 weeks (Zalvidea et al. 2012). Delapril treated mice myocytes showed significant reduction in diastolic Ca^{2+} overload induced by MI and cardiomyocytes also displayed improved contraction (Zalvidea et al. 2012). Quinaprilat (active metabolite of ACE inhibitor Quinapril), Enalapril and Enalaprilat were protective against Ca^{2+} overload induced by lysophosphatidylcholine (LPC) (biomolecule derived from cleavage of membrane phospholipids) (Hong et al. 1999). Ventricular myocytes isolated from male Sprague-Dawley rats were pre-treated with the ACE inhibitors and the active metabolites for 5 minutes, then treated with LPC. All 3 compounds significantly attenuated Ca^{2+} overload induced by LPC treatment (Hong et al. 1999). The above highlights the efficacy of ACE inhibition in the attenuation of Ca^{2+} overload.

In this present study it was observed that there was an increase in ROS generation associated with crizotinib treatment and treatment with ramipril and crizotinib yielded a significant reduction in ROS generation. Similarly, there was significant reduction in Calcium ion detection in H9C2 myoblasts treated with ramipril & crizotinib compared to crizotinib treatment alone.

The data produced during this study further supports the beneficial properties of ACE inhibitor administration such as ramipril on not only blood pressure but

through direct action on the myocardium which led to left ventricular hypertrophy regression and decreased fibrosis in the myocardium (Ha and Oh 2009). Prevention of myocardial fibrosis limits alteration or limitation of left ventricular diastolic function through maintenance of cardiac elasticity (Ha and Oh 2009).

In conclusion, ramipril administered in combination with crizotinib appeared to produce improvement LVDP, non-significant reduction & stabilisation of heart rate and improvement in coronary flow compared to rat hearts treated with crizotinib alone. Ramipril treatment was also effective at showing improvement in cardiomyocyte viability as well as increases in mitochondrial superoxide & calcium ion detection compared with crizotinib treatment alone. Ramipril co-treatment resulted in decreases in activity of caspase 3 detection. All of these effects appear to oppose the effects induced by crizotinib treatment alone.

Chapter 5: Angiotensin Receptor Antagonist Losartan Reverses Crizotinib Induced Cardiotoxicity

5.1 Abstract

Anticancer treatment with tyrosine kinase inhibitors has been associated with adverse effects on the myocardium. Acute crizotinib treatment is associated with episodes of QT prolongation and cardiac rhythm disturbances. Losartan is usually prescribed for the treatment of hypertension but has also been shown to possess protective properties against drug induced cardiotoxicity. The ability of losartan treatment to reverse on crizotinib induced cardiotoxicity was evaluated.

Isolated perfused hearts were treated with losartan in combination with crizotinib for 175 minutes, haemodynamic performance and infarct development were assessed. Western blot analysis of left ventricular tissue was conducted to evaluate p-AKT expression. Ramipril in combination with crizotinib was administered to H9C2 cardiac myoblasts which were evaluated for cleaved caspase-3 expression, mitochondrial superoxide generation and calcium signalling disturbances.

Losartan co-administration with crizotinib significantly improved left ventricular developed pressure performance. Losartan co-administration with crizotinib significantly decreased infarct risk ratio (%) developed. Losartan co-administration with crizotinib significantly increased myoblast viability. Losartan co-administration with crizotinib decreased cleaved caspase-3 expression, superoxide generation and calcium ion detection. All compared to treatment with crizotinib alone.

This study advocates the use of losartan in combination with crizotinib to attenuate cardiotoxicity induced by crizotinib treatment.

5.2 Introduction

Despite the vast advancements made in the fields of medicine pertaining the treatment of malignancies, cancer still ranks as a leading cause of death globally and also presents the greatest obstruction to life expectancy in the 21st century (Bray et al. 2018). Over the last few decades lung cancer has been of particular interest; widely considered as one of the leading causes of death in both males and females globally (Costa et al. 2015). In 2013, approximately 1.4 million deaths worldwide were attributed to lung cancer (Lindeman et al. 2013). Non-small cell lung cancer (NSCLC) accounts for the highest incidence of lung cancer cases with up to 90% of cases and are split into adenocarcinoma, squamous cell carcinoma and large-cell carcinoma as variants (Yang et al. 2020). With a dismal 5-year survival rate, with a peak less than 20% rate of survival post diagnosis; the need for timely diagnosis in at-risk individuals would go a long way to delay lung cancer progression (Molina et al. 2008b). Metastatic NSCLC is widely considered a debilitating condition, resulting in a high burden of symptoms and decreased quality of life, with estimated prognosis established as under a year which is a major cause for concern (Temel et al. 2010).

As a result of the poor patient prognosis and often late stage diagnosis, treatment often ends up being mainly palliative in individuals diagnosed with metastatic NSCLC (Temel et al. 2010). Chemotherapy is considered the standard of care for patients with advanced stage of the disease, but more recently conventional chemotherapeutics have plateaued in terms of efficacy which led to drives aimed

at the identification of compounds and strategies with more targeted methods of action (Molina et al. 2008). A rearrangement within the anaplastic lymphoma kinase (ALK) gene and echinoderm microtubule-associated protein-line 4(EML4) gene, results in constitutive activation of ALK signalling which leads to apoptotic inhibition and promotion of tumour progression by upregulating tumour cell proliferation within the ALK positive non-small cell lung cancer C(O'Bryant et al. 2013).

Under normal conditions, ALK activation is mediated through ligand induced phosphorylation and homo-dimerization; and inactivated through dephosphorylation in the absence of ligand binding (Figure 5.2.1) (Huang 2018). ALK activates multiple pathways with the resulting signalling regulating cellular growth, transformation as well as anti-apoptotic signalling (Figure 5.2.1) (Della Corte et al. 2018).
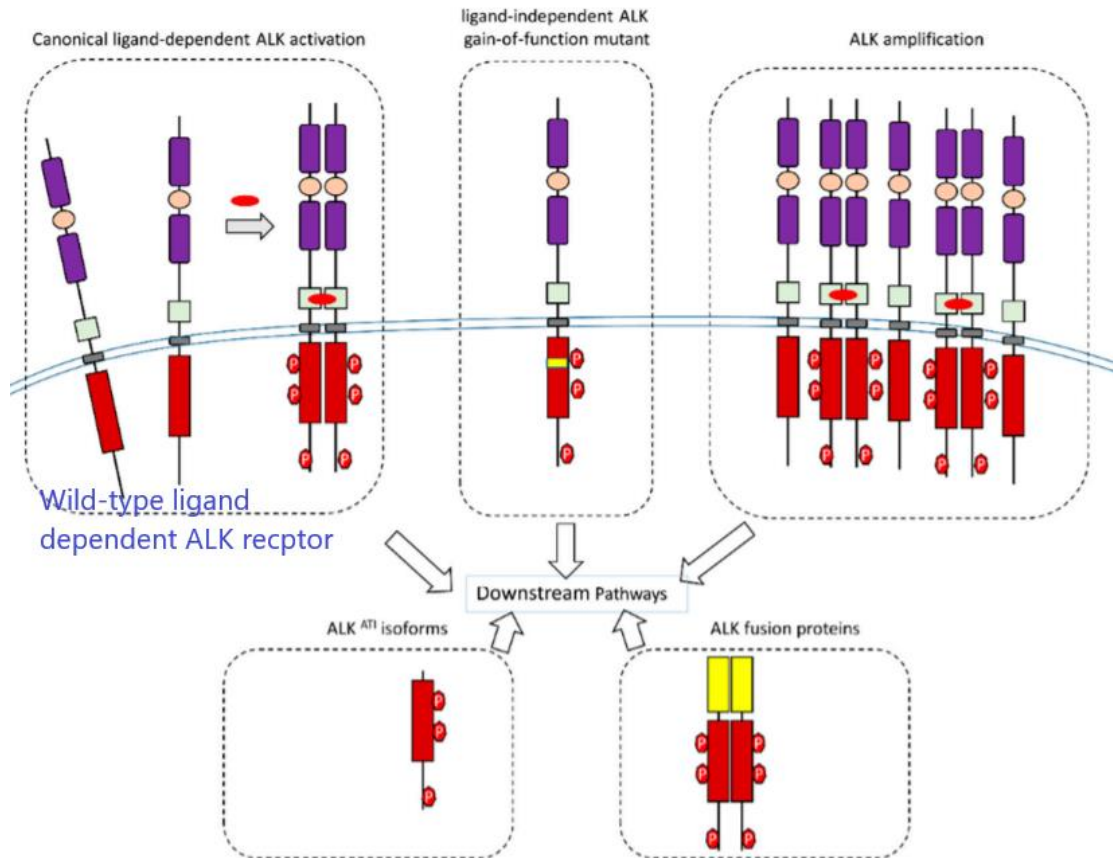
Figure 5.2.1 ALK receptor transmembrane receptor illustration with the wild-type receptor highlighted along with some aberrant variants which contribute to overactive signalling [Adapted from (Huang 2018)].

ALK rearrangements are reportedly discovered in approximately 5% of NSCLC cases (O'Bryant et al. 2013; Sasaki et al. 2010). This led to the discovery of crizotinib, which is described as an oral ATP-competitive selective inhibitor of tyrosine kinase receptors (Anaplastic lymphoma kinase or ALK and hepatocyte growth factor receptor or MET) causes inhibition of receptor phosphorylation even at nanomolecular concentrations (Kwak et al. 2010). Crizotinib treatment is associated with positive tumour responses in up to 60% of patients with ALK-positive NSCLC and also associated with cancer progression-free survival up to 10 months (Shaw et al. 2013; Solomon et al. 2014). A prospective study comparing

crizotinib treatment against standard chemotherapy (pemetrexed or docetaxel) in patients treated for advanced ALK-positive non-small cell lung cancer, concluded that crizotinib treatment was associated with significant & greater sustained patient cancer progression-free survival, greater response rates, symptom reduction and overall significantly improved quality of life (Shaw et al. 2013).
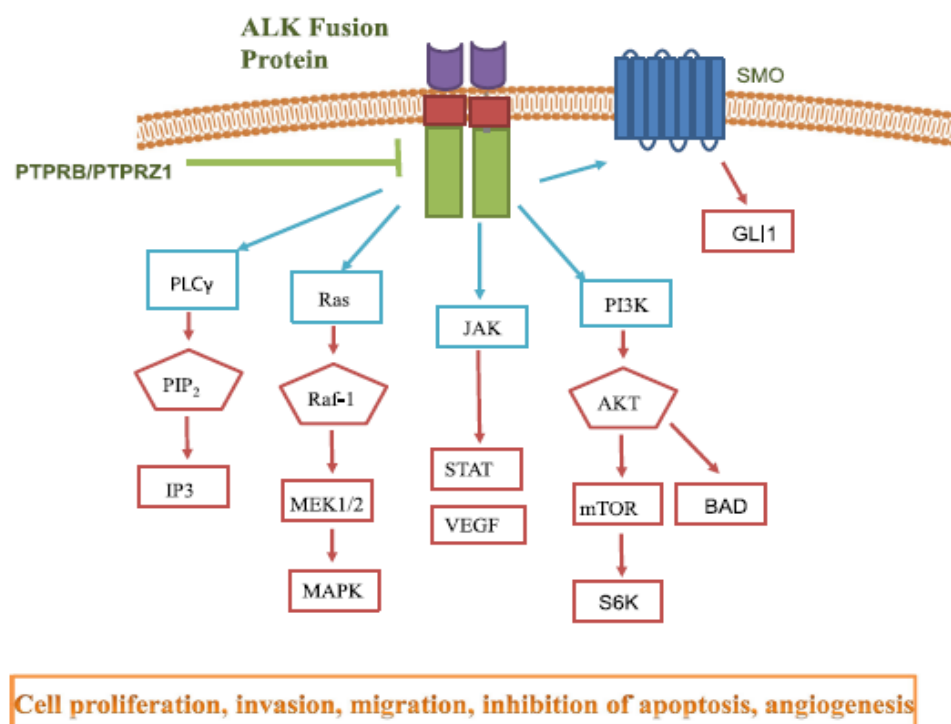
Figure 5.2.2 The ALK signalling cascade governing activation of multiple pathways and signalling cascades which regulate key processes within cells such as proliferation, invasion, migration, cell survival (apoptosis avoidance) and angiogenesis [Adapted from (Della Corte et al. 2018)].

The main hinderance associated with anticancer treatment and improvements in patient survivorship, is unfortunately the associated injuries afflicted to other

organs/systems within the body, with effects on the cardiovascular system being particularly concerning (Curigliano et al. 2016). Cardiotoxicity refers to the negative impact cancer therapy inflicts on the heart and cardiovascular system as a whole (Dent et al. 2015).

Cardiotoxicity related cardiovascular disease presents as one of the leading causes of long-term morbidity and mortality experienced by individuals recovering after anticancer therapy (Curigliano et al. 2016). The more conventional methods of chemotherapy and targeted therapies have been associated with an increased risk of damage to the myocardium leading to adverse events such as left ventricular dysfunction and heart failure as some of the more extreme manifestations (Curigliano et al. 2016). For instance, a retrospective cohort study was conducted to assess the risk of heart failure in primarily young breast cancer patients treated with anthracycline and trastuzumab (Bowles et al. 2012). The study concluded that significant increases in the risk of heart failure development was observed when both treatment groups were compared to a group treated without chemotherapy (Bowles et al. 2012).

Similarly, a separate study was undertaken to estimate heart failure and cardiomyopathy development following treatment with either adjuvant trastuzumab or chemotherapy in a population of older women with early-stage breast cancer (Chen et al. 2012). The study identified that greater rates of heart failure or cardiomyopathy were reported in individuals treated with trastuzumab compared to the non-adjuvant chemotherapy or non-trastuzumab, reporting up to

a 14% greater adjusted incidence rates for heart failure and cardiomyopathy over 3 years post treatment (Chen et al. 2012). The study also reported that individuals administered adjunctive anthracycline and trastuzumab therapy presented a 23.8% greater rate of heart failure compared to non-adjuvant chemotherapy or non-trastuzumab treatment (Chen et al. 2012).

Some of the less imminently life-threatening cardiovascular related conditions include treatment induced hypertension, ischemia which could be either vasoconstrictive or thromboembolic in origin, cardiac rhythm disturbances, conduction system disturbances are also associated (Curigliano et al. 2016). These conditions may be minor in isolation but could contribute towards cardiovascular disease state much later when left poorly managed (Curigliano et al. 2016).

Tyrosine kinase inhibitors are not exempt from cardiotoxicity, with asymptomatic Q wave T wave interval prolongation, left ventricular ejection fraction reduction, symptomatic congestive heart failure and myocardial infarction in severe situations are associated with TKI therapy (Orphanos, Ioannidis, and Ardavanis 2009; Tartarone et al. 2015a). Imatinib (STI571) has been attributed with cell death in cultured mouse cardiac myocytes linked with endoplasmic stress response (Pattacini et al. 2004; Ron and Walter 2007). In myocardial biopsies from 2 individuals and wild-type C57BL6 mice were treated with imatinib mesylate for between 3 to 6 weeks assessed for cardiotoxicity, there was evidence of mitochondrial abnormalities (with scattered cytosolic lipid droplets, pleomorphic mitochondria with stretched cristae and presence of vacuoles). In the mice

mitochondria, significant Ca^{2+} opening of the mitochondrial permeability transition pore was associated with imatinib treatment and collapse of mitochondrial membrane potential and significant cytochrome C release and cleavage of caspase 3 all linked to cell death (Kerkelä et al. 2006).

Anti-tumour activity tyrosine kinase inhibitor treatment must be balanced against cardiotoxicity as preservation of cardiomyocyte health must be prioritised (Hui and Thomas 2010). Cardiomyocyte cell death is a key contributor to drug induced cardiotoxicity with apoptosis and necrosis regularly implicated (Galluzzi et al. 2018; Ma et al. 2020). In the multi-parameter in vitro testing of tyrosine kinase inhibitors, crizotinib and nilotinib treatment on human cardiomyocytes were linked with apoptosis as the cultures showed an increase in activation of caspase 3/7 and a decrease in cell viability (Doherty et al. 2013). Regarding necrosis, TKI imatinib treatment was associated with caspase independent, necrosis-like cell death mediated by serine protease activity (Okada et al. 2004). BV173 (leukemic cell line from patient with chronic myelogenous leukaemia lymphoid blastic crisis) and K562 (cell line from patient with chronic myelogenous leukaemia erythroid blastic crisis) cells were treated with imatinib. Inhibition of caspases could not attenuate cell death by imatinib treatment which led investigators to suggest necrotic death (Okada et al. 2004).

Cell death is also regulated by a number of cellular pathways such as phosphatidylinositol3-kinase /protein kinase B (PI3K/AKT) pathway (Roskoski 2013). The phosphorylated AKT regulates cell survival as p-AKT inhibits pro-

apoptotic proteins which allow cells avoid apoptosis (Chiarle et al. 2008). In primary mouse embryonic fibroblasts, wild type cells with normal AKT expression were significantly more susceptible to hydrogen peroxide (ROS) induced cell death compared to AKT knockout fibroblasts (Nogueira et al. 2008). AKT was also shown to inhibit non-apoptotic cell death induced by ceramide (molecule generated in response to cell death stimulus such as oxidative stress and ionizing radiation) (Mochizuki et al. 2002). In U251 glioma cells induced with constitutive activation of AKT kinase, significant inhibition of cell death with significant increases in cell viability was observed after 48 hours of treatment with ceramide (Mochizuki et al. 2002).

Tyrosine kinase inhibitors nilotinib & sunitinib treatment have been linked to increased caspase activation also indicative of cell death (Doherty et al. 2013; Ron and Walter 2007). Human induced pluripotent cardiomyocytes treated for 72 hours with sunitinib and nilotinib were linked with significant reduction in cardiomyocyte viability while nilotinib treatment was associated with increased caspase 3/7 activation (Doherty et al. 2013). In the same study, crizotinib treatment was shown to increase caspase 3/7 activation as well as increase superoxide generation in cardiomyocytes indicative of increased oxidative stress (Doherty et al. 2013).

The onus then falls on researchers and medical practitioners to develop strategies to balance retaining anticancer treatment efficacy while also seeking to minimise adverse cardiac effects. A number of agents have been shown to display beneficial

effects to patients who have been treated with anticancer agents known to induce cardiotoxicity such as angiotensin antagonists, statins and dexrazoxane all offer varying levels of cardiac protection (Acar et al. 2011; Cadeddu et al. 2010a; Cardinale et al. 2006; Curigliano et al. 2016; Seicean et al. 2012).

The renin angiotensin system is a complex multitude of mechanisms that plays a central role in a number of physiological processes including cardiovascular regulation (Shetty and DelGrande 2000; Sobczuk et al. 2020). The system also contributes towards progression of cardiovascular disease states such as arterial hypertension, heart failure and cardiotoxicity linked to agents such as anthracyclines (Dessì et al. 2011; Shetty and DelGrande 2000; Sobczuk et al. 2020). Angiotensin receptor blockers are compounds which act antagonistically to angiotensin receptor type 1 (AT1) receptor (Sobczuk et al. 2020). Angiotensin II is the major effector peptide which binds to the AT1 receptor contributing to blood pressure control and fluid homeostasis (Figure 5.2.2)(Sandmann et al. 2006b).

It has previously been established that AT1 receptor antagonism enacts beneficial cardioprotective effects in individuals with myocardial infarction and hypertension (Schieffer et al. 1994; Schieffer et al. 2004). Patients with coronary artery disease and arterial hypertension were administered enalapril or irbesartan to assess RAS blockage on attenuation of adverse cardiovascular events (Schieffer et al. 2004). AT1 receptor blockade exerted greater systemic anti-inflammatory and anti-aggregatory effects with increased interleukin-10 levels

and reduced serum metalloprotease 9, as well as reduced interleukin 6 (Schieffer et al. 2004).
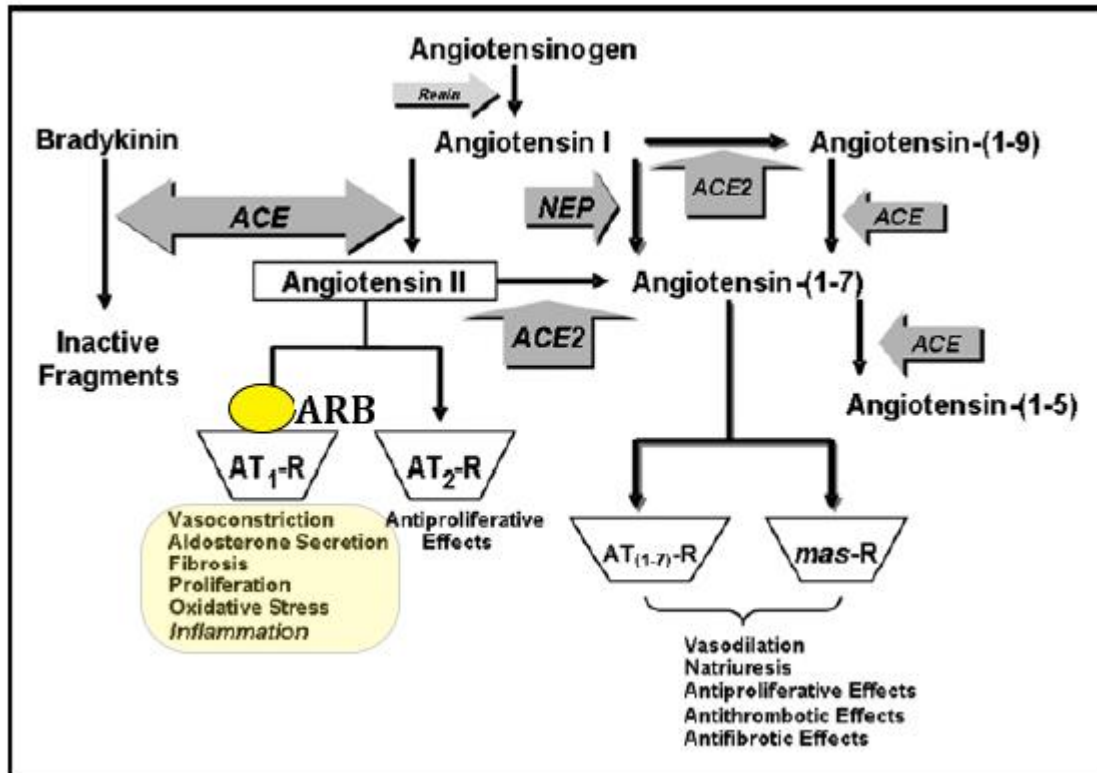
Figure 5.2.2 Illustration of the angiotensin pathway highlighting the production of angiotensin peptides. The yellow marker indicates action sites for angiotensin receptor blocker losartan with subsequent inhibition of the listed processes [Adapted from (Ferrario and Strawn 2006)].

Losartan is an angiotensin receptor antagonist or angiotensin receptor blocker (ARB)(Akershoek et al. 2017; Schieffer et al. 1994). It is a competitive antagonist selective for the AT1 receptor and is FDA approved for the treatment of hypertension administered alone or in combination with other antihypertensives (Díez 2006; Ripley and Hirsch 2010).

Losartan inhibits systemic renin angiotensin system functions to alleviate hypertensive symptoms (Akershoek et al. 2017). In an adriamycin-induced rat heart failure study, losartan treatment was successful at inducing cardioprotection with significant improvements in left ventricular ejection fraction (Zong et al. 2011). Losartan co-treatment also increased plasma angiotensin (Ang-(1-7) within treated animals compared to the adriamycin heart failure models alone. Ang-(1-7) is capable of induction of vasodilation, diuresis, anti-hypertrophy, anti-fibrosis amongst other effects, again demonstrating cardioprotection (Iwai and Horiuchi 2009; Zong et al. 2011).

Losartan treatment significantly attenuated doxorubicin induced cardiotoxicity and additional cardioprotection was achieved during was co-administered with quercetin (flavonoid) (Matouk et al. 2013). Adult male Wistar rats administered with different combinations doxorubicin, losartan and or quercetin. Losartan administration concurrently with doxorubicin significantly decreased tumour necrosis factor alpha (TNF-α) detection (proinflammatory indicative of damage) compared to doxorubicin treatment alone (Matouk et al. 2013). Losartan co-treatment with doxorubicin also significantly decreased serum levels of lactase dehydrogenase and creatine kinase compared to the levels achieved with doxorubicin treatment alone (Matouk et al. 2013).

Similarly, losartan treatment was associated with anti-hypertensive effects in doxorubicin induced congestive heart failure model study (Lovric-Bencic et al. 2004). Male Wistar rats or NMRI mice were subjected to congestive heart failure

and treated with doxorubicin with and without losartan. Losartan and doxorubicin treated animals showed significant decrease in blood pressure compared to the animals treated with doxorubicin alone (Lovric-Bencic et al. 2004).

In another study, male Wistar rats were treated with sorafenib with and without losartan for 30 days (Abdelgalil et al. 2020). Losartan treatment with sorafenib was credited with improvements in left ventricular pressure and also perfusion pressure compared to sorafenib treatment alone, although improvements were not statistically significant (Abdelgalil et al. 2020). Losartan co-treatment with sorafenib was also credited with reduction of plasma metabolites associated with sorafenib induced cardiotoxicity as well as reduction in changes in cardiac tissue morphology associated with sorafenib cardiotoxicity (Abdelgalil et al. 2020).

Losartan treatment was associated with reduction of angiotensin II (Ang II) induced apoptosis in adult male Sprague-Dawley rats (Diep et al. 2002). The animals were first administered external ang II for 7 days with or without losartan. Blockage of Angiotensin I receptor by losartan administration significantly reduced cleaved caspase-3 activity compared to animals that were not treated with losartan. Similarly, Losartan treated animals were associated with significantly reduced bax/bcl2 ratio indicative of apoptosis reduction compared to animals not treated with losartan (Diep et al. 2002).

In hypertensive patients, losartan treatment was associated with decreased apoptosis of cardiomyocytes (González Arantxa et al. 2002). Study participants were treated with losartan for 12 months and biopsies were collected after a year

of treatment. Losartan treated patient biopsies were associated with significantly diminished apoptotic index observed in cardiomyocytes as well as reduction in immunostaining for caspase-3 compared to non-treated patient biopsies. In addition, Losartan treatment was also associated with decreased bax/bcl-2 ratio compared to non-treated control, however, was not statistically significant (González Arantxa et al. 2002). Losartan treatment was credited with preserving cardiomyocyte size and preventing myocardial dysfunction in tail-suspended mice (Liang et al. 2019).

Adult male mice (C57BL/6 mice) with their tails suspended to simulate microgravity were treated with losartan for 28 days. Losartan treatment was associated with significant reduction of ROS generation and in turn oxidative damage induced by sustained tail suspension in analysed heart lysates (Liang et al. 2019).

Losartan treatment was successful at reversing subcellular remodelling in response to heart failure induced by myocardial infarction (Babick et al. 2012). Sprague Dawley rats subjected to left anterior coronary artery occlusion to induce heart failure model, were treated with oral losartan for 8 weeks and tissues analysed later. Losartan treatment was credited with restoring Sarcoplasmic Ca^{2+} uptake pump protein preventing calcium overload and cardiomyocyte dysfunction (Babick et al. 2012). Similarly, in a model to assess the effects of losartan on cardiac hypertrophy, losartan treatment was associated with improvement of cardiomyocyte contractility and calcium regulation in rat heart failure model.

Female Sprague Dawley rats were subjected to left coronary artery ligation and administered losartan orally after 7 days. Losartan treatment significantly improved systolic and diastolic calcium overload (detection) as well as significant decrease in cytosolic Ca^{2+} (Loennechen Jan et al. 2002).

In a separate study, intermittent treatment with losartan was able to induce cardiac preconditioning in isolated Sprague Dawley rat hearts (Sgarra et al. 2014). The animals were subject to ischaemia reperfusion then intermittently administered losartan resulted in significant increase in phosphorylation of Akt (p-Akt) (Sgarra et al. 2014). Similarly, losartan treatment restored skeletal muscle remodelling and offered protection against atrophy in mice sarcopenia (Burks et al. 2011). Male C57BL/6 mice were treated with losartan for 1 week and subjected to injury (immobilisation) and continued losartan treatment and then administered cardiotoxin in the tibialis anterior muscle to stimulate regeneration. Losartan improved muscle remodelling and significantly increased p-AKT expression compared to the placebo treated animals and prevented atrophy (Burks et al. 2011).

The literature and prior studies conducted with losartan provide evidence to highlight cardioprotective properties with success observed when administered with agents capable of inducing cardiotoxicity.

The purpose of this study was to assess the potential of angiotensin receptor blocking through losartan co-administration to attenuate the severity of myocardial injury resulting from crizotinib induced cardiotoxicity. The effects of

ARB were assessed in *in vitro* whole heart model and cardiomyocyte studies. Haemodynamic performance was evaluated, infarct development and cell death were considered. Analysis of cleaved caspase-3 expression, mitochondrial superoxide generation and calcium dysregulation was also evaluated in cultured cardiac myoblasts

5.3 Materials and Methods

5.3.1 Materials

Crizotinib was purchased from Carbosynth limited (UK) and dissolved in dimethyl sulphoxide prior to storage at -20 °C. Krebs-Henseleit buffer (KH) salts (118.5 mM NaCl, 25 mM NaHCO$_3$, 4.8 mM KCl, 1.2 mM MgSO$_4$, 1.2 mM KH$_2$PO$_4$, 1.7 mM CaCl$_2$, and 12 mM glucose), were purchased from Fisher scientific (UK). The antibodies anti-rabbit antibody for phospho-Akt at Ser473 (Cell Signalling), Akt (pan) (11E7) Rabbit mAb (cell signalling) as well as anti-biotin and anti-rabbit IgG were purchased from cell signalling. Triphenlytetrazolium chloride (TTC) was purchased from Sigma Aldrich, UK. DMEM (Dulbecco's modified eagle medium) which was purchased from ThermoFisher scientific ™. Penicillin streptomycin (10,000 U/mL) purchased from Gibco ™. Foetal bovine serum (FBS) purchased from Gibco ™. Phosphate buffer saline was purchased from Gibco ™. Losartan chloride purchased from Tocris, Bio-techne limited (UK) and dissolved in DMSO then stored in -20°C.

5.3.2 Animals and ethics

Adult male Sprague-Dawley rats with body weight range approximately 350±50g were purchased from Charles River UK limited (Margate, UK) were used for the purpose of this study (Ethics number P66861). Animals were kept in humane conditions, suitably housed, and had free access to standard pellet diet and water. Handling and treatment procedures were in full accordance with the Guidelines regarding the operation and handlings of Animals (Scientific Procedures Act 1986). Animals were selected at random for treatment. Tissue collected for infarct analysis were blinded and stored for later analysis.

5.3.3 Langendorff isolated perfused heart preparation

Adult male Sprague-Dawley rats were humanely sacrificed by cervical dislocation and the hearts were quickly excised and placed in ice-cool KH buffer. The rat hearts were then mounted unto the langendorff apparatus and perfused continually with KH buffer. The KH buffer was maintained at PH 7.4 by continuous gas supply of 95% O_2 and 5% CO_2 with the temperature maintained at 37 °C using a water-jacketed organ chamber. The left atria were excised and a latex iso-volumic balloon was carefully inserted into the left ventricle via the opening created from excision of the left atria and inflated to between 5-10mmHg. Heart functional parameters measured, which were the left ventricular developed pressure (LVDP), heart rate (HR) and coronary flow (CF) were monitored and recorded at regular intervals. The LVDP and HR were measured and recorded with a physiological pressure transducer and Powerlab Software, AD Instruments (UK). CF was

measured by collecting volume of perfusate for a minute. The functional parameters measured were expressed as mean of the stabilisation period to facilitate standardisation between different treatment groups. At the end of the perfusion protocol, the hearts were carefully removed from the apparatus, weighed and frozen at -20°C for infarct analysis.

5.3.4 Infarct size analysis

The now frozen hearts were sliced into about 2mm thick transverse sections and incubated in 2, 3, 5-Triphenyltetrazolium chloride (TTC) solution (1% phosphate buffer solution) and kept at 37°C for 12 minutes to stain infarct regions. The slices were then fixed in 10% formaldehyde solution for at least 4 hours. Regions of risk stained red while regions of infarct in tissue stained white/pale. The risk areas and infarct areas were traced onto acetate sheets and used to calculate a percentage of infarct to risk ratio (%). The sheets were scanned, and traces were assessed using the image J software. A ratio of infarct to risk size was calculated for each of the heart slices. The mean infarct to risk ratio (%) was then normalised to the weight of each heart.

5.3.5 Langendorff perfused heart experimental protocol

The hearts following excision were allowed a stabilisation period of 20 minutes prior to drug treatment for 155 minutes outlined by figure 5.3.1 below. Hearts were randomly assigned to the following treatment groups; 1) perfusion with KH buffer alone (vehicle control), 2) hearts treated with crizotinib 1µM, 3) hearts treated with losartan 4.5µM ± crizotinib 1µM.
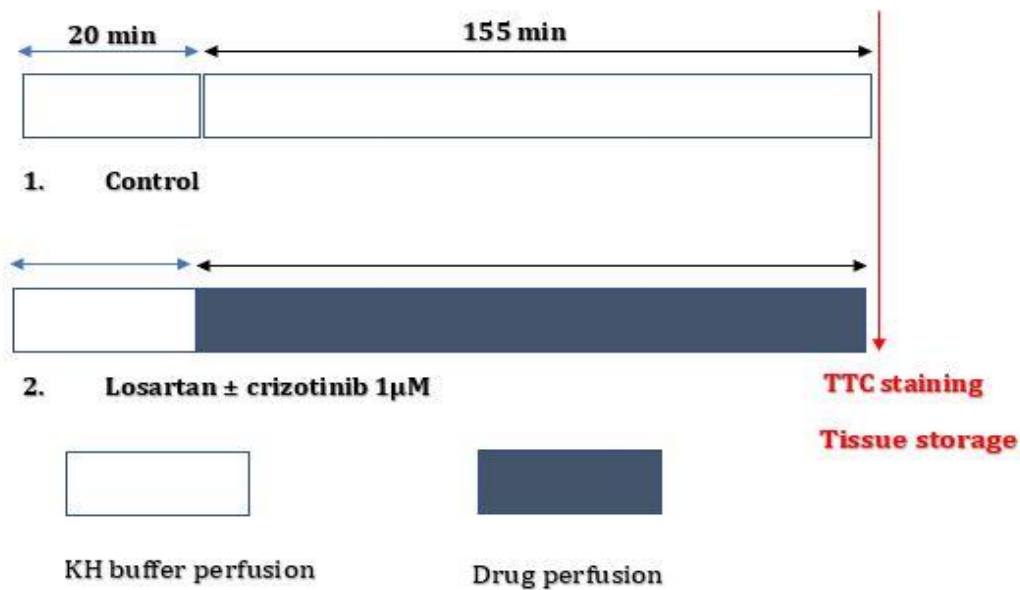
Figure 5.3.1 Langendorff drug treatment protocol

5.3.6 Western Blot analysis

For the western blot protein studies, the hearts were carefully removed from the langendorff apparatus following completion of perfusion period. The left ventricles were then excised and quickly flash-frozen in liquid nitrogen and stored away at -80°C for later analysis.

After thawing on ice, into a 2ml Eppendorf 400µl of lysis buffer (NaCl 0.1 M,Tris base 10 µM, EDTA 1 mM, sodium pyrophosphate 2 mM, NaF 2 mM, β-glycaophosphate2 mM, 4-(2-Aminoethyl) benzene sulfonyl fluoride hydrochloride + PhosSTOP™ (Phosphatase stop) + Protease cocktail tablet (Roche, Switzerland) was added and between 70-100 mg of frozen cardiac tissue. All done over ice to prevent unnecessary heating of samples to prevent protein denaturation.

The eppendorf with the samples were homogenised at 11000 Rpm for 2 minutes and returned on ice as soon as possible. The samples were homogenised until a paste-like consistency was achieved. Homogenised samples were then subjected to BCA assay for protein quantification. Then 30μg of protein was loaded to 4–15 % Mini-Protean TGX Gel from Bio-Rad (UK) and separated at 10 V for 45 – 50 minutes. After separation, the proteins were transferred to the Bond-P polyvinylidene difluoride membrane from Bio-Rad (UK) by using the Trans-Blot Turbo transfer system from Bio-Rad (UK). Following successful transfer, the gel area was cut with a scalpel on the membrane. The membranes were then placed in a tub with blocking buffer(solution of 15ml 10X TBST ; 10x TBST – 50mM Tris Base, 150mM NaCl, 0.05% Tween-20; pH 7.6) , 5% milk - 0.75 g) and then was incubated at room temperature on the orbital shaker for at least 1 hour. After blocking, blots were washed 3 times in 10 X TBST & probed for the phospho-Akt (Ser473 Cell Signalling). The blots were placed into falcon tubes containing solution of 10ml TBST + 5% BSA with 5 μl primary antibody and incubated overnight on a roller at 4 °C.

Following overnight incubation (8-12 hours), the blots were taken out of the falcon tubes and washed twice in 10 x TBST. The secondary antibody was then prepared (15ml TBST, 0.5g BSA and 3μl anti-rabbit IgG). The blots were then incubated in the secondary solution for 2 hours (no longer than 2 hours to prevent oversaturation) at room temperature on the orbital shaker. After incubation the blots were then washed 3 times in TBST.

A 1:1 solution of the West Femto™ reagents was made (usually about 2-3ml for 2 blots). The blot was then placed on a clear acetate film taking care to remove bubbles underneath the membranes. 1ml of the solution was then pipetted over the membrane generously and then placed into the Bio-rad ChemiDoc™ for imaging. The appropriate chemiluminescence settings were then selected, and imaging conducted.

Following imaging of the bands phospho-Akt at Ser473 (Cell Signalling), the membranes were stripped (0.1 L pre-warmed Stripping buffer for 5 minutes – 20ml SDS 10%, 12.5ml Tris HCl ,pH 6.8, 0.5M, 67.5ml distilled water, add 0.8ml β-mercaptoethanol under the fume hood and warmed to 50°C) and washed 3 times 10 x TBST. The blots were then blocked again for 2 hours and then incubated overnight in Akt (pan) (11E7) Rabbit mAb (cell signalling) 10ml TBST + 5% BSA with 5 µl primary antibody and incubated overnight on a roller at 4 °C.

Following overnight incubation, the blots were taken out of the falcon tubes and washed twice in 10 x TBST. The secondary antibody was then prepared (15ml TBST, 0.5g BSA and 3µl anti-rabbit IgG). The blots were then incubated in the secondary solution for 2 hours at room temperature on the orbital shaker. After incubation the blots were then washed 3 times in TBST.

A 1:1 solution of the west femto™ reagents was made (usually about 2-3ml for 2 blots). The blot was then placed on a clear acetate film taking care to remove bubbles underneath the membranes. 1ml of the solution was then pipetted over the membrane generously and then placed into the Bio-rad ChemiDoc™ for

imaging. The appropriate chemiluminescence settings were then selected, and imaging conducted.

5.3.7 Culturing H9C2 cells

H9C2 cells were cultured in T75 flasks and supplemented with modified DMEM (Dulbecco's Modified Eagle Medium) which contained 10% FBS (Foetal bovine serum) and 1% PEN-STREP (Penicillin streptomycin). Cultured cells were then seeded on 6-well plates and given about 48 hours for the plates to achieve 70% confluency. The first step was the culture the cells unto well plates as required. The cell density per well for this study was about 1×10^5 per well.

The plates were then treated with the appropriate drug treatments and incubated overnight (24 hours). The treatment media was then discarded, and the cells were trypsinised. The dislodged cells were then transferred into eppendorf tubes with equal volume of modified media to inactivate trypsin and pelleted (100-300g for 5 minutes at 4°C). The pellets were then analysed for cleaved-caspase 3, cell death, mitochondrial superoxide, and calcium overload studies.

5.3.8 Cell viability analysis via MTT assay

Cultured cells in T75 flasks were first trypsinised and incubated for 5 minutes in 5% CO_2 incubator and temperature of 37°C to remove them from the culture flasks. About 2-3ml of supplemented media was added into the flasks to inactivate the trypsin. The cells were then pelleted and resuspended in fresh media, counted, and then seeded unto plates with a density of about 1×10^5 per well about 48 hours

prior to allow enough time to adhere and reach full confluency on a 24-well plate. A few wells were filled with media alone to serve as background control.

The outer wells were filled with media alone to serve as background control. The cells were then incubated for 24 hours with crizotinib 1µM ± losartan 4.5µM and crizotinib 1µM. Following the incubation period, the media was discarded, and the wells directly inoculated with 100µl of 5mg/ml MTT reagent and the wells were then incubated for 3 hours.

Following incubation, the solution was discarded and 100% DMSO solution was added to lyse the cells as previously described in methods section. The absorbances were then read at 590nm. The data was normalised using the formula below.

Normalised absorbance reading = Mean absorbance value minus (-) Mean absorbance of cell free medium

Percentage cytotoxicity (%) = (Control (Untreated)absorbance / treated absorbance) x 100

5.3.9 Analysis of protein expression in isolated perfused left ventricular tissue following drug treatment through western blotting

Following protein separation via electrophoresis, the protein bands were transferred onto the PVDF membrane and probed for the phosphorylated and total forms of AKT (Ser 473). The resultant banding on the membranes were analysed

with the aid of Image J© software. The changes in relative expression were assessed and calculated and corrected for differences in protein loading as established by probing for total protein (total AKT).

5.3.10 Assessment of crizotinib cytotoxicity in cultured H9C2 cardiac fibroblasts following drug treatment via annexin v detection (Abcam™ Annexin V-FITC apoptosis detection kit)

The cultured cells were first trypsinised from flasks and plated to a density of about 1×10^5 per well about 48 hours prior to allow enough time to adhere and reach full confluency on a 24-well plate. The plates were then inoculated with the required drug treatments and then incubated for 24 hours at 37°C. Following the incubation period, the plates were recovered from the incubator and transferred to a laminar flow hood for the rest of the protocol.

The treatment media was firstly discarded, and the cells required trypsinisation for detachment from the plate. The trypsinised cell suspension was then transferred into eppendorf tubes. The trypsin was then inactivated with equal volume of supplemented media. The cells were then pelleted in a cold centrifuge (100-300g for 5 minutes at 4°C) and the pellet was then resuspended in 500μl of 1 X binding buffer. To each of the eppendorf tubes, 5 μl of annexin V-FITC and 5 μl of propidium iodide (for necrosis) was added. The tubes were then transferred into a dark drawer at room temperature for 5 minutes. Upon completion of the incubation period, the samples were then analysed BD Accuri™ C6 Plus personal flow cytometer set to count 5000 cells.

5.3.11 Assessment of cleaved caspase 3 activity (asp175) in cultured H9C2 fibroblasts following drug treatment

Cultured cells were first stripped from T75 flasks and plated to a density of about 1×10^5 per well about 48 hours prior to allow enough time to adhere and reach full confluency on a 24-well plate. The plates were then inoculated with the required drug treatments and then incubated for 24 hours at 37°C.

The treatment media was discarded, and the cells required trypsinisation for detachment from the plate. The trypsinised cell suspension was then transferred into eppendorf tubes. The trypsin was then inactivated with equal volume of modified media. The cells were then pelleted in a cold centrifuge (100-300g for 5 minutes at 4°C) and the resultant pellet was resuspended in 100μl of 4% formaldehyde solution to fix the cells at room temperature for 15 minutes. The suspension was then washed afterwards in excess 1 X PBS solution and pellet and discard the supernatant. The samples were then resuspended in 0.5 – 1ml of PBS solution.

The fixed cells were then permeabilized with ice chilled 100% methanol added dropwise to the prechilled cells bringing the final concentration to 90% methanol solution. The samples were left for 10 minutes on ice and transferred to then be stored at – 20 °C or could be carried further for immunostaining.

The first step leading up to the immunostaining procedure was to count cells and aliquot desired number of cells into tubes (approximately 5×10^5). The samples were then washed in PBS to remove methanol and the resultant pellet was then

diluted in 100µL of diluted primary antibody solution (Cleaved caspase-3 antibody dilution buffer based). This was then allowed to incubate for 1 hour at room temperature. The samples were then washed in 1 x PBS, pelleted, and washed again for a second time. The samples were then resuspended in the secondary antibody solution (Alexa Flour 488® conjugate) which was also prepared in antibody dilution buffer. This was then allowed to incubate for 30 minutes at room temperature in dark condition. The samples were then washed 2 times in 1 x PBS. The pellet was finally resuspended in 500 µl of 1 x PBS ready for analysis on the BD Accuri™ C6 Plus personal flow cytometer set to count 10000 cells.

5.3.12 Assessment of mitochondrial superoxide generation following treatment of cultured H9C2 cardiac fibroblasts

Cultured cells were first stripped from T75 flasks and plated to a density of about 1×10^5 per well about 48 hours prior to allow enough time to adhere and reach full confluency on a 24-well plate. The plates were then inoculated with the required drug treatments and then incubated for 24 hours at 37°C.

The following day, the treatment media was then discarded. The adherent cells were then washed twice with phenol free media twice and not PBS to ensure signal stability. The cells were then covered with 300-500µl of 5µM solution of mitochondrial superoxide red (MitoSox™ reagent). Original stock solution (5mM stock in DMSO) of MitoSox red was reconstituted in DMSO, however working (5 µM) solution was diluted in media. The plates were incubated for 20-25 minutes

at 37^{0}C covered from light. Following the incubation period, the mitosox reagent was carefully aspirated off and transferred to the Epoch 2 microplate spectrophotometer (Biotek UK). The absorbance was then measured between 510/580nm wavelengths.

5.3.13 Assessment of calcium ion detection following treatment of cultured H9C2 cardiac fibroblasts

Disruptions in calcium signalling and homeostasis could contribute towards apoptosis, with increases in Ca^{2+} a hallmark of early and late stage apoptotic pathway (Pinton et al 2008).

Cultured cells were first trypsinised from T75 flasks and plated to a density of about 1 X 10^5 per well about 48 hours prior to allow enough time to adhere and reach full confluency on a 24-well plate. The plates were then inoculated with the required drug treatments and then incubated for 24 hours at 37°C.

The treatment media was discarded, and the cells required trypsinisation for detachment from the plate. The trypsinised the cell suspension was then transferred into eppendorf tubes. The trypsin was then inactivated with equal volume of modified media. The cells were then pelleted in a cold centrifuge (100-300g for 5 minutes at 4°C). Pellets were then resuspended in 1ml of 5μM Fluo-3, AM, Calcium Indicator solution and incubated for 30 minutes 37°C. Following this the cells were then washed twice and resuspended in 1ml 1 X PBS. The samples were than analysed on the BD Accuri™ C6 Plus personal flow cytometer set to count 5000 cells.

5.3.14 Statistical analysis

As previously stated, the processed data was presented as mean ± Standard error of the mean (SEM). Haemodynamic data was tested for differences using Two-way analysis of variance (ANOVA) with Fischer's LSD post hoc tests for the different time points using GraphPad prism 8 software. Infarct data was assessed so statistical differences between the individual groups using the one-way ANOVA and Tukeys post hoc test. MTT data was assessed so statistical differences between the individual groups using the two-way ANOVA and Fischer's LSD post hoc tests. Fold changes for AKT expression was assessed so statistical differences between the individual groups using one-way ANOVA and Fischer's LSD post hoc tests. One-way ANOVA was employed for the other sets of data with Fischer's LSD post hoc tests. P-values less than 0.05(P< 0.05) were considered statistically significant.

5.4 Results

5.4.1 The effects of losartan co-treatment on myocardial dysfunction in isolated perfused rat hearts (haemodynamic assessment)

In order to assess the effects of losartan co-treatment on cardiac dysfunction induced by crizotinib treatment, isolated rat heats were perfused with the different treatment compounds for a total of 175 minutes. The haemodynamic performance in each of the hearts was assessed for their performance in left ventricular developed pressure (LVDP), heart rate (HR) and coronary flow (CF) and the figures generated were recorded. During the first 55-minute perfusion

period, readings were collected at 5-minute intervals, after which, readings were collected at 15-minute intervals.

5.4.1.a Variation in LVDP (%) in isolated adult male rat hearts treated with losartan 4.5 µM ± crizotinib 1µM

Isolated rat hearts treated with crizotinib alone performed the worst with regards overall LVDP (%) across the monitoring period. Hearts treated with combination of losartan and crizotinib produced significant improvement in the LVDP (%) compared to hearts treated with crizotinib alone over a number measured time point (Figure5.4.1)
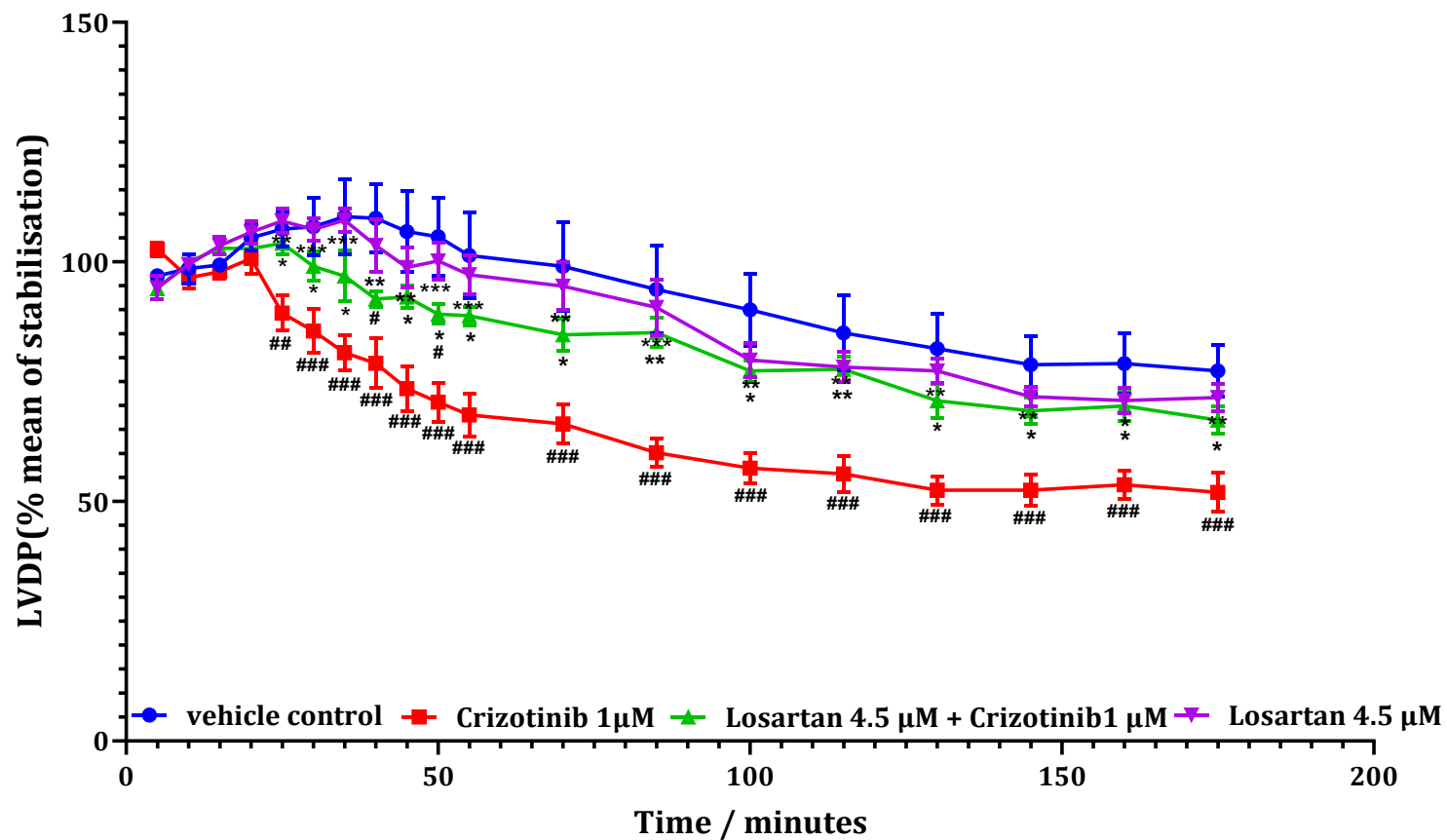
Figure 5.4.1 The effects of losartan co-administration with crizotinib on adult male Sprague Dawley rat hearts left ventricular developed pressure treated for 175 minutes. The hearts were all allowed a 20-minute stabilisation period

and 155 minutes of drug perfusion. (# P<0.05, ## P<0.01, ### P<0.001 versus time matched vehicle control treatment, * P<0.05, ** P<0.01 *** P<0.001 versus time matched treatment with crizotinib 1μM treatment, N=6 for all samples).

During the stabilisation period, any differences between the groups were not deemed statistically significant.

After 40 minutes, the hearts treated with losartan co-administered with crizotinib and crizotinib alone significantly reduced the LVDP (%) compared to the isolated rat hearts treated with the vehicle control (109.1±7.165% versus 92.29±1.660% P<0.05 and 109.1±7.165% versus 78.83±5.141% respectively, P<0.001). Hearts treated with crizotinib alone significantly reduced the LVDP (%) compared to the isolated rat hearts treated with losartan 4.5 μM alone (78.83±5.141% versus 103.42±5.56%, where P<0.001) (Figure 5.4.2).
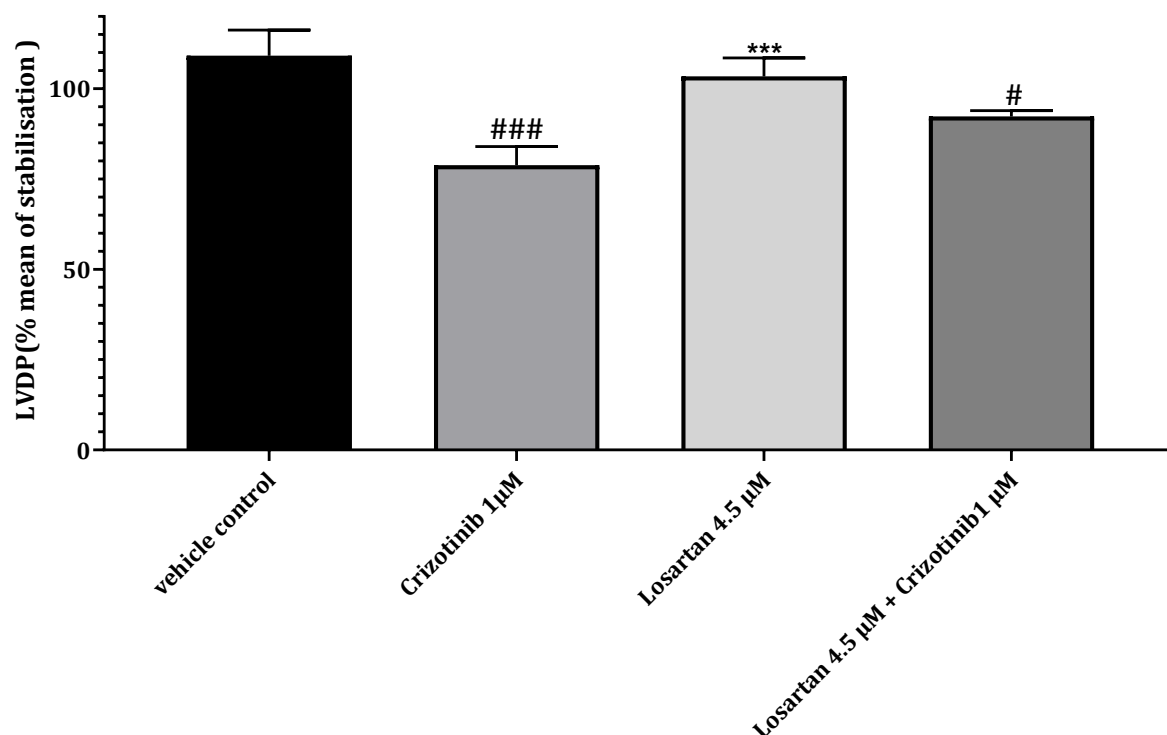
Figure 5.4.2 Assessment of LVDP (%) in isolated adult rat hearts at 40 minutes. The hearts treated with losartan co-administration and crizotinib alone significantly reduced LVDP (%) compared to non-treated control. (# P<0.05, ### P <0.001 versus non-treated vehicle controls, *** P<0.001 versus crizotinib 1μM treatment).

At 50 minutes, the hearts treated with losartan co-administered with crizotinib and crizotinib alone significantly reduced the LVDP (%) compared to the isolated rat hearts treated with the vehicle control (105.23±8.98% versus 89.10±2.24% P<0.05 and 105.23±8.98% versus 71.16±4.46% respectively, P<0.001). The hearts treated with losartan co-administered with crizotinib significantly improved LVDP (%) compared to the time matched hearts treated with crizotinib alone (89.10±2.24% versus 71.16±4.46% respectively, P<0.05). Treatment of the

isolated hearts with crizotinib alone significantly reduced the LVDP (%) compared to the isolated rat hearts treated with losartan 4.5 µM alone (71.16±4.46% versus 100.2± 3.53% respectively, P<0.001) (Figure 5.4.3).
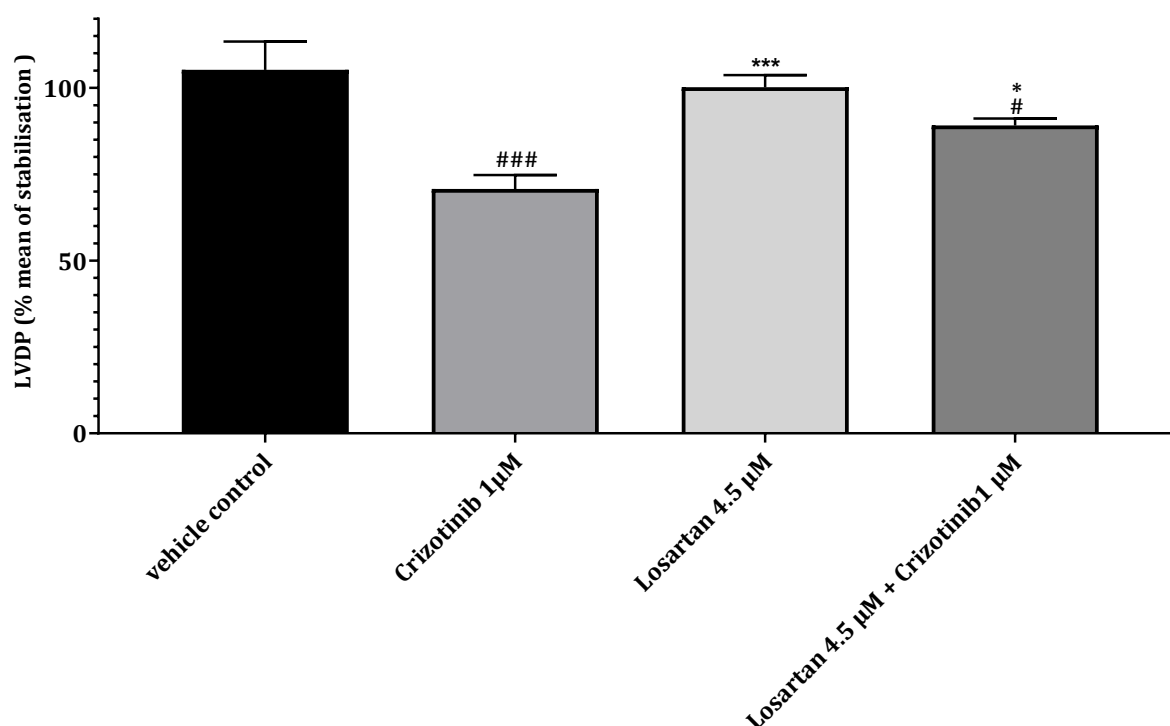
Figure 5.4.3 Assessment of LVDP (%) in isolated rat hearts at 50 minutes. Treatment with losartan in combination with crizotinib significantly increased LVDP (%) in isolated hearts compared to hearts treated with crizotinib alone. (# P<0.05, ### P<0.001 versus non-treated control treated hearts; * P<0.05, *** P<0.001 versus treatment with crizotinib alone)

After 85 minutes, losartan co-administered with crizotinib significantly improved LVDP (%) compared to isolated adult rat hearts treated with crizotinib alone (85.2±3.35% versus 60.55±3.33% respectively, P<0.01). Treatment of isolated rat hearts with crizotinib alone significantly decreased LVDP (%) compared to hearts

treated with losartan alone (60.55±3.33% versus 90.5±5.25% respectively, where P<0.001) (Figure 5.4.4).
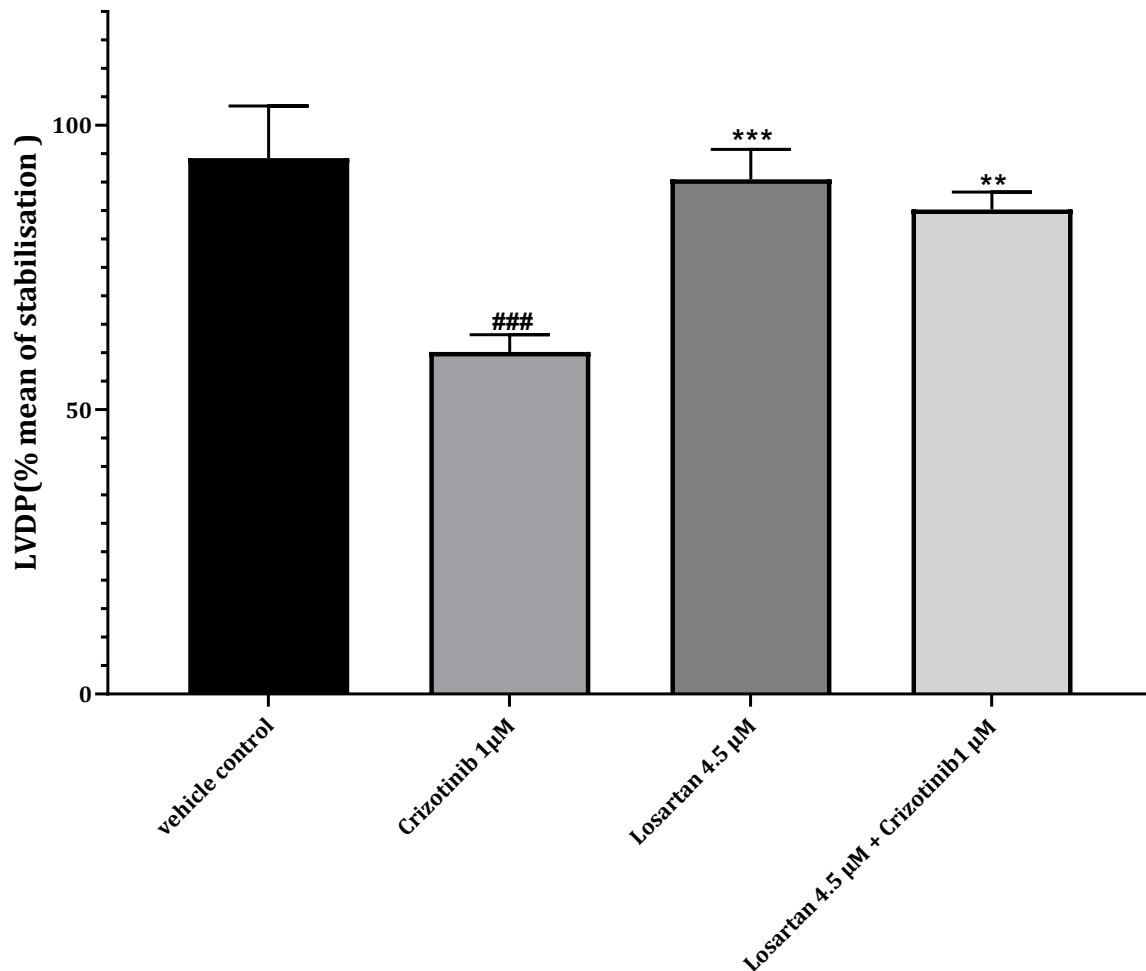
Figure 5.4.4 Assessment of LVDP (%) in isolated rat hearts at 85 minutes. Treatment with losartan in combination with crizotinib significantly increased LVDP (%) in isolated hearts compared to hearts treated with crizotinib alone. (### P<0.001 versus treatment with non-treated control; ** P<0.01 versus treatment with crizotinib alone).

Overall, losartan co-administration significantly improved LVDP (%) in isolated rat hearts compared with hearts treated with crizotinib alone. The improvements

were statistically significant as indicated in figure 5.4.1. This appears suggestive that losartan was limiting the impairment of left ventricular pressure.

5.4.1.b Variation in heart rate (%) in isolated adult male rat hearts treated with crizotinib ± Losartan

Treatment with losartan in combination with crizotinib did not significantly change heart rate (%) response compared to isolated hearts treated with crizotinib alone. Overall, losartan ± crizotinib treatment resulted in lower heart rate values compared to the other regimens but again any differences were not deemed statistically significant.

However, within the stabilisation period all the treatment regimens appeared to generate similar readings with no significant differences between the treatment groups (Figure 5.4.5 and Figure 5.4.6).
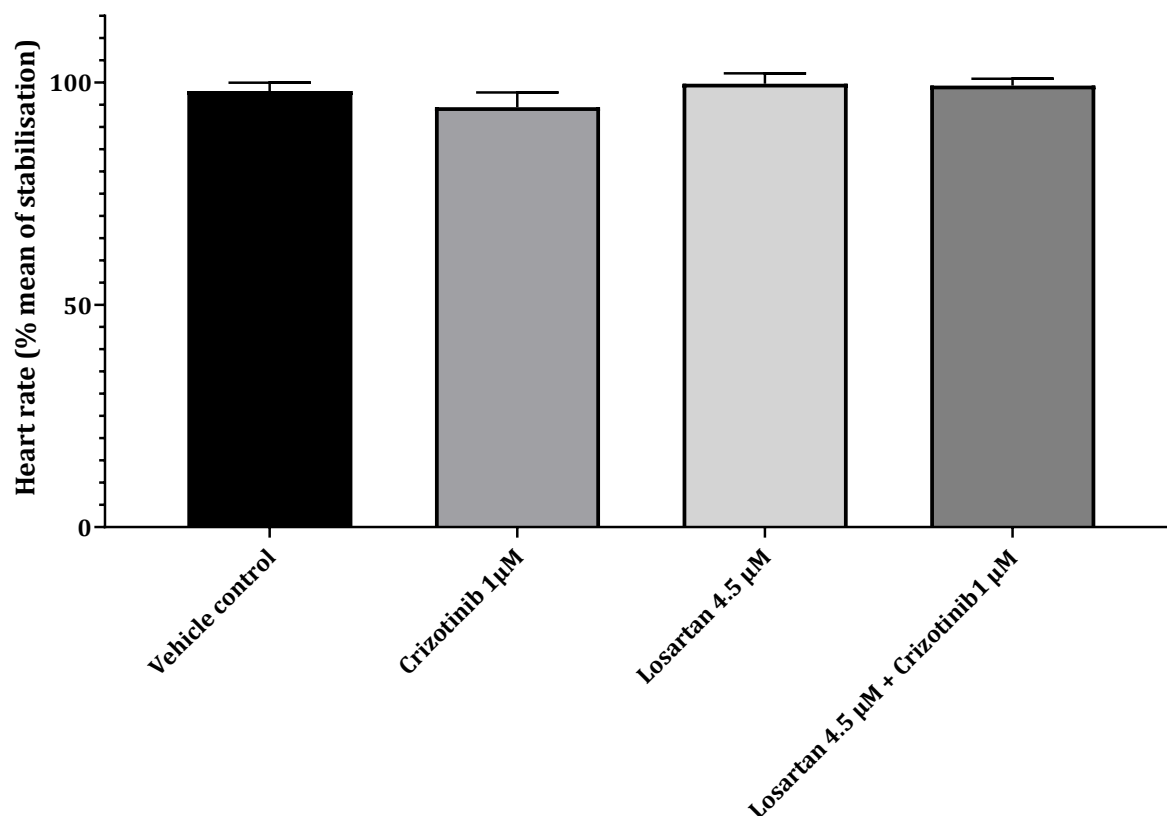
Figure 5.4.5 Assessment of heart rate (%) in isolated rat hearts at 20 minutes during stabilisation. No significant differences observed between the different treatments with regards heart rate.

The figure illustrating the whole treatment period denotes no significant differences between hearts of the studied treatments (Figure 5.4.6).
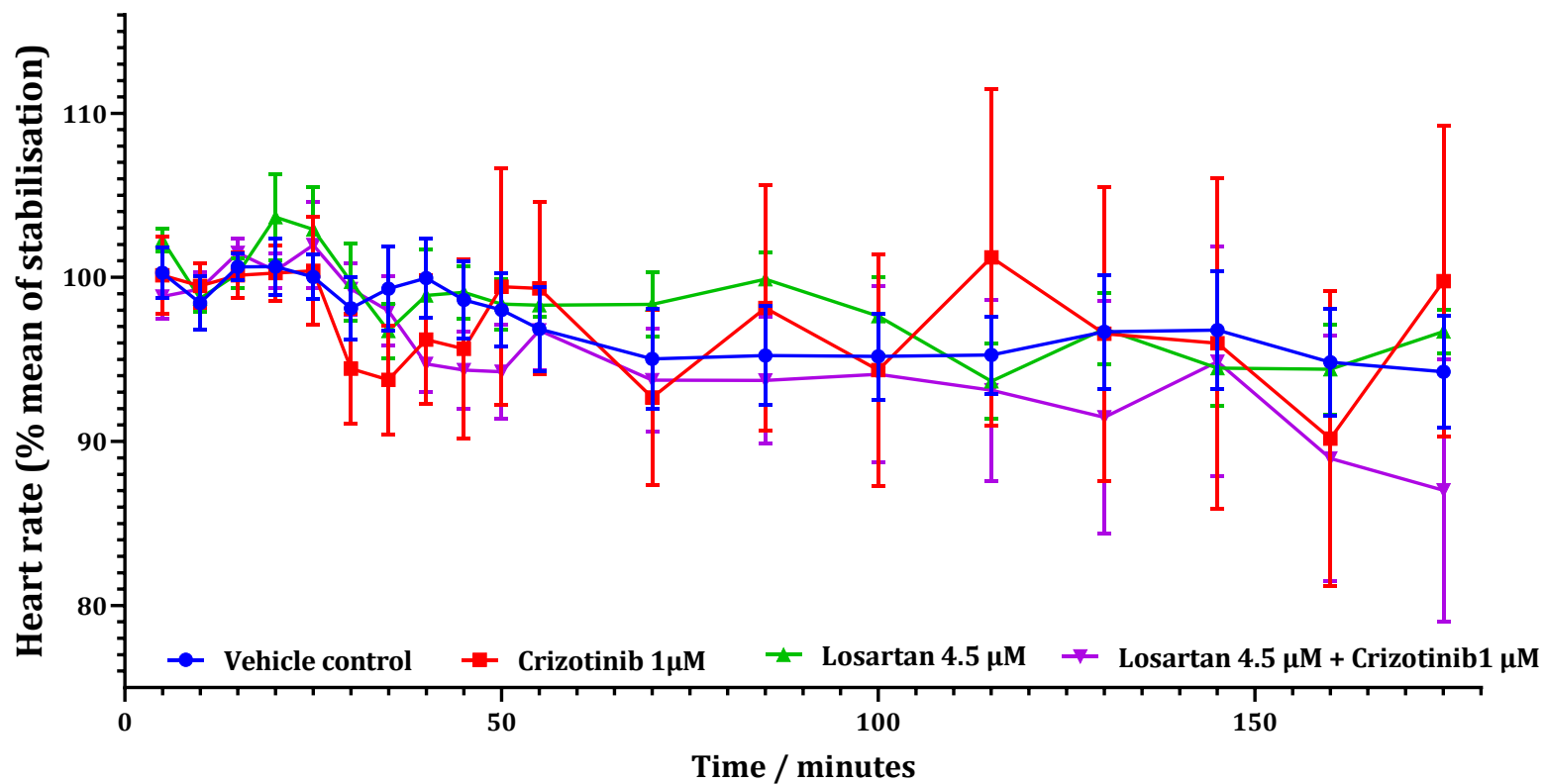
Figure 5.4.6 The effects of losartan co-administration with crizotinib on adult male Sprague Dawley rat hearts recorded heart rates treated for 175 minutes. The hearts were all allowed a 20-minute stabilisation period and 155

minutes of drug perfusion. Losartan co-administration with crizotinib did not significantly change the heartrates compared to that ho hearts treated with crizotinib alone.

5.4.1.c Observed variation in coronary flow in isolated adult male rat hearts treated with crizotinib ± Losartan

Isolated rat hearts treated with losartan co-administered with crizotinib appeared to increase coronary flow (%) about 5 minutes into drug perfusion compared to hearts treated with crizotinib alone & the non-treated control, however only the increase compared to the non-treated control was statistically significant(Figure 5.4.7 and Figure 5.4.8).
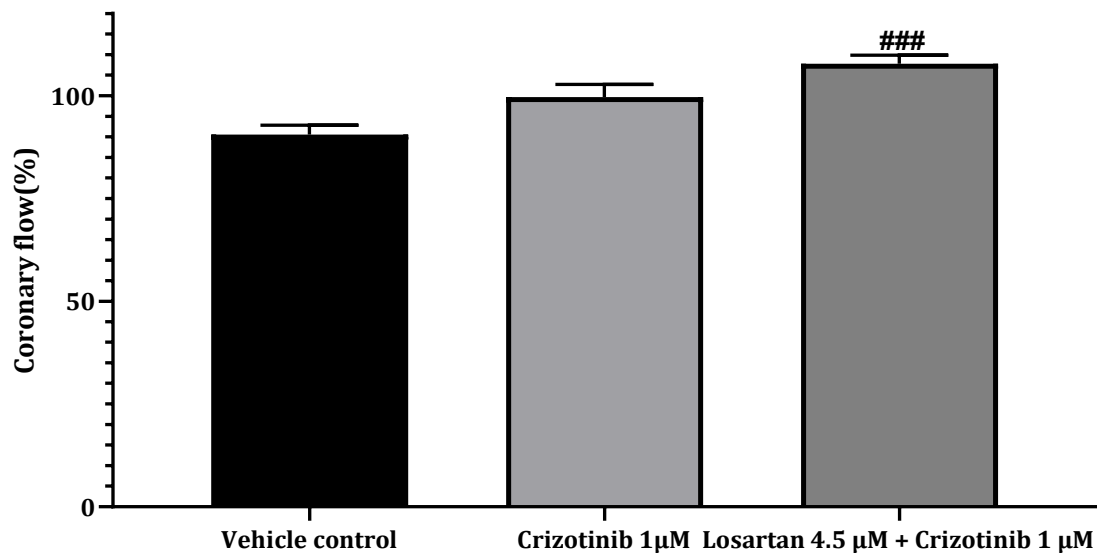
Figure 5.4.7 Assessment of coronary flow (%) changes in isolated rat hearts 5 minutes into drug perfusion. Losartan co-administered with crizotinib treatment significantly increased coronary flow compared to non-treated control (### P<0.001 versus vehicle control treatment).
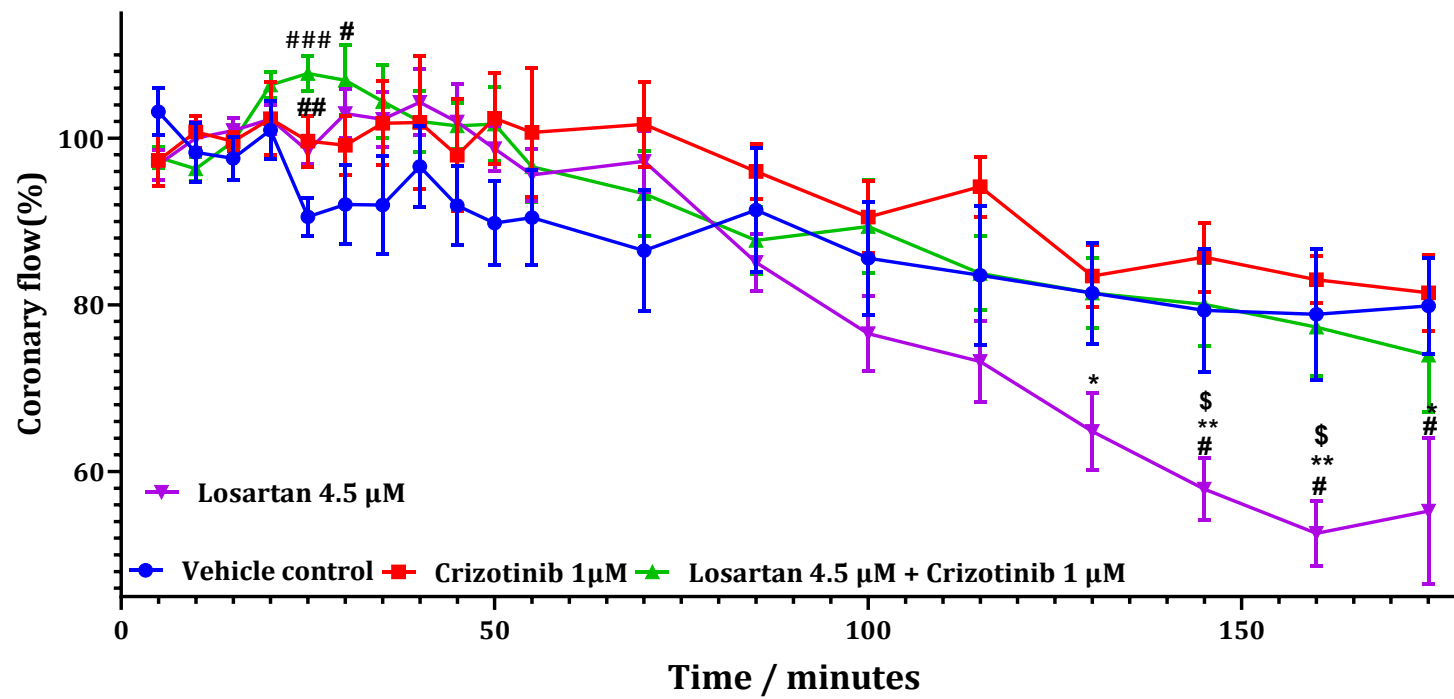
Figure 5.4.8 The effects of co-administration of losartan and crizotinib on coronary flow generated from isolated male

Sprague Dawley rat hearts treated for 175 minutes. Hearts were treated for 175 minutes allowing a 20-minute stabilisation period. Co-administration of losartan and crizotinib significantly increased the coronary flow compared to non-treated control (### P<0.001 versus vehicle control treatment). After 5 minutes of drug perfusion (25-minute measurement interval), losartan administration concomitantly with crizotinib significantly increased coronary flow compared to the non-treated vehicle control rat hearts (107.7±2.066% versus 90.55±2.275% respectively, P<0.001). Losartan alone treatment on rat hearts also significantly increased coronary flow (%) compared to hearts with non-treated vehicle controls (98.44±1.72% versus 90.55±2.275% respectively, where P<0.05).

5.4.2 The effects of co-administration of losartan and crizotinib on mean infarct to risk ratio (%) development in isolated adult male Sprague-Dawley rat hearts during langendorff perfusion.

Whole heart sections were stained with 2, 3, 5-Triphenyltetrazolium Chloride (TTC™) for infarct region development and incubated prior to analysis of infarct size to risk ratio (%) with the Image J software (Image J®).

Losartan administration simultaneously with crizotinib significantly reduced infarct to risk ratio (%) compared to treatment with crizotinib alone on isolated rat hearts (13.7±0.561% versus 23.4±5.58% respectively, P<0.01). Losartan administration concomitantly with crizotinib significantly increased infarct to risk

ratio (%) developed compared to non-treated control (13.7±0.561% versus

6.88±0.88% respectively, P<0.001) (Figure 5.4.9).
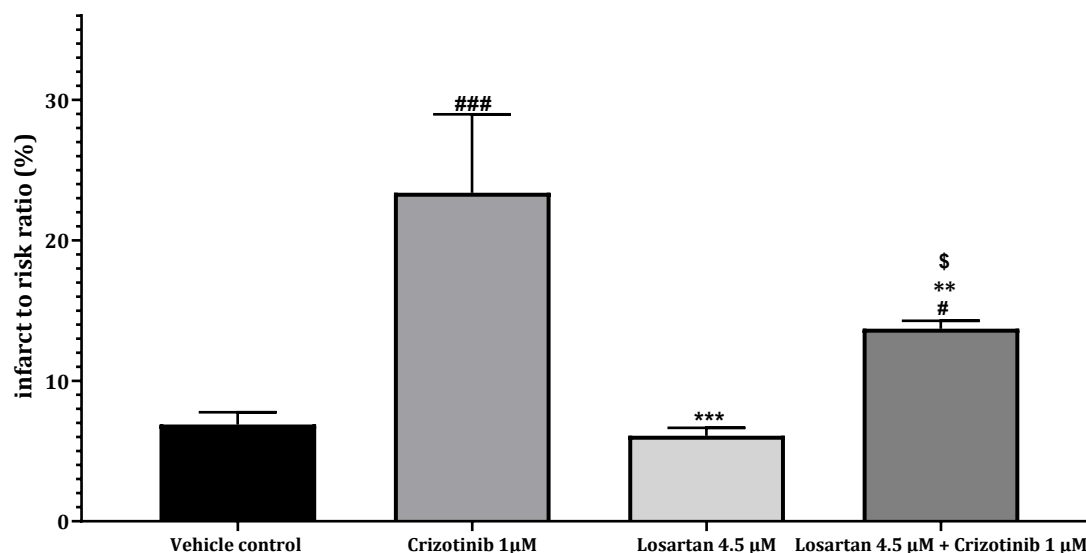
Figure 5.4.9 Assessment of mean infarct size to risk ratio (%) developed in isolated male Sprague-Dawley rat hearts treated with vehicle control, Crizotinib 1μM and losartan 4.5μM + Crizotinib 1μM for 155 minutes (Data was presented as mean ± SEM. ** P<0.01 ***P<0.001 vs Crizotinib 1μM, #P<0.05 ###P<0.001 vs vehicle control (DMSO 0.04%), $ P<0.05 versus treatment with losartan 4.5μM)

Losartan administration concomitantly with crizotinib significantly increased infarct to risk ratio (%) developed compared to hearts treated with losartan 4.5μM alone (13.7±0.561% versus 6.082±0.57%, where P<0.05).

5.4.3 The effects of co-administration of losartan and crizotinib on cellular viability in cultured H9C2 myoblasts Assessment of viability via MTT assay

The MTT (3-(4,5-dimethylthiazol-2-yl)-2-5-diphenlytetrazolium bromide) assay was employed as a means to assess cell viability.

Treatment of the cultured H9C2 cardiac myoblasts with losartan and crizotinib significantly improved cell viability assessed compared to the cultures treated with crizotinib alone ($67.21 \pm 2.05\%$ versus $35.51 \pm 3.98\%$ respectively, $P < 0.001$). Treatment with co-administered losartan and crizotinib significantly reduced viability in cultured H9C2 myoblasts compared to non-treated controls ($67.21 \pm 2.05\%$ versus $104.8 \pm 5.62\%$ respectively).
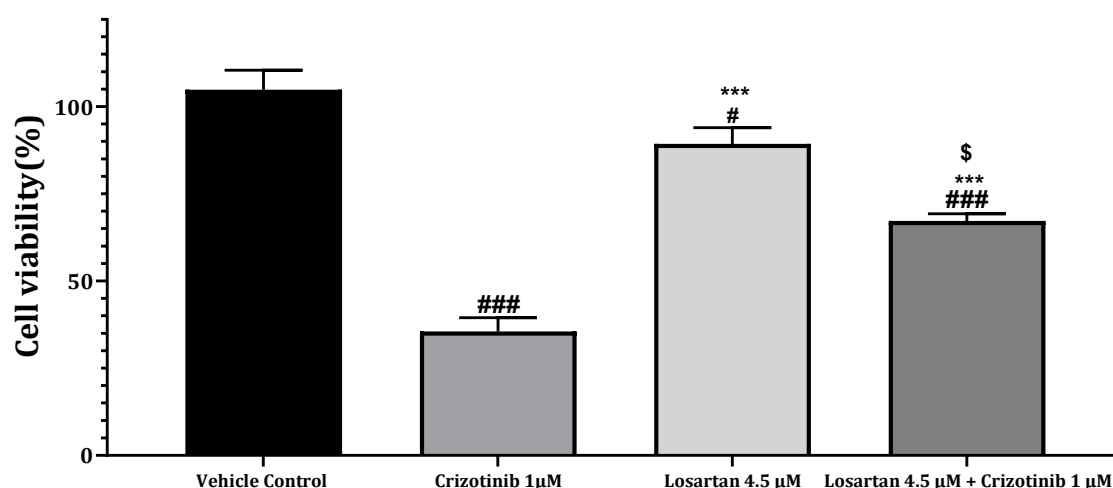
Figure 5.4.10 Assessment of H9C2 cultured myoblast viability assessed by MTT (3-(4,5-dimethylthiazol-2-yl)-2-5-diphenlytetrazolium bromide) assay after 24-hour treatment in vehicle control (0.04% DMSO), losartan 4.5μM ±

crizotinib 1μM(Data was presented as mean ± SEM;### P<0.001 versus vehicle control treatment and *** P<0.001 versus Crizotinib 1μM treatment).

Treatment with losartan and crizotinib significantly decreased viability in cultured H9C2 myoblasts compared to H9C2 cultures treated with losartan 4.5μM alone (67.21±2.05% versus 89.32±4.62%, where P<0.05). H9C2 cultures treated with losartan 4.5μM alone showed significantly improved viability compared top cultures treated with crizotinib 1μM alone (89.32±4.62% versus 35.51±3.98%, where P<0.001).

5.4.4 The effect of losartan administration concomitantly with crizotinib on expression of phosphorylated AKT (ser473) in left ventricular tissue of adult male Sprague-Dawley rat hearts

Upon completion of the protocol outlined in section 5.3.9, the comparative band intensities were quantified and analysed.

Although there appeared to be variation between the expressions between the individual groups, losartan in combination with crizotinib did not significantly appear to alter crizotinib expression. Interestingly, it appeared losartan treatment alone increased relative AKT expression however this was not statistically significant.

B)
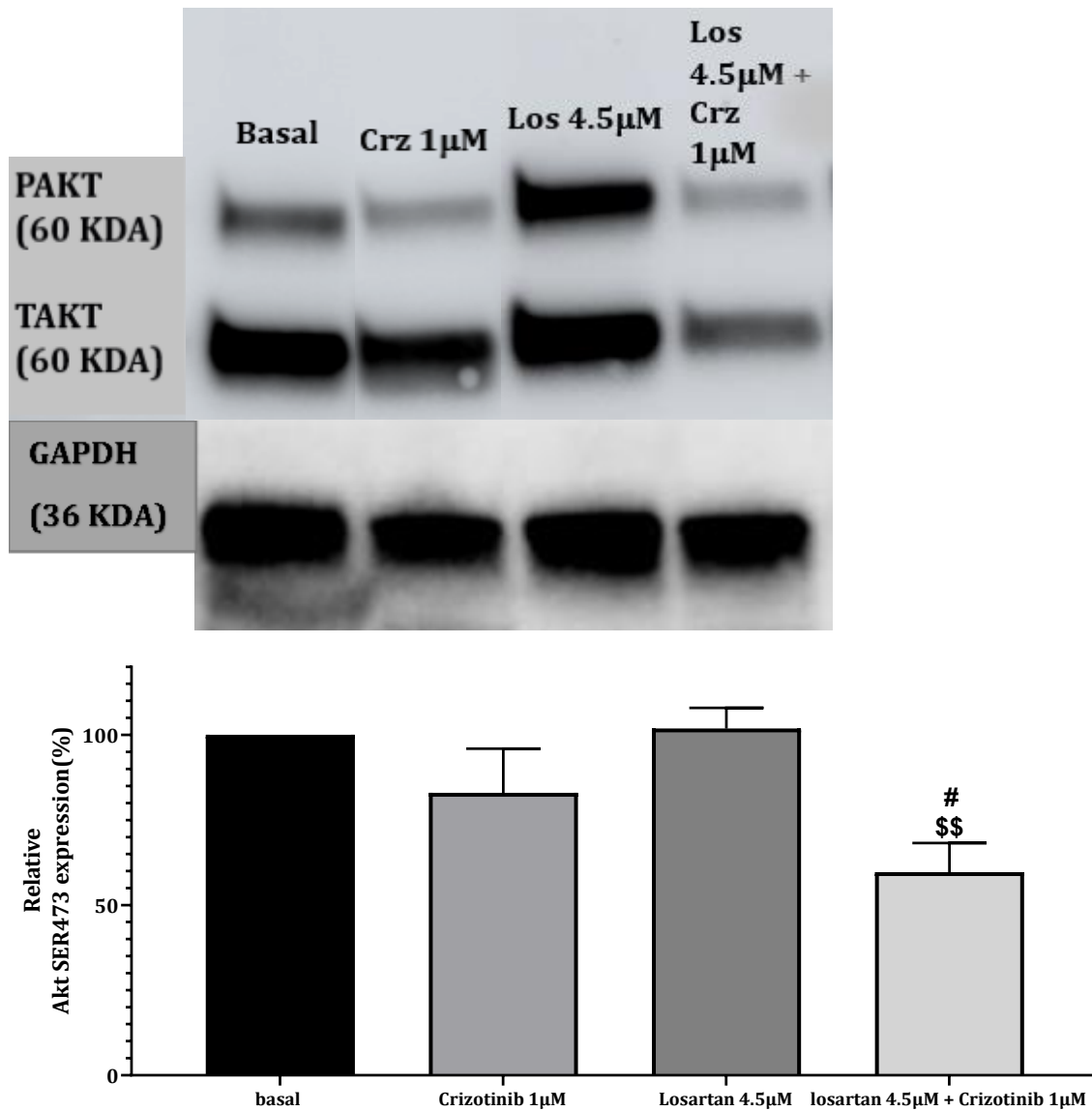
Figure 5.4.12 Assessment of relative phosphorylated AKT expression in adult isolated Sprague-Dawley rat hearts treated for 175 minutes with Losartan ± Crizotinib which were added 20 minutes into perfusion period (Data presented as mean ± SEM, #P<0.05 versus basal vehicle control and $$P<0.01 versus treatment with losartan 4.5μM alone).

5.4.5 The effect of losartan administration concomitantly with crizotinib treatment on cleaved caspase-3 expression in cultured H9C2 cardiac myoblasts

As an indicator of cellular apoptosis, cleaved caspase 3 expression was evaluated. 10000 cells were counted on the flow cytometer and assessed for cleaved caspase-3 expression.

Treatment of cultured cells with losartan concomitantly with crizotinib for 24 hours significantly decreased cleaved caspase 3 expression in H9C2 cultures compared to cultures treated with crizotinib alone (3416 ± 599.4 RFU versus 5292 ± 283.9 RFU, $P<0.05$) (Figure 5.4.13).
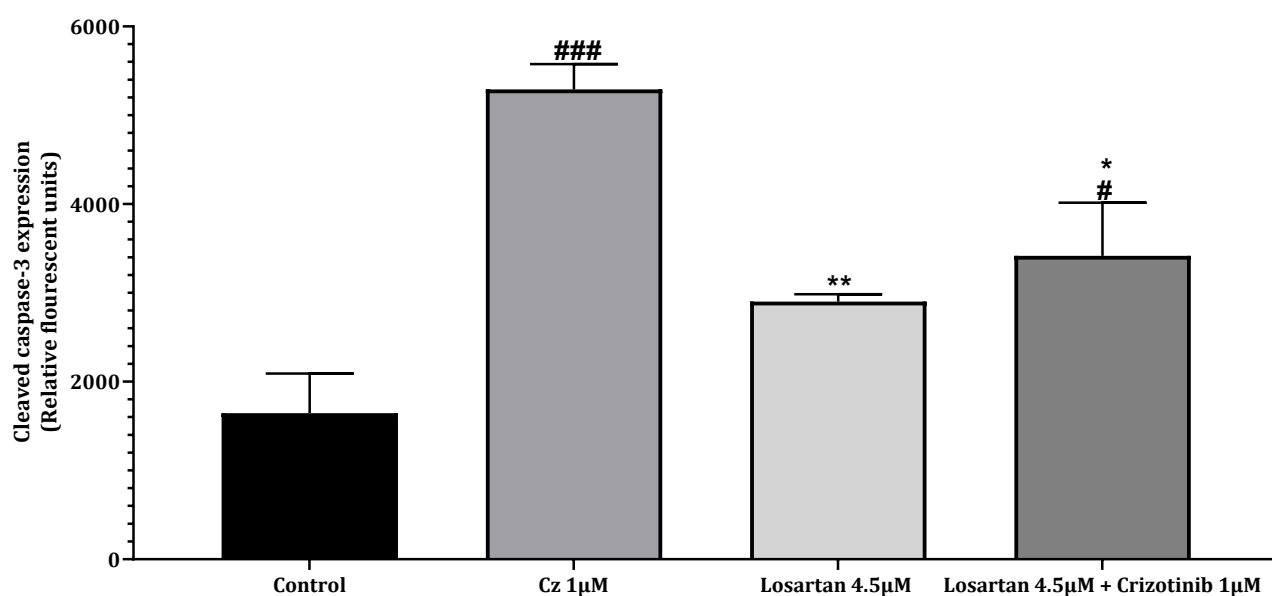
Figure 5.4.13 Assessment of cleaved caspase 3 expression in cultured H9C2 myoblasts treated for 24 hours with crizotinib ± Losartan (Data presented as mean ± SEM, # P<0.05 ### P<0.001 versus non-treated vehicle control, * P<0.05 versus treatment with crizotinib alone).

Treatment of cultured H9C2 myoblasts with losartan concomitantly with crizotinib for 24 hours significantly increased cleaved caspase-3 detection compared to myoblasts treated with the vehicle control treatment (3416±599.4 RFU versus 1644±447.3 RFU, P<0.05) (Figure 5.4.13).

Treatment of cultured H9C2 myoblasts with losartan alone significantly reduced cleaved caspase-3 expression compared to samples treated with crizotinib alone (2901±84 RFU versus 5292±284 RFU, where P<0.01).

The losartan and crizotinib co-treatment brought about significant reduction in cleaved caspase-3 expression compared with crizotinib treatment alone.

5.4.6 The effects losartan administration concomitantly with crizotinib treatment on mitochondrial superoxide generation in cultured H9C2 cardiac myoblasts

MitoSox Red mitochondrial superoxide indictor was employed for the assessment for this study. Detection was carried out with microplate reader.

The H9C2 cell cultures treated with Losartan administered in combination with crizotinib significantly decreased the percentage of superoxide that was generated compared to cultures that were treated with crizotinib alone (54.84±4.29% versus 82.98±1.69%, P<0.001). Suggestive that losartan was attenuating the effects of crizotinib. Interestingly, the H9C2 cell cultures treated with Losartan administered in combination with crizotinib showed a decrease percentage of superoxide that was generated compared to cultures with the non-treated vehicle control however this was deemed not statistically significant (Figure 5.4.14). The

samples treated with losartan alone also showed significant reduction in superoxide generation compared to hearts treated with crizotinib alone. Interestingly, treatment with losartan alone showed significant reduction in mitochondrial superoxide generation compared to samples treated with vehicle control.
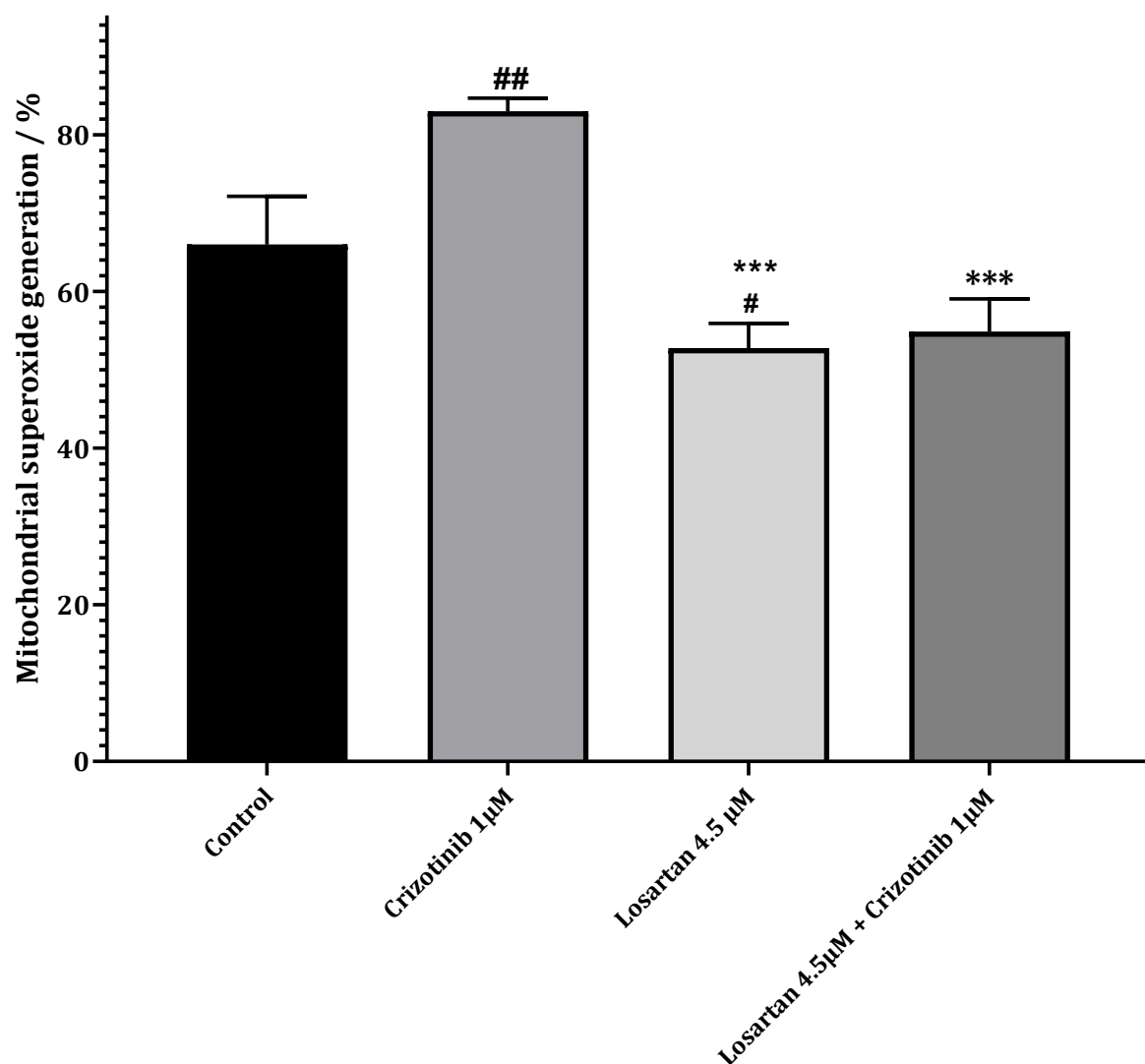
Figure 5.4.14 Assessment of mitochondrial superoxide generation in cultured H9C2 myoblasts subjected to 24 hours treatment with either vehicle control, Crizotinib 1μM ± losartan 4.5μM (Data presented as mean ±

SEM #P<0.05 and ##P<0.01 versus Vehicle control, ***P<0.001 versus treatment with crizotinib treatment alone).

The deductions from the data support the notion inclusion of losartan during crizotinib administration significantly decreased superoxide generation.

5.3.7 The effects of losartan co-treatment on crizotinib induced disruption of calcium of ion metabolism in H9C2 cardiac myoblast

Treatment of cultured H9C2 myoblasts with either vehicle control, Crizotinib 1μM ± losartan 4.5μM for 24 hours was conducted.

Treatment of cultured H9C2 myoblasts with Losartan administered in combination with crizotinib significantly reduced the percentage of fluo-3am detected in the treated myoblast cultures compared to the samples treated with crizotinib alone (73.48±5.327% versus 95.38±3.615%, P<0.01). Losartan coadministration appeared being about significant attenuation of the action of crizotinib (Figure 5.4.15).
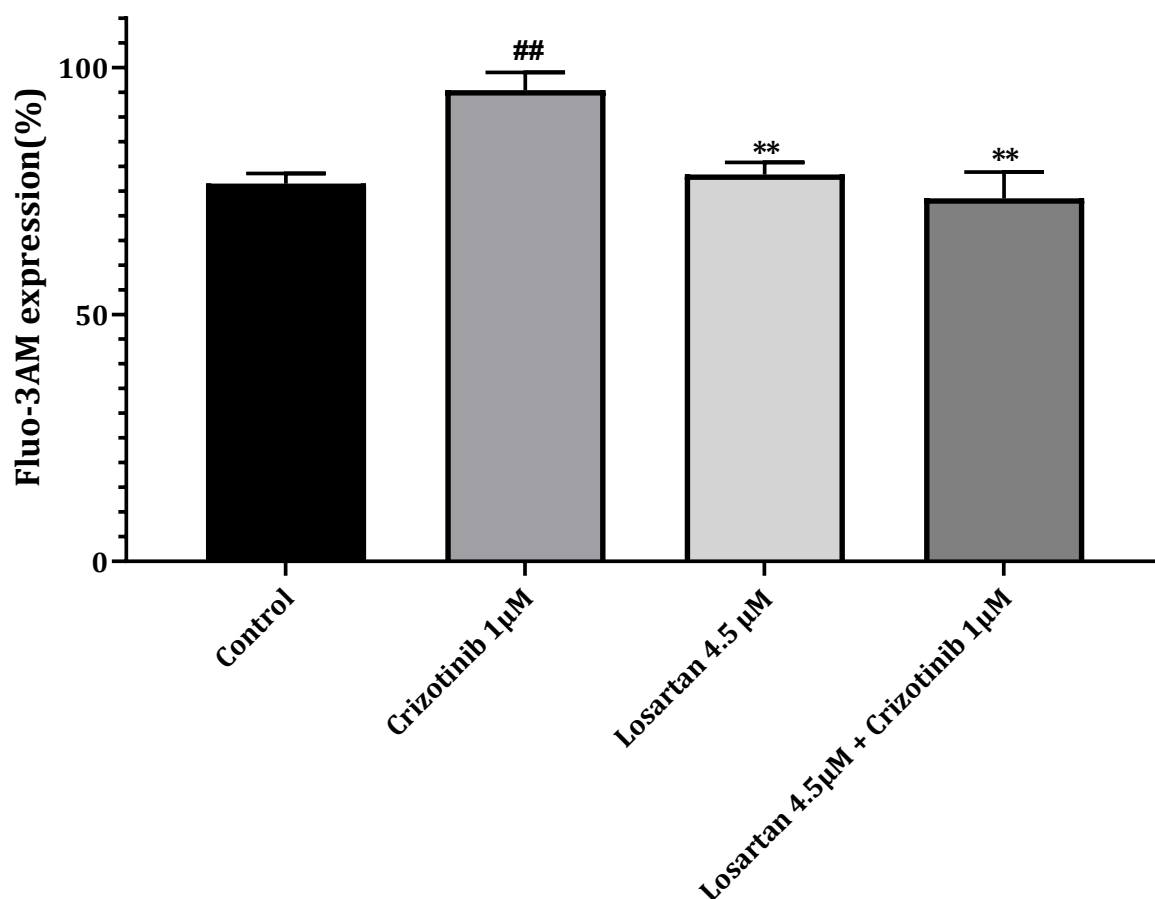
Figure 5.4.15 Assessment of calcium ion activity in cultured H9C2 myoblasts subjected to 24 hours treatment with either vehicle control, Crizotinib 1µM ± losartan 4.5µM (Where ## P<0.05 versus vehicle control, ** P<0.01 versus treatment with crizotinib alone).

Treatment of cultured H9C2 myoblasts with Losartan administered in combination with crizotinib however did not significantly alter fluo-3am detection compared to the non-treated control cultured H9C2 myoblasts. Treatment of cultured H9C2 myoblasts with Losartan alone significantly reduced fluo-3am detection compared to samples treated with crizotinib alone.

5.4 Discussion

The purpose of this study was to assess the potential for angiotensin receptor blocker losartan, to attenuate the cardiotoxic effects of tyrosine kinase inhibitor crizotinib. Tyrosine kinase inhibitors have been invaluable towards improvement in patient outcome during the treatment of a number of malignancies with perceivably reduced of incidence toxicity compared to traditional chemotherapeutics in a number of patients (Chu et al. 2007). Previous literature has argued renin angiotensin system overactivity contributes to anticancer cardiotoxicity, hence inhibitory agents limiting RAS activity provide beneficial effects in limiting cardiotoxicity and cardiovascular complications (Akolkar et al. 2015; Pinter, Kwanten, and Jain 2018). The benefits of Angiotensin receptor blockage are well documented to protect against chemotherapy induced cardiotoxicity by agents such as anthracyclines (Doxorubicin)(Cadeddu et al. 2010; Rashikh, Pillai, and Najmi 2014). Tyrosine kinase inhibitors do not have same mechanism of action as anthracyclines. Losartan which is regarded as an effective anti-hypertensive but is also renowned for its beneficial effects against cardiovascular diseases and complications (Akershoek et al. 2017; Iwai and Horiuchi 2009; Zong et al. 2011). This study investigated the role of losartan in reversing crizotinib induced cardiotoxicity.

With regards the experiments conducted to observe changes in haemodynamic parameters (Section 5.3.1), the overall observation was losartan co-administration with crizotinib significantly improved left ventricular developed

pressure at a number of time points in isolated hearts (figure 5.4.1) and there was an overall reduction in coronary output measured (however not deemed statistically significant) (Figure 5.4.8) compared to hearts treated with crizotinib alone. Hearts treated with losartan co-administration with crizotinib were associated with a more stable heart rate, however, was not significant different to hearts treated with crizotinib alone (Figure 5.4.6).

Activation of AT1 receptor by ang-II is associated with undesired effects such as fibrosis, inflammation, hypertrophy, increased blood pressure and increased ROS generation under stressed conditions (Schieffer et al. 1994; Schieffer et al. 2004; Sobczuk et al. 2020). The significant improvements in haemodynamic function observed in this current study appear consistent with prior literature which credits losartan for attenuation of left ventricular dysfunction initiated by anticancer treatment (Matouk et al. 2013; Sobczuk et al. 2020; Zong et al. 2011). Healthy male Wistar rats were treated with sorafenib with and without losartan for 30 days (Abdelgalil et al. 2020). Losartan co-administration with sorafenib was associated with improved left ventricular pressure also perfusion pressure compared to hearts treated with sorafenib alone, although improvements were not statistically significant (Abdelgalil et al. 2020). Treatment of hearts with losartan and sorafenib yielded significant improvement in heart rate compared to hearts treated with sorafenib alone (Abdelgalil et al. 2020). Similar results were observed in a study involving ARB telmisartan in which co-administration with epirubicin significantly reversed early left ventricular impairment induced by cardiotoxicity (Cadeddu et al. 2010b). The study which enrolled 49 individuals

involving epirubicin co-treated with telmisartan showed that telmisartan was effective at initially limiting epirubicin induced ventricular impairment and afterwards (3 weeks into telmisartan treatment) significantly reverse epirubicin induced impairment (Cadeddu et al. 2010). In a follow up study, angiotensin receptor blocker administration was credited with long term protective effects against epirubicin-induced inflammation and oxidative stress (Dessì et al. 2013). The phase II single blind placebo-controlled randomised trial with a 49-patient sample were included. Over the 18-month telmisartan and epirubicin treated patients showed sustained diastolic function while epirubicin alone treatment associated with significant diastolic impairment in patients (Dessì et al. 2013).

Losartan co-treatment with crizotinib in this present study significantly reduced infarct to risk ratio (%) development compared with hearts treated with crizotinib alone (Figure 5.4.2). ARB's have been credited for their ability to prevent cardiac damage through attenuating cardiac cell death, fibrosis, and inflammation (Sobczuk et al. 2020). Reduction in the infarct risk ratio (%) indicates losartan co-treatment with crizotinib may have been attenuating effects of crizotinib significantly in the current study. This was consistent with prior studies which showed losartan treatment was associated with almost conserved histological profiles following co-treatment with doxorubicin and sorafenib compared to more disarranged cardiomyocytes arrangement, increased inflammatory cells and inflammation which could all be indication of infarcted tissue (Abdelgalil et al. 2020; Matouk et al. 2013). Healthy Wistar rats subjected to sorafenib induced

cardiotoxicity, losartan treatment with sorafenib significantly attenuated sorafenib induced cardiac tissue changes (Abdelgalil et al. 2020).

Losartan treatment with sorafenib reduced morphological changes induced by treatment with sorafenib alone on hematoxylin and eosin stained heart tissue slides (Abdelgalil et al. 2020). Similarly, losartan treatment along with doxorubicin in male Wistar rats significantly reduced oxidative stress damage in treated rats as evidenced by reduced lipid peroxidation product thiobarbituric acid reactive substances (TBARS) (Matouk et al. 2013). Losartan and telmisartan treatment were associated with significant reduction in proinflammatory cytokine TNF α and serum cardiac enzymes lactate dehydrogenase & creatine kinase following treatment with doxorubicin and Sorafenib indicative of cardiac tissue preservation (Abdelgalil et al. 2020; Ibrahim et al. 2009b; Matouk et al. 2013). In the study by Ibrahim et al (2009), male albino rats treated with doxorubicin and telmisartan, telmisartan was effective at limiting doxorubicin induced cardiotoxicity. Telmisartan co-treatment with doxorubicin significantly reduced serum enzyme (Creatine kinase and lactic dehydrogenase) detection compared to samples with doxorubicin treatment alone (Ibrahim et al. 2009). Telmisartan co-treatment with doxorubicin also improved histological heart sections with observable reduction in incidences of interstitial oedema, vacuolation and general degeneration of the myocardial tissue compared to treatment with doxorubicin alone (Ibrahim et al. 2009).

Losartan treatment induced significant reduction of cardioskeletal muscle fibrosis in dystrophin deficient Mdx mice (Spurney et al. 2011). Losartan treatment on the mice induced significant decrease in fibrotic tissue development, along with small but significant decrease in cardiomyocyte cross-sectional area compared to untreated animals (Spurney et al. 2011). The studies introduced earlier Caddedu et al. (2010) and Dessi et al (2013), showed adjuvant treatment with epirubicin and telmisartan was effective at reduction of serum interleukin 6 (Pro-inflammatory) both acutely as well as in the long term (18-months) indictive of reduced dysfunction/inflamation (Cadeddu et al. 2010; Dessì et al. 2013).

In this current study, co-administration of losartan with crizotinib significantly improved cell viability (Figure 5.4.10), and decreased caspase 3 expression compared to treatment with crizotinib alone (Figure 5.4.13). Losartan co-administration with crizotinib appeared to attenuate the effects of crizotinib treatment alone. With regards cell viability, the current study shows consistency with a prior study crediting losartan with significantly improved cell viability when administered alone against Ang-II treatment alone (Xu et al. 2009). Neonate rat cardiomyocytes were supplemented with external Ang-II treatment with and without losartan. Losartan administration significantly improved MTT derived cell viability and decreased bax/bcl-2 ratio suggesting decreased apoptosis compared to myocytes not treated with losartan (Xu et al. 2009). In a study conducted to assess the ability of losartan to improve successful myoblast transplantation, losartan was associated with improved cell viability compared to the control adding credence to its protective capabilities (Fakhfakh et al. 2012). Losartan was

administered orally to transplanted animals. Losartan treatment on myoblasts reversed hydrogen peroxide induced apoptosis and necrosis (Fakhfakh et al. 2012). Losartan treatment induced significant reduction of apoptosis in primary cardiac myocytes induced by ang-II and significant reduction of overall cell death induced by hydrogen peroxide (apoptotic and necrotic) in skeletal muscle myoblasts respectively (Fakhfakh et al. 2012; Xu et al. 2009).

Losartan treatment was also associated with significant increased anti-apoptotic mediator bcl-2 and significant decrease in pro-apoptotic mediator bax against ang-II induced apoptosis in the study by Xu et al (2009) previously introduced (Xu et al. 2009). Similarly, ARB Telmisartan significantly attenuated cleaved caspase 3 activity induced by doxorubicin treatment in myocardium (Rashikh, Pillai, and Najmi 2014). Albino Wistar rats were treated with doxorubicin with and without telmisartan, and telmisartan treatment along with doxorubicin significantly decreased caspase-3 activity compared to doxorubicin treatment alone (Rashikh, Pillai, and Najmi 2014). These provide evidence supporting the results of this study attributing angiotensin receptor blockade on reduced observed cell death & apoptosis.

P-AKT is an important intracellular protein, regulates cell survival as p-AKT inhibits pro-apoptotic proteins which allows cells avoid apoptosis (Chiarle et al. 2008). In this present study, Losartan co-administration with crizotinib decreased p-AKT expression however, not significantly compared to isolated hearts treated with crizotinib alone. It did however decrease p-AKT expression significantly

compared to hearts treated with losartan alone and the basal control. In the study to evaluate ponatinib included cardiotoxicity, there was significant decrease in expression of p-AKT associated with ponatinib treatment in cardiomyocytes (Singh et al. 2019). In rats with myocardial infarction, losartan treatment significantly reversed the decreased expression of p-AKT induced by myocardial infarction (Wen et al. 2018). Male Sprague Dawley rats were subjected to left coronary artery ligation to simulate myocardial infarction and treatment commenced 48 hours post-surgery. Heart tissue was collected and analysed via western blotting. Myocardial infarction significantly decreased p-AKT expression compared to non-MI animals, myocardial infarcted animals treated with losartan showed significant restoration of p-AKT expression (Wen et al. 2018). Although, previous studies have shown losartan treatment increased expression of p-AKT following cardiac injury, in this present study losartan co-administration did not significantly increase p-AKT expression.

In this current study, losartan co-administration with crizotinib was credited with significant reduction in the mitochondrial superoxide generation and Ca^{2+} detection compared to cultures treated with crizotinib alone (Figures 5.4.14 and 5.4.15 respectively). This was consistent with the multi-parameter in vitro toxicity testing of tyrosine kinase inhibitors on human cardiomyocytes study by Doherty et al. (2013), crizotinib treatment induced increased cardiomyocyte superoxide (ROS) generation and blocked calcium (Ca^{2+}) ion uptake channels (Doherty et al. 2013). Cultured human cardiomyocytes cultured in media on culture plates and human induced pluripotent stem cell-derived cardiomyocytes were treated with

crizotinib. Dihydroethidium probing for intracellular superoxide and impedance recording xcelligence RTCA cardio instrument were employed to assess superoxide generation and calcium ion channel activity. Crizotinib treatment increased intracellular mitochondrial superoxide generation and inhibited Ca^{2+} channel (Doherty et al. 2013).

ROS have been considered by-products of mitochondrial metabolism which under normal conditions internal homeostasis would prevent excessive accumulation of ROS (Zorov, Juhaszova, and Sollott 2014). However certain therapeutic agents directly or indirectly promote ATP depletion leading mitochondria to take compensatory measures inducing oxidative stress promoting the accumulation of ROS (superoxide) and calcium overload (Li et al. 2013; Zoltán et al. 2015). Excessive ROS generation has been described as one of the key pathways involved in drug induced cardiotoxicity agents such as doxorubicin, sunitinib and sorafenib, all credit ROS generation as one of the major mechanisms in their cardiotoxic properties (Bouitbir et al. 2019; Chaar, Kamta, and Ait-Oudhia 2018; Deng et al. 2007; Ma et al. 2020; Zorov, Juhaszova, and Sollott 2014).

ARB losartan co-administration significantly decreased mitochondrial superoxide & calcium overload detected compared to treatment with crizotinib alone in this present study. This was consistent with findings in a number of prior literatures. Losartan treatment along with doxorubicin in male Wistar rats was effective at significantly increasing superoxide dismutase (SOD) against doxorubicin induced cardiotoxicity, and losartan combination with quercetin (flavonoid molecule)

yielded significant improvement versus losartan alone (Matouk et al. 2013). Based on the premise that increased SOD would correlate to increased catalysis of degradation of superoxide radicals to oxygen and hydrogen peroxide reducing the number of superoxide radicals present (Fukai and Ushio-Fukai 2011; Nojima et al. 2019). In the study by Rashikh, Pillai and Najmi (2014) introduced above, ARB telmisartan treatment significantly increased cardiac SOD activity in response to doxorubicin induced cardiotoxicity assessed in murine model which the researchers suggested would lead to facilitate metabolism of superoxide (ROS) (Rashikh, Pillai, and Najmi 2014).

Losartan treatment was also associated with prevention of myocardial atrophy and significantly prevented superoxide generation induced by doxorubicin treatment (Zhao et al. 2010). Male Nox2−/− and WT littermate mice were treated with doxorubicin for 3 weeks (1 injection a week) and analysed 8 weeks following initial injection and the losartan treated animals were administered losartan for 7 days. Ventricular cardiomyocytes were isolated from the wild type mice for cardiomyocyte studies. Losartan treatment decreased myocardial atrophy and reduced NADPH-dependent superoxide production; however, the decrease was not statistically significant (Zhao et al. 2010).

Adult male Sprague Dawley rats supplemented with tumour necrosis factor with or without losartan to observe the contribution of tumour necrosis factor interaction with angiotensin II resulting in cardiac damage and oxidative stress (Mariappan et al. 2012). Concomitant administration of tumour necrosis factor

and losartan proved effective at significant attenuation of increases in mitochondrial superoxide and hydrogen peroxide induced by TNF- induced mitochondrial dysfunction (Mariappan et al. 2012). Losartan treatment was also associated with upregulation of myocardial catalase activity to catalyse the decomposition of hydrogen peroxide compared to doxorubicin treatment alone suggesting reduction in oxidative stress induced by doxorubicin cardiotoxicity (Matouk et al. 2013). The studies introduced earlier Caddedu et al (2010) and Dessi et al (2013), ARB telmisartan was also credited with attenuation of epirubicin induced ROS generation in acute and long term epirubicin treatment (Cadeddu et al. 2010; Dessì et al. 2013).

With regards calcium overload, losartan treatment crucially restored Sarcoplasmic Ca^{2+} uptake pump protein preventing calcium overload and cardiomyocyte dysfunction (Babick et al. 2012). Sprague Dawley rats subjected to left anterior coronary artery occlusion to induce heart failure model, were treated with oral losartan for 8 weeks and losartan treatment was effective at reinstating calcium pump in the sarcoplasmic reticulum preventing calcium overload. Similarly, losartan treatment was effective at improving calcium overload in cardiac hypertrophy in a rat heart failure model (Loennechen Jan et al. 2002). Female Sprague Dawley rats subjected to left coronary artery ligation (to induce hypertrophy) and administered losartan orally for after 7 days. Losartan administration induced significant reduction in systolic and diastolic calcium overload (detection) as well as significant decrease in cytosolic Ca^{2+} compared to

ligated control animals (Loennechen Jan et al. 2002). Further providing credence to the cardioprotective properties of ARB blocking by losartan.

The data collected in this study shows consistency with past studies highlighting the benefits of concomitant administration of losartan as being beneficial during myocardial injury. Direct antagonism of AT1 receptor by losartan appears to promote a number of pathways protecting the myocardium (Figure 5.2.2) (Ferrario and Strawn 2006).

In conclusion, co-administration of losartan with crizotinib produced significant improvements in left ventricular developed pressure, reduced Infarct risk ratio (%) development, improved cell viability, decreased caspase 3 activity, and reduced expression of oxidative stress markers compared to crizotinib treatment alone.

Chapter 6: General conclusions

6.1 Summary of findings

This present study highlights crizotinib induced cardiotoxicity in naïve male Sprague Dawley rats using langendorff isolated heart perfusion model. The effects of crizotinib administration on haemodynamic performance and infarct development were considered. Left ventricular tissue was also evaluated for p-AKT expression in response to crizotinib induced cardiotoxicity. Following this, the ability of losartan and ramipril, which act on the renin angiotensin pathway (RAS), to attenuate some of the cardiotoxic properties induced by crizotinib treatment was then evaluated.

This study revealed that crizotinib treatment induced significant impairment in haemodynamic function, specifically with left ventricular developed pressure during the langendorff perfusion experiments. The impairment was particularly pronounced at the crizotinib concentration 1µM when compared to naïve hearts from control groups. In addition, crizotinib 1µM treated hearts displayed significant increase in infarct to risk ratio (%) developed versus hearts from control groups.

These results were similar to past studies involving other tyrosine kinase inhibitors. During the cardiac safety patient pool for lapatinib, the tyrosine kinase inhibitor was associated with declines in left ventricular ejection fraction (Perez et al. 2008). Similarly, Imatinib treatment in patients and mice was associated with left ventricular dysfunction (Kerkelä et al. 2006).

Crizotinib treatment also induced significant decrease in cell viability and increased expression of cleaved caspase-3, compared to the non-treated control group. This was consistent with the study conducted by Doherty et al. (2013), as crizotinib treatment on isolated human cardiac myocytes resulted in increased activation of caspase 3/7 and crizotinib treatment also induced cardiomyocyte death (Doherty et al. 2013). In a study to evaluate imatinib cardiotoxicity, imatinib treatment on C7BL6 mice was associated with early apoptosis and necrosis (Kerkelä et al. 2006). In the multiparameter study introduced early carried out by Doherty et al., nilotinib treatment also induced caspase 3 activation (Doherty et al. 2013).

Crizotinib treatment also induced increased mitochondrial superoxide generation and intracellular calcium levels compared to the non-treated control myoblasts. Disruption of intracellular calcium signalling, and mitochondrial superoxide generation contribute to cardiomyocyte and inherently cardiac dysfunction (Rodríguez-Hernández et al. 2020). Similar to this present study, imatinib treatment on isolated neonate ventricular myocytes resulted in significant Ca^{2+} transient peak amplitudes and significant phosphorylation of Ca^{2+} regulatory

proteins (Barr et al. 2014). In the multiparameter study introduced earlier, crizotinib and nilotinib treatment induced significant increase in cardiomyocyte superoxide generation with significant increases in reactive oxygen species detection (Doherty et al. 2013).

In summary, chapter 3 of this study shows that crizotinib induces significant cardiotoxic around the concentration 1µM in isolated rat heart and also similar indications were observed in cultured myoblast studies.

The protective properties of ramipril and losartan were assessed against crizotinib induced cardiotoxicity again in langendorff perfused isolated rat heart experiments and H9C2 cardiac myoblast models. Ramipril is an angiotensin converting enzyme inhibitor usually prescribed for the treatment of hypertensive symptoms (López-Sendón et al. 2004).

In this current study, ramipril treatment was successful at significantly improving left ventricular developed pressure performance induced by crizotinib cardiotoxicity as well as reduce infarct development in langendorff perfused rat hearts. These properties of ramipril were consistent with Rouleau Jean et al. (2001), where ramipril treatment on induced cardiac hypertrophy in rabbit model showed reduction in ventricular hypertrophy and maintained cardiac contractility (Rouleau Jean et al. 2001). Similarly, in a study involving induction of myocardial infarction model in female Wistar rats, ramipril treatment improved animal haemodynamic performance with improved systolic and diastolic pressures and ventricular systolic pressure compared to the non-ramipril treated animals (Wei

et al. 2016). Ramipril treatment also prevented morphological changes to the heart following myocardial infarction in male Wistar rats, limiting infarct length and size (Sandmann et al. 2006).

Ramipril co-administration also improved cell viability and significantly decreased superoxide generation and calcium detection. This was consistent with previous literature. Ramiprilat treatment on isolated guineapig hearts subjected to free radical damage (oxidative stress) resulted in reduced indicator of cardiomyocyte breakdown with reduced lactate dehydrogenase in cardiac effluent (Jin and Chen 2000). Ramipril treatment on male albino rats subjected to ischemia reperfusion significantly reduced thiobarbituric acid reactive substances produced by cardiomyocytes indicative of decreased cardiomyocyte damage (Sheik Uduman et al. 2016). Delapril treatment for 6 weeks on myocardial infarcted swiss mice induced significant attenuation of diastolic Ca^{2+} overload and improved contraction (Zalvidea et al. 2012).

Angiotensin receptor blocker losartan is regarded as an effective anti-hypertensive medication (Iwai and Horiuchi 2009). Losartan treatment improved decline in haemodynamic performance induced by crizotinib treatment. Losartan co-administration significantly improved left ventricular developed pressure and decreased infarct developed compared to hearts treated with crizotinib 1μM. This was similar to a study involving sorafenib treated Wistar rats. Losartan co-treated animals showed improved left ventricular developed pressure compared with animals treated with sorafenib alone (Abdelgalil et al. 2020). Losartan co-

administration on Wistar rats was also effective at reducing cardiomyocyte morphological changes and inflammation associated with cardiotoxic agent's doxorubicin and sorafenib (Matouk et al. 2013). Losartan co-treatment with doxorubicin in male albino rats reduced appearance of interstitial oedema, vacuole formation and myocardial degradation associated with doxorubicin treatment alone (Matouk et al. 2013).

Losartan co-administration with crizotinib significantly increased myoblast viability and decreased cleaved caspase-3 activity compared to crizotinib treatment alone. In animals subjected to myoblast transplantation, losartan treatment induced improved cardiomyocyte survival against hydrogen peroxide induced cell death (Fakhfakh et al. 2012). Losartan treatment attenuated angiotensin II induced apoptosis in Sprague Dawley rats, with significant reduction in cleaved caspase 3 expression and reduction in bax/bcl2 ratio compared non-losartan treated animals (Diep et al. 2002).

In this present study Losartan co-administration with crizotinib significantly decreased mitochondrial superoxide generation and calcium ion detection compared to treatment with crizotinib alone. This was consistent with a heart failure model on Sprague Dawley rats, treatment with losartan restored the function of sarcoplasmic Ca^{2+} uptake pump protein preventing calcium overload and further cardiomyocyte (Babick et al. 2012)(Babick et al. 2012). Similarly, in female Sprague Dawley rat heart failure model, oral administration of losartan significantly decreased cytosolic Ca^{2+} preventing overload (Loennechen Jan et al.

2002). Adult male Sprague Dawley rats were administered tumour necrosis factor with or without losartan to assess cardiac damage and oxidative stress induced by angiotensin II (Mariappan et al. 2012). Losartan administration with tumour necrosis factor attenuated mitochondrial superoxide generation and mitochondrial dysfunction (Mariappan et al. 2012).

6.2 Limitations and future prospects

6.2.1 The use of animal and cellular models

The use of animal and cell-based models present a challenge when attempting to extrapolate data from *in vitro* models to translate into human studies. Common issues such as interspecies differences and different pharmacokinetics between rodent species and humans present a challenge (Hartung 2008). A possible improvement would be to employ cardiac models more similar to human myocytes.

6.2.2 Cardiotoxicity induced by crizotinib treatment

The results of this study agree that crizotinib treatment induced cardiotoxic effects, however, the exact mechanisms or key mechanisms that fuel the toxicity remain. Further study would be important to shed more light in this study. It is still unclear if the extent of toxicity observed in the animal and cell models would be the same with more human models again due to species variability. For instance, crizotinib treatment in individuals was associated with QT prolongation

and bradycardia during clinical trials (Lamore et al. 2020). This would be more challenging to replicate in animal studies.

Similarly, with regards the adjunctive therapies it is difficult to predict the responses *in vivo* studies. The langendorff system is useful for isolating the whole heart model and limiting external influences. However, this may not be the case *in vivo* as the influence of other systems could play a part.

6.3 Conclusions

This study provides evidence for crizotinib induced cardiotoxicity in whole rat heart model and cardiac myoblast studies. Treatment with crizotinib (1µM), significantly impaired left ventricular developed pressure performance, increased infarct development. Crizotinib treatment also significantly, decreased cardiac myoblast viability, increased cleaved caspase-3 activity, mitochondrial superoxide generation and increased calcium detection. Angiotensin converting enzyme inhibitor ramipril and angiotensin receptor blocker losartan treatment abrogated features of crizotinib induced cardiotoxicity.

Word count – 52,000 words

References

Abdelgalil, A. A., Mohamed, O. Y., Ahamad, S. R., and Al-Jenoobi, F. I. (2020) 'The Protective Effect of Losartan Against Sorafenib Induced Cardiotoxicity: Ex-Vivo Isolated Heart and Metabolites Profiling Studies in Rat'. *European Journal of Pharmacology* 882, 173229

Acar, Z., Kale, A., Turgut, M., Demircan, S., Durna, K., Demir, S., Meriç, M., and Ağaç, M. T. (2011) 'Efficiency of Atorvastatin in the Protection of Anthracycline-Induced Cardiomyopathy'. *Journal of the American College of Cardiology* 58 (9), 988-989

Akershoek, J. J., Brouwer, K. M., Vlig, M., Boekema, B. K. H. L., Beelen, R. H. J., Middelkoop, E., and Ulrich, M. M. W. (2017) 'Differential Effects of Losartan and Atorvastatin in Partial and Full Thickness Burn Wounds'. *PloS One* 12 (6), e0179350

Akolkar, G., Bhullar, N., Bews, H., Shaikh, B., Premecz, S., Bordun, K. A., Cheung, D. Y., Goyal, V., Sharma, A. K., Garber, P., Singal, P. K., and Jassal, D. S. (2015) 'The Role of Renin Angiotensin System Antagonists in the Prevention of Doxorubicin and Trastuzumab Induced Cardiotoxicity'. *Cardiovascular Ultrasound* 13, 18-x

Albini, A., Pennesi, G., Donatelli, F., Cammarota, R., De Flora, S., and Noonan, D. M. (2010) 'Cardiotoxicity of Anticancer Drugs: The Need for Cardio-Oncology and Cardio-Oncological Prevention'. *JNCI: Journal of the National Cancer Institute* 102 (1), 14-25

Al-Khatib, S. M., LaPointe, N. M. A., Kramer, J. M., and Califf, R. M. (2003) 'What Clinicians should Know about the QT Interval'. *Jama* 289 (16), 2120-2127

Angsutararux, P., Luanpitpong, S., and Issaragrisil, S. (2015a) 'Chemotherapy-Induced Cardiotoxicity: Overview of the Roles of Oxidative Stress'. *Oxidative Medicine and Cellular Longevity* 2015, 795602

Angsutararux, P., Luanpitpong, S., and Issaragrisil, S. (2015b) 'Chemotherapy-Induced Cardiotoxicity: Overview of the Roles of Oxidative Stress'. *Oxidative Medicine and Cellular Longevity* 2015, 795602

Anju, N. (2013) 'B-Adrenergic Blockade for Anthracycline- and Trastuzumab-Induced Cardiotoxicity'. *Circulation: Heart Failure* 6 (3), 358-361

Armenian, S. H., Armstrong, G. T., Aune, G., Chow, E. J., Ehrhardt, M. J., Ky, B., Moslehi, J., Mulrooney, D. A., Nathan, P. C., Ryan, T. D., van der Pal, Helena J., van Dalen, E. C., and Kremer, L. C. M. (2018) 'Cardiovascular Disease in Survivors of Childhood Cancer: Insights into Epidemiology, Pathophysiology, and Prevention'. *Jco* 36 (21), 2135-2144

Aronow, W. S. (2016) 'Update of Treatment of Heart Failure with Reduction of Left Ventricular Ejection Fraction'. *Archives of Medical Sciences.Atherosclerotic Diseases* 1 (1), e106-e116

Ayoub, N. M., Al-Shami, K., Alqudah, M. A., and Mhaidat, N. M. (2017) 'Crizotinib, a MET Inhibitor, Inhibits Growth, Migration, and Invasion of Breast Cancer Cells in Vitro and Synergizes with Chemotherapeutic Agents'. *OncoTargets and Therapy* 10, 4869-4883

Babick, A., Chapman, D., Zieroth, S., Elimban, V., and Dhalla, N. S. (2012) 'Reversal of Subcellular Remodelling by Losartan in Heart Failure due to Myocardial Infarction'. *Journal of Cellular and Molecular Medicine* 16 (12), 2958-2967

Baines, C. P. (2009) 'The Mitochondrial Permeability Transition Pore and Ischemia-Reperfusion Injury'. *Basic Research in Cardiology* 104 (2), 181-188

Bang, Y. (2011) 'The Potential for Crizotinib in Non-Small Cell Lung Cancer: A Perspective Review'. *Therapeutic Advances in Medical Oncology* 3 (6), 279-291

Bansal, N., Adams, M. J., Ganatra, S., Colan, S. D., Aggarwal, S., Steiner, R., Amdani, S., Lipshultz, E. R., and Lipshultz, S. E. (2019) 'Strategies to Prevent Anthracycline-Induced Cardiotoxicity in Cancer Survivors'. *Cardio-Oncology* 5 (1), 18

Bansal, N., Amdani, S., Lipshultz, E. R., and Lipshultz, S. E. (2017) 'Chemotherapy-Induced Cardiotoxicity in Children'. *Null* 13 (8), 817-832

Barr, L. A., Makarewich, C. A., Berretta, R. M., Gao, H., Troupes, C. D., Woitek, F., Recchia, F., Kubo, H., Force, T., and Houser, S. R. (2014) 'Imatinib Activates Pathological Hypertrophy by Altering Myocyte Calcium Regulation'. *Clinical and Translational Science* 7 (5), 360-367

Bello, C. L., Mulay, M., Huang, X., Patyna, S., Dinolfo, M., Levine, S., Van Vugt, A., Toh, M., Baum, C., and Rosen, L. (2009) 'Electrocardiographic Characterization of the QTc Interval in Patients with Advanced Solid Tumors: Pharmacokinetic-Pharmacodynamic Evaluation of Sunitinib'. *Clinical Cancer Research : An Official Journal of the American Association for Cancer Research* 15 (22), 7045-7052

Bertero, E. and Maack, C. (2018) 'Calcium Signaling and Reactive Oxygen Species in Mitochondria'. *Circulation Research* 122 (10), 1460-1478

Bertero, E., Ameri, P., and Maack, C. (2019) 'Bidirectional Relationship between Cancer and Heart Failure: Old and New Issues in Cardio-Oncology'. *Cardiac Failure Review* 5 (2), 106-111

Blackhall, F., Ross Camidge, D., Shaw, A. T., Soria, J., Solomon, B. J., Mok, T., Hirsh, V., Jänne, P. A., Shi, Y., Yang, P., De Pas, T., Hida, T., De Carpeño, J. C., Lanzalone, S., Polli, A., Iyer, S., Reisman, A., Wilner, K. D., and Kim, D. (2017a) 'Final Results of the Large-Scale Multinational Trial PROFILE 1005: Efficacy and Safety of Crizotinib in Previously Treated Patients with Advanced/Metastatic ALK-Positive Non-Small-Cell Lung Cancer'. *ESMO Open* 2 (3)

Blackhall, F., Ross Camidge, D., Shaw, A. T., Soria, J., Solomon, B. J., Mok, T., Hirsh, V., Jänne, P. A., Shi, Y., Yang, P., De Pas, T., Hida, T., De Carpeño, J. C., Lanzalone, S., Polli, A., Iyer, S., Reisman, A., Wilner, K. D., and Kim, D. (2017b) 'Final Results of the Large-Scale Multinational Trial PROFILE 1005: Efficacy and Safety of Crizotinib in Previously Treated Patients with Advanced/Metastatic ALK-Positive Non-Small-Cell Lung Cancer'. *ESMO Open* 2 (3)

Blaes, A., Duprez, D., Defor, T., Shanley, R., Beckwith, H., Haddad, T., Potter, D., Yee, D., Sanghavi, K., and Jacobson, P. (2015) 'Angiotensin Converting Enzyme Inhibitors (ACEI) and Doxorubicin Pharmacokinetics in Women Receiving Adjuvant Breast Cancer Treatment'. *SpringerPlus* 4, 32

Bloom, M. W., Hamo, C. E., Cardinale, D., Ky, B., Nohria, A., Baer, L., Skopicki, H., Lenihan, D. J., Gheorghiade, M., Lyon, A. R., and Butler, J. (2016) 'Cancer Therapy-Related Cardiac Dysfunction and Heart Failure: Part 1: Definitions, Pathophysiology, Risk Factors, and Imaging'. *Circulation.Heart Failure* 9 (1), e002661

Bouitbir, J., Alshaikhali, A., Panajatovic, M. V., Abegg, V. F., Paech, F., and Krähenbühl, S. (2019a) 'Mitochondrial Oxidative Stress Plays a Critical Role in the Cardiotoxicity of Sunitinib: Running Title: Sunitinib and Oxidative Stress in Hearts'. *Toxicology* 426, 152281

Bouitbir, J., Alshaikhali, A., Panajatovic, M. V., Abegg, V. F., Paech, F., and Krähenbühl, S. (2019b) 'Mitochondrial Oxidative Stress Plays a Critical Role in the Cardiotoxicity of Sunitinib: Running Title: Sunitinib and Oxidative Stress in Hearts'. *Toxicology* 426, 152281

Bou-Teen, D., Kaludercic, N., Weissman, D., Turan, B., Maack, C., Di Lisa, F., and Ruiz-Meana, M. (2021) 'Mitochondrial ROS and Mitochondria-Targeted Antioxidants in the Aged Heart'. *Free Radical Biology and Medicine* 167, 109-124

Bovelli, D., Plataniotis, G., Roila, F., and ESMO Guidelines Working Group (2010) 'Cardiotoxicity of Chemotherapeutic Agents and Radiotherapy-Related Heart Disease: ESMO Clinical Practice Guidelines'. *Annals of Oncology : Official Journal of the European Society for Medical Oncology* 21 Suppl 5, 277

Bowles, E. J., Wellman, R., Feigelson, H. S., Onitilo, A. A., Freedman, A. N., Delate, T., Allen, L. A., Nekhlyudov, L., Goddard, K. A., Davis, R. L., Habel, L. A., Yood, M. U., McCarty, C., Magid, D. J., Wagner, E. H., and Pharmacovigilance Study Team (2012) 'Risk of Heart Failure in Breast Cancer Patients After Anthracycline and Trastuzumab Treatment: A Retrospective Cohort Study'. *Journal of the National Cancer Institute* 104 (17), 1293-1305

Brave, M., Goodman, V., Kaminskas, E., Farrell, A., Timmer, W., Pope, S., Harapanhalli, R., Saber, H., Morse, D., Bullock, J., Men, A., Noory, C., Ramchandani, R., Kenna, L., Booth, B., Gobburu, J., Jiang, X., Sridhara, R., Justice, R., and Pazdur, R. (2008) 'Sprycel for Chronic Myeloid Leukemia and Philadelphia Chromosome–Positive Acute Lymphoblastic Leukemia Resistant to Or Intolerant of Imatinib Mesylate'. *Clinical Cancer Research* 14 (2), 352-359

Bray, F., Ferlay, J., Soerjomataram, I., Siegel, R. L., Torre, L. A., and Jemal, A. (2018a) 'Global Cancer Statistics 2018: GLOBOCAN Estimates of Incidence and Mortality Worldwide for 36 Cancers in 185 Countries'. *CA: A Cancer Journal for Clinicians* 68 (6), 394-424

Bray, F., Ferlay, J., Soerjomataram, I., Siegel, R. L., Torre, L. A., and Jemal, A. (2018b) 'Global Cancer Statistics 2018: GLOBOCAN Estimates of Incidence and Mortality Worldwide for 36 Cancers in 185 Countries'. *CA: A Cancer Journal for Clinicians* 68 (6), 394-424

Brentnall, M., Rodriguez-Menocal, L., De Guevara, R. L., Cepero, E., and Boise, L. H. (2013) 'Caspase-9, Caspase-3 and Caspase-7 have Distinct Roles during Intrinsic Apoptosis'. *BMC Cell Biology* 14 (1), 32

Bröker, L. E., Kruyt, F. A. E., and Giaccone, G. (2005) 'Cell Death Independent of Caspases: A Review'. *Clin Cancer Res* 11 (9), 3155

Brookes, P. S., Yoon, Y., Robotham, J. L., Anders, M. W., and Shey-Shing Sheu (2004) 'Calcium, ATP, and ROS: A Mitochondrial Love-Hate Triangle'. *American Journal of Physiology-Cell Physiology* 287 (4), C817-C833

Brown, H. D. and Hahn, R. C. (2018) 'WHO Cancer 2018'. *Cancer*

Burke, M. J., Walmsley, R., Munsey, T. S., and Smith, A. J. (2019) 'Receptor Tyrosine Kinase Inhibitors Cause Dysfunction in Adult Rat Cardiac Fibroblasts in Vitro'. *Toxicology in Vitro* 58, 178-186

Burks, T. N., Andres-Mateos, E., Marx, R., Mejias, R., Van Erp, C., Simmers, J. L., Walston, J. D., Ward, C. W., and Cohn, R. D. (2011) 'Losartan Restores Skeletal Muscle Remodeling and Protects Against Disuse Atrophy in Sarcopenia'. *Science Translational Medicine* 3 (82), 82ra37

Burton, G. J. and Jauniaux, E. (2011) 'Oxidative Stress'. *Best Practice & Research Clinical Obstetrics & Gynaecology* 25 (3), 287-299

Cadeddu, C., Piras, A., Mantovani, G., Deidda, M., Dessì, M., Madeddu, C., Massa, E., and Mercuro, G. (2010a) 'Protective Effects of the Angiotensin II Receptor Blocker Telmisartan on Epirubicin-Induced Inflammation, Oxidative Stress, and Early Ventricular Impairment'. *American Heart Journal* 160 (3), 487.e1-487.e7

Cadeddu, C., Piras, A., Mantovani, G., Deidda, M., Dessì, M., Madeddu, C., Massa, E., and Mercuro, G. (2010b) 'Protective Effects of the Angiotensin II Receptor Blocker Telmisartan on Epirubicin-Induced Inflammation, Oxidative Stress, and Early Ventricular Impairment'. *American Heart Journal* 160 (3), 487.e1-487.e7

Cardinale, D., Colombo, A., Sandri, M. T., Lamantia, G., Colombo, N., Civelli, M., Martinelli, G., Veglia, F., Fiorentini, C., and Cipolla, C. M. (2006) 'Prevention of High-Dose Chemotherapy-Induced Cardiotoxicity in High-Risk Patients by Angiotensin-Converting Enzyme Inhibition'. *Circulation* 114 (23), 2474-2481

Chaar, M., Kamta, J., and Ait-Oudhia, S. (2018a) 'Mechanisms, Monitoring, and Management of Tyrosine Kinase Inhibitors-Associated Cardiovascular Toxicities'. *OncoTargets and Therapy* 11, 6227-6237

Chaar, M., Kamta, J., and Ait-Oudhia, S. (2018b) 'Mechanisms, Monitoring, and Management of Tyrosine Kinase Inhibitors-Associated Cardiovascular Toxicities'. *OncoTargets and Therapy* 11, 6227-6237

Chambers, T. P., Santiesteban, L., Gomez, D., and Chambers, J. W. (2017) 'Sab Mediates Mitochondrial Dysfunction Involved in Imatinib Mesylate-Induced Cardiotoxicity'. *Toxicology* 382, 24-35

Chatterjee, K., Zhang, J., Honbo, N., and Karliner, J. S. (2010a) 'Doxorubicin Cardiomyopathy'. *Cardiology* 115 (2), 155-162

Chatterjee, K., Zhang, J., Honbo, N., and Karliner, J. S. (2010b) 'Doxorubicin Cardiomyopathy'. *Cardiology* 115 (2), 155-162

Chen, D., yu, J., and Zhang, L. (2016) 'Necroptosis: An Alternative Cell Death Program Defending Against Cancer'. *Biochimica Et Biophysica Acta (BBA) - Reviews on Cancer* 1865

Chen, G., Chen, X., Zhang, Y., Yan, F., Fang, W., Yang, Y., Hong, S., Miao, S., Wu, M., Huang, X., Luo, Y., Zhou, C., Gong, R., Huang, Y., Zhou, N., Zhao, H., and Zhang, L. (2017) 'A Large, Single-center, Real-world Study of Clinicopathological Characteristics and Treatment in Advanced ALK-positive Non-small-cell Lung Cancer'. *Cancer Medicine (Malden, MA)* 6 (5), 953-961

Chen, J., Long, J. B., Hurria, A., Owusu, C., Steingart, R. M., and Gross, C. P. (2012) 'Incidence of Heart Failure Or Cardiomyopathy After Adjuvant Trastuzumab Therapy for Breast Cancer'. *Journal of the American College of Cardiology* 60 (24), 2504-2512

Chen, M. H., Kerkelä Risto, and Thomas, F. (2008) 'Mechanisms of Cardiac Dysfunction Associated with Tyrosine Kinase Inhibitor Cancer Therapeutics'. *Circulation* 118 (1), 84-95

Chiarle, R., Voena, C., Ambrogio, C., Piva, R., and Inghirami, G. (2008) 'The Anaplastic Lymphoma Kinase in the Pathogenesis of Cancer [J]' 8, 11-23

Chiong, M., Wang, Z. V., Pedrozo, Z., Cao, D. J., Troncoso, R., Ibacache, M., Criollo, A., Nemchenko, A., Hill, J. A., and Lavandero, S. (2011) 'Cardiomyocyte Death: Mechanisms and Translational Implications'. *Cell Death & Disease* 2 (12), e244

Chiou, J., Tai, C., Wang, Y., Liu, T., Jen, Y., and Shiau, C. (2009) 'Sorafenib Induces Preferential Apoptotic Killing of a Drug- and Radio-Resistant Hep G2 Cells through a Mitochondria-Dependent Oxidative Stress Mechanism'. *Null* 8 (20), 1904-1913

Chu, T. F., Rupnick, M. A., Kerkela, R., Dallabrida, S. M., Zurakowski, D., Nguyen, L., Woulfe, K., Pravda, E., Cassiola, F., Desai, J., George, S., Morgan, J. A., Harris, D. M., Ismail, N. S.,

Chen, J., Schoen, F. J., Van den Abbeele, Annick D., Demetri, G. D., Force, T., and Chen, M. H. (2007) 'Cardiotoxicity Associated with Tyrosine Kinase Inhibitor Sunitinib'. *Lancet (London, England)* 370 (9604), 2011-2019

Codony-Servat, J., Albanell, J., Lopez-Talavera, J., Arribas, J., and Baselga, J. (1999) 'Cleavage of the HER2 Ectodomain is a Pervanadate-Activable Process that is Inhibited by the Tissue Inhibitor of Metalloproteases-1 in Breast Cancer Cells'. *Cancer Res* 59 (6), 1196

Coriat, R., Nicco, C., Chéreau, C., Mir, O., Alexandre, J., Ropert, S., Weill, B., Chaussade, S., Goldwasser, F., and Batteux, F. (2012) 'Sorafenib-Induced Hepatocellular Carcinoma Cell Death Depends on Reactive Oxygen Species Production in Vitro and in Vivo'. *Molecular Cancer Therapeutics* 11 (10), 2284-2293

Costa, D. B., Shaw, A. T., Ou, S. I., Solomon, B. J., Riely, G. J., Ahn, M., Zhou, C., Shreeve, S. M., Selaru, P., Polli, A., Schnell, P., Wilner, K. D., Wiltshire, R., Camidge, D. R., and Crinò, L. (2015) 'Clinical Experience with Crizotinib in Patients with Advanced ALK-Rearranged Non–Small-Cell Lung Cancer and Brain Metastases'. *Jco* 33 (17), 1881-1888

Crinò, L., Kim, D., Riely, G. J., Janne, P. A., Blackhall, F. H., Camidge, D. R., Hirsh, V., Mok, T., Solomon, B. J., Park, K., Gadgeel, S. M., Martins, R., Han, J., De Pas, T. M., Bottomley, A., Polli, A., Petersen, J., Tassell, V. R., and Shaw, A. T. (2011) 'Initial Phase II Results with Crizotinib in Advanced ALK-Positive Non-Small Cell Lung Cancer (NSCLC): PROFILE 1005'. *Jco* 29 (15), 7514

Cross, M. J., Berridge, B. R., Clements, P. J. M., Cove-Smith, L., Force, T. L., Hoffmann, P., Holbrook, M., Lyon, A. R., Mellor, H. R., Norris, A. A., Pirmohamed, M., Tugwood, J. D., Sidaway, J. E., and Park, B. K. (2015) 'Physiological, Pharmacological and Toxicological Considerations of Drug-Induced Structural Cardiac Injury'. *British Journal of Pharmacology* 172 (4), 957-974

Crow Michael, T., Kartik, M., Nam Young-Jae, and Kitsis Richard, N. (2004) 'The Mitochondrial Death Pathway and Cardiac Myocyte Apoptosis'. *Circulation Research* 95 (10), 957-970

Cruz, M., Duarte-Rodrigues, J., and Campelo, M. (2016) 'Cardiotoxicidade Na Terapêutica Com Antraciclinas: Estratégias De Prevenção'. *Revista Portuguesa De Cardiologia* 35 (6), 359-371

Csapo, M. and Lazar, L. (2014a) 'Chemotherapy-Induced Cardiotoxicity: Pathophysiology and Prevention'. *Clujul Medical (1957)* 87 (3), 135-142

Csapo, M. and Lazar, L. (2014b) 'Chemotherapy-Induced Cardiotoxicity: Pathophysiology and Prevention'. *Clujul Medical (1957)* 87 (3), 135-142

Cui, J. J., Tran-Dubé, M., Shen, H., Nambu, M., Kung, P. P., Pairish, M., Jia, L., Meng, J., Funk, L., Botrous, I., McTigue, M., Grodsky, N., Ryan, K., Padrique, E., Alton, G., Timofeevski, S., Yamazaki, S., Li, Q., Zou, H., Christensen, J., Mroczkowski, B., Bender, S., Kania, R. S.,

and Edwards, M. P. (2011) 'Structure Based Drug Design of Crizotinib (PF-02341066), a Potent and Selective Dual Inhibitor of Mesenchymal-Epithelial Transition Factor (C-MET) Kinase and Anaplastic Lymphoma Kinase (ALK)'. *Journal of Medicinal Chemistry* 54 (18), 6342-6363

Curigliano, G., Lenihan, D., Fradley, M., Ganatra, S., Barac, A., Blaes, A., Herrmann, J., Porter, C., Lyon, A. R., Lancellotti, P., Patel, A., DeCara, J., Mitchell, J., Harrison, E., Moslehi, J., Witteles, R., Calabro, M. G., Orecchia, R., de Azambuja, E., Zamorano, J. L., Krone, R., Iakobishvili, Z., Carver, J., Armenian, S., Ky, B., Cardinale, D., Cipolla, C. M., Dent, S., Jordan, K., and ESMO Guidelines Committee. Electronic address: clinicalguidelines@esmo.org (2020) 'Management of Cardiac Disease in Cancer Patients Throughout Oncological Treatment: ESMO Consensus Recommendations'. *Annals of Oncology : Official Journal of the European Society for Medical Oncology* 31 (2), 171-190

Curigliano, G., Cardinale, D., Dent, S., Criscitiello, C., Aseyev, O., Lenihan, D., and Cipolla, C. M. (2016a) 'Cardiotoxicity of Anticancer Treatments: Epidemiology, Detection, and Management'. *CA: A Cancer Journal for Clinicians* 66 (4), 309-325

Curigliano, G., Cardinale, D., Dent, S., Criscitiello, C., Aseyev, O., Lenihan, D., and Cipolla, C. M. (2016b) 'Cardiotoxicity of Anticancer Treatments: Epidemiology, Detection, and Management'. *CA: A Cancer Journal for Clinicians* 66 (4), 309-325

D. Lekes, I. SZADVARI, O. KRIZANOVA, K. LOPUSNA, I. REZUCHOVA, M. NOVAKOVA, Z. NOVAKOVA, T. PARAK, and P. BABULA (2016) 'Nilotinib Induces ER Stress and Cell Death in H9c2 Cells'. *Physiological Research* 65 (Suppl. 4), S505-S514

Dan Dunn, J., Alvarez, L. A., Zhang, X., and Soldati, T. (2015) 'Reactive Oxygen Species and Mitochondria: A Nexus of Cellular Homeostasis'. *Redox Biology* 6, 472-485

Daniela, C., Alessandro, C., Sandri Maria, T., Giuseppina, L., Nicola, C., Maurizio, C., Giovanni, M., Fabrizio, V., Cesare, F., and Cipolla Carlo, M. (2006) 'Prevention of High-Dose Chemotherapy–Induced Cardiotoxicity in High-Risk Patients by Angiotensin-Converting Enzyme Inhibition'. *Circulation* 114 (23), 2474-2481

de Groot, P.,M., Wu, C. C., Carter, B. W., and Munden, R. F. (2018) 'The Epidemiology of Lung Cancer'. *Translational Lung Cancer Research* 7 (3), 220-233

Della Corte, C. M., Viscardi, G., Di Liello, R., Fasano, M., Martinelli, E., Troiani, T., Ciardiello, F., and Morgillo, F. (2018) 'Role and Targeting of Anaplastic Lymphoma Kinase in Cancer'. *Molecular Cancer* 17 (1), 30

Deng, S., Kruger, A., Kleschyov, A. L., Kalinowski, L., Daiber, A., and Wojnowski, L. (2007) 'Gp91phox-Containing NAD(P)H Oxidase Increases Superoxide Formation by Doxorubicin and NADPH'. *Free Radical Biology and Medicine* 42 (4), 466-473

Dent, S., Liu, P., Brezden-Masley, C., and Lenihan, D. (2015) 'Cancer and Cardiovascular Disease: The Complex Labyrinth'. *Journal of Oncology* 2015, 516450

Deres, P., Halmosi, R., Toth, A., Kovacs, K., Palfi, A., Habon, T., Czopf, L., Kalai, T., Hideg, K., Sumegi, B., and Toth, K. (2005) 'Prevention of Doxorubicin-Induced Acute Cardiotoxicity by an Experimental Antioxidant Compound'. *Journal of Cardiovascular Pharmacology* 45 (1), 36-43

Desai, V. G., Herman, E. H., Moland, C. L., Branham, W. S., Lewis, S. M., Davis, K. J., George, N. I., Lee, T., Kerr, S., and Fuscoe, J. C. (2013) 'Development of Doxorubicin-Induced Chronic Cardiotoxicity in the B6C3F1 Mouse Model'. *Toxicology and Applied Pharmacology* 266 (1), 109-121

Dessì, M., Piras, A., Madeddu, C., Cadeddu, C., Deidda, M., Massa, E., Antoni, G., Mantovani, G., and Mercuro, G. (2011) 'Long-Term Protective Effects of the Angiotensin Receptor Blocker Telmisartan on Epirubicin-Induced Inflammation, Oxidative Stress and Myocardial Dysfunction'. *Experimental and Therapeutic Medicine* 2 (5), 1003-1009

Dessì, M., Madeddu, C., Piras, A., Cadeddu, C., Antoni, G., Mercuro, G., and Mantovani, G. (2013) 'Long-Term, Up to 18 Months, Protective Effects of the Angiotensin II Receptor Blocker Telmisartan on Epirubin-Induced Inflammation and Oxidative Stress Assessed by Serial Strain Rate'. *SpringerPlus* 2 (1), 198

Dhalla, N. S., Elmoselhi, A. B., Hata, T., and Makino, N. (2000) 'Status of Myocardial Antioxidants in Ischemia-Reperfusion Injury'. *Cardiovascular Research* 47 (3), 446-456

Diep, Q. N., Mabrouk, M. E., Yue, P., and Schiffrin, E. L. (2002) 'Effect of AT_1 Receptor Blockade on Cardiac Apoptosis in Angiotensin II-Induced Hypertension'. *American Journal of Physiology-Heart and Circulatory Physiology* 282 (5), H1635-H1641

Díez, J. (2006) 'Review of the Molecular Pharmacology of Losartan and its Possible Relevance to Stroke Prevention in Patients with Hypertension'. *Clinical Therapeutics* 28 (6), 832-848

Dl, L., H, C., and Lx, Y. (2014) 'Cardiotoxicity of Molecular-Targeted Drug Therapy.'. *Anticancer Research* 34 (7), 3243-3249

Doebele, R. C., Pilling, A. B., Aisner, D. L., Kutateladze, T. G., Le, A. T., Weickhardt, A. J., Kondo, K. L., Linderman, D. J., Heasley, L. E., Franklin, W. A., Varella-Garcia, M., and Camidge, D. R. (2012) 'Mechanisms of Resistance to Crizotinib in Patients with ALK Gene Rearranged Non–Small Cell Lung Cancer'. *Clinical Cancer Research* 18 (5), 1472-1482

Doherty, K. R., Talbert, D. R., Trusk, P. B., Moran, D. M., Shell, S. A., and Bacus, S. (2015) 'Structural and Functional Screening in Human Induced-Pluripotent Stem Cell-Derived Cardiomyocytes Accurately Identifies Cardiotoxicity of Multiple Drug Types'. *Toxicology and Applied Pharmacology* 285 (1), 51-60

Doherty, K. R., Wappel, R. L., Talbert, D. R., Trusk, P. B., Moran, D. M., Kramer, J. W., Brown, A. M., Shell, S. A., and Bacus, S. (2013) 'Multi-Parameter in Vitro Toxicity Testing of

Crizotinib, Sunitinib, Erlotinib, and Nilotinib in Human Cardiomyocytes'. *Toxicology and Applied Pharmacology* 272 (1), 245-255

Drew Barbara, J., Ackerman Michael, J., Marjorie, F., Brian, G. W., Paul, K., Venu, M., Philippides George, J., Roden Dan, M., and Wojciech, Z. (2010) 'Prevention of Torsade De Pointes in Hospital Settings'. *Circulation* 121 (8), 1047-1060

Dumoulin, M. J., Adam, A., Burnett, J., Heublein, D., Yamaguchi, N., and Lamontagne, D. (2005) 'The Cardioprotective Effect of Dual Metallopeptidase Inhibition: Respective Roles of Endogenous Kinins and Natriuretic Peptides'. *Canadian Journal of Physiology and Pharmacology* 83 (2), 166-173

Duprez, L., Vanlangenakker, N., Festjens, N., Herreweghe, F., Vanden Berghe, T., and Vandenabeele, P. (2009) 'Necrosis: Molecular Mechanisms and Physiological Roles'. in . ed. by Anon, 599-633

Dzau Victor, J. (2001) 'Tissue Angiotensin and Pathobiology of Vascular Disease'. *Hypertension* 37 (4), 1047-1052

Edoardo, B. and Christoph, M. (2018) 'Calcium Signaling and Reactive Oxygen Species in Mitochondria'. *Circulation Research* 122 (10), 1460-1478

Eiki, T. and Kass David, A. (2007) 'Role of Oxidative Stress in Cardiac Hypertrophy and Remodeling'. *Hypertension* 49 (2), 241-248

Fakhfakh, R., Lamarre, Y., Skuk, D., and Tremblay, J. P. (2012) 'Losartan Enhances the Success of Myoblast Transplantation'. *Cell Transplant* 21 (1), 139-152

Ferlay, J., Soerjomataram, I., Dikshit, R., Eser, S., Mathers, C., Rebelo, M., Parkin, D. M., Forman, D., and Bray, F. (2015) 'Cancer Incidence and Mortality Worldwide: Sources, Methods and Major Patterns in GLOBOCAN 2012'. *International Journal of Cancer* 136 (5), E359-E386

Ferrario, C. M. and Strawn, W. B. (2006) 'Role of the Renin-Angiotensin-Aldosterone System and Proinflammatory Mediators in Cardiovascular Disease'. *The American Journal of Cardiology* 98 (1), 121-128

Force, T., Krause, D. S., and Van Etten, R. A. (2007) 'Molecular Mechanisms of Cardiotoxicity of Tyrosine Kinase Inhibition'. *Nature Reviews.Cancer* 7 (5), 332-344

Förstermann, U. and Sessa, W. C. (2012) 'Nitric Oxide Synthases: Regulation and Function'. *European Heart Journal* 33 (7), 829-837d

Franke, T. F., Hornik, C. P., Segev, L., Shostak, G. A., and Sugimoto, C. (2003) 'PI3K/Akt and Apoptosis: Size Matters'. *Oncogene* 22 (56), 8983-8998

Freudenheim, J. L., Ritz, J., Smith-Warner, S. A., Albanes, D., Bandera, E. V., van den Brandt, P. A., Colditz, G., Feskanich, D., Goldbohm, R. A., Harnack, L., Miller, A. B., Rimm, E., Rohan, T. E., Sellers, T. A., Virtamo, J., Willett, W. C., and Hunter, D. J. (2005) 'Alcohol

Consumption and Risk of Lung Cancer: A Pooled Analysis of Cohort Studies'. *The American Journal of Clinical Nutrition* 82 (3), 657-667

Fukai, T. (2011) *Superoxide Dismutases: Role in Redox Signaling, Vascular Function, and Diseases* [online]

Fukai, T. and Ushio-Fukai, M. (2011) 'Superoxide Dismutases: Role in Redox Signaling, Vascular Function, and Diseases'. *Antioxidants & Redox Signaling* 15 (6), 1583-1606

Fulda, S. and Debatin, K. (2006) 'Extrinsic Versus Intrinsic Apoptosis Pathways in Anticancer Chemotherapy'. *Oncogene* 25 (34), 4798-4811

Galkin, A. V., Melnick, J. S., Kim, S., Hood, T. L., Li, N., Li, L., Xia, G., Steensma, R., Chopiuk, G., Jiang, J., Wan, Y., Ding, P., Liu, Y., Sun, F., Schultz, P. G., Gray, N. S., and Warmuth, M. (2007) 'Identification of NVP-TAE684, a Potent, Selective, and Efficacious Inhibitor of NPM-ALK'. *Proceedings of the National Academy of Sciences* 104 (1), 270-275

Galluzzi, L., Vitale, I., Aaronson, S. A., Abrams, J. M., Adam, D., Agostinis, P., Alnemri, E. S., Altucci, L., Amelio, I., Andrews, D. W., Annicchiarico-Petruzzelli, M., Antonov, A. V., Arama, E., Baehrecke, E. H., Barlev, N. A., Bazan, N. G., Bernassola, F., Bertrand, M. J. M., Bianchi, K., Blagosklonny, M. V., Blomgren, K., Borner, C., Boya, P., Brenner, C., Campanella, M., Candi, E., Carmona-Gutierrez, D., Cecconi, F., Chan, F. K. -., Chandel, N. S., Cheng, E. H., Chipuk, J. E., Cidlowski, J. A., Ciechanover, A., Cohen, G. M., Conrad, M., Cubillos-Ruiz, J., Czabotar, P. E., D'Angiolella, V., Dawson, T. M., Dawson, V. L., De Laurenzi, V., De Maria, R., Debatin, K., DeBerardinis, R. J., Deshmukh, M., Di Daniele, N., Di Virgilio, F., Dixit, V. M., Dixon, S. J., Duckett, C. S., Dynlacht, B. D., El-Deiry, W., Elrod, J. W., Fimia, G. M., Fulda, S., García-Sáez, A. J., Garg, A. D., Garrido, C., Gavathiotis, E., Golstein, P., Gottlieb, E., Green, D. R., Greene, L. A., Gronemeyer, H., Gross, A., Hajnoczky, G., Hardwick, J. M., Harris, I. S., Hengartner, M. O., Hetz, C., Ichijo, H., Jäättelä, M., Joseph, B., Jost, P. J., Juin, P. P., Kaiser, W. J., Karin, M., Kaufmann, T., Kepp, O., Kimchi, A., Kitsis, R. N., Klionsky, D. J., Knight, R. A., Kumar, S., Lee, S. W., Lemasters, J. J., Levine, B., Linkermann, A., Lipton, S. A., Lockshin, R. A., López-Otín, C., Lowe, S. W., Luedde, T., Lugli, E., MacFarlane, M., Madeo, F., Malewicz, M., Malorni, W., Manic, G., Marine, J., Martin, S. J., Martinou, J., Medema, J. P., Mehlen, P., Meier, P., Melino, S., Miao, E. A., Molkentin, J. D., Moll, U. M., Muñoz-Pinedo, C., Nagata, S., Nuñez, G., Oberst, A., Oren, M., Overholtzer, M., Pagano, M., Panaretakis, T., Pasparakis, M., Penninger, J. M., Pereira, D. M., Pervaiz, S., Peter, M. E., Piacentini, M., Pinton, P., Prehn, J. H. M., Puthalakath, H., Rabinovich, G. A., Rehm, M., Rizzuto, R., Rodrigues, C. M. P., Rubinsztein, D. C., Rudel, T., Ryan, K. M., Sayan, E., Scorrano, L., Shao, F., Shi, Y., Silke, J., Simon, H., Sistigu, A., Stockwell, B. R., Strasser, A., Szabadkai, G., Tait, S. W. G., Tang, D., Tavernarakis, N., Thorburn, A., Tsujimoto, Y., Turk, B., Vanden Berghe, T., Vandenabeele, P., Vander Heiden, M. G., Villunger, A., Virgin, H. W., Vousden, K. H., Vucic, D., Wagner, E. F., Walczak, H., Wallach, D., Wang, Y., Wells, J. A., Wood, W., Yuan, J., Zakeri, Z., Zhivotovsky, B., Zitvogel, L., Melino, G., and Kroemer, G. (2018) 'Molecular Mechanisms of Cell Death: Recommendations of the Nomenclature Committee on Cell Death 2018'. *Cell Death & Differentiation* 25 (3), 486-541

Gharanei, M., Hussain, A., Janneh, O., and Maddock, H. L. (2013) 'Doxorubicin Induced Myocardial Injury is Exacerbated Following Ischaemic Stress Via Opening of the

Mitochondrial Permeability Transition Pore'. *Toxicology and Applied Pharmacology* 268 (2), 149-156

Ghazi-Khansari, M. and Mohammadi-Bardbori, A. (2007) 'Captopril Ameliorates Toxicity Induced by Paraquat in Mitochondria Isolated from the Rat Liver'. *Toxicology in Vitro* 21 (3), 403-407

Giorgi, C., Romagnoli, A., Pinton, P., and Rizzuto, R. (2008) 'Ca2+ Signaling, Mitochondria and Cell Death'. *Current Molecular Medicine* 8 (2), 119-130

Giorgi, C., Baldassari, F., Bononi, A., Bonora, M., De Marchi, E., Marchi, S., Missiroli, S., Patergnani, S., Rimessi, A., Suski, J. M., Wieckowski, M. R., and Pinton, P. (2012) 'Mitochondrial Ca2+ and Apoptosis'. *Cell Calcium* 52 (1), 36-43

González Arantxa, López Begoña, Susana, R., Querejeta Ramón, Mariano, L., Díez Javier, and Fortuño María, A. (2002) 'Stimulation of Cardiac Apoptosis in Essential Hypertension'. *Hypertension* 39 (1), 75-80

Gorini, S., De Angelis, A., Berrino, L., Malara, N., Rosano, G., and Ferraro, E. (2018) 'Chemotherapeutic Drugs and Mitochondrial Dysfunction: Focus on Doxorubicin, Trastuzumab, and Sunitinib'. *Oxidative Medicine and Cellular Longevity* 2018, 7582730

Görlach, A., Bertram, K., Hudecova, S., and Krizanova, O. (2015) 'Calcium and ROS: A Mutual Interplay'. *Redox Biology* 6, 260-271

Gridelli, C., de Marinis, F., Cappuzzo, F., Di Maio, M., Hirsch, F. R., Mok, T., Morgillo, F., Rosell, R., Spigel, D. R., Yang, J. C., and Ciardiello, F. (2014) 'Treatment of Advanced Non-Small-Cell Lung Cancer with Epidermal Growth Factor Receptor (EGFR) Mutation Or ALK Gene Rearrangement: Results of an International Expert Panel Meeting of the Italian Association of Thoracic Oncology'. *Clinical Lung Cancer* 15 (3), 173-181

Gridelli, C., Peters, S., Sgambato, A., Casaluce, F., Adjei, A. A., and Ciardiello, F. (2014) 'ALK Inhibitors in the Treatment of Advanced NSCLC'. *Cancer Treatment Reviews* 40 (2), 300-306

Guglin, M., Krischer, J., Tamura, R., Fink, A., Bello-Matricaria, L., McCaskill-Stevens, W., and Munster, P. N. (2019) 'Randomized Trial of Lisinopril Versus Carvedilol to Prevent Trastuzumab Cardiotoxicity in Patients with Breast Cancer'. *Journal of the American College of Cardiology* 73 (22), 2859

Gujral, D. M., Lloyd, G., and Bhattacharyya, S. (2018) 'Effect of Prophylactic Betablocker Or ACE Inhibitor on Cardiac Dysfunction & Heart Failure during Anthracycline Chemotherapy ± trastuzumab'. *Breast (Edinburgh, Scotland)* 37, 64-71

Gutierrez, C. and Schiff, R. (2011) 'HER2: Biology, Detection, and Clinical Implications'. *Archives of Pathology & Laboratory Medicine* 135 (1), 55-62

Ha, J. and Oh, J. K. (2009) 'Therapeutic Strategies for Diastolic Dysfunction: A Clinical Perspective'. *Journal of Cardiovascular Ultrasound* 17 (3), 86-95

Hallberg, B. and Palmer, R. H. (2016) 'The Role of the ALK Receptor in Cancer Biology'. *Annals of Oncology* 27, iii4-iii15

Han, X., Zhou, Y., and Liu, W. (2017) 'Precision Cardio-Oncology: Understanding the Cardiotoxicity of Cancer Therapy'. *Npj Precision Oncology* 1 (1), 31

Hanif, K., Bid, H. K., and Konwar, R. (2010) 'Reinventing the ACE Inhibitors: Some Old and New Implications of ACE Inhibition'. *Hypertension Research* 33 (1), 11-21

Hartung, T. (2008) 'Thoughts on Limitations of Animal Models'. *Parkinsonism & Related Disorders* 14, S81-S83

Hemmings, B. A. and Restuccia, D. F. (2015) 'The PI3K-PKB/Akt Pathway'. *Cold Spring Harbor Perspectives in Biology* 7 (4), 10.1101/cshperspect.a026609

Hempel, N. and Trebak, M. (2017) 'Crosstalk between Calcium and Reactive Oxygen Species Signaling in Cancer'. *Cell Calcium* 63, 70-96

Henderson, K. A., Borders, R. B., Ross, J. B., Huwar, T. B., Travis, C. O., Wood, B. J., Ma, Z. J., Hong, S. P., Vinci, T. M., and Roche, B. M. (2013) 'Effects of Tyrosine Kinase Inhibitors on Rat Isolated Heart Function and Protein Biomarkers Indicative of Toxicity'. *Journal of Pharmacological and Toxicological Methods* 68 (1), 150-159

Heran, B. S., Wong, M. M., Heran, I. K., and Wright, J. M. (2008) 'Blood Pressure Lowering Efficacy of Angiotensin Converting Enzyme (ACE) Inhibitors for Primary Hypertension'. *The Cochrane Database of Systematic Reviews* 2008 (4), CD003823

Herman, E. H., Knapton, A., Rosen, E., Thompson, K., Rosenzweig, B., Estis, J., Agee, S., Lu, Q., Todd, J. A., Lipshultz, S., Hasinoff, B., and Zhang, J. (2011) 'A Multifaceted Evaluation of Imatinib-Induced Cardiotoxicity in the Rat'. *Toxicol Pathol* 39 (7), 1091-1106

Hicks, B. M., Filion, K. B., Yin, H., Sakr, L., Udell, J. A., and Azoulay, L. (2018) 'Angiotensin Converting Enzyme Inhibitors and Risk of Lung Cancer: Population Based Cohort Study'. *Bmj* 363, k4209

Hiona, A., Lee, A. S., Nagendran, J., Xie, X., Connolly, A. J., Robbins, R. C., and Wu, J. C. (2011) 'Pretreatment with Angiotensin-Converting Enzyme Inhibitor Improves Doxorubicin-Induced Cardiomyopathy Via Preservation of Mitochondrial Function'. *The Journal of Thoracic and Cardiovascular Surgery* 142 (2), 396-403.e3

Hirokazu, O., Hitoshi, T., Hideyasu, O., Kiyoshi, S., Izumi, S., Noriko, M., Akiyoshi, U., Daisuke, W., Tomoaki, M., Takeshi, S., Akiyoshi, F., and Yoshihito, H. (2004) 'Phosphatidylinositol 3-Kinase/Akt Regulates Angiotensin II–Induced Inhibition of Apoptosis in Microvascular Endothelial Cells by Governing Survivin Expression and Suppression of Caspase-3 Activity'. *Circulation Research* 94 (6), 785-793

Holla, V. R., Elamin, Y. Y., Bailey, A. M., Johnson, A. M., Litzenburger, B. C., Khotskaya, Y. B., Sanchez, N. S., Zeng, J., Shufean, M. A., Shaw, K. R., Mendelsohn, J., Mills, G. B., Meric-Bernstam, F., and Simon, G. R. (2017) 'ALK: A Tyrosine Kinase Target for Cancer Therapy'. *Cold Spring Harbor Molecular Case Studies* 3 (1), a001115

Hong, M., Hiroko, H., Akiyoshi, H., Kazuto, Y., and Yasushi, A. (1999) 'Protective Effect of Quinaprilat, an Active Metabolite of Quinapril, on Ca2+-Overload Induced by Lysophosphatidylcholine in Isolated Rat Cardiomyocytes'. *Japanese Journal of Pharmacology* 79 (1), 17-24

Houston Miller, N. (2010) 'Cardiovascular Risk Reduction with Renin-Angiotensin Aldosterone System Blockade'. *Nursing Research and Practice* 2010, 101749

Huang, H. (2018) 'Anaplastic Lymphoma Kinase (ALK) Receptor Tyrosine Kinase: A Catalytic Receptor with Many Faces'. *International Journal of Molecular Sciences* 19 (11), 3448

Hui, C. and Thomas, F. (2010) 'Molecular Mechanisms of Cardiovascular Toxicity of Targeted Cancer Therapeutics'. *Circulation Research* 106 (1), 21-34

Ibrahim, M. A., Ashour, O. M., Ibrahim, Y. F., El-Bitar, H. I., Gomaa, W., and Abdel-Rahim, S. R. (2009a) 'Angiotensin-Converting Enzyme Inhibition and Angiotensin AT(1)-Receptor Antagonism Equally Improve Doxorubicin-Induced Cardiotoxicity and Nephrotoxicity'. *Pharmacological Research* 60 (5), 373-381

Ibrahim, M. A., Ashour, O. M., Ibrahim, Y. F., El-Bitar, H. I., Gomaa, W., and Abdel-Rahim, S. R. (2009b) 'Angiotensin-Converting Enzyme Inhibition and Angiotensin AT(1)-Receptor Antagonism Equally Improve Doxorubicin-Induced Cardiotoxicity and Nephrotoxicity'. *Pharmacological Research* 60 (5), 373-381

Ichihara, S., Yamada, Y., Kawai, Y., Osawa, T., Furuhashi, K., Duan, Z., and Ichihara, G. (2007) 'Roles of Oxidative Stress and Akt Signaling in Doxorubicin Cardiotoxicity'. *Biochemical and Biophysical Research Communications* 359 (1), 27-33

Inamura, K., Takeuchi, K., Togashi, Y., Nomura, K., Ninomiya, H., Okui, M., Satoh, Y., Okumura, S., Nakagawa, K., Soda, M., Lim Choi, Y., Niki, T., Mano, H., and Ishikawa, Y. (2008) 'EML4-ALK Fusion is Linked to Histological Characteristics in a Subset of Lung Cancers'. *Journal of Thoracic Oncology* 3 (1), 13-17

Indo, H. P., Yen, H., Nakanishi, I., Matsumoto, K., Tamura, M., Nagano, Y., Matsui, H., Gusev, O., Cornette, R., Okuda, T., Minamiyama, Y., Ichikawa, H., Suenaga, S., Oki, M., Sato, T., Ozawa, T., Clair, D. K. S., and Majima, H. J. (2015) 'A Mitochondrial Superoxide Theory for Oxidative Stress Diseases and Aging'. *Journal of Clinical Biochemistry and Nutrition* 56 (1), 1-7

Iwai, M. and Horiuchi, M. (2009) 'Devil and Angel in the Renin-Angiotensin System: ACE-Angiotensin II-AT1 Receptor Axis Vs. ACE2-Angiotensin-(1-7)-Mas Receptor Axis'. *Hypertension Research : Official Journal of the Japanese Society of Hypertension* 32 (7), 533-536

Izzo, V., Bravo-San Pedro, J. M., Sica, V., Kroemer, G., and Galluzzi, L. (2016) 'Mitochondrial Permeability Transition: New Findings and Persisting Uncertainties'. *Trends in Cell Biology* 26 (9), 655-667

Jackie Bosch, Eva Lonn, Janice Pogue, J. Malcolm O. Arnold, Gilles R. Dagenais, and Salim Yusuf (2005) 'Long-Term Effects of Ramipril on Cardiovascular Events and on Diabetes'. *Circulation* 112 (9), 1339-1346

Jacob, F., Yonis, A. Y., Cuello, F., Luther, P., Schulze, T., Eder, A., Streichert, T., Mannhardt, I., Hirt, M. N., Schaaf, S., Stenzig, J., Force, T., Eschenhagen, T., and Hansen, A. (2016) 'Analysis of Tyrosine Kinase Inhibitor-Mediated Decline in Contractile Force in Rat Engineered Heart Tissue'. *PloS One* 11 (2), e0145937

Jain, S. D., Biradar, S., Periyandavar, I., Singh Sodhi, S., Anwaruddin, K., Gawde, A., Baliga, V., Gandewar, K., and Desai, A. (2005) 'Effects of Oral Fixed-Dose Combinations of Telmisartan Plus Ramipril and Losartan Plus Ramipril in Hypertension: A Multicenter, Prospective, Randomized, Double-Blind, Phase Iii Trial in Adult Indian Patients'. *Current Therapeutic Research* 66 (6), 630-642

Jemal, A., Bray, F., Center, M. M., Ferlay, J., Ward, E., and Forman, D. (2011) 'Global Cancer Statistics'. *CA: A Cancer Journal for Clinicians* 61 (2), 69-90

Jin, Z. Q. and Chen, X. (2000) 'Pretreatment with Ramiprilat Induces Cardioprotection Against Free Radical Injury in Guinea-Pig Isolated Heart: Involvement of Bradykinin, Protein Kinase C and Prostaglandins'. *Clinical and Experimental Pharmacology & Physiology* 27 (4), 257-262

Kahan, T. and Eliasson, K. (1999) 'The Influence of Long-Term ACE Inhibitor Treatment on Circulatory Responses to Stress in Human Hypertension*'. *American Journal of Hypertension* 12 (12), 1188-1194

Kawabata, M., Umemoto, N., Shimada, Y., Nishimura, Y., Zhang, B., Kuroyanagi, J., Miyabe, M., and Tanaka, T. (2015) 'Downregulation of Stanniocalcin 1 is Responsible for Sorafenib-Induced Cardiotoxicity'. *Toxicological Sciences : An Official Journal of the Society of Toxicology* 143 (2), 374-384

Kerkela, R., Woulfe, K. C., Durand, J., Vagnozzi, R., Kramer, D., Chu, T. F., Beahm, C., Chen, M. H., and Force, T. (2009) 'Sunitinib-Induced Cardiotoxicity is Mediated by Off-Target Inhibition of AMP-Activated Protein Kinase'. *Clinical and Translational Science* 2 (1), 15-25

Kerkelä, R., Grazette, L., Yacobi, R., Iliescu, C., Patten, R., Beahm, C., Walters, B., Shevtsov, S., Pesant, S., Clubb, F. J., Rosenzweig, A., Salomon, R. N., Van Etten, R.,A., Alroy, J., Durand, J., and Force, T. (2006a) 'Cardiotoxicity of the Cancer Therapeutic Agent Imatinib Mesylate'. *Nature Medicine* 12 (8), 908-916

Kerkelä, R., Grazette, L., Yacobi, R., Iliescu, C., Patten, R., Beahm, C., Walters, B., Shevtsov, S., Pesant, S., Clubb, F. J., Rosenzweig, A., Salomon, R. N., Van Etten, R.,A., Alroy, J.,

Durand, J., and Force, T. (2006b) 'Cardiotoxicity of the Cancer Therapeutic Agent Imatinib Mesylate'. *Nature Medicine* 12 (8), 908-916

Kerkelä, R., Grazette, L., Yacobi, R., Iliescu, C., Patten, R., Beahm, C., Walters, B., Shevtsov, S., Pesant, S., Clubb, F. J., Rosenzweig, A., Salomon, R. N., Van Etten, R.,A., Alroy, J., Durand, J., and Force, T. (2006c) 'Cardiotoxicity of the Cancer Therapeutic Agent Imatinib Mesylate'. *Nature Medicine* 12 (8), 908-916

Khakoo, A. Y. and Yeh, E. T. (2008) 'Therapy Insight: Management of Cardiovascular Disease in Patients with Cancer and Cardiac Complications of Cancer Therapy'. *Nature Clinical Practice Oncology* 5 (11), 655-667

Kim, T. D., le Coutre, P., Schwarz, M., Grille, P., Levitin, M., Fateh-Moghadam, S., Giles, F. J., Dörken, B., Haverkamp, W., and Köhncke, C. (2012) 'Clinical Cardiac Safety Profile of Nilotinib'. *Haematologica* 97 (6), 883

Kuramochi, Y., Guo, X., and Sawyer, D. B. (2006) 'Neuregulin Activates erbB2-Dependent Src/FAK Signaling and Cytoskeletal Remodeling in Isolated Adult Rat Cardiac Myocytes'. *Journal of Molecular and Cellular Cardiology* 41 (2), 228-235

Kuttikrishnan, S., Siveen, K. S., Prabhu, K. S., Khan, A. Q., Ahmed, E. I., Akhtar, S., Ali, T. A., Merhi, M., Dermime, S., Steinhoff, M., and Uddin, S. (2019) 'Curcumin Induces Apoptotic Cell Death Via Inhibition of PI3-Kinase/AKT Pathway in B-Precursor Acute Lymphoblastic Leukemia'. *Frontiers in Oncology* 9, 484

Kwak, E. L., Bang, Y. J., Camidge, D. R., Shaw, A. T., Solomon, B., Maki, R. G., Ou, S. H., Dezube, B. J., Jänne, P. A., Costa, D. B., Varella-Garcia, M., Kim, W. H., Lynch, T. J., Fidias, P., Stubbs, H., Engelman, J. A., Sequist, L. V., Tan, W., Gandhi, L., Mino-Kenudson, M., Wei, G. C., Shreeve, S. M., Ratain, M. J., Settleman, J., Christensen, J. G., Haber, D. A., Wilner, K., Salgia, R., Shapiro, G. I., Clark, J. W., and Iafrate, A. J. (2010a) 'Anaplastic Lymphoma Kinase Inhibition in Non-Small-Cell Lung Cancer'. *The New England Journal of Medicine* 363 (18), 1693-1703

Kwak, E. L., Bang, Y. J., Camidge, D. R., Shaw, A. T., Solomon, B., Maki, R. G., Ou, S. H., Dezube, B. J., Jänne, P. A., Costa, D. B., Varella-Garcia, M., Kim, W. H., Lynch, T. J., Fidias, P., Stubbs, H., Engelman, J. A., Sequist, L. V., Tan, W., Gandhi, L., Mino-Kenudson, M., Wei, G. C., Shreeve, S. M., Ratain, M. J., Settleman, J., Christensen, J. G., Haber, D. A., Wilner, K., Salgia, R., Shapiro, G. I., Clark, J. W., and Iafrate, A. J. (2010b) 'Anaplastic Lymphoma Kinase Inhibition in Non-Small-Cell Lung Cancer'. *The New England Journal of Medicine* 363 (18), 1693-1703

Lal, H., Kolaja, K. L., and Force, T. (2013) 'Cancer Genetics and the Cardiotoxicity of the Therapeutics'. *Journal of the American College of Cardiology* 61 (3), 267-274

Lamore, S. D., Kohnken, R. A., Peters, M. F., and Kolaja, K. L. (2020) 'Cardiovascular Toxicity Induced by Kinase Inhibitors: Mechanisms and Preclinical Approaches'. *Chemical Research in Toxicology* 33 (1), 125-136

Le, D. L., Cao, H., and Yang, L. X. (2014) 'Cardiotoxicity of Molecular-Targeted Drug Therapy'. *Anticancer Research* 34 (7), 3243-3249

Lee, C. J., Liao, C. L., and Lin, Y. L. (2005) 'Flavivirus Activates Phosphatidylinositol 3-Kinase Signaling to Block Caspase-Dependent Apoptotic Cell Death at the Early Stage of Virus Infection'. *Journal of Virology* 79 (13), 8388-8399

Lekes, D., Szadvari, I., Krizanova, O., Lopusna, K., Rezuchova, I., Novakova, M., Novakova, Z., Parak, T., and Babula, P. (2016) 'Nilotinib Induces ER Stress and Cell Death in H9c2 Cells'. *Physiological Research* 65 (Suppl 4), S505-S514

Li, L., Wei, L., Zhang, N., Wei, W., Hu, C., Deng, W., and Tang, Q. (2020) 'Levosimendan Protects Against Doxorubicin-Induced Cardiotoxicity by Regulating the PTEN/Akt Pathway'. *BioMed Research International* 2020, 1-11

Li, X. and Hemminki, K. (2004) 'Inherited Predisposition to Early Onset Lung Cancer According to Histological Type'. *International Journal of Cancer* 112 (3), 451-457

Li, X., Fang, P., Mai, J., Choi, E. T., Wang, H., and Yang, X. (2013) 'Targeting Mitochondrial Reactive Oxygen Species as Novel Therapy for Inflammatory Diseases and Cancers'. *Journal of Hematology & Oncology* 6 (1), 19

Li, Y., Ye, X., Liu, J., Zha, J., and Pei, L. (2011) 'Evaluation of EML4-ALK Fusion Proteins in Non–Small Cell Lung Cancer using Small Molecule Inhibitors'. *Neoplasia* 13 (1), 1-IN1

Liang, L., Yuan, W., Qu, L., Li, H., Zhang, L., Fan, G., and Peng, T. (2019) 'Administration of Losartan Preserves Cardiomyocyte Size and Prevents Myocardial Dysfunction in Tail-Suspended Mice by Inhibiting p47phox Phosphorylation, NADPH Oxidase Activation and MuRF1 Expression'. *Journal of Translational Medicine* 17 (1), 279

Lim, S. Y., Davidson, S. M., Mocanu, M. M., Yellon, D. M., and Smith, C. C. T. (2007) 'The Cardioprotective Effect of Necrostatin Requires the Cyclophilin-D Component of the Mitochondrial Permeability Transition Pore'. *Cardiovascular Drugs and Therapy* 21 (6), 467-469

Lindeman, N. I., Cagle, P. T., Beasley, M. B., Chitale, D. A., Dacic, S., Giaccone, G., Jenkins, R. B., Kwiatkowski, D. J., Saldivar, J. -., Squire, J., Thunnissen, E., and Ladanyi, M. (2013) 'Molecular Testing Guideline for Selection of Lung Cancer Patients for EGFR and ALK Tyrosine Kinase Inhibitors: Guideline from the College of American Pathologists, International Association for the Study of Lung Cancer, and Association for Molecular Pathology'. *Archives of Pathology and Laboratory Medicine* 137 (6), 828-860

Linkermann, A. and Green, D. (2014) 'Necroptosis'. *New England Journal of Medicine* 370, 455-465

Liu, P., Cheng, H., Roberts, T. M., and Zhao, J. J. (2009) 'Targeting the Phosphoinositide 3-Kinase Pathway in Cancer'. *Nature Reviews.Drug Discovery* 8 (8), 627-644

Liu, R., Chen, Y., Liu, G., Li, C., Song, Y., Cao, Z., Li, W., Hu, J., Lu, C., and Liu, Y. (2020) 'PI3K/AKT Pathway as a Key Link Modulates the Multidrug Resistance of Cancers'. *Cell Death & Disease* 11 (9), 797

Loennechen Jan, P., Wisløff Ulrik, Geir, F., and Ellingsen Øyvind (2002) 'Effects of Cariporide and Losartan on Hypertrophy, Calcium Transients, Contractility, and Gene Expression in Congestive Heart Failure'. *Circulation* 105 (11), 1380-1386

Lonn, E., Shaikholeslami, R., Yi, Q., Bosch, J., Sullivan, B., Tanser, P., Magi, A., and Yusuf, S. (2004) 'Effects of Ramipril on Left Ventricular Mass and Function in Cardiovascular Patients with Controlled Blood Pressure and with Preserved Left Ventricular Ejection Fraction: A Substudy of the Heart Outcomes Prevention Evaluation (HOPE) Trial'. *Journal of the American College of Cardiology* 43 (12), 2200-2206

López-Sendón, J., Swedberg, K., McMurray, J., Tamargo, J., Maggioni, A. P., Dargie, H., Tendera, M., Waagstein, F., Kjekshus, J., Lechat, P., Torp-Pedersen, C., and Task Force on ACE-inhibitors of the European Society of Cardiology (2004) 'Expert Consensus Document on Angiotensin Converting Enzyme Inhibitors in Cardiovascular Disease. the Task Force on ACE-Inhibitors of the European Society of Cardiology'. *European Heart Journal* 25 (16), 1454-1470

Loreto, C., La Rocca, G., Anzalone, R., Caltabiano, R., Vespasiani, G., Castorina, S., Ralph, D. J., Cellek, S., Musumeci, G., Giunta, S., Djinovic, R., Basic, D., and Sansalone, S. (2014) 'The Role of Intrinsic Pathway in Apoptosis Activation and Progression in Peyronie's Disease'. *BioMed Research International* 2014, 616149

Los, M., Maddika, S., Erb, B., and Schulze-Osthoff, K. (2009) 'Switching Akt: From Survival Signaling to Deadly Response'. *BioEssays : News and Reviews in Molecular, Cellular and Developmental Biology* 31 (5), 492-495

Lovric-Bencic, M., Sikiric, P., Hanzevacki, J. S., Seiwerth, S., Rogic, D., Kusec, V., Aralica, G., Konjevoda, P., Batelja, L., and Blagaic, A. B. (2004) 'Doxorubicine-Congestive Heart Failure-Increased Big Endothelin-1 Plasma Concentration: Reversal by Amlodipine, Losartan, and Gastric Pentadecapeptide BPC157 in Rat and Mouse'. *Journal of Pharmacological Sciences* 95 (1), 19-26

Lozano, R., Naghavi, M., Foreman, K., Lim, S., Shibuya, K., Aboyans, V., Abraham, J., Adair, T., Aggarwal, R., Ahn, S. Y., Alvarado, M., Anderson, H. R., Anderson, L. M., Andrews, K. G., Atkinson, C., Baddour, L. M., Barker-Collo, S., Bartels, D. H., Bell, M. L., Benjamin, E. J., Bennett, D., Bhalla, K., Bikbov, B., Bin Abdulhak, A., Birbeck, G., Blyth, F., Bolliger, I., Boufous, S., Bucello, C., Burch, M., Burney, P., Carapetis, J., Chen, H., Chou, D., Chugh, S. S., Coffeng, L. E., Colan, S. D., Colquhoun, S., Colson, K. E., Condon, J., Connor, M. D., Cooper, L. T., Corriere, M., Cortinovis, M., de Vaccaro, K. C., Couser, W., Cowie, B. C., Criqui, M. H., Cross, M., Dabhadkar, K. C., Dahodwala, N., De Leo, D., Degenhardt, L., Delossantos, A., Denenberg, J., Des Jarlais, D. C., Dharmaratne, S. D., Dorsey, E. R., Driscoll, T., Duber, H., Ebel, B., Erwin, P. J., Espindola, P., Ezzati, M., Feigin, V., Flaxman, A. D., Forouzanfar, M. H., Fowkes, F. G., Franklin, R., Fransen, M., Freeman, M. K., Gabriel, S. E., Gakidou, E., Gaspari, F., Gillum, R. F., Gonzalez-Medina, D., Halasa, Y. A., Haring, D., Harrison, J. E., Havmoeller, R., Hay, R. J., Hoen, B., Hotez, P. J., Hoy, D.,

Jacobsen, K. H., James, S. L., Jasrasaria, R., Jayaraman, S., Johns, N., Karthikeyan, G., Kassebaum, N., Keren, A., Khoo, J. P., Knowlton, L. M., Kobusingye, O., Koranteng, A., Krishnamurthi, R., Lipnick, M., Lipshultz, S. E., Ohno, S. L., Mabweijano, J., MacIntyre, M. F., Mallinger, L., March, L., Marks, G. B., Marks, R., Matsumori, A., Matzopoulos, R., Mayosi, B. M., McAnulty, J. H., McDermott, M. M., McGrath, J., Mensah, G. A., Merriman, T. R., Michaud, C., Miller, M., Miller, T. R., Mock, C., Mocumbi, A. O., Mokdad, A. A., Moran, A., Mulholland, K., Nair, M. N., Naldi, L., Narayan, K. M., Nasseri, K., Norman, P., O'Donnell, M., Omer, S. B., Ortblad, K., Osborne, R., Ozgediz, D., Pahari, B., Pandian, J. D., Rivero, A. P., Padilla, R. P., Perez-Ruiz, F., Perico, N., Phillips, D., Pierce, K., Pope, C. A.,3rd, Porrini, E., Pourmalek, F., Raju, M., Ranganathan, D., Rehm, J. T., Rein, D. B., Remuzzi, G., Rivara, F. P., Roberts, T., De León, F. R., Rosenfeld, L. C., Rushton, L., Sacco, R. L., Salomon, J. A., Sampson, U., Sanman, E., Schwebel, D. C., Segui-Gomez, M., Shepard, D. S., Singh, D., Singleton, J., Sliwa, K., Smith, E., Steer, A., Taylor, J. A., Thomas, B., Tleyjeh, I. M., Towbin, J. A., Truelsen, T., Undurraga, E. A., Venketasubramanian, N., Vijayakumar, L., Vos, T., Wagner, G. R., Wang, M., Wang, W., Watt, K., Weinstock, M. A., Weintraub, R., Wilkinson, J. D., Woolf, A. D., Wulf, S., Yeh, P. H., Yip, P., Zabetian, A., Zheng, Z. J., Lopez, A. D., Murray, C. J., AlMazroa, M. A., and Memish, Z. A. (2012) 'Global and Regional Mortality from 235 Causes of Death for 20 Age Groups in 1990 and 2010: A Systematic Analysis for the Global Burden of Disease Study 2010'. *Lancet (London, England)* 380 (9859), 2095-2128

Lv, X., Zhang, Y., Niu, Y., Song, Q., and Zhao, Q. (2018) 'Comparison of Angiotensin-Converting Enzyme Inhibitors and Angiotensin II Receptor Blockers on Cardiovascular Outcomes in Hypertensive Patients with Type 2 Diabetes Mellitus: A PRISMA-Compliant Systematic Review and Meta-Analysis'. *Medicine* 97 (15), e0256

Ma, W., Liu, M., Liang, F., Zhao, L., Gao, C., Jiang, X., Zhang, X., Zhan, H., Hu, H., and Zhao, Z. (2020a) 'Cardiotoxicity of Sorafenib is Mediated through Elevation of ROS Level and CaMKII Activity and Dysregulation of Calcium Homoeostasis'. *Basic & Clinical Pharmacology & Toxicology* 126 (2), 166-180

Ma, W., Wei, S., Zhang, B., and Li, W. (2020b) 'Molecular Mechanisms of Cardiomyocyte Death in Drug-Induced Cardiotoxicity'. *Frontiers in Cell and Developmental Biology* 8, 434

Maharsy, W. (2015) 'Chemotherapy Induced Cardiotoxicity: Facts, Breakthroughs, and Challenges'. *University of Ottawa Journal of Medicine* 5 (1), 51-56

Malvezzi, M., Bertuccio, P., Rosso, T., Rota, M., Levi, F., La Vecchia, C., and Negri, E. (2015) 'European Cancer Mortality Predictions for the Year 2015: Does Lung Cancer have the Highest Death Rate in EU Women?'. *Annals of Oncology : Official Journal of the European Society for Medical Oncology* 26 (4), 779-786

Mariappan, N., Elks, C. M., Haque, M., and Francis, J. (2012) 'Interaction of TNF with Angiotensin II Contributes to Mitochondrial Oxidative Stress and Cardiac Damage in Rats'. *PloS One* 7 (10), e46568

Marroquin, L. D., Hynes, J., Dykens, J. A., Jamieson, J. D., and Will, Y. (2007) 'Circumventing the Crabtree Effect: Replacing Media Glucose with Galactose Increases Susceptibility

of HepG2 Cells to Mitochondrial Toxicants'. *Toxicological Sciences : An Official Journal of the Society of Toxicology* 97 (2), 539-547

Martelli, M. P., Sozzi, G., Hernandez, L., Pettirossi, V., Navarro, A., Conte, D., Gasparini, P., Perrone, F., Modena, P., Pastorino, U., Carbone, A., Fabbri, A., Sidoni, A., Nakamura, S., Gambacorta, M., Fernández, P. L., Ramirez, J., Chan, J. K. C., Grigioni, W. F., Campo, E., Pileri, S. A., and Falini, B. (2009) 'EML4-ALK Rearrangement in Non-Small Cell Lung Cancer and Non-Tumor Lung Tissues'. *The American Journal of Pathology* 174 (2), 661-670

Matouk, A. I., Taye, A., Heeba, G. H., and El-Moselhy, M. A. (2013) 'Quercetin Augments the Protective Effect of Losartan Against Chronic Doxorubicin Cardiotoxicity in Rats'. *Environmental Toxicology and Pharmacology* 36 (2), 443-450

McLachlan, J., Beattie, E., Murphy, M. P., Koh-Tan, C., Olson, E., Beattie, W., Dominiczak, A. F., Nicklin, S. A., and Graham, D. (2014) 'Combined Therapeutic Benefit of Mitochondria-Targeted Antioxidant, MitoQ10, and Angiotensin Receptor Blocker, Losartan, on Cardiovascular Function'. *Journal of Hypertension* 32 (3)

Meng, Y., Wang, W., Kang, J., Wang, X., and Sun, L. (2017) 'Role of the PI3K/AKT Signalling Pathway in Apoptotic Cell Death in the Cerebral Cortex of Streptozotocin-Induced Diabetic Rats'. *Experimental and Therapeutic Medicine* 13 (5), 2417-2422

Meredith, A. and Dass, C. R. (2016) 'Increasing Role of the Cancer Chemotherapeutic Doxorubicin in Cellular Metabolism'. *Journal of Pharmacy and Pharmacology* 68 (6), 729-741

Min, L., Mogi, M., Iwai, M., and Horiuchi, M. (2009) 'Signaling Mechanisms of Angiotensin II in Regulating Vascular Senescence'. *Ageing Research Reviews* 8 (2), 113-121

Mochizuki, T., Asai, A., Saito, N., Tanaka, S., Katagiri, H., Asano, T., Nakane, M., Tamura, A., Kuchino, Y., Kitanaka, C., and Kirino, T. (2002) 'Akt Protein Kinase Inhibits Non-Apoptotic Programmed Cell Death Induced by Ceramide *'. *Journal of Biological Chemistry* 277 (4), 2790-2797

Molina, J. R., Yang, P., Cassivi, S. D., Schild, S. E., and Adjei, A. A. (2008a) 'Non-Small Cell Lung Cancer: Epidemiology, Risk Factors, Treatment, and Survivorship'. *Mayo Clinic Proceedings* 83 (5), 584-594

Molina, J. R., Yang, P., Cassivi, S. D., Schild, S. E., and Adjei, A. A. (2008b) 'Non-Small Cell Lung Cancer: Epidemiology, Risk Factors, Treatment, and Survivorship'. *Mayo Clinic Proceedings* 83 (5), 584-594

Montaigne, D., Hurt, C., and Neviere, R. (2012a) 'Mitochondria Death/Survival Signaling Pathways in Cardiotoxicity Induced by Anthracyclines and Anticancer-Targeted Therapies'. *Biochemistry Research International* 2012, 951539

Montaigne, D., Hurt, C., and Neviere, R. (2012b) 'Mitochondria Death/Survival Signaling Pathways in Cardiotoxicity Induced by Anthracyclines and Anticancer-Targeted Therapies'. *Biochemistry Research International* 2012, 951539

Mossé, Y. P., Wood, A., and Maris, J. M. (2009) 'Inhibition of ALK Signaling for Cancer Therapy'. *Clinical Cancer Research* 15 (18), 5609-5614

Munger, M. A. (2011) 'Use of Angiotensin Receptor Blockers in Cardiovascular Protection: Current Evidence and Future Directions'. *P & T : A Peer-Reviewed Journal for Formulary Management* 36 (1), 22-40

Murabito, A., Hirsch, E., and Ghigo, A. (2020a) 'Mechanisms of Anthracycline-Induced Cardiotoxicity: Is Mitochondrial Dysfunction the Answer?'. *Frontiers in Cardiovascular Medicine* 7, 35

Murabito, A., Hirsch, E., and Ghigo, A. (2020b) 'Mechanisms of Anthracycline-Induced Cardiotoxicity: Is Mitochondrial Dysfunction the Answer?'. *Frontiers in Cardiovascular Medicine* 7, 35

Nitulescu, G.,Mihai, Van De Venter, M., Nitulescu, G., Ungurianu, A., Juzenas, P., Peng, Q., Olaru, O.,Tudorel, Grădinaru, D., Tsatsakis, A., Tsoukalas, D., Spandidos, D.,A., and Margina, D. (2018) 'The Akt Pathway in Oncology Therapy and Beyond (Review)'. *Int J Oncol; International Journal of Oncology* 53 (6), 2319-2331

Nogueira, V., Park, Y., Chen, C., Xu, P., Chen, M., Tonic, I., Unterman, T., and Hay, N. (2008) 'Akt Determines Replicative Senescence and Oxidative Or Oncogenic Premature Senescence and Sensitizes Cells to Oxidative Apoptosis'. *Cancer Cell* 14 (6), 458-470

Nojima, Y., Bono, H., Yokoyama, T., Iwabuchi, K., Sato, R., Arai, K., and Tabunoki, H. (2019) 'Superoxide Dismutase Down-Regulation and the Oxidative Stress is Required to Initiate Pupation in Bombyx Mori'. *Scientific Reports* 9 (1), 14693

O'Bryant, C. L., Wenger, S. D., Kim, M., and Thompson, L. A. (2013) 'Crizotinib: A New Treatment Option for ALK-Positive Non-Small Cell Lung Cancer'. *The Annals of Pharmacotherapy* 47 (2), 189-197

Octavia, Y., Tocchetti, C. G., Gabrielson, K. L., Janssens, S., Crijns, H. J., and Moens, A. L. (2012) 'Doxorubicin-Induced Cardiomyopathy: From Molecular Mechanisms to Therapeutic Strategies'. *Journal of Molecular and Cellular Cardiology* 52 (6), 1213-1225

Okada, M., Adachi, S., Imai, T., Watanabe, K., Toyokuni, S., Ueno, M., Zervos, A. S., Kroemer, G., and Nakahata, T. (2004) 'A Novel Mechanism for Imatinib Mesylate–induced Cell Death of BCR-ABL–positive Human Leukemic Cells: Caspase-Independent, Necrosis-Like Programmed Cell Death Mediated by Serine Protease Activity'. *Blood* 103 (6), 2299-2307

Orphanos, G. S., Ioannidis, G. N., and Ardavanis, A. G. (2009) 'Cardiotoxicity Induced by Tyrosine Kinase Inhibitors'. *Acta Oncologica* 48 (7), 964-970

O'Sullivan, C. C. and Smith, K. L. (2014) 'Therapeutic Considerations in Treating HER2-Positive Metastatic Breast Cancer'. *Current Breast Cancer Reports* 6 (3), 169-182

Ou, S. H., Janne, P. A., Bartlett, C. H., Tang, Y., Kim, D. W., Otterson, G. A., Crino, L., Selaru, P., Cohen, D. P., Clark, J. W., and Riely, G. J. (2014) 'Clinical Benefit of Continuing ALK Inhibition with Crizotinib Beyond Initial Disease Progression in Patients with Advanced ALK-Positive NSCLC'. *Annals of Oncology : Official Journal of the European Society for Medical Oncology* 25 (2), 415-422

Ou, S. I. (2011) 'Crizotinib: A Novel and First-in-Class Multitargeted Tyrosine Kinase Inhibitor for the Treatment of Anaplastic Lymphoma Kinase Rearranged Non-Small Cell Lung Cancer and Beyond'. *Drug Design, Development and Therapy* 5, 471-485

Özdoğru, İ (2014) 'Anthracycline-Induced Cardiotoxicity'. *Turk Kardiyoloji Dernegi Arsivi : Turk Kardiyoloji Derneginin Yayin Organidir* 42 (3), 274-276

Paech, F., Mingard, C., Grünig, D., Abegg, V. F., Bouitbir, J., and Krähenbühl, S. (2018) 'Mechanisms of Mitochondrial Toxicity of the Kinase Inhibitors Ponatinib, Regorafenib and Sorafenib in Human Hepatic HepG2 Cells'. *Toxicology* 395, 34-44

Park, Y. H., Park, H. J., Kim, B. S., Ha, E., Jung, K. H., Yoon, S. H., Yim, S. V., and Chung, J. H. (2006) 'BNP as a Marker of the Heart Failure in the Treatment of Imatinib Mesylate'. *Cancer Letters* 243 (1), 16-22

Pattacini, L., Mancini, M., Mazzacurati, L., Brusa, G., Benvenuti, M., Martinelli, G., Baccarani, M., and Santucci, M. A. (2004) 'Endoplasmic Reticulum Stress Initiates Apoptotic Death Induced by STI571 Inhibition of p210 Bcr–abl Tyrosine Kinase'. *Leukemia Research* 28 (2), 191-202

Paul, W., David, P., Caroline, H., Shah Anoop, S. V., David, M., Andrew, B., Charles, B., Alex, M., Sandosh, P., Claire, W., Mark, W., Archie, C., David, P., Mills Nicholas, L., and Naveed, S. (2019) 'Cardiac Troponin T and Troponin I in the General Population'. *Circulation* 139 (24), 2754-2764

Perez, E. A., Koehler, M., Byrne, J., Preston, A. J., Rappold, E., and Ewer, M. S. (2008) 'Cardiac Safety of Lapatinib: Pooled Analysis of 3689 Patients Enrolled in Clinical Trials'. *Mayo Clinic Proceedings* 83 (6), 679-686

Peter, A. K., Bjerke, M. A., and Leinwand, L. A. (2016) 'Biology of the Cardiac Myocyte in Heart Disease'. *Molecular Biology of the Cell* 27 (14), 2149-2160

Pinter, M., Kwanten, W. J., and Jain, R. K. (2018) 'Renin-Angiotensin System Inhibitors to Mitigate Cancer Treatment-Related Adverse Events'. *Clinical Cancer Research*, clincanres.0236.2018

Pinto, A. C., Ades, F., de Azambuja, E., and Piccart-Gebhart, M. (2013) 'Trastuzumab for Patients with HER2 Positive Breast Cancer: Delivery, Duration and Combination Therapies'. *Breast (Edinburgh, Scotland)* 22 Suppl 2, 152

Pinton, P., Giorgi, C., Siviero, R., Zecchini, E., and Rizzuto, R. (2008) 'Calcium and Apoptosis: ER-Mitochondria Ca2+ Transfer in the Control of Apoptosis'. *Oncogene* 27 (50), 6407-6418

Pituskin, E., Mackey, J. R., Koshman, S., Jassal, D., Pitz, M., Haykowsky, M. J., Pagano, J. J., Chow, K., Thompson, R. B., Vos, L. J., Ghosh, S., Oudit, G. Y., Ezekowitz, J. A., and Paterson, D. I. (2017) 'Multidisciplinary Approach to Novel Therapies in Cardio-Oncology Research (MANTICORE 101–Breast): A Randomized Trial for the Prevention of Trastuzumab-Associated Cardiotoxicity'. *Jco* 35 (8), 870-877

Porter, A. G. and Jänicke, R. U. (1999) 'Emerging Roles of Caspase-3 in Apoptosis'. *Cell Death and Differentiation* 6 (2), 99-104

Qi, W., Lin, F., Sun, Y., Tang, L., He, A., Yao, Y., and Shen, Z. (2013) 'Incidence and Risk of Hypertension with Pazopanib in Patients with Cancer: A Meta-Analysis'. *Cancer Chemotherapy and Pharmacology* 71 (2), 431-439

Raschi, E., Vasina, V., Ursino, M. G., Boriani, G., Martoni, A., and De Ponti, F. (2010) 'Anticancer Drugs and Cardiotoxicity: Insights and Perspectives in the Era of Targeted Therapy'. *Pharmacology & Therapeutics* 125 (2), 196-218

Rashikh, A., Pillai, K. K., and Najmi, A. K. (2014) 'Protective Effect of a Direct Renin Inhibitor in Acute Murine Model of Cardiotoxicity and Nephrotoxicity'. *Fundamental & Clinical Pharmacology* 28 (5), 489-500

Reck, M., Heigener, D. F., Mok, T., Soria, J. C., and Rabe, K. F. (2013) 'Management of Non-Small-Cell Lung Cancer: Recent Developments'. *Lancet (London, England)* 382 (9893), 709-719

Richards, C. J., Je, Y., Schutz, F. A., Heng, D. Y., Dallabrida, S. M., Moslehi, J. J., and Choueiri, T. K. (2011) 'Incidence and Risk of Congestive Heart Failure in Patients with Renal and Nonrenal Cell Carcinoma Treated with Sunitinib'. *Journal of Clinical Oncology : Official Journal of the American Society of Clinical Oncology* 29 (25), 3450-3456

Ripley, E. and Hirsch, A. (2010) 'Fifteen Years of Losartan: What have we Learned about Losartan that can Benefit Chronic Kidney Disease Patients?'. *International Journal of Nephrology and Renovascular Disease* 3, 93-98

Roche (2018) 'Lung Cancer'. *Lung Cancer*

Rodig, S. J. and Shapiro, G. I. (2010) 'Crizotinib, a Small-Molecule Dual Inhibitor of the C-Met and ALK Receptor Tyrosine Kinases'. *Current Opinion in Investigational Drugs (London, England : 2000)* 11 (12), 1477-1490

Rodríguez-Hernández, M. A., de la Cruz-Ojeda, P., López-Grueso, M. J., Navarro-Villarán, E., Requejo-Aguilar, R., Castejón-Vega, B., Negrete, M., Gallego, P., Vega-Ochoa, Á, Victor, V. M., Cordero, M. D., Del Campo, J. A., Bárcena, J. A., Padilla, C. A., and Muntané, J. (2020a) 'Integrated Molecular Signaling Involving Mitochondrial Dysfunction and

Alteration of Cell Metabolism Induced by Tyrosine Kinase Inhibitors in Cancer'. *Redox Biology* 36, 101510

Rodríguez-Hernández, M. A., de la Cruz-Ojeda, P., López-Grueso, M. J., Navarro-Villarán, E., Requejo-Aguilar, R., Castejón-Vega, B., Negrete, M., Gallego, P., Vega-Ochoa, Á, Victor, V. M., Cordero, M. D., Del Campo, J. A., Bárcena, J. A., Padilla, C. A., and Muntané, J. (2020b) 'Integrated Molecular Signaling Involving Mitochondrial Dysfunction and Alteration of Cell Metabolism Induced by Tyrosine Kinase Inhibitors in Cancer'. *Redox Biology* 36, 101510

Ron, D. and Walter, P. (2007) 'Signal Integration in the Endoplasmic Reticulum Unfolded Protein Response'. *Nature Reviews.Molecular Cell Biology* 8 (7), 519-529

Roskoski, R. (2013) 'Anaplastic Lymphoma Kinase (ALK): Structure, Oncogenic Activation, and Pharmacological Inhibition'. *Pharmacological Research* 68 (1), 68-94

Rouleau Jean, L., Gaston, K., Pelletier Stéphane, Hugues, G., Albert, A., Caroline, G., Chantal, L., and Sylvain, M. (2001) 'Cardioprotective Effects of Ramipril and Losartan in Right Ventricular Pressure Overload in the Rabbit'. *Circulation* 104 (8), 939-944

Ruschitzka, F. and Taddei, S. (2012) 'Angiotensin-Converting Enzyme Inhibitors: First-Line Agents in Cardiovascular Protection?'. *European Heart Journal* 33 (16), 1996-1998

Sahu, A., Prabhash, K., Noronha, V., Joshi, A., and Desai, S. (2013a) 'Crizotinib: A Comprehensive Review'. *South Asian Journal of Cancer* 2 (2), 91-97

Sahu, A., Prabhash, K., Noronha, V., Joshi, A., and Desai, S. (2013b) 'Crizotinib: A Comprehensive Review'. *South Asian Journal of Cancer* 2 (2), 91-97

Sandmann, S., Li, J., Fritzenkötter, C., Spormann, J., Tiede, K., Fischer, J. W., and Unger, T. (2006a) 'Differential Effects of Olmesartan and Ramipril on Inflammatory Response After Myocardial Infarction in Rats'. *Blood Pressure* 15 (2), 116-128

Sandmann, S., Li, J., Fritzenkötter, C., Spormann, J., Tiede, K., Fischer, J. W., and Unger, T. (2006b) 'Differential Effects of Olmesartan and Ramipril on Inflammatory Response After Myocardial Infarction in Rats'. *Blood Pressure* 15 (2), 116-128

Sanguinetti, M. and Mitcheson, J. (2005) 'Sanguinetti MC, Mitcheson JSPredicting Drug-hERG Channel Interactions that Cause Acquired Long QT Syndrome. Trends Pharmacol Sci 26(3): 119-124'. *Trends in Pharmacological Sciences* 26, 119-24

Sasaki, T., Rodig, S. J., Chirieac, L. R., and Jänne, P. A. (2010a) 'The Biology and Treatment of EML4-ALK Non-Small Cell Lung Cancer'. *European Journal of Cancer (Oxford, England : 1990)* 46 (10), 1773-1780

Sasaki, T., Rodig, S. J., Chirieac, L. R., and Jänne, P. A. (2010b) 'The Biology and Treatment of EML4-ALK Non-Small Cell Lung Cancer'. *European Journal of Cancer (Oxford, England : 1990)* 46 (10), 1773-1780

Sasaki, T., Rodig, S. J., Chirieac, L. R., and Jänne, P. A. (2010c) 'The Biology and Treatment of EML4-ALK Non-Small Cell Lung Cancer'. *European Journal of Cancer (Oxford, England : 1990)* 46 (10), 1773-1780

Schieffer, B., Wirger, A., Meybrunn, M., Seitz, S., Holtz, J., Riede, U. N., and Drexler, H. (1994) 'Comparative Effects of Chronic Angiotensin-Converting Enzyme Inhibition and Angiotensin II Type 1 Receptor Blockade on Cardiac Remodeling After Myocardial Infarction in the Rat'. *Circulation* 89 (5), 2273-2282

Schieffer, B., Bünte, C., Witte, J., Hoeper, K., Böger, R. H., Schwedhelm, E., and Drexler, H. (2004) 'Comparative Effects of AT1-Antagonism and Angiotensin-Converting Enzyme Inhibition on Markers of Inflammation and Platelet Aggregation in Patients with Coronary Artery Disease'. *Journal of the American College of Cardiology* 44 (2), 362-368

Schmidinger, M., Zielinski, C. C., Vogl, U. M., Bojic, A., Bojic, M., Schukro, C., Ruhsam, M., Hejna, M., and Schmidinger, H. (2008) 'Cardiac Toxicity of Sunitinib and Sorafenib in Patients with Metastatic Renal Cell Carcinoma'. *Jco* 26 (32), 5204-5212

Schneider, C., Wallner, M., Kolesnik, E., Herbst, V., Mächler, H., Pichler, M., von Lewinski, D., Sedej, S., and Rainer, P. P. (2018) 'The Anti-Cancer Multikinase Inhibitor Sorafenib Impairs Cardiac Contractility by Reducing Phospholamban Phosphorylation and Sarcoplasmic Calcium Transients'. *Scientific Reports* 8 (1), 5295

Schwach, V., Slaats, R. H., and Passier, R. (2020) 'Human Pluripotent Stem Cell-Derived Cardiomyocytes for Assessment of Anticancer Drug-Induced Cardiotoxicity'. *Frontiers in Cardiovascular Medicine* 7, 50

Seicean, S., Seicean, A., Plana, J. C., Budd, G. T., and Marwick, T. H. (2012) 'Effect of Statin Therapy on the Risk for Incident Heart Failure in Patients with Breast Cancer Receiving Anthracycline Chemotherapy: An Observational Clinical Cohort Study'. *Journal of the American College of Cardiology* 60 (23), 2384-2390

Sgarra, L., Leo, V., Addabbo, F., Iacobazzi, D., Carratù, M. R., Montagnani, M., and Potenza, M. A. (2014) 'Intermittent Losartan Administration Triggers Cardiac Post-Conditioning in Isolated Rat Hearts: Role of BK2 Receptors'. *Plos One* 9 (2), e88542

Shah, R. R., Morganroth, J., and Shah, D. R. (2013) 'Cardiovascular Safety of Tyrosine Kinase Inhibitors: With a Special Focus on Cardiac Repolarisation (QT Interval)'. *Drug Safety* 36 (5), 295-316

Shaw, A. T., Kim, D. W., Nakagawa, K., Seto, T., Crinó, L., Ahn, M. J., De Pas, T., Besse, B., Solomon, B. J., Blackhall, F., Wu, Y. L., Thomas, M., O'Byrne, K. J., Moro-Sibilot, D., Camidge, D. R., Mok, T., Hirsh, V., Riely, G. J., Iyer, S., Tassell, V., Polli, A., Wilner, K. D., and Jänne, P. A. (2013) 'Crizotinib Versus Chemotherapy in Advanced ALK-Positive Lung Cancer'. *The New England Journal of Medicine* 368 (25), 2385-2394

Sheik Uduman, M.,Saleem Thattakudian, Reddy, R. B., Punuru, P., Chakka, G., and Karunakaran, G. (2016) 'Protective Role of Ramipril and Candesartan Against

Myocardial Ischemic Reperfusion Injury: A Biochemical and Transmission Electron Microscopical Study'*. Advances in Pharmacological Sciences* 2016, 4608979

Shetty, S. S. and DelGrande, D. (2000) 'Differential Inhibition of the Prejunctional Actions of Angiotensin II in Rat Atria by Valsartan, Irbesartan, Eprosartan, and Losartan'*. J Pharmacol Exp Ther* 294 (1), 179

Shi, Q., Abusarah, J., Baroudi, G., Fernandes, J. C., Fahmi, H., and Benderdour, M. (2012) 'Ramipril Attenuates Lipid Peroxidation and Cardiac Fibrosis in an Experimental Model of Rheumatoid Arthritis'*. Arthritis Research & Therapy* 14 (5), R223

Shinmura, K., Kageyama, S., Tao, H., Bunai, T., Suzuki, M., Kamo, T., Takamochi, K., Suzuki, K., Tanahashi, M., Niwa, H., Ogawa, H., and Sugimura, H. (2008) 'EML4-ALK Fusion Transcripts, but no NPM-, TPM3-, CLTC-, ATIC-, Or TFG-ALK Fusion Transcripts, in Non-Small Cell Lung Carcinomas'*. Lung Cancer* 61 (2), 163-169

Shopp, G. M., Helson, L., Bouchard, A., Salvail, D., and Majeed, M. (2014) 'Liposomes Ameliorate Crizotinib- and Nilotinib-Induced Inhibition of the Cardiac IKr Channel and QTc Prolongation'*. Anticancer Research* 34 (9), 4733-4740

Siegel, R. L., Miller, K. D., and Jemal, A. (2018) 'Cancer Statistics, 2018'*. CA: A Cancer Journal for Clinicians* 68 (1), 7-30

Siegel, R. L., Miller, K. D., and Jemal, A. (2017) 'Cancer Statistics, 2017'*. CA: A Cancer Journal for Clinicians* 67 (1), 7-30

Simonis, G., Braun, M. U., Kirrstetter, M., Schön, S. P., and Strasser, R. H. (2003) 'Mechanisms of Myocardial Remodeling: Ramiprilat Blocks the Expressional Upregulation of Protein Kinase C-Epsilon in the Surviving Myocardium Early After Infarction'*. Journal of Cardiovascular Pharmacology* 41 (5), 780-787

Singh, A. P., Glennon, M. S., Umbarkar, P., Gupte, M., Galindo, C. L., Zhang, Q., Force, T., Becker, J. R., and Lal, H. (2019) 'Ponatinib-Induced Cardiotoxicity: Delineating the Signalling Mechanisms and Potential Rescue Strategies'*. Cardiovascular Research* 115 (5), 966-977

Singla, D. K. (2015) 'Akt—mTOR Pathway Inhibits Apoptosis and Fibrosis in Doxorubicin-Induced Cardiotoxicity Following Embryonic Stem Cell Transplantation'*. Cell Transplant* 24 (6), 1031-1042

Siu, P. M. and Alway, S. E. (2009) 'Response and Adaptation of Skeletal Muscle to Denervation Stress: The Role of Apoptosis in Muscle Loss'*. Frontiers in Bioscience (Landmark Edition)* 14, 432-452

Smiseth, O. A., Edvardsen, T., and Skulstad, H. (2013) 'Cardioprotection during Chemotherapy: Need for Faster Transfer of Knowledge from Cardiology to Oncology and Role for a Cardio-Oncologist*'*. Journal of the American College of Cardiology* 61 (23), 2363-2364

Smith, T. A. D., Phyu, S. M., and Akabuogu, E. U. (2016) 'Effects of Administered Cardioprotective Drugs on Treatment Response of Breast Cancer Cells'. *Anticancer Res* 36 (1), 87

Sobczuk, P., Czerwińska, M., Kleibert, M., and Cudnoch-Jędrzejewska, A. (2020) 'Anthracycline-Induced Cardiotoxicity and Renin-Angiotensin-Aldosterone System—from Molecular Mechanisms to Therapeutic Applications'. *Heart Failure Reviews*

Soda, M., Choi, Y. L., Enomoto, M., Takada, S., Yamashita, Y., Ishikawa, S., Fujiwara, S., Watanabe, H., Kurashina, K., Hatanaka, H., Bando, M., Ohno, S., Ishikawa, Y., Aburatani, H., Niki, T., Sohara, Y., Sugiyama, Y., and Mano, H. (2007) 'Identification of the Transforming EML4–ALK Fusion Gene in Non-Small-Cell Lung Cancer'. *Nature* 448 (7153), 561-566

Solomon, B. J., Mok, T., Kim, D., Wu, Y., Nakagawa, K., Mekhail, T., Felip, E., Cappuzzo, F., Paolini, J., Usari, T., Iyer, S., Reisman, A., Wilner, K. D., Tursi, J., and Blackhall, F. (2014) 'First-Line Crizotinib Versus Chemotherapy in ALK-Positive Lung Cancer'. *N Engl J Med* 371 (23), 2167-2177

Spurney, C. F., Sali, A., Guerron, A. D., Iantorno, M., Yu, Q., Gordish-Dressman, H., Rayavarapu, S., van der Meulen, J., Hoffman, E. P., and Nagaraju, K. (2011) 'Losartan Decreases Cardiac Muscle Fibrosis and Improves Cardiac Function in Dystrophin-Deficient Mdx Mice'. *Journal of Cardiovascular Pharmacology and Therapeutics* 16 (1), 87-95

Srikanthan, A., Ethier, J., Ocana, A., Seruga, B., Krzyzanowska, M. K., and Amir, E. (2015) 'Cardiovascular Toxicity of Multi-Tyrosine Kinase Inhibitors in Advanced Solid Tumors: A Population-Based Observational Study'. *Plos One* 10 (3), e0122735

Sun, H. and Wang, Y. (2012) 'Prostaglandin E2 in Remote Control of Myocardial Remodeling'. *Circulation* 125 (23), 2818-2820

Syrigos, K. N., Karapanagiotou, E., Boura, P., Manegold, C., and Harrington, K. (2011) 'Bevacizumab-Induced Hypertension: Pathogenesis and Management'. *BioDrugs : Clinical Immunotherapeutics, Biopharmaceuticals and Gene Therapy* 25 (3), 159-169

Tait, S. W. G. and Green, D. R. (2008) 'Caspase-Independent Cell Death: Leaving the Set without the Final Cut'. *Oncogene* 27 (50), 6452-6461

Takashi, M., Jingzang, T., del, M. F., Lee Kyung-Han, Ling, L., Michael, P., Force Thomas, L., Franke Thomas, F., Hajjar Roger, J., and Anthony, R. (2001) 'Akt Activation Preserves Cardiac Function and Prevents Injury After Transient Cardiac Ischemia in Vivo'. *Circulation* 104 (3), 330-335

Takemura, G. and Fujiwara, H. (2007) 'Doxorubicin-Induced Cardiomyopathy: From the Cardiotoxic Mechanisms to Management'. *Progress in Cardiovascular Diseases* 49 (5), 330-352

Tartarone, A., Gallucci, G., Lazzari, C., Lerose, R., Lombardi, L., and Aieta, M. (2015a) 'Crizotinib-Induced Cardiotoxicity: The Importance of a Proactive Monitoring and Management'. *Future Oncology (London, England)* 11 (14), 2043-2048

Tartarone, A., Gallucci, G., Lazzari, C., Lerose, R., Lombardi, L., and Aieta, M. (2015b) 'Crizotinib-Induced Cardiotoxicity: The Importance of a Proactive Monitoring and Management'. *Future Oncology (London, England)* 11 (14), 2043-2048

Temel, J. S., Greer, J. A., Muzikansky, A., Gallagher, E. R., Admane, S., Jackson, V. A., Dahlin, C. M., Blinderman, C. D., Jacobsen, J., Pirl, W. F., Billings, J. A., and Lynch, T. J. (2010) 'Early Palliative Care for Patients with Metastatic Non–Small-Cell Lung Cancer'. *N Engl J Med* 363 (8), 733-742

Teppo, H., Soini, Y., and Karihtala, P. (2017) 'Reactive Oxygen Species-Mediated Mechanisms of Action of Targeted Cancer Therapy'. *Oxidative Medicine and Cellular Longevity* 2017, 1485283

Tisdale, J. E. (2016) 'Drug-Induced QT Interval Prolongation and Torsades De Pointes: Role of the Pharmacist in Risk Assessment, Prevention and Management'. *Canadian Pharmacists Journal : CPJ = Revue Des Pharmaciens Du Canada : RPC* 149 (3), 139-152

Tokudome, T., Mizushige, K., Noma, T., Manabe, K., Murakami, K., Tsuji, T., Nozaki, S., Tomohiro, A., and Matsuo, H. (2000) 'Prevention of Doxorubicin (Adriamycin)-Induced Cardiomyopathy by Simultaneous Administration of Angiotensin-Converting Enzyme Inhibitor Assessed by Acoustic Densitometry'. *Journal of Cardiovascular Pharmacology* 36 (3), 361-368

Torre, L. A., Siegel, R. L., Ward, E. M., and Jemal, A. (2016) 'Global Cancer Incidence and Mortality Rates and Trends—An Update'. *Cancer Epidemiol Biomarkers Prev* 25 (1), 16

Toyokawa, G. and Seto, T. (2014) 'Anaplastic Lymphoma Kinase Rearrangement in Lung Cancer: Its Biological and Clinical Significance'. *Respiratory Investigation* 52 (6), 330-338

Ueno, M., Kakinuma, Y., Yuhki, K., Murakoshi, N., Iemitsu, M., Miyauchi, T., and Yamaguchi, I. (2006) 'Doxorubicin Induces Apoptosis by Activation of Caspase-3 in Cultured Cardiomyocytes in Vitro and Rat Cardiac Ventricles in Vivo'. *Journal of Pharmacological Sciences* 101 (2), 151-158

Vaduganathan, M., Vardeny, O., Michel, T., McMurray, J. J. V., Pfeffer, M. A., and Solomon, S. D. (2020) 'Renin–Angiotensin–Aldosterone System Inhibitors in Patients with Covid-19'. *N Engl J Med* 382 (17), 1653-1659

van Loo, G., Saelens, X., van Gurp, M., MacFarlane, M., Martin, S. J., and Vandenabeele, P. (2002) 'The Role of Mitochondrial Factors in Apoptosis: A Russian Roulette with More than One Bullet'. *Cell Death & Differentiation* 9 (10), 1031-1042

van Thiel, B. S., van der Pluijm, I., te Riet, L., Essers, J., and Danser, A. H. J. (2015) 'The Renin–angiotensin System and its Involvement in Vascular Disease'. *European Journal of Pharmacology* 763, 3-14

Vanlangenakker, N., Vanden Berghe, T., Krysko, D. V., Festjens, N., and Vandenabeele, P. (2008) 'Molecular Mechanisms and Pathophysiology of Necrotic Cell Death'. *Current Molecular Medicine* 8 (3), 207-220

Vaynblat, M., Shah, H. R., Bhaskaran, D., Ramdev, G., Davis, W. J.,3rd, Cunningham, J. N.,Jr, and Chiavarelli, M. (2002) 'Simultaneous Angiotensin Converting Enzyme Inhibition Moderates Ventricular Dysfunction Caused by Doxorubicin'. *European Journal of Heart Failure* 4 (5), 583-586

Veeravalli, K. K., Akula, A., Routhu, K. V., and Kota, M. K. (2003) 'Infarct Size Limiting Effect of Apstatin Alone and in Combination with Enalapril, Lisinopril and Ramipril in Rats with Experimental Myocardial Infarction'. *Pharmacological Research* 48 (6), 557-563

Volkova, M. and Russell, R.,3rd (2011) 'Anthracycline Cardiotoxicity: Prevalence, Pathogenesis and Treatment'. *Current Cardiology Reviews* 7 (4), 214-220

Wallace, K. B., Sardão, V. A., and Oliveira, P. J. (2020) 'Mitochondrial Determinants of Doxorubicin-Induced Cardiomyopathy'. *Circulation Research* 126 (7), 926-941

Warner, G. T. and Perry, C. M. (2002) 'Ramipril : A Review of its use in the Prevention of Cardiovascular Outcomes'. *Drugs* 62 (9), 1381-1405

Wei, Q., Liu, H., Liu, M., Yang, C., Yang, J., Liu, Z., and Yang, P. (2016) 'Ramipril Attenuates Left Ventricular Remodeling by Regulating the Expression of Activin A-Follistatin in a Rat Model of Heart Failure'. *Scientific Reports* 6 (1), 33677

Wen, Z., Mai, Z., Chen, Y., Wang, J., and Geng, D. (2018) 'Angiotensin II Receptor Blocker Reverses Heart Failure by Attenuating Local Oxidative Stress and Preserving Resident Stem Cells in Rats with Myocardial Infarction'. *American Journal of Translational Research* 10 (8), 2387-2401

Will, Y., Dykens, J. A., Nadanaciva, S., Hirakawa, B., Jamieson, J., Marroquin, L. D., Hynes, J., Patyna, S., and Jessen, B. A. (2008) 'Effect of the Multitargeted Tyrosine Kinase Inhibitors Imatinib, Dasatinib, Sunitinib, and Sorafenib on Mitochondrial Function in Isolated Rat Heart Mitochondria and H9c2 Cells'. *Toxicological Sciences : An Official Journal of the Society of Toxicology* 106 (1), 153-161

Wu, S., Chen, J. J., Kudelka, A., Lu, J., and Zhu, X. (2008) 'Incidence and Risk of Hypertension with Sorafenib in Patients with Cancer: A Systematic Review and Meta-Analysis'. *The Lancet.Oncology* 9 (2), 117-123

Xiongwen, C., Xiaoying, Z., Hajime, K., Harris David, M., Mills Geoffrey, D., Jed, M., Remus, B., Potts, S. T., Marsh James, D., and Houser Steven, R. (2005) 'Ca2+ Influx–Induced Sarcoplasmic Reticulum Ca2+ Overload Causes Mitochondrial-Dependent Apoptosis in Ventricular Myocytes'. *Circulation Research* 97 (10), 1009-1017

Xu, F., Na, L., Li, Y., and Chen, L. (2020) 'Roles of the PI3K/AKT/mTOR Signalling Pathways in Neurodegenerative Diseases and Tumours'. *Cell & Bioscience* 10 (1), 54

Xu, J., Lü, X., Huang, Y., Zhu, P., and Li, J. (2009) 'Synergism of Simvastatin with Losartan Prevents Angiotensin II-Induced Cardiomyocyte Apoptosis in Vitro'. *Journal of Pharmacy and Pharmacology* 61 (4), 503-510

Yang, G., Xu, H., Yang, L., Xu, F., Zhang, S., Yang, Y., and Wang, Y. (2020) 'Apatinib in Combination with Pemetrexed-Platinum Chemotherapy for Chemo-Naive Non-Squamous Non-Small Cell Lung Cancer: A Phase II Clinical Study'. *Lung Cancer* 147, 229-236

Yang, Q., Wen, L., Meng, Z., and Chen, Y. (2018) 'Blockage of Endoplasmic Reticulum Stress Attenuates Nilotinib-Induced Cardiotoxicity by Inhibition of the Akt-GSK3β-Nox4 Signaling'. *European Journal of Pharmacology* 822, 85-94

Zahedmehr, A. (2018) 'Chapter 17 - Hypertension'. in *Practical Cardiology*. ed. by Maleki, M., Alizadehasl, A., and Haghjoo, M. : Elsevier, 291-302

Zalvidea, S., André, L., Loyer, X., Cassan, C., Sainte-Marie, Y., Thireau, J., Sjaastad, I., Heymes, C., Pasquié, J. L., Cazorla, O., Aimond, F., and Richard, S. (2012) 'ACE Inhibition Prevents Diastolic Ca2+ Overload and Loss of Myofilament Ca2+ Sensitivity After Myocardial Infarction'. *Current Molecular Medicine* 12 (2), 206-217

Zamorano, J. L., Lancellotti, P., Rodriguez Muñoz, D., Aboyans, V., Asteggiano, R., Galderisi, M., Habib, G., Lenihan, D. J., Lip, G. Y. H., Lyon, A. R., Lopez Fernandez, T., Mohty, D., Piepoli, M. F., Tamargo, J., Torbicki, A., Suter, T. M., Zamorano, J. L., Aboyans, V., Achenbach, S., Agewall, S., Badimon, L., Barón-Esquivias, G., Baumgartner, H., Bax, J. J., Bueno, H., Carerj, S., Dean, V., Erol, Ç, Fitzsimons, D., Gaemperli, O., Kirchhof, P., Kolh, P., Lancellotti, P., Lip, G. Y. H., Nihoyannopoulos, P., Piepoli, M. F., Ponikowski, P., Roffi, M., Torbicki, A., Vaz Carneiro, A., Windecker, S., Authors/Task, F. M., ESC Committee for Practice Guidelines, (CPG), and Reviewers, D. (2017) '2016 ESC Position Paper on Cancer Treatments and Cardiovascular Toxicity Developed Under the Auspices of the ESC Committee for Practice Guidelines'. *European Journal of Heart Failure* 19 (1), 9-42

Zang, J., Wu, S., Tang, L., Xu, X., Bai, J., Ding, C., Chang, Y., Yue, L., Kang, E., and He, J. (2012) 'Incidence and Risk of QTc Interval Prolongation among Cancer Patients Treated with Vandetanib: A Systematic Review and Meta-Analysis'. *PloS One* 7 (2), e30353

Zarogoulidis, K., Zarogoulidis, P., Darwiche, K., Boutsikou, E., Machairiotis, N., Tsakiridis, K., Katsikogiannis, N., Kougioumtzi, I., Karapantzos, I., Huang, H., and Spyratos, D. (2013) 'Treatment of Non-Small Cell Lung Cancer (NSCLC)'. *Journal of Thoracic Disease* 5 Suppl 4, S389-S396

Zhang, J., Liu, D., Zhang, M., and Zhang, Y. (2019a) 'Programmed Necrosis in Cardiomyocytes: Mitochondria, Death Receptors and Beyond'. *British Journal of Pharmacology* 176 (22), 4319-4339

Zhang, X., Zhu, Y., Dong, S., Zhang, A., Lu, Y., Li, Y., Lv, S., and Zhang, J. (2019b) 'Role of Oxidative Stress in Cardiotoxicity of Antineoplastic Drugs'. *Life Sciences* 232, 116526

Zhao, Y. Y., Sawyer, D. R., Baliga, R. R., Opel, D. J., Han, X., Marchionni, M. A., and Kelly, R. A. (1998) 'Neuregulins Promote Survival and Growth of Cardiac Myocytes. Persistence of ErbB2 and ErbB4 Expression in Neonatal and Adult Ventricular Myocytes'. *The Journal of Biological Chemistry* 273 (17), 10261-10269

Zhao, Y., McLaughlin, D., Robinson, E., Harvey, A. P., Hookham, M. B., Shah, A. M., McDermott, B. J., and Grieve, D. J. (2010) 'Nox2 NADPH Oxidase Promotes Pathologic Cardiac Remodeling Associated with Doxorubicin Chemotherapy'. *Cancer Res* 70 (22), 9287

Zhu, X., Stergiopoulos, K., and Wu, S. (2009) 'Risk of Hypertension and Renal Dysfunction with an Angiogenesis Inhibitor Sunitinib: Systematic Review and Meta-Analysis'. *Null* 48 (1), 9-17

Zoltán, V. V., Ferdinandy, P., Liaudet, L., and Pál Pacher (2015) 'Drug-Induced Mitochondrial Dysfunction and Cardiotoxicity'. *American Journal of Physiology-Heart and Circulatory Physiology* 309 (9), H1453-H1467

Zong, W. N., Yang, X. H., Chen, X. M., Huang, H. J., Zheng, H. J., Qin, X. Y., Yong, Y. H., Cao, K., Huang, J., and Lu, X. Z. (2011) 'Regulation of Angiotensin-(1-7) and Angiotensin II Type 1 Receptor by Telmisartan and Losartan in Adriamycin-Induced Rat Heart Failure'. *Acta Pharmacologica Sinica* 32 (11), 1345-1350

Zorov, D. B., Juhaszova, M., and Sollott, S. J. (2014) 'Mitochondrial Reactive Oxygen Species (ROS) and ROS-Induced ROS Release'. *Physiological Reviews* 94 (3), 909-950